CHARACTERIZATION OF CYANOBACTERIAL CELL SURFACE FOR REMOVAL OF HEAVY METALS FROM AQUEOUS SOLUTIONS

A THESIS SUBMITTED IN PARTIAL FULFILLMENT OF THE REQUIREMENTS FOR THE DEGREE OF DOCTOR OF PHILOSOPHY

SENGJRANG CH MOMIN

MZU Reg. No.: 7050 of 2014

Ph. D Reg. No.: MZU/Ph.D./1014 of 26.05.2017

DEPARTMENT OF BOTANY

SCHOOL OF LIFE SCIENCES

MAY, 2024

CHARACTERIZATION OF CYANOBACTERIAL CELL SURFACE FOR REMOVAL OF HEAVY METALS FROM AQUEOUS SOLUTIONS

By

SENGJRANG CH MOMIN

DEPARTMENT OF BOTANY

SUPERVISOR

DR. SURYA KANT MEHTA

SUBMITTED

IN PARTIAL FULFILLMENT OF THE REQUIREMENT OF THE DEGREE OF DOCTOR OF PHILOSOPHY IN BOTANY OF MIZORAM UNIVERSITY, AIZAWL

MIZORAM UNIVERSITY
MIZORAM: AIZAWL- 796 004

Botany Department

Dr. S. K. MEHTA
Professor

Post Box No. 190
Gram: MZU
Phone: 0389-2330733
Fax: 0389-2330532
Email: skmehta@mzu.edu.in

CERTIFICATE

This is to certify that **Mr. Sengjrang Ch Momin,** Registration No. **MZU/Ph.D/1014 of 26.05.2017** has submitted the thesis entitled "**Characterization of cyanobacterial cell surface for removal of heavy metals from aqueous solutions**" under my supervision, for the requirement of the award of the Degree of Doctor of Philosophy in the Department of Botany, Mizoram University, Aizawl. The work is authentic, content of the thesis is the original work of the Research Scholar, and the nature and the presentation of the work are the first of its kind.

It is further certified that no portion(s) or part(s) of the content of the thesis has been submitted for any degree in Mizoram University or any other University or Institute.

Date

Sincerely yours,

Place

(Dr. Surya Kant Mehta)
Supervisor
Department of Botany
Mizoram University

MIZORAM UNIVERSITY

May 2024

DECLARATION

I, Mr. Sengjrang Ch Momin**,** hereby declare that the subject matter of this thesis is the record of work done by me, that the contents of this thesis did not form basis of the award of any previous degree to me or to the best of my knowledge to anybody else, and that the thesis has not been submitted by me for any research degree in any other University/Institute.

This is being submitted to the Mizoram University for the degree of Doctor of Philosophy in Botany.

Date:
Place: Aizawl, Mizoram

(Mr. Sengjrang Ch Momin)
Department of Botany
Mizoram University
Aizawl- 796004

(Prof. F. Lalnunmawia)
Head
Department of Botany
Mizoram University
Aizawl-796004

(Dr. Surya Kant Mehta)
Supervisor
Department of Botany
Mizoram University
Aizawl- 796004

Acknowledgement

First and foremost I would like to express my humble gratitude to Almighty God for giving me a good heath throughout my journey and for all His blessings upon me.

I would like to express my sincere gratitude to my **supervisor Dr. Surya Kant Mehta** for his invaluable guidance, patience, and support throughout the research process. His expertise and encouragement were instrumental in shaping this thesis.

I am thankful to **Head, Department of Botany Prof. F. Lalnunmawia** and all the faculties of the Botany department including non-teaching staffs for their unconditional help and support during my work.

I would like to give my sincere gratitude to **Dean of Life Science Prof. N. Senthil Kumar** for his kind support and cooperation. Particularly, I would like to acknowledge **Prof. Y. T. Singh** for allowing me to utilized his laboratory instruments for my experiments.

I acknowledge my gratitude to the Ministry of Tribal Affairs, Scholarship Division, Government of India for financial support in the form of **National Fellowship for ST candidates** (Award No. - 201819-NFST-MEG-00069).

I am indebted to **Mizoram University** for providing the resources and facilities necessary for conducting this research and also for providing financial assistant through University Non-NET fellowship.

I would like to express my sincere gratitude to **Mr. Brojen Singh**, Laboratory Technician, Chemistry Department, Mizoram University for helping me in Heavy metal analysis in Atomic Adsorption Spectrophotometer without any hesitation.

Special thanks to all my lab mates, who were another blessing to me, who made the laboratory atmosphere a home away from home, **Miss Ruthi Lalmuanzeli, Mr. Lalremdika, Mrs. Chawngthantluangi, Mr. Ran Bahadur Pradhan, Miss Jyotishma Nath, Mr. Agniv Kar, Miss Lalchhanhimi Khiangte and Miss Semima Farhin.**

It will be amiss if I don't mention my friends from Buannel hostel, **Dr. Ao Sanen, Dr. R. Yaongam, Dr. Sari Kokba, Dr. Gabriel Lalchandama** and others. A humble gratitude to all the friends from Garo community specially **Miss. Bidanchi Momin and Mr. Brilliant Marak**, and would like to mentioned other close friends and well-wishers **Dr. Wistful In excelsis Nongrem, Dr. Ng. Polbina Monsang and Miss Fedalia Bamon** for all their unwavering support and encouragement during challenging times.

I am grateful to the participants who generously contributed their time and insights to this study.

Finally, I would like to **dedicate this thesis to my family** and would like to offer my sincere gratitude to my family for their unconditional love and encouragement throughout my academic journey.

Date: Sengjrang Ch Momin

Mizoram University

PREFACE

The ominous shadow of heavy metal contamination in our water resources looms ever larger, posing a significant threat to human health and ecological well-being. Industrial activities, agricultural practices, and even natural geological processes can all contribute to the accumulation of these toxic elements in water bodies. These heavy metals, unlike organic pollutants, are not readily biodegradable and persist in the environment, entering the food chain and causing detrimental effects at various levels.

This thesis delves into the exciting realm of bioremediation, a burgeoning field that harnesses the power of living organisms to cleanse contaminated environments. Specifically, it explores the potential of cyanobacteria, a diverse group of photosynthetic microorganisms, as nature's warriors in the fight against heavy metal pollution. The research focuses on two promising cyanobacterial strains: *Microcystis aeruginosa* and *Anabaena doliolum*.

This study goes beyond simply establishing the efficacy of these cyanobacteria in removing heavy metals. It delves deeper, meticulously dissecting the underlying mechanisms governing this metal removal process. By unravelling these mechanisms, we can not only optimize bioremediation strategies but also gain a deeper understanding of the fascinating interplay between cyanobacteria and heavy metals. The research investigates the effectiveness of both live cyanobacteria (biomass) and their intriguing biomolecules, Exopolysaccharides (EPS), in capturing specific heavy metal ions, namely Cu^{2+}, Ni^{2+}, and Cd^{2+}.

Furthermore, the research extends its focus by examining the impact of these very metals on the cyanobacteria themselves. It analyzes the tolerance mechanisms employed by these microorganisms and their response to the cellular stress caused by metal exposure. Understanding how cyanobacteria cope with these environmental stressors is crucial for developing robust bioremediation strategies that can withstand the harsh realities of contaminated water bodies.

The thesis is organized for optimal comprehension. Chapter I, the “Introduction”, lays the groundwork by outlining the problem of heavy metal contamination and the promise of bioremediation using cyanobacteria. Chapter II, “Materials and Methods”, serves as a blueprint, meticulously detailing the experimental design, the materials employed, and the analytical techniques used to gather the data. Chapter III, “Results”, presents the findings of the research in a clear and concise manner, often utilizing figures and tables for enhanced visualization. Finally, Chapter IV, “Discussion”, interprets the results within the context of existing scientific knowledge, highlighting the most significant findings and their implications for the field of bioremediation. An abstract precedes the main body of the thesis,

providing a concise overview of the research objectives, methodology, key findings, and conclusions. Following Chapter IV, a “Summary” recapitulates the major research questions, summarizes the key findings, and reiterates the significance of this work in the fight against water pollution.

The research journey documented in this thesis has been both intellectually stimulating and profoundly rewarding. It is my sincere hope that the findings presented here contribute to the development of sustainable and effective bioremediation strategies that can help us reclaim our water resources from the clutches of heavy metal contamination. By harnessing the power of nature's warriors, the cyanobacteria, we can move towards a future with cleaner water and a healthier planet.

Date: Sengjrang Ch Momin

Mizoram University

CONTENTS

Chapter-3 Results

ABBREVIATION

AAS	Atomic Adsorption Spectroscopy
ABC	ATP-Binding Cassette
Ag	Silver
Al	Aluminium
Ala	Alanine
APX	Ascorbate Peroxidase
Ar	Arsenic
Arg	Arginine
ASC	Ascorbate
Asn	Asparagine
Asp	Aspartic
ATP	Adenosine Triphosphate
Au	Gold
BSA	Bovine Serum Albumin
CAR	Carotenoids
CAT	Catalase
CAX	Cation Exchangers
CCU	Carbon Capture and Utilization
Cd	Cadmium
CDF	Cation Diffusion Facilitators
CDI	Capacitive Deionization Systems
Chl-a	Chlorophyll-a
Co	Cobalt
CO_2	Carbon-dioxide
COPT	Copper Transporters
Cr	Chromium
Cu	Copper
DNA	Deoxyribonucleic acid
EDTA	Ethylenediaminetetraacetic acid
EDX	Energy-dispersive X-ray
EPA	European Protection Agency
EPA	European Protection Agency
EPS	Extracellular Polymeric Substance
ETC	Electron Transport Chain
Fe	Iron
FTIR	Fourier Transform Infrared Spectroscopy
Gly	Glycine
GR	Glutathione Reductase

H_2O_2	Hydrogen Peroxide
Hg	Mercury
HM	Heavy Metals
HMA	Heavy-Metal P-type ATPases
HSAB	Hard and soft acids and bases
Ile	Isoleucine
LB-EPS	Loosely bound EPS
LCMS	Liquid Chromatography Mass Spectrometry
Leu	Leucine
Lys	Lysine
MDA	Malondialdehyde
MDHA	Monodehydroascorbate
Mn	Manganese
Mo	Molybdenum
MTs	Metallothioneins
N_2	Nitrogen
NBT	Nitro blue tetrazolium
NH_3	Ammonia
Ni	Nickel
NRAMP	Natural Resistance-Associated Macrophage Proteins
O_2	Oxygen
O_2^-	Superoxide Radicals
OH^-	Hydroxyl Radicals
Pb	Lead
PFO	Pseudo-First-Order
PHAs	Polyhydroxyalkanoates
Phe	Phenylalanine
Pro	Proline
PS-I	Photosystem I
PS-II	Photosystem II
PSO	Pseudo-Second-Order
SEM	Scanning Electron Microscopy
Ser	Serine
SOD	Superoxide Dismutase
TBARS	2-Thiobarbituric acid reactive substances
TB-EPS	Tightly bound EPS
TEM	Transmission Electron Microscopy
Thr	Threonine
UV/VIS	Ultra-violet Visible spectroscopy
Val	Valine

WHO	World Health Organization
ZIP	Zrt- Irt-like Proteins
Zn	Zinc

LIST OF FIGURES

Figure.10. Liquid Chromatography- Mass Spectrometry (LCMS) chromatogram of isolated EPS from *M. aeruginosa*.

Figure.11. Liquid Chromatography- Mass Spectrometry (LCMS) chromatogram of isolated EPS from *A. doliolum*.

Figure 12. Surface protonation of cyanobacterial biomass and EPS assessed by Acid-Base Titration. (A) *Microcystis* biomass untreated, Cd^{2+}, Cu^{2+} and Ni^{2+} treated, (B) *Anabaena* biomass untreated, Cd^{2+}, Cu^{2+} and Ni^{2+} treated, (C) *Microcystis* -EPS untreated, Cd^{2+}, Cu^{2+} and Ni^{2+} treated and (D) *Anabaena* EPS untreated, Cd^{2+}, Cu^{2+} and Ni^{2+} treated.

Figure.13. Equivalence Point of pH Titration for *M. aeruginosa, A. doliolum*, and EPS with and without metal treatment. (A) *Microcystis* biomass untreated, Cd^{2+}, Cu^{2+} and Ni^{2+} treated, (B) *Anabaena* biomass untreated, Cd^{2+}, Cu^{2+} and Ni^{2+} treated, (C) *Microcystis* EPS untreated, Cd^{2+}, Cu^{2+} and Ni^{2+} treated and (D) *Anabaena*-EPS untreated, Cd^{2+}, Cu^{2+} and Ni^{2+} treated.

Figure.14. Gran's plot. (A) pH titration of untreated *M. aeruginosa* biomass, (B) pH titration of Cd^{2+} treated biomass (C) pH titration of Cu^{2+} treated biomass, and (D) pH titration of Ni^{2+} treated biomass.

Figure.15. Gran's plot. (A) pH titration of untreated *A. doliolum* biomass, (B) pH titration of Cd^{2+} treated biomass (C) pH titration of Cu^{2+} treated biomass, and (D) pH titration of Ni^{2+} treated biomass.

Figure.16. Gran's plot. (A) pH titration of untreated *Microcystis* EPS, (B) pH titration of Cd^{2+} treated EPS (C) pH titration of Cu^{2+} treated EPS, and (D) pH titration of Ni^{2+} treated EPS.

Figure.17. Gran's plot. (A) pH titration of untreated *Anabaena* EPS, (B) pH titration of Cd^{2+} treated EPS (C) pH titration of Cu^{2+} treated EPS, and (D) pH titration of Ni^{2+} treated EPS.

Figure.18. Impact of pH on metal removal efficiency (A) Native biomass of the cyanobacteria *M. aeruginosa* and (B) Native biomass of cyanobacteria *A. doliolum.* The experiments were carried out with an initial concentration of 5 mg L^{-1} for both Ni^{2+} and Cu^{2+}, maintaining a consistent incubation period of 1 h. The values shown represent the mean results from three replicates, accompanied by their corresponding standard deviations (SD).

Figure.19. Impact of pH on metal removal efficiency. (A) EPS isolated from *M. aeruginosa* and (B) EPS isolated from *A. doliolum*. The experiments were carried out with an initial concentration of 5 mg L^{-1} for both Ni^{2+} and Cu^{2+}, maintaining a consistent incubation period of 1 hour. The values shown represent the mean results from three replicates, accompanied by their corresponding standard deviations (SD).

Figure.20. Kinetic profile of metal sorption by living biomass of *M. aeruginosa*. (A) Cd^{2+}, (B) Cu^{2+} and (C) Ni^{2+}. The curves correspond to the predicted values from the PFO and PSO models. Kinetic parameters for each metal can be found in Table 6.

Figure.21. Kinetic profile of metal sorption by living biomass of *A. doliolum* (A) Cd^{2+}, (B) Cu^{2+} and (C) Ni^{2+}.The curves correspond to the predicted values from the PFO and PSO models. Kinetic parameters for each metal can be found in Table 7.

Figure.22. Kinetic profile of metal sorption by isolated EPS of *M. aeruginosa*. The curves represent the predicted sorption trends based on the PFO and PSO. Kinetic parameters for each metal can be found in Table 8.

Figure.23. Kinetic profile of metal sorption by isolated EPS of *M. aeruginosa*. The curves represent the predicted sorption trends based on the PFO and PSO. Kinetic parameters for each metal can be found in Table 8.

Figure.24. Intraparticle diffusion analysis for metal sorption by *M. aeruginosa* biomass (A) Cd^{2+} biosorption, (B) Cu^{2+} biosorption and (C) Ni^{2+} biosorption. Experimental data points are denoted by symbols, while model predictions are depicted by the corresponding curves.

Figure.25. Intraparticle diffusion analysis for metal sorption by *A. doliolum* biomass (A) Cd^{2+} biosorption, (B) Cu^{2+} biosorption and (C) Ni^{2+} biosorption. Experimental data points are denoted by symbols, while model predictions are depicted by the corresponding curves.

Figure.26. Intraparticle diffusion analysis for metal sorption by isolated EPS of *M. aeruginosa.* (A) Cd^{2+} biosorption, (B) Cu^{2+} biosorption and (C) Ni^{2+} biosorption. Experimental data points are denoted by symbols, while model predictions are depicted by the corresponding curves.

Figure.27. Intraparticle diffusion analysis for metal sorption by isolated EPS of *A. doliolum.* (A) Cd^{2+} biosorption, (B) Cu^{2+} biosorption and (C) Ni^{2+} biosorption. Experimental data points are denoted by symbols, while model predictions are depicted by the corresponding curves.

Figure.28. Van't Hoff plot for the biosorption of Ni^{2+} (A), Cu^{2+} (B), and Cd^{2+} (C) ions onto *M. aeruginosa* biomass. The data points represent the experimental values of ln kc at different temperatures. The corresponding thermodynamic parameters (ΔG^{o}, ΔH^{o}, and ΔS^{o}) for each metal ion can be found in Table 11.

Figure.29. Van't Hoff plot for the biosorption of Ni^{2+} (A), Cu^{2+} (B), and Cd^{2+} (C) ions onto *A. doliolum* biomass. The data points represent the experimental values of ln kc at different temperatures. The corresponding thermodynamic parameters (ΔG^{o}, ΔH^{o}, and ΔS^{o}) for each metal ion can be found in Table 12.

Figure.30. Van't Hoff plot for the biosorption of Ni^{2+} (A), Cu^{2+} (B), and Cd^{2+} (C) ions onto isolated EPS from *M. aeruginosa*. The data points represent the experimental values of ln kc at different temperatures. The corresponding thermodynamic parameters (ΔG^{o}, ΔH^{o}, and ΔS^{o}) for each metal ion can be found in Table 13.

Figure.31. Van't Hoff plot for the biosorption of Ni^{2+} (A), Cu^{2+} (B), and Cd^{2+} (C) ions onto isolated EPS of *A. doliolum*. The data points represent the experimental values of ln kc at different temperatures. The corresponding thermodynamic parameters (ΔG^{o}, ΔH^{o}, and ΔS^{o}) for each metal ion can be found in Table 14.

Figure.32. Equilibrium isotherms for the biosorption of Ni^{2+} (A), Cu^{2+} (B), and Cd^{2+} (C) ions onto *M. aeruginosa* biomass. The curves represent the fitting of the Langmuir, Freundlich, and Temkin isotherm models to the experimental data points.

Figure.33. Equilibrium isotherms for the biosorption of Ni^{2+} (A), Cu^{2+} (B), and Cd^{2+} (C) ions onto *A. doliolum* biomass. The curves represent the fitting of the Langmuir, Freundlich, and Temkin isotherm models to the experimental data points.

Figure.34. Equilibrium isotherms for the biosorption of Ni^{2+} (A), Cu^{2+} (B), and Cd^{2+} (C) ions onto *M. aeruginosa* EPS (Extracellular Polymeric Substances). The curves represent the fitting of the Langmuir, Freundlich, and Temkin isotherm models to the experimental data points.

Figure.35. Equilibrium isotherms for the biosorption of Ni^{2+} (A), Cu^{2+} (B), and Cd^{2+} (C) ions onto *A. doliolum* EPS. The curves represent the fitting of the Langmuir, Freundlich, and Temkin isotherm models to the experimental data points.

Figure.36. Influence of Ni^{2+} Co-existence on Cu^{2+} Biosorption. This figure depicts the biosorption behavior of Cu^{2+} ions onto *M. aeruginosa* and *A. doliolum* biomass (A and B) and their respective EPS (C and D) in the presence of co-existing Ni^{2+} ions. The initial concentration of Cu^{2+} varied from 0 to 10 mg L^{-1}, while a constant concentration of Ni^{2+} (5 mg L^{-1}) was introduced in the binary systems. The solid lines represent the fitting of the Langmuir (blue), Freundlich (red), and Temkin (green) isotherm models to the experimental data points (symbols).

Figure.37. Influence of Cu^{2+} Co-existence on Ni^{2+} Biosorption. This figure depicts the biosorption behavior of Ni^{2+} ions onto M. aeruginosa and *A. doliolum* biomass (A and B) and their respective EPS (C and D) in the presence of co-existing Cu^{2+} ions. The initial concentration of Ni^{2+} varied from 0 to 10 mg L^{-1}, while a constant concentration of Cu^{2+} (5 mg L^{-1}) was introduced in the binary systems. The solid lines represent the fitting of the Langmuir (blue), Freundlich (red), and Temkin (green) isotherm models to the experimental data points (symbols).

Figure.38. Desorption of Cd^{2+}, Cu^{2+}, and Ni^{2+} from *M. aeruginosa* biomass and EPS. This figure illustrates the desorption efficiency of de-ionized water for Cd^{2+}, Cu^{2+}, and Ni^{2+} ions previously adsorbed onto M. aeruginosa biomass (A-C) and its EPS (D-F). A-C: Depict the desorption percentage of Cd^{2+} (A), Cu^{2+} (B), and Ni^{2+} (C) from M. aeruginosa biomass. D-F: Show the desorption percentage of Cd^{2+} (D), Cu^{2+} (E), and Ni^{2+} (F) from M. aeruginosa EPS.

Figure.39. Desorption of Cd^{2+}, Cu^{2+}, and Ni^{2+} from *A. doliolum* biomass and EPS. This figure illustrates the desorption efficiency of de-ionized water for Cd^{2+}, Cu^{2+}, and Ni^{2+} ions previously adsorbed onto *A. doliolum* biomass (A-C) and its EPS (D-F). A-C: Depict the desorption percentage of Cd^{2+} (A), Cu^{2+} (B), and Ni^{2+} (C) from *A. doliolum* biomass. D-F: Show the desorption percentage of Cd^{2+} (D), Cu^{2+} (E), and Ni^{2+} (F) from *A. doliolum* EPS.

Figure 40. Growth patterns of *M. aeruginosa* and *A. doliolum*. Absorbance of culture at 663 nm was measured every other day to monitor growth over a 36-day period. Error bars represent the standard error of the mean (n=3).

Figure 41. Effect of Cu^{2+}, Ni^{2+}, and Cd^{2+} on the specific growth rate of *M. aeruginosa*. The specific growth rate of *M. aeruginosa* treated with copper (Cu^{2+}), nickel (Ni^{2+}), and cadmium (Cd^{2+}) is shown. Vertical bars represent the standard error of the mean (n=3).

Figure 42. Effect of Cu^{2+}, Ni^{2+}, and Cd^{2+} on the specific growth rate of *A. doliolum*. The specific growth rate of *M. aeruginosa* treated with copper (Cu^{2+}), nickel (Ni^{2+}), and cadmium (Cd^{2+}) is shown. Vertical bars represent the standard error of the mean (n=3).

Figure 43. Total protein content ($\mu g\ ml^{-1}$) of *M. aeruginosa* treated with Cu^{2+}, Ni^{2+}, and Cd^{2+} for 96 h. Protein content showed statistically significant differences compared to the untreated control according to a two-tailed Student's T-Test. Asterisks indicate significance level: * ($p = 0.05$).

Figure.44. Total protein content (µg ml^{-1}) of *A. doliolum* treated with Cu^{2+}, Ni^{2+}, and Cd^{2+} for 96 h. Total protein content (µg ml^{-1}) of *M. aeruginosa* treated with Cu^{2+}, Ni^{2+}, and Cd^{2+} for 96 h. Protein content showed statistically significant differences compared to the untreated control according to a two-tailed Student's T-Test. Asterisks indicate significance level: * ($p = 0.05$).

Figure.45. Total carbohydrate content of *M. aeruginosa* treated with Cu^{2+}, Ni^{2+}, and Cd^{2+} for 96 h. Vertical bars represent the standard error of the means (n=3). Total carbohydrate content showed statistically significant differences compared to the untreated control according to a two-tailed Student's T-Test. Asterisks indicate significance level: * ($p = 0.05$)

Figure.46. Total carbohydrate content of *A. doliolum* treated with Cu^{2+}, Ni^{2+}, and Cd^{2+} for 96 h. Vertical bars represent the standard error of the means (n=3). Total carbohydrate content showed statistically significant differences compared to the untreated control according to a two-tailed Student's T-Test. Asterisks indicate significance level: * ($p = 0.05$).

Figure.47. Chlorophyll-a (Chl-a) content of *M. aeruginosa* treated with Cu^{2+}, Ni^{2+}, and Cd^{2+} for 96 h. Vertical bars represent the standard error of the mean (n=3). Total chlorophyll-a content showed statistically significant differences compared to the untreated control according to a two-tailed Student's T-Test. Asterisks indicate significance level: * ($p = 0.05$).

Figure.48. Chlorophyll-a (Chl-a) content of *A. doliolum* treated with Cu^{2+}, Ni^{2+}, and Cd^{2+} for 96 h. Vertical bars represent the standard error of the mean (n=3). Total Chlorophyll-a content showed statistically significant differences compared to the untreated control according to a two-tailed Student's T-Test. Asterisks indicate significance level: * ($p = 0.05$).

Figure.49. Carotenoid content of *M. aeruginosa* treated with Cu^{2+}, Ni^{2+}, and Cd^{2+} for 96 h. Vertical bars represent the standard error of the mean (n=3). Total carotenoids content showed statistically significant differences compared to the untreated control

according to a two-tailed Student's T-Test. Asterisks indicate significance level: * (p = 0.05).

Figure.50. Carotenoid content of *A. doliolum* treated with Cu^{2+}, Ni^{2+}, and Cd^{2+} for 96 h. Vertical bars represent the standard error of the mean (n=3). Total carotenoids content showed statistically significant differences compared to the untreated control according to a two-tailed Student's T-Test. Asterisks indicate significance level: * (p = 0.05).

Figure.51. Malondialdehyde (MDA) content of *M. aeruginosa* treated with Cu^{2+}, Ni^{2+}, and Cd^{2+} for 96 h. Vertical bars represent the standard error of the mean (n=3). All treatments with Cu^{2+}, Ni^{2+}, and Cd^{2+} resulted in statistically significant (P > 0.05, Two-tailed Student's T-test) increases in MDA content compared to the untreated control.

Figure.52. Malondialdehyde (MDA) content of *A. doliolum* treated with Cu^{2+}, Ni^{2+}, and Cd^{2+} for 96 h. Vertical bars represent the standard error of the mean (n=3). All treatments with Cu^{2+}, Ni^{2+}, and Cd^{2+} resulted in statistically significant (P > 0.05, Two-tailed Student's T-test) increases in MDA content compared to the untreated control.

Figure.53. Hydrogen Peroxide (H_2O_2) production in *M. aeruginosa* treated with Cu^{2+}, Ni^{2+}, and Cd^{2+} for 96 h. Vertical bars represent the standard error of the mean (n=3). All treatments with Cu^{2+}, Ni^{2+}, and Cd^{2+} resulted in statistically significant (P > 0.05, Two-tailed Student's T-test) increases in H_2O_2 levels compared to the untreated control.

Figure.54. Hydrogen Peroxide (H_2O_2) production in *A. doliolum* treated with Cu^{2+}, Ni^{2+}, and Cd^{2+} for 96 h. Vertical bars represent the standard error of the mean (n=3). All treatments with Cu^{2+}, Ni^{2+}, and Cd^{2+} resulted in statistically significant (P > 0.05, Two-tailed Student's T-test) increases in H_2O_2 levels compared to the untreated control.

Figure.55. Superoxide radical production in *M. aeruginosa* treated with Cu^{2+}, Ni^{2+}, and Cd^{2+} for 96 h. Vertical bars represent the standard error of the mean (n=3). All

treatments with Cu^{2+}, Ni^{2+}, and Cd^{2+} resulted in statistically significant (P > 0.05, Two-tailed Student's T-test) increases in O_2^- levels compared to the untreated control.

Figure.56. Superoxide radical production in *A. doliolum* treated with Cu^{2+}, Ni^{2+}, and Cd^{2+} for 96 h. Vertical bars represent the standard error of the mean (n=3). All treatments with Cu^{2+}, Ni^{2+}, and Cd^{2+} resulted in statistically significant (P > 0.05, Two-tailed Student's T-test) increases in O_2^- levels compared to the untreated control.

Figure.57. Hydroxyl radical production in *M. aeruginosa* treated with Cu^{2+}, Ni^{2+}, and Cd^{2+} for 96 h. Vertical bars represent the standard error of the mean (n=3). All treatments with Cu^{2+}, Ni^{2+}, and Cd^{2+} resulted in statistically significant (P > 0.05, Two-tailed Student's T-test) increases in OH^- levels compared to the untreated control.

Figure.58. Hydroxyl radical production in *A. doliolum* treated with Cu^{2+}, Ni^{2+}, and Cd^{2+} for 96 h. Vertical bars represent the standard error of the mean (n=3). All treatments with Cu^{2+}, Ni^{2+}, and Cd^{2+} resulted in statistically significant (P > 0.05, Two-tailed Student's T-test) increases in OH^- levels compared to the untreated control.

Figure.59. SOD enzyme activity in *M. aeruginosa* treated with Cu^{2+}, Ni^{2+}, and Cd^{2+} for 96 h. Vertical bars represent the standard error of the mean (n=3). All treatments with Cu^{2+}, Ni^{2+}, and Cd^{2+} resulted in statistically significant (P > 0.05, Two-tailed Student's T-test) increases in SOD levels compared to the untreated control.

Figure.60. SOD enzyme activity in *A. doliolum* treated with Cu^{2+}, Ni^{2+}, and Cd^{2+} for 96 h. Vertical bars represent the standard error of the mean (n=3). All treatments with Cu^{2+}, Ni^{2+}, and Cd^{2+} resulted in statistically significant (P > 0.05, Two-tailed Student's T-test) increases in SOD levels compared to the untreated control.

Figure.61. Catalase enzyme activity in *M. aeruginosa* treated with Cu^{2+}, Ni^{2+}, and Cd^{2+} for 96 h. Vertical bars represent the standard error of the mean (n=3). All treatments with Cu^{2+}, Ni^{2+}, and Cd^{2+} resulted in statistically significant (P > 0.05, Two-tailed Student's T-test) increases in CAT levels compared to the untreated control.

Figure.62. Catalase enzyme activity in *A. doliolum* treated with Cu^{2+}, Ni^{2+}, and Cd^{2+} for 96 h. Vertical bars represent the standard error of the mean (n=3). All treatments with Cu^{2+}, Ni^{2+}, and Cd^{2+} resulted in statistically significant ($P > 0.05$, Two-tailed Student's T-test) increases in CAT levels compared to the untreated control.

Figure.63. Ascorbate peroxidase (APX) enzyme activity in *M. aeruginosa* treated with Cu^{2+}, Ni^{2+}, and Cd^{2+} for 96 h. Vertical bars represent the standard error of the mean (n=3). All treatments with Cu^{2+}, Ni^{2+}, and Cd^{2+} resulted in statistically significant ($P > 0.05$, Two-tailed Student's T-test) increases in APX levels compared to the untreated control.

Figure.64. Ascorbate peroxidase (APX) enzyme activity in *A. doliolum* treated with Cu^{2+}, Ni^{2+}, and Cd^{2+} for 96 h. Vertical bars represent the standard error of the mean (n=3). All treatments with Cu^{2+}, Ni^{2+}, and Cd^{2+} resulted in statistically significant ($P > 0.05$, Two-tailed Student's T-test) increases in APX levels compared to the untreated control.

Figure.65. Glutathione reductase (GR) enzyme activity in *M. aeruginosa* treated with Cu^{2+}, Ni^{2+}, and Cd^{2+} for 96 h. Vertical bars represent the standard error of the mean (n=3). All treatments with Cu^{2+}, Ni^{2+}, and Cd^{2+} resulted in statistically significant ($P > 0.05$, Two-tailed Student's T-test) increases in GR levels compared to the untreated control.

Figure.66. Glutathione reductase (GR) enzyme activity in *A. doliolum* treated with Cu^{2+}, Ni^{2+}, and Cd^{2+} for 96 h. Vertical bars represent the standard error of the mean (n=3). All treatments with Cu^{2+}, Ni^{2+}, and Cd^{2+} resulted in statistically significant ($P > 0.05$, Two-tailed Student's T-test) increases in GR levels compared to the untreated control.

LIST OF TABLES

CHAPTER-1

INTRODUCTION

1.1. HEAVY METAL POLLUTION

1.1.1 Water and Its Importance

Water is precious and indispensable habitat for a wide range of organisms, serving as the cornerstone of life on Earth. Water ecosystems must be protected and preserved in order to sustain biodiversity, provide ecosystem services, and ensure the health and well-being of both natural and human societies. Moreover, clean water is critical for sustaining life and enhancing human health, as well as supporting ecosystems and driving economic growth.

Drinking water is an integral element of our lives and is critical for our health. Clean water is utilized for a variety of purposes, including cooking, personal hygiene, and agriculture. It can assist to avoid water-borne infectious illnesses, keep the body functioning normally, and encourage a healthy lifestyle. It is essential for good sanitation and hygiene habits including handwashing, bathing, and waste disposal. Improved sanitation facilities, together with access to clean water, help to reduce the transmission of infectious illnesses and promote general health.

Clean water is necessary for agricultural production, such as irrigation, livestock farming, and aquaculture. Adequate water quality and availability are vital for agricultural and farm animals, maintaining food security and providing livelihoods for millions of people throughout the world.

The Earth's water cycle is a complicated system that includes evaporation, precipitation, groundwater, rivers, lakes, and the ocean. Clean water is an important component of this cycle since it acts as an evaporator and precipitator. When water quality deteriorates, contaminants in precipitation rise, which can have a severe influence on ecosystems and the climate.

Clean water is crucial for climate regulation. First, clean water maintains atmospheric humidity and promotes precipitation. Second, bodies of water like lakes

and rivers retain a lot of fresh water, which helps to regulate temperatures (Cosgrove and Loucks 2015). Most significantly, aquatic bodies, such as wetlands, serve as vital sites for carbon sequestration. Wetlands and other aquatic ecosystems have the ability to absorb and retain significant amounts of carbon. These ecosystems retain organic matter from plants and soil, lowering the quantity of carbon dioxide in the atmosphere and contributing to lower greenhouse gas emissions, delaying climate change (Villa and Bernal 2018; Were et al. 2019).

Providing access to clean water is a worldwide requirement that necessitates collective efforts from governments, communities, corporations, and people to protect human health, ecosystems, and promote sustainable development.

1.1.2. Heavy Metals

The term "heavy metal" lacks a universally accepted definition and can vary based on density, atomic weight, or toxicity. One definition considers density, classifying metals exceeding 5 g/cm³ as heavy metals (Tchounwou et al. 2012). However, Duffus (2002) argues that this definition is problematic as it may include non-toxic elements and excludes metalloids, which often exhibit similar environmental behaviors. Another approach defines heavy metals based on atomic mass greater than 23 or atomic number exceeding 20. This method, however, is prone to errors and confusion due to the inclusion of non-metals (Koller and Saleh 2018).

Despite the lack of a single, agreed-upon definition, certain elements are widely recognized as heavy metals due to their high density and potential environmental risks. These include titanium, vanadium, chromium, manganese, iron, cobalt, nickel, copper, zinc, arsenic, molybdenum, silver, cadmium, tin, platinum, gold, mercury, and lead (Briffa et al. 2020). This research specifically investigates the biosorption of three prevalent heavy metals: nickel (Ni), copper (Cu), and cadmium (Cd). These elements are frequently encountered in various environmental settings and pose significant ecological concerns.

Heavy metals are divided into two types i.e. essential and non-essential heavy metals. Essential heavy metals such as cobalt (Co), copper (Cu), iron (Fe), manganese (Mn), molybdenum (Mo), nickel (Ni), and zinc (Zn) plays an important role in growth

and development of plants (Arif et al. 2016). In low concentrations, essential heavy metals are regarded less harmful and function as co-enzymes in the biological process. For example, iron is found in hemoglobin and myoglobin, whereas cobalt is found in vitamin B12 (Rama Jyothi 2021). Essential heavy metals, although necessary for some biological functions, can also become hazardous to health and physiological function at high cellular concentrations. In extreme cases, they may even be carcinogenic (Kim et al. 2019). Unlike essential heavy metals, chromium (Cr), lead (Pb), arsenic (As), cadmium (Cd), and mercury (Hg) pose a significant threat to living organisms. These non-essential metals are highly toxic even at low concentrations, non-biodegradable, and have a multitude of harmful impacts (Slobodian et al. 2021). Essential elements can be further classified into three distinct categories: major elements, macrominerals, and trace elements. The fundamental building blocks of most living organisms are constituted by the major elements: hydrogen, carbon, nitrogen, and oxygen (Mitra 2015).

Macrominerals, on the other hand, comprise integral elements crucial for maintaining ionic balance within structural compounds, amino acids, and nucleic acids. These include sodium, magnesium, phosphorus, sulfur, chlorine, potassium, and calcium, with their categorization often based on atomic number (Ali 2023). Trace elements, encompassing thirteen elements identified by their atomic number, encompass silicon, vanadium, chromium, manganese, iron, cobalt, nickel, copper, zinc, arsenic, selenium, molybdenum, and iodine. Notably, essential elements play a multifaceted role in biological processes, including fostering skeletal structure formation, regulating acid-base equilibrium, and maintaining colloidal systems. They further serve as vital constituents of key enzymes, structural proteins, and hormones (Nimbalkar et al. 2018). For example, zinc is a component of numerous enzymes, iron is a critical element in hemoglobin, and selenium is essential for the enzyme glutathione peroxidase (Sedighi et al. 2014; Jeng and Chen 2022). Conversely, non-essential heavy metals lack any known beneficial role within the human body. However, they can still exert detrimental effects through their potential to disrupt the homeostasis of essential elements within the body (Ali et al. 2019; Briffa et al. 2020).

1.1.3. Sources of Heavy Metal Pollution

Since the planet's formation, heavy metals have been constituents of Earth's crust. The exponential increase in heavy metal use has led to a concomitant rise in their bioavailability within aquatic and terrestrial ecosystems, resulting in heavy metal pollution. This pollution primarily stems from anthropogenic activities, including mining, metal processing facilities (foundries and smelters), and other metal-based industries. Additionally, various sources contribute to heavy metal leaching into the environment, such as improperly disposed waste (garbage and landfills), animal waste (urine, manure), agricultural runoff, vehicle emissions, and road construction activities (Zhou et al. 2020; Masindi et al. 2021; Rama Jyothi 2021).

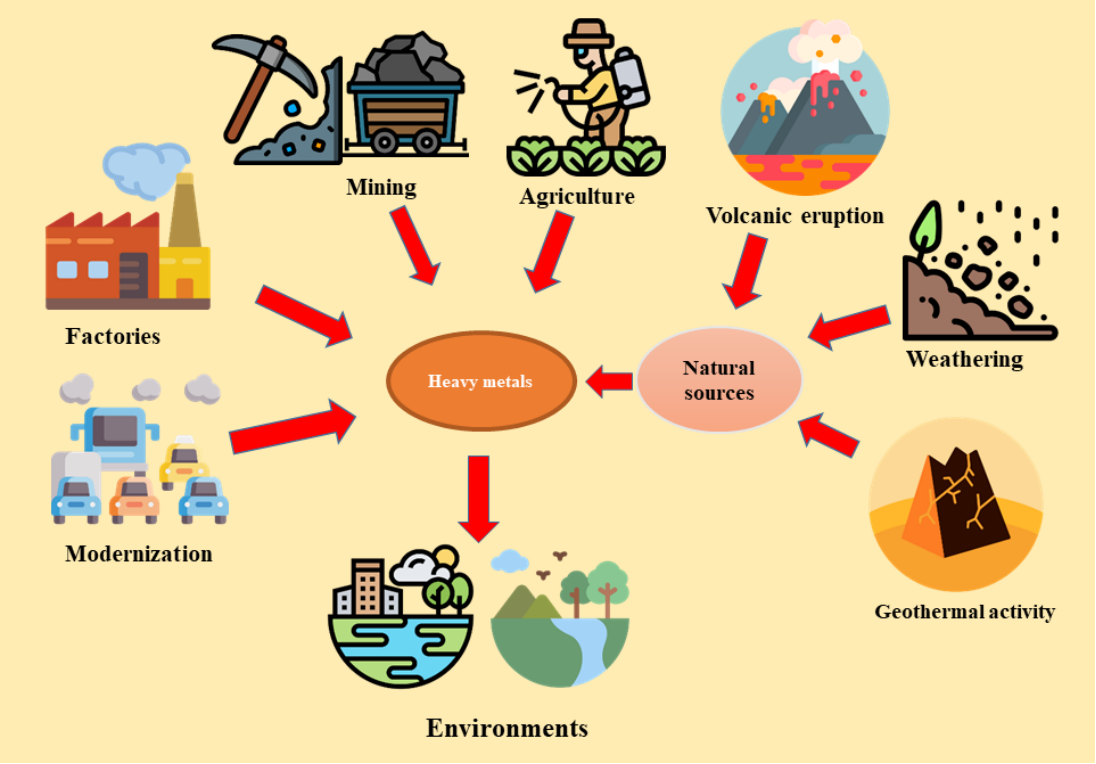

Fig.1.1. Different sources of heavy metal pollution discharge into the environment.

Agriculture fields are also a secondary source of heavy metal contamination from herbicides, insecticides, fertilizers, and other chemicals. Heavy metals can also be released into the environment through natural processes such as volcanic activity, metal corrosion, metal evaporation from soil water and sand, soil erosion, and

geological weathering (Mohammed et al. 2011; Srivastava et al. 2016; Masindi et al. 2021; Alengebawy et al. 2021; Sodhi et al. 2022; Wu et al. 2022).

Heavy metals may travel large distances in the atmosphere and may be deposited on land and water surfaces by precipitation (rain, snow, and dust) (He et al. 2023). Industrial emissions, automobile exhaust, and natural occurrences such as volcanic eruptions and wildfires all contribute to atmospheric heavy metal levels (Malik and Kaur Sandhu 2023).

1.1.4. Growing Threat of Heavy Metal Contamination in Water Resources

Heavy metal contamination is a major threat to the environment and human health, particularly in developing nations. Heavy metals can infiltrate the food chain through plants' roots, contaminating crops, vegetables, and soil. These metals can also interact with DNA and nuclear proteins, causing DNA damage and affecting the cell cycle (Agbemafle et al. 2019). This poses the greatest risk for the land, crops, and communities surrounding dumpsites. Heavy metal-polluted soil poses health concerns to humans, pollutes groundwater, causes phytotoxicity in plants, and reduces crop and soil output. Plant roots act as the primary pathway for heavy metal uptake, leading to their subsequent bioaccumulation within the food chain, posing a significant threat to animal and human health (Nyiramigisha et al. 2021). Unlike biodegradable contaminants of biological origin, heavy metals persist in the environment for extended periods, potentially lasting for decades or even centuries. This persistence is compounded by their ability to bioaccumulate within living organisms. Through this process, heavy metals progressively concentrate in tissues and are magnified as they move up the food chain, ultimately posing a significant threat to higher trophic levels, including humans (Uddin et al. 2021).

Heavy metal pollution in aqueous environments poses significant threats to both ecosystems and human health due to the non-degradability, bioaccumulation, and biomagnification of these heavy metals in organisms, either directly or indirectly through the food chain (Fu and Wang 2011; Ali and Khan 2018). These heavy metals can adversely affect various organs, including the kidneys, central nervous system, and lungs (Gybina and Prohaska 2008; Reglero et al. 2009), with the majority being reported as carcinogenic (Afroze and Sen 2018; Leong and Chang 2020). Furthermore,

heavy metal ions can be hazardous to plants and animals in the soil environment as they are absorbed by plants and eventually find their way into humans and other organisms (Mallampati et al. 2013; Dubey et al. 2018).

The escalating threat posed by heavy metal contamination in water resources demands a holistic approach encompassing pollution prevention, rigorous monitoring programs, robust regulatory frameworks, and effective remediation strategies. Sustainable water management practices, including stringent pollution control measures, watershed conservation efforts, and ecological restoration initiatives, are crucial for safeguarding water quality and ensuring the health of both human populations and the environment for present and future generations.

1.2. HEAVY METAL ACCUMULATION IN ALGAE AND CYANOBACTERIA

The process of metal accumulation in algae and cyanobacteria is a complex interplay between uptake mechanisms and detoxification strategies. These microorganisms have evolved a range of sophisticated mechanisms to fight with challenge of acquiring essential elements while avoiding the detrimental effects of heavy metals.

1.2.1. Mechanism of Heavy Metal Uptake in Algae and Cyanobacteria

The detrimental effects of heavy metal pollution on aquatic ecosystems are well-documented. Algae and cyanobacteria, being primary producers at the base of the food chain, play a crucial role in these ecosystems. Understanding their mechanisms of heavy metal uptake is essential for assessing their tolerance and potential bioremediation applications.

I. Intracellular Uptake

Intracellular uptake refers to the movement of heavy metals across the cell membrane and into the cytoplasm of algae and cyanobacteria. This process can be further divided into two main categories:

a. Active Transport:

This is a highly regulated and energy-dependent mechanism. Specific transport proteins embedded in the cell membrane play a crucial role. These proteins recognize and bind to specific metal ions or complexes containing metal ions. The binding triggers a conformational change in the protein, facilitating the translocation of the metal ion across the membrane and into the cytoplasm (Dhir 2021; Radzymińska-Lenarcik et al. 2022). This process requires energy derived from the hydrolysis of ATP (adenosine triphosphate), the cell's primary energy currency. The selectivity of these transporters is crucial, as they often have some affinity for essential elements with similar chemical properties to certain heavy metals. This can lead to the unintentional co-transport of essential elements alongside heavy metals, highlighting the delicate balance algae and cyanobacteria must maintain (Tangahu et al. 2011).

Recent research has shed light on a team of membrane transport proteins crucial players in management of metal ions across the cell membrane system. These proteins act like specialized gatekeepers embedded in the plant's cell membrane. Just like a symphony relies on various sections, plants including algae and cyanobacteria utilize a diverse array of these transport protein families, including the CDF (cation diffusion facilitators), ZIP (Zrt-, Irt-like proteins), CAX (cation exchangers), COPT (copper transporters), HMA (heavy-metal P-type ATPases), NRAMP (natural resistance-associated macrophage proteins), and ABC (ATP-binding cassette) transporters (Paulsen and Jr. 1997; Bowers and Srai 2018; He et al. 2020, 2022; Rekha et al. 2021; Wang et al. 2021; Bozzi and Gaudet 2021). Interestingly, these families are quite extensive. For instance, the *Arabidopsis* plant boasts 15 ZIP genes, 12 MTP (metal tolerance protein) genes, and 8 HMA genes (Zheng et al. 2018; Zhang et al. 2021; Wang et al. 2022). Despite this impressive lineup, much remains to be discovered about their specific roles. Studies are still deciphering the exact metals each transporter handles, how their activity is regulated, and where within the cell they operate.

b. Membrane Transport Mechanisms

Specific transport proteins located in the cell membrane play a critical role in facilitating the uptake of essential elements (Pizzagalli et al. 2021). These transmembrane proteins are highly selective and utilize ATP to actively transport

nutrients against their concentration gradient, ensuring a sufficient supply for cellular processes (Ryu et al. 2019). Examples of such transporters include those specific for phosphate (P), iron (Fe), and nitrogen (N). These essential elements often share similar chemical properties with certain heavy metals. For instance, some phosphate transporters exhibit unintended affinity for arsenic (As), which has a similar structure to phosphate (Blaby-Haas and Merchant 2012; Gill et al. 2021). This can lead to the unintentional co-transport of As into the cell, even though it is not essential and can be detrimental. Similarly, iron transporters may take up other divalent metal ions like cadmium (Cd) or copper (Cu) if they are present in the environment (Shcolnick and Keren 2006; Huertas et al. 2014). This non-specific uptake highlights the challenge faced by algae and cyanobacteria in maintaining a balance between acquiring essential nutrients and avoiding harmful heavy metals.

Channel proteins also play a significant role in heavy metal uptake, particularly for smaller ions. These transmembrane proteins form pores that allow the passage of ions and molecules across the cell membrane. The size and charge selectivity of these channels are determined by their specific amino acid composition and conformation. Channel-mediated uptake of heavy metals can be passive, relying on the concentration gradient across the membrane, or facilitated by chelating molecules that bind to the metal ion and influence its passage through the channel (Pasricha et al. 2021; Witkowska et al. 2021). Tight regulation of channel opening and closing is crucial for maintaining cellular homeostasis. Overly permissive channels can lead to excessive uptake of heavy metals, while overly restrictive channels can hinder the uptake of essential nutrients. Understanding the specific mechanisms of channel-mediated heavy metal uptake and its regulation is an essential area of research in this field (Ma et al. 2009; Bird 2015).

c. Facilitated Diffusion:

Facilitated diffusion offers a rapid and efficient way for plants to acquire essential metal ions across their cell membranes. Unlike active transport, which requires energy input in the form of ATP, facilitated diffusion relies solely on the concentration gradient across the cell membrane. Embedded within the cell membrane are specialized channel proteins. These proteins act like selective pores, allowing the

passage of specific ions and molecules based on size, charge, and sometimes even specific chemical properties. In the case of metal transport, certain channel proteins have evolved to recognize and facilitate the movement of essential metal ions like iron (Fe), copper (Cu), and zinc (Zn) across the membrane (Puckett et al. 2010; Jain et al. 2018; Briffa et al. 2020).

Facilitated diffusion relies on the principle of diffusion, where molecules move from an area of high concentration to an area of low concentration. This passive movement continues until equilibrium is reached, where the concentration of the metal ion is equal on both sides of the membrane. While channel proteins facilitate the influx of essential metal ions, their selectivity isn't always perfect. Factors like size and charge similarity can sometimes lead to the unintentional passage of non-essential heavy metals. For instance, a channel protein designed for copper (Cu^{2+}) might also allow the passage of cadmium (Cd^{2+}) due to their similar ionic charge (Thévenod et al. 2019). Various factors, such as the presence or absence of specific signal molecules or changes in environmental conditions, can influence the opening and closing of these channels (Briffa et al. 2020).

Energy Requirements for Intracellular Uptake: As mentioned earlier, active transport mechanisms involve significant energy expenditure in the form of ATP hydrolysis. This energy cost ensures that the uptake process is tightly regulated and allows the algae/cyanobacteria to prioritize the acquisition of essential elements while minimizing the influx of potentially toxic heavy metals.

II. Extracellular uptake

Extracellular uptake refers to the accumulation of heavy metals on the outer surface of the cell, primarily on the cell wall and the surrounding EPS (extracellular polymeric substances) layer. This process is passive and does not require energy input. Functional groups present on the cell wall (e.g., carboxyl, hydroxyl, sulfate, phosphate) can interact with metal ions through electrostatic interactions, chelation, or ion exchange (Pagliaccia et al. 2022; Raji et al. 2023). These interactions lead to the non-covalent binding of metal ions to the cell wall, effectively sequestering them outside the cell. The EPS layer also plays a significant role in biosorption. The complex carbohydrates

present in the EPS can bind metal ions through similar mechanisms, reducing their bioavailability in the surrounding environment (Vijayaraghavan and Yun 2008). This extracellular accumulation serves as a first line of defense, preventing the heavy metals from directly entering the cell and minimizing the need for energy-intensive intracellular uptake processes.

1.3. CELLULAR DETOXIFICATION MECHANISMS

I. Role of Cell Wall and Extracellular Polymeric Substances (EPS):

Algae and cyanobacteria possess cell walls that act as the first barrier against heavy metal influx. The composition of the cell wall varies considerably among different algal and cyanobacterial species (Woitzik et al. 1988; Popper et al. 2014; Spain and Funk 2022). For example, diatom cell walls are primarily composed of silica (SiO_2) frustules (Kröger and Poulsen 2008), while green algae often have cell walls rich in cellulose and hemicellulose (Domozych et al. 2012). These polysaccharides can contain functional groups like carboxyl, hydroxyl, sulphate, amino and phosphate, which can interact with metal ions through electrostatic interactions, chelation, or ion exchange (Okajima et al. 2008). Proteins embedded within the cell wall can also play a role in heavy metal binding. The specific composition and structure of the cell wall thus influence its affinity for different heavy metals and can determine the initial extent of metal ion interaction and potential uptake.

Extracellular Polymeric Substances (EPS) are complex secretions produced by algae and cyanobacteria that surround the cell wall and form a mucilaginous layer. This layer is composed of a variety of biopolymers, including carbohydrates (such as polysaccharides), proteins, nucleic acids, and lipids (Kawaguchi and Decho 2000; Ramirez-Mora et al. 2018). The specific composition of EPS can vary depending on the algal/cyanobacterial species and environmental conditions. However, carbohydrates are generally the most abundant component, and they play a significant role in heavy metal interactions (Jiao et al. 2010). The functional groups present on these carbohydrates, like carboxyl, hydroxyl, sulfate, and phosphate, can form complexes with metal ions through chelation, adsorption, or ion exchange (Oleńska et al. 2021). This EPS layer acts as a biosorption matrix, reducing the bioavailability of

free metal ions in the surrounding environment. By binding metals to its EPS, algae and cyanobacteria can limit their uptake and potential toxicity. Additionally, EPS can influence the speciation of heavy metals, affecting their mobility and transport in aquatic systems.

II. Role of Redox Transformations

Heavy metals can undergo redox transformations at the cell surface, altering their charge and potentially influencing their uptake. This process is mediated by enzymes on the cell surface cyanobacteria. For instance, some cyanobacteria can reduce toxic Cr(VI), the chromate ion, to the less toxic Cr(III), the chromic ion (Barakat 2011; Reddy et al. 2024). This reduction changes the chromium's oxidation state, making it less soluble and bioavailable. As a result, the chromium is less likely to be taken up by the cyanobacteria. Similarly, some microbes can oxidize As (III) to As (V), which is less toxic and more easily sequestered (Cavalca et al. 2013; Drewniak and Sklodowska 2013). These redox transformations are a crucial detoxification mechanism employed by algae and cyanobacteria to protect themselves from heavy metal exposure.

III. Intracellular Detoxification Strategies

Once heavy metals cross the initial barriers of the cell wall and membrane, algae and cyanobacteria face the challenge of minimizing their intracellular toxicity. They have evolved a sophisticated detoxification strategies to neutralize these threats.

a. Chelation with Ligands: A Molecular Cage

Chelation is an important detoxification strategy employed by algae and cyanobacteria. It involves the binding of heavy metal ions with specific organic molecules called ligands (Sears 2013; Chugh et al. 2022). These ligands act like molecular cages, sequestering the metal ion within their structure and reducing its interaction with vital cellular components. Common ligands used in this process include:

i. Glutathione: This low-molecular-weight thiol (sulfhydryl group-containing) peptide is ubiquitous in most living organisms and plays a vital role in

detoxification. In algae and cyanobacteria, glutathione can bind to various heavy metals, including Cu, Cd, Pb, and Hg (Burford et al. 2005; Rubino 2015). The thiol group on the glutathione molecule readily forms strong covalent bonds with the metal ion, effectively neutralizing its potential for cellular damage.

ii. Metallothioneins (MTs): These are small, cysteine-rich proteins with a high affinity for heavy metals. The cysteine residues in MTs contain thiol groups that form strong complexes with metal ions, effectively sequestering them (Carpenè et al. 2007; Ruttkay-Nedecky et al. 2013). MTs offer several advantages for detoxification (Amiard et al. 2006; Yu et al. 2019): (i) Their high affinity for heavy metals allows them to bind even low concentrations effectively; (ii) The cysteine residues can participate in redox reactions, potentially transforming the metal ion to a less toxic form; (iii) MTs can be localized in specific cellular compartments, further isolating the metals from sensitive cellular processes.

b. Compartmentalization: Cellular Segregation

Plant cell and certain algae can compartmentalize heavy metals within the cell, further minimizing their potential for disrupting cellular functions (De Caroli et al. 2020). This primarily involves sequestering the metals in vacuoles, which are membrane-bound sacs within the cytoplasm. These vacuoles act as storage compartments for various unwanted substances, including heavy metals. By transporting metals into vacuoles, plant cells can isolate them from the rest of the cell's essential machinery. This not only reduces the potential for direct interaction between the metal ions and sensitive cellular components but also allows for the accumulation of high metal concentrations within the vacuole without disrupting the overall cellular homeostasis. The transport process is mediated by specific transport proteins located in the vacuolar membrane (Etxeberria et al. 2012; Sharma et al. 2016). These proteins recognize and bind to metal ions or complexes containing metal ions, facilitating their translocation across the membrane and into the lumen (internal space) of the vacuole. The vacuolar membrane can also contain ATP-dependent pumps that actively transport metal ions against their

concentration gradient, ensuring efficient sequestration (Martinoia et al. 2000; Collins and Forgac 2020). Additionally, vacuoles may contain enzymes that can further modify or detoxify the sequestered metals (Nowicka 2022). This comprehensive compartmentalization strategy allows plant cell to effectively mitigate the threat posed by heavy metals.

c. Active Efflux Pumps: Pumping Out the Threat

Some algae and cyanobacteria possess active efflux pumps embedded in their cell membrane (Kato et al. 2015). These pumps are transmembrane proteins that utilize the energy derived from the hydrolysis of ATP to transport heavy metal ions out of the cytoplasm and across the cell membrane. This active transport process is crucial for eliminating excess metal ions that may have entered the cell inadvertently through passive diffusion or non-specific transporters. The specific type and efficiency of these efflux pumps can vary across different species. Some efflux pumps are specific for a particular metal ion (Hajiagha and Kafil 2023), while others can transport a wider range of metals (Hasani et al. 2019). Additionally, the expression and activity of these pumps can be influenced by various environmental factors, such as the concentration of the metal ion in the surrounding environment, pH, and nutrient availability (Blanco et al. 2016; Nové et al. 2020). Understanding the regulation of these efflux pumps is an important area of research, as it could provide insights into how algae and cyanobacteria adapt to different environmental metal burdens.

1.4. REMOVAL OF HEAVY METALS BY ALGAE AND CYANOBACTERIA AND REGENERATION

Heavy metal removal by algae or cyanobacteria can be carried out through two main mechanisms, i.e. bioaccumulation and biosorption. Bioaccumulation is a metabolically driven active process that requires living cells, whereas the biosorption is a passive process that can be performed by both dead or living cells (Bloch and Ghosh 2022; Pandey et al. 2022).

Biosorption is a main method for removing heavy metals from wastewater, including a variety of processes such as ion exchange, adsorption, surface

complexation, precipitation, and chelation (Volesky and Holan 1995; Kanamarlapudi et al. 2018). Metal ions can be rapidly sorbed to the surface of cyanobacteria in the first stage because their cell walls are generally rich in negatively charged groups that can serve as heavy metal binding sites. As a result, metal ions can be transferred into cells via active transporters and carriers, where they are converted into less harmful forms and stored in vacuoles (Cui et al. 2020; Nowicka 2022).

Biosorption has been considered as a more viable strategy for heavy metal removal from wastewater than bioaccumulation because it has faster kinetics and does not harm cells when heavy metal concentrations are high enough to be harmful (Yaashikaa et al. 2021). Another advantage of biosorption is the capacity to reuse the cells for several desorption and adsorption cycles, increasing shelf life and, as a result, economic value (Ciani and Adessi 2023). Various solutions may be employed during desorption, including strong acid or base, EDTA, and water, depending on the strength of the binding between metal ions and binding groups, as well as the mechanical and physical strength of the biosorbents.. (Chatterjee and Abraham, 2019; Agarwal et al., 2020; Satya et al., 2021). However, numerous parameters are known to influence the biosorption process, such as pH, temperature, biosorbent dosage, and pretreatment, which require attention to optimise adsorption capability (Al-Amin et al. 2021).

Algae and cyanobacteria biosorption is generally recognised as an effective, rapid, low-cost, and eco-friendly treatment method because to the huge surface-to-volume ratio, the strong anionic character of EPS, and the potential to renew, reuse, and simply recover the biosorbents (Singh et al. 2016; Agarwal et al. 2022).

1.4.1 Types of Biosorbent

A wide range of biomaterials available in nature has been employed as biosorbent for the desired pollutant removal. All kinds of microbial, plant and animal biomass and their derivative products, have received great interest in a variety of ways and in relation to a variety of substances (Volesky and Holan 1995). Various microorganisms, including bacteria, fungi, microalgae, and protozoa, have been studied for their potential in bioremediation of heavy metals. Certain bacterial that contribute in heavy metals removal include *Bacillus* sp., *Pseudomonas* sp, *Arthrobacter* sp, *Alcaligenes*

sp, *Azotobacter* sp, *Rhodococcus* sp, and methanogens (Girma 2015). Among those bacteria, *Bacillus* sp. is considered to be a most potential organism for removing various heavy metals, particularly Gram-positive bacteria (Alotaibi et al. 2021). Fungi such as *Auricularia polytricha*, *Flammulina velutipes* (Li et al. 2018) has been employed for removal of heavy metals. *Chlorococcum humicola* (Borah et al. 2020), *Scenedesmus almeriensisis* (Saavedra et al. 2018), *Phormidium ambiguum* (Shanab et al. 2012), *Cladophora glomerata* (Al-Homaidan et al. 2018), and *Chlorella vulgaris* (Saavedra et al. 2018) are some of the microalgae that has been utilized for the removal of heavy metals.

Various cyanobacteria species such as *Anabaena, Cyanobium, Nostoc, Cyanothece, Arthrospira, Microcystis , Synechocystis, Spirulina platenis* and *Leptolyngbya*, have shown effective results on Cu, Cd, Zn, Cr, Pb, Ni, Co or Hg removal (Zinicovscaia et al. 2015; Mota et al. 2015; Yadav et al. 2021; Bloch and Ghosh 2022; Pandey et al. 2022). Furthermore, the use of consortia of several cyanobacteria species or microalgae and other microorganisms might potentially aid to achieve improved metal tolerance and increased metabolite synthesis, favourably contributing to metal removal. (Anand et al. 2023).

Besides from the aforementioned natural biosorbents, the following biomaterials have garnered significant attention in the literature: rice husk (Chuah et al. 2005), coconut shell (Pino et al. 2006), plant barks (Ighalo and Adeniyi 2020), leaves (Dey et al. 2023), sawdust (Meez et al. 2021), sugarcane bagasse (Raj et al. 2022), and peat moss (Brown et al. 2000).

EPS derived from various organisms such as bacteria (Tsuneda et al. 2003; Marvasi et al. 2010; Costa et al. 2018; Angelin and Kavitha 2020), cyanobacteria and microalgae (Parikh and Madamwar 2006; Boonchai et al. 2015; Xiao and Zheng 2016; Babiak and Krzemińska 2021), yeasts (Rahbar Saadat et al. 2021; Hamidi et al. 2023), fungi (Osińska-Jaroszuk et al. 2015; Op De Beeck et al. 2021; Breitenbach et al. 2022), and protists (Jain et al. 2005; Lee Chang et al. 2014). EPS plays an important role in metal sequestration because it contains negatively charged groups such as sulphate, phosphate, carboxyl, and hydroxyl, which can function as chelating agents for positively charged heavy metals (De Philippis et al. 2011; Oleńska et al. 2021). It has been widely demonstrated using molecular and biophysical approaches such as

mutagenesis, X-ray spectroscopy, Fourier transformed infrared spectroscopy (FTIR), and scanning or transmission electron microscopy (Kawaguchi and Decho 2000).

1.4.2 Biosorption by Live and Dead Cells

The biosorption process can occur in either living or dead cells. However, dead biomass is more often employed since it offers several advantages than living algae cells. Indeed, dead cells require no nutrition or special environmental conditions and may be employed with a wide variety of experimental variables (temperature, pH, and so on). Dead biomass may readily be kept for extended periods of time without losing efficacy (Huang et al. 2013; Hasyimah et al. 2021). Unlike non-living material, live algae cells may bioaccumulate heavy metals. This has a significant impact on their metabolism and is often very poisonous to the cells (Leong and Chang 2020).

Furthermore, since enzymatic activity is sustained in live cells, enzymes may modify the pollutant through biotransformation or biodegradation, making pollutant recovery more challenging (Torres 2020). Other often stated benefits of employing dead biomass over living cells include the ability to renew and reuse the biomass, simple immobilisation of the dead cells, and easier mathematical modelling of the kinetics (Chu and Phang 2019). Finally, and most crucially, dead microalgal cells have been shown to absorb heavy metals more efficiently than living cells (Aksu and Kutsal 1990). Sibi (2014) demonstrated that the biosorption rate of As(III) by several types of microalgae was much greater when dead biomass was used rather than active cells.

1.4.3 Cell Wall Components

Algae and cyanobacteria's cell walls are mostly made up of carbohydrates, proteins, and lipids, all of which have negatively charged functional groups on their surfaces. These groups can capture and hence remove metal ions from their surroundings through counter-ion interactions, making the cell wall the primary participant in heavy metal removal (Pradhan et al. 2022).

Cell walls are classified based on the layers that make up their structure. Three unique conformations have been identified: the cell wall can be made up of a single microfibrillar layer or both an inner and exterior layer. Depending on the species, the

outer layer can have one of two structures: a mono-electron-dense layer or three sub-layers, the latter of which typically contains algaenan (Hoiczyk and Hansel 2000). The outermost layer of the *Chlorella* trilaminar layer is made up of sporopollenin, the middle layer of mannose and chitin-like polysaccharides, and the innermost layer of a phospholipid bilayer (Dixon and Wilken 2018). The biochemical makeup of microalgal cell walls varies substantially not only across genera but also between strains, and it is not consistently comparable to higher plants, where carbohydrates are always and by far the most important component of the cell wall (Siegel and Siegel 1973).

The functional groups on the outer layer of the algal cell wall interact with the surrounding environment and can serve as binding sites for positively charged metal ions that interact with negatively charged groups on the cell wall surface. Understanding processes like biosorption requires understanding of their characteristics. Biosorption is the fast and reversible binding of ions from aqueous solutions to functional groups present on the surface of (Spain et al. 2021).

1.4.4 Biosorption Mechanism

Heavy metals are absorbed by the biosorbent through a variety of ways, various studies propose different mechanisms dependent on the kind of biosorbent and categorization criteria. Furthermore, most processes are not completely known due to complexities in chemical composition of biosorbents. The processes are either defined according to (a) their dependency on cell metabolism or (b) the site within the cell where the metal is accumulated, which is separated into three types: extracellular accumulation/precipitation, cell surface sorption/precipitation, and intracellular accumulation (Aquino et al. 2011).

Cell metabolism-dependent biosorption or bioaccumulation involves transport across the cell membrane and precipitation, whereas cell metabolism-independent biosorption involves precipitation, physical adsorption, ion exchange, and complexation (Javanbakht et al. 2014; Priya et al. 2022).

Physical adsorption

Physical adsorption occurs on the surface of biosorbent, may be with the cell walls when dealing with microorganisms, and is facilitated by electrostatic interactions such as van der Waals forces. The surface area of the biosorbent, as well as the pH of the solution, influence the physical adsorption mechanism. (Raji et al. 2023).

Ion exchange

The ion exchange mechanism involves replacing an ion bonded to the solid phase that is easily exchanged with another ion in solution. Considering the biosorption in microorganisms such as bacteria and fungi, it has been discovered that *Gandoderma lucidium* biosorbs copper ions by ion exchange mechanism, this is possible in microorganisms due to the composition of their cell walls, which have polysaccharides that can ion exchange with their counter ions (Chang et al. 2020). *Spirulina*, a cyanobacteria, was capable of biosorbing chromium(III), cadmium(II), and copper(II) by ion exchange through identified functional groups including carboxyl, phosphate, and hydroxyl groups (Kanamarlapudi et al. 2018).

Complexation

Complexation is the process of forming complexes by electrostatic attraction or covalent bonding between metal ions and organic molecules that act as electron donors. Chelation is a more complicated sort of complexation in which the organic ligand forms coordination bonds with the metal ion from many places at the same time, resulting in a more stable complex. (Nickisch et al. 2023). The affinity of metal ions and organic ligands which is the most significant factor in complexation is based on the Hard and soft acids and bases (HSAB) theory, which implies that elements are classified into hard or soft acids (mainly metals) and hard or soft bases (mainly nonmetals), hard acids have stronger affinity to hard bases, and so the weak acids and bases (Lawson et al. 1984; Melnikov et al. 2020). .

Precipitation

Precipitation is the generation of insoluble metal in the form of precipitate, which is one of the few processes involved in metabolism-dependent biosorption; however,

precipitation may also be used for metabolism-independent biosorption. In metabolism-dependent biosorption, precipitation occurs as a reaction by the microorganisms' active defence mechanism in the presence of an environment containing hazardous metal ions (Benalia et al. 2022). In metabolism-independent biosorption, precipitation occurs because of chemical interactions between the functional groups of the cell wall of the biosorbent and the metal ion; the processes could involve oxidation-reduction reactions (Abid et al. 2011).

Transport across cell membrane

Heavy metal ion transport across cell membranes is mostly found in microorganisms. This mechanism consists of two stages: in the first stage, the metal ion binds to binding sites on the microorganism's cell wall, which is referred to as independent binding metabolism, and in the second stage, the metal ion is transported across the cell membrane into the cell, which is referred to as metabolism dependent intracellular uptake (Foulkes 2000). The mechanism replicates the process of absorption of vital ions by the cell; it has been suggested that cellular metal transport systems are misled by heavy metal ions with the same ionic radius and charge as the essential metal ions; nevertheless, the process is not yet well understood (Kerkhove et al. 2013).

1.4.5 Factors Affecting Biosorption

Various different factors can contribute in controlling the mechanisms that include chemical, stereochemical and coordination characteristics of the metal of interest which involves the ion mass, ionic radius and the oxidation state of the metal ion (Kanamarlapudi et al. 2018). The number of reactive binding sites, accessibility and availability of binding sites, type of binding site, and affinity between the biosorbent's binding site and the metal ion of interest all have an impact on the biosorption mechanism (Shamim 2018; Salam 2019). Other parameters that influence biosorption include pH, temperature, and the complexity of the solution containing the metal ion (Kanamarlapudi et al. 2018). In certain circumstances, many mechanisms may occur in a multi-step process. For example, the biosorption of uranium by Aloe vera waste

comprised physical adsorption, ion exchange, complexation, and precipitation (Ali Redha 2020).

The surface area of the biosorbent material also affects its biosorption ability, a larger surface area would boost biosorption under same circumstances. A research evaluated the biosorption of lead, copper, and zinc ions by (a) dried lettuce leaves and (b) powdered lettuce leaves (in dry form). Under all circumstances, powdered lettuce leaves removed more metal than dried ones (Shartooh et al. 2014). .

The presence of more than one metal ion in the same media might affect the removal of one metal ion on another, since one metal ion may have stronger affinity to the binding sites of the biosorbent, resulting in competition for the availability of binding sites (Morales-Barrera et al. 2020).

1.4.6 Kinetics of Biosorption

There are two distinct kinetic models, pseudo-first and pseudo-second order, that are used to describe biosorption under nonequilibrium conditions. The equations contain the first and second order constants, k_1 (min^{-1}) and k_2 ($g\,mg^{-1}\,min^{-1}$), as well as the quantity of heavy metal adsorbed q_t at time (t) and the maximum amount of heavy metal adsorbed q_e at equilibrium. The huge number of chemical groups within the algal cell wall allows for a wide range of interactions. The pseudo-first order equation given by Lagergren (Tseng et al. 2010) describes biosorption in the liquid phase. It discusses the relationship between solid capacity and the adsorption of liquid solid systems. As a result, the various microalgal surfaces will have an effect on the kinetics and parameters.

The pseudo-second order kinetic was proposed by Blanchard et al. (Plazinski et al. 2013) and has been developed further (Ho 2000). Like the pseudo-first-order equation, it is heavily dependent on solid capacity, but the presence of two surface sites is required for the theory to work. The pseudo second order equation also involves adsorption on the surface inside the first phase and the inclusion of the second phase (Bullen et al. 2021).

Both equations are often used in tandem to explain the kinetics of biosorption. Based on the data, these equations have slightly different regression (r^2) values.

Because many of these models are based on empirical data, the kinetic constants will vary and must be calculated by study-specific curve fitting. Despite being one of the most feasible techniques, nonlinear regression frequently replaces linear regression because it permits the use of multiple error functions for the best possible predictions. (Wang and Guo 2020; Hegazy et al. 2023).

The Intraparticle Diffusion Model is another important kinetic model that describes the rate-limiting step in the adsorption process, which is frequently the intraparticle diffusion of adsorbate molecules within biosorbent particles (Das et al. 2014). This model sheds light on the function of intraparticle diffusion in regulating the overall adsorption kinetics. The model assumes that the rate-limiting stage in the adsorption process is the diffusion of adsorbate molecules within biosorbent particles. Intraparticle diffusion is the migration of adsorbate molecules from the bulk solution into the interior of biosorbent particles. The model takes into consideration the boundary layer or film diffusion, which happens when mass transfers between the bulk solution and the biosorbent particles' surfaces (Wu et al. 2009; Wang and Guo 2022).

1.4.7 Biosorption Isotherm

Heavy metal biosorption isotherms can utilized various models, each with a different number of dependent factors (Chen et al. 2022). These models may explain the amount of metal ions adsorbed at equilibrium (q_e mg g^{-1}) corresponding to their concentration in the solution (C_e mg L^{-1}). Langmuir and Freundlich equations are two main parameter isotherm models that are often used to estimate heavy metal adsorption on algal surfaces (Raji et al. 2023).

The Langmuir empirical model for gas adsorption on a monolayer surface was created over 100 years ago (Langmuir 1918). The Langmuir model describes the equilibrium adsorption of molecules on a surface with a finite number of identical binding sites. It is assumed that adsorption occurs in a single layer on the surface of the adsorbent material, with no interaction between the adsorbed molecules. The model assumes that the adsorbent's surface is uniform and homogeneous, with all binding sites having identical energies. According to the Langmuir model, once a

molecule has occupied a binding site, no more adsorption may occur (Swenson and Stadie 2019).

The Freundlich Isotherm (Freundlich 1907) model is another important equation used to describe the adsorption of molecules onto a surface, especially in biosorption processes involving pollutants and biological materials. Unlike the Langmuir model, the Freundlich model depicts multilayer adsorption, which occurs when adsorbate molecules form multiple layers on the adsorbent's surface. The model considers a heterogeneous surface with varying adsorption energies and surface locations, allowing for non-uniform adsorption behaviour. Adsorption is considered to have an exponential connection between the concentration of the adsorbate in solution and the amount adsorbed on the surface. The Freundlich model applies to non-ideal adsorption systems in which the adsorbate-adsorbent interactions are not specifically monolayer and uniform (Vigdorowitsch et al. 2021; Kalam et al. 2021).

The given models may be used to characterise the interaction of heavy metal ions with the microalgal surface, as well as to make inferences about the quantities of heavy metals that are adsorbed. Several alternative isotherm models (e.g., Dubinin-Radushkevich, Temkin, Flory-Huggins, Hill, Elovich, Sips, Redlich Peterson, etc.) concentrate on other characteristics, such as the adsorption of aromatics by activated carbon or the structure of the adsorbent (A.O 2012; Tzabar and Ter Brake 2016; Ayawei et al. 2017; Hu and Zhang 2019; Chu et al. 2023).

1.4.8 Desorption or Regeneration of Biosorbent

If the biosorption process is employed as an alternative to wastewater treatment, the regeneration of the biosorbent may be critical for lowering process costs and opening up the prospect of recovering metals removed from liquid phase. For this, it is preferable to desorb the sorbed metals and renew the biosorbent material for a subsequent application cycle. The desorption process should produce concentrated metals, return the biosorbent to near to its original condition for successful reuse, with no reduction in metal absorption and no physical changes or damage to the biosorbent (Park et al. 2010; Bayuo et al. 2020).

While the biosorbent can be regenerated by washing it with a suitable solution, the type and strength of this solution are determined by the amount to which the deposited metal is bound. Dilute solutions of mineral acids, such as hydrochloric, sulphuric, acetic, and nitric acid, can be employed for metal desorption from biomass (Pagnanelli et al. 2002; Sudha Bai and Abraham 2003).

Desorbing agents are typically classified into three types: acids (hydrochloric acid, sulphuric acid, nitric acid, and acetic acid), alkalis (sodium hydroxide, sodium hydrogen carbonate, sodium carbonate, and potassium hydroxide), and chelating agents (ethylenediaminetetraacetic acid) (Lata et al. 2015). In terms of speed and desorption %, acidic desorbing agents outperformed basic and neutral agents. A suitable desorbing agent should not change the chemical or physical characteristics of the biosorbent (Patel 2021).

Deionized water (DI water) is utilised in desorption, a step in capacitive deionization (CDI) systems when electrodes are regenerated. In CDI, a potential difference is provided between electrodes to adsorb ions from water during adsorption, and the electrodes are regenerated during desorption. DI water has a higher stripping capacity than other kinds of water, which helps improve desorption (Al-Juboori et al. 2022; Li et al. 2024). Deionized water contains no trace of ions and pollutants; thus, it does not introduce new contaminants during the desorption process. This is critical for ensuring the desorbed substances' integrity and purity.

1.5. HEAVY METAL-INDUCED OXIDATIVE STRESS AND TOLERANCE MECHANISMS IN ALGAE AND CYANOBACTERIA

In response to heavy metals, algae or cyanobacteria produce a variety of antioxidants, including superoxide dismutase, catalase, glutathione peroxidase, and ascorbate peroxidase, as well as low molecular weight molecules like carotenoids and glutathione. High, or acute, quantities of metal pollution induce harm to algal cells because ROS (reactive oxygen species) levels surpass the cell's ability to cope. At lower or chronic levels, algae collect heavy metals and can transfer them on to creatures at other trophic levels such as molluscs, crustaceans, and fishes (Pinto et al. 2003; Cassier-Chauvat and Chauvat 2014).

ROS generation in response to heavy metal stress

Aerobic organisms produce a variety of ROS, such as superoxide anion (O_2^-), hydrogen peroxide (H_2O_2), singlet oxygen ($^1O_2^-$), and hydroxyl radical (OH^-) (Juan et al. 2021). These substances are natural byproducts of oxidative metabolism and constitute an ongoing hazard to all aerobic organisms. Although some of them may work as key signalling molecules, altering gene expression and modulating the activity of certain defence proteins, all ROS may be exceedingly toxic to organisms at large doses (Sharma et al. 2012; Xie et al. 2021). ROS may oxidise proteins, lipids, and nucleic acids, causing cell structural changes and mutations (Halliwell 2006; Juan et al. 2021). Many environmental factors can cause oxidative stress in cells by producing $O2^-$. Thus, modulating antioxidant levels is a key adaptive response to enduring unfavourable environments. Indeed, maintaining a high antioxidant capacity in cells has been associated to enhanced resistance to several types of environmental stress (Xie et al. 2019).

ROS are constantly generated as byproducts of several metabolic processes that are localised in distinct cellular compartments such as chloroplasts, mitochondria, and peroxisomes. (Mandal et al. 2011). Photosynthesis occurs in chloroplasts of algae and higher plants, which feature a highly organised thylakoid membrane system that includes all components of the light-capturing photosynthetic apparatus and offers all structural qualities for effective light harvesting. During photosynthesis, O_2 is produced in the chloroplasts and can receive electrons flowing through the photosystems, resulting in the formation of superoxide radicals (O_2^-). Normally, electron flow in the PSI is directed to NADP+ from the activated photosystem, which is then reduced into NADPH. Then it enters the Calvin cycle, reducing the terminal electron acceptor CO_2. However, when ETC is overloaded (due to different stressors), a portion of the electron flow from ferredoxin is redirected to O_2, which is then reduced to superoxide via the Mehler reaction. PSII additionally supplies electron transfer sites (QA, QB) for O_2 (Kozuleva et al. 2020; Foyer and Hanke 2022).

Finally, the chloroplast contains CuZn-SOD, which converts superoxide into H2O2. As a result, triplet chl, ETC in PSI and PSII make the chloroplast a primary

source of ROS generation. In darkness, mitochondria appear to be the primary ROS generators. It is believed that 1-5% of the O_2 consumed by isolated mitochondria results in ROS generation (Pilon et al. 2011). In mitochondria, complex I, II, and ubiquinone of the electron transport chain (ETC) are the primary sites for O_2^- production. Furthermore, SOD reduces it to superoxide. In the presence of appropriate transition metals, particularly Fe, O_2 converts superoxide and hydrogen peroxide to OH at neutral pH and ambient temperature-driven Fenton reaction (Asada 2006).

Cellular defense mechanisms against ROS

Organisms have evolved a diverse set of defensive mechanisms to eliminate ROS before they may harm sensitive areas of the cellular machinery. These are classified as low molecular weight molecules such as GSH, phenolics, ascorbate, flavonoids, tocopherols, and carotenoids, as well as high molecular weight enzymatic catalysts.

Superoxide dismutase (SOD)

Superoxide dismutase (SOD) is a metalloprotein that catalyses the dismutation of superoxide radicals into hydrogen peroxide and molecular oxygen (Sheng et al. 2014). It serves as the first line of defence against ROS, which are formed in various organelles such as chloroplasts, mitochondria, and peroximes. It is the most efficient intracellular enzymatic antioxidant in all aerobic species and subcellular compartments susceptible to ROS-mediated oxidative damage. It eliminates superoxide radical ($O2^-$), lowering the danger of the most effective OH^- through a metal-catalyzed Haber-Weiss type reaction (Wang et al. 2018; Fujii et al. 2022).

The enzyme activity of SOD has been observed to increase in response to numerous environmental factors, indicating a defence mechanism. Choudhary et al. (2007) investigated the effect of heavy metals (Pb, Cu, and Zn) on *Spirulina platensis* and discovered increased SOD activity with increasing metal concentration, indicating the presence of a ROS scavenging mechanism ($O2^-$) and improving *Spirulina platensis* resistance. SOD activity was also elevated in the nitrogen-fixing Cyanobacterium *Anabaena variabilis* in the presence of metals (Aftab and Ahmad 2013).

Catalase (CAT)

Catalase (CAT) is a very important antioxidant enzyme and it is found in nearly all aerobic organisms. Catalase degrades two hydrogen peroxide molecules into one molecule of oxygen and two molecules of water in a two-step process (Yuzugullu Karakus 2020). The chemical pathway begins with the reduction of one hydrogen peroxide molecule, resulting in the creation of a spectroscopically distinctive intermediate compound I, a covalent oxyferryl species (FeIVO) with a porphyrin π-cation radical. In the second step process, component I is reduced by redox reactions with a two-electron transfer from an electron donor (the second molecule of hydrogen peroxide) to create free enzyme, oxygen, and water (Heck et al. 2010; Napolitano et al. 2021) .

It is produced in peroxisomes by oxidases engaged in β-oxidation of fatty acids, photorespiration, and purine catabolism. When cells are under energy stress, they rapidly produce H_2O_2 through catabolic mechanisms. Then, catalase offers an energy-efficient method for degrading H_2O_2. Thus, Catalase eliminates H_2O_2 without utilising cellular reducing equivalents, such as NADPH (Kirkman et al. 1999; Lismont et al. 2019).

Ascorbate Peroxidase (APX) and Glutathione reductase (GR)

Ascorbate peroxidase and glutathione reductase are the key enzyme antioxidants of the Ascorbate-Glutathione cycle, commonly known as the Halliwell-Asada pathway. The ascorbate-glutathione cycle includes the oxidation and reduction of ascorbate, glutathione, and NADPH by the enzymes APX, GR, and dehydroascorbate reductase. APX and GR are critical in the detoxification of ROS produced in a subcellular compartment of higher plants, algae, and other organisms (Foyer and Noctor 2011; Hasanuzzaman et al. 2019).

APX is a heme-containing protein that converts H_2O_2 to H_2O in the chloroplast through O_2^- dismutation. To avoid inhibition of calvin cycle enzymes, H_2O_2 must be decomposed in chloroplasts (Caccamo et al. 2023). APX degrade H_2O_2 into H_2O molecules by utilising ascorbate as an electron donor and oxidising it to monodehydroascorbate (MDHA). MDHA can spontaneously dismutase into

dehydroascorbate (DHA). Dehydroascorbate reductase regenerates ascorbate by converting NAD(P)H into reducing equivalents. Ascorbate regeneration occurs through the oxidation of GSH (reduced glutathione) to GSSG (oxidised glutathione). Finally, GR regenerates GSH from GSSG, utilising NADPH as a reducing equivalent (Karyotou and Donaldson 2005; Zhang et al. 2023).

Glutathione reductase (GR) is a flavoprotein oxidoreductase present in both eukaryotic and prokaryotic cells. It is mostly present in chloroplasts, although a small amount has also been discovered in mitochondria and the cytosol. It is an essential enzyme in the ascorbate-glutathione cycle that maintains the Glutathione (GSH) pool, which is particularly important for many metabolic regulatory and antioxidative activities in plants. Glutathione peroxidase, like Ascorbate peroxidase, decomposes H_2O_2 to H_2O by directly reducing it with GSH (Bashir et al. 2007; Harshavardhan et al. 2017). GR expression is elevated during stress such as changes in salinity, drought, high light intensity, mechanical wounding, cold, and exposure to heavy metals (Romero-Puertas et al. 2006).

1.5. BASIS FOR RESEARCH EXPLORATION

Recent interest has turned towards harnessing the potential of biological materials, such as plants and microorganisms, and their byproducts, for heavy metal removal (Nnaji et al. 2023). Of particular interest are native biomass and (EPS) derived from microorganisms, which have demonstrated promising capabilities as effective sorbents for a wide range of heavy metals (Sudhakar et al. 2020; Yadav et al. 2020; Zeng et al. 2022).

In comparison to conventional heavy metal removal methods, cyanobacteria-mediated heavy metal removal shows promise as a cost-effective, in vitro operable, and environmentally friendly approach. Cyanobacteria, such as *M. aeruginosa* and *A. doliolum* predominantly harness EPS for the biosorption of metal ions due to the prevalence of negatively charged functional groups within their structure. This distinctive attribute renders them highly promising chelating agents, particularly well-suited for targeting and removing positively charged heavy metal ions from aqueous solutions (De Philippis 1998; Al-Amin et al. 2021).

Extensive research investigations have elucidated the efficacy of EPS derived from diverse microorganisms, encompassing cyanobacteria and bacteria, in their capacity to adsorb and subsequently eliminate heavy metal contaminants from aqueous solutions (Pal and Paul 2008; Gupta and Diwan 2017; Concórdio-Reis et al. 2020). Microbial EPS contain a variety of functional groups that contribute to their metal-binding capacity. Commonly identified functional groups within EPS include carboxyl, phosphate, amine, sulfhydryl and hydroxyl groups (Huang et al. 2022). These functional groups serve as binding sites for heavy metal ions, forming coordination complexes through chemical interactions such as ion exchange, chelation, and electrostatic interactions.

M. aeruginosa and *A. doliolum*, a commonly occurring and bloom forming cyanobacterium, exhibits substantial EPS production and metal-binding properties (Pradhan et al. 2007). While previous studies have explored the metal-binding potential of EPS derived from various bacterial and cyanobacterial species, limited research has been specifically conducted on the EPS of *M. aeruginosa* and *A. doliolum* (De Philippis 1998; Gupta and Diwan 2017). Therefore, further investigation is needed to explore the sorption and removal efficiency of cadmium, copper and nickel using native biomass and EPS derived from these cyanobacteria in aqueous solutions. This study aims to comprehensively investigate the sorption and removal of cadmium, copper and nickel using native biomass and EPS derived from *M. aeruginosa* and *A. doliolum* in aqueous solutions. The underlying research hypothesis postulates that the EPS derived from both cyanobacteria will demonstrate a notable affinity towards cadmium, copper and nickel, consequently leading to the proficient extraction of these metals from the aqueous phase. The proposed mechanisms of sorption encompass the coordination of metal ions with the functional groups inherent to the EPS structure, alongside electrostatic interactions and complexation processes (Duan et al. 2020).

1.5. OBJECTIVES OF THE RESEARCH

i) Identification and quantification of cell surface associated proteins, sugars, amino acids and other metal binding ligands and functional groups in the test cyanobacterium.

ii) To estimate the densities of the proton binding site in the intact cell and isolated sheath.

iii) To study the kinetics and mechanisms of metal binding on to intact cyanobacterial cell and isolated sheath.

iv) To study the defence mechanism against heavy metal toxicity on live cells of cyanobacteria.

CHAPTER 2

MATERIAL AND METHODS

SECTION I. BIOSORPTION EXPERIMENTS

2.1. Organism and Growth Condition

The freshwater cyanobacterium, *Anabaena doliolum* and *Microcystis aeruginosa* were selected for the present study. In this study the cyanobacteria samples were collected from a paddy field located in Aizawl, Mizoram, India. To ensure purity, the collected sample underwent a purification process using the agar-plating method. Subsequently, the purified cyanobacterial strains were cultured and maintained in CHU-10 growth medium (Table 1.1). The pH of the growth medium was carefully maintained at 7.2 ± 0.2 to create an optimal environment for the growth and development of the cyanobacteria culture.

Table 2.1.1 Composition of Chu-10 Medium for Cyanobacteria Culture:

Macronutrients	g L^{-1}	Micronutrients	g L^{-1}
KNO_3	0.04	$MnCl_2.4H_2O$	0.5
K_2HPO_4	0.01	$Na_2MoO_4.2H_2O$	0.01
$MgSO_4.7H_2O$	0.04	H_3BO_3	0.5
Na_2SiO_3	0.02	$CuSO_4.5H_2O$	0.02
Ferric citrate	0.003	$CoCl_2$	0.04
Citric acid	0.003	$ZnSO_4$	0.05

The culture was subjected to a controlled light-dark photoperiod of 10-14 h, simulating natural day-night cycles, within a specially designed culture room equipped with air conditioning. The culture room was maintained at a temperature range of 30-35°C, as it is conducive to the optimal growth of Cyanobacteria. These culture conditions were

implemented to provide the ideal growth conditions for Cyanobacteria and ensure the reliability and consistency of the experimental results obtained in this study.

2.2. Chemical and Reagents

All the chemicals used in the studies were analytical grade from Merck, India. Milli-Q ultrapure water was used throughout the investigation. Heavy metals (Copper, Cadmium and Nickel) were selected for this study and stock solutions of 1000 mg L^{-1} concentrations were prepared by dissolving copper chloride ($CuCl_2$), cadmium chloride ($CdCl_2.H_2O$) and nickel chloride ($NiCl_2.6H_2O$) in Milli-Q water.

2.3. Extrapolymeric Substances (EPS) production

To induce EPS production in cyanobacteria, a 250 mL aliquot of sterilized Chu-10 medium is added to a sterilized 1.0 L Erlenmeyer flask. Following aseptic transfer, 50 mL of prepared cyanobacterial culture inoculum is introduced into the flask containing the growth medium. The contents are then gently hand-shaken to ensure proper mixing and aeration. This inoculated flask is subsequently placed in an incubator set at the optimal temperature for the specific cyanobacterial species, mimicking the light conditions described earlier (refer to "Culture of cyanobacteria for both species" section). To maintain culture homogeneity and prevent settling, the flask is shaken twice daily using a shaker. The culture is then allowed to grow and produce EPS under these controlled conditions for a period of 30 days, although this duration may require optimization depending on the chosen species and desired EPS yield.

2.4. Extraction of EPS

This section describes the extraction of EPS from cyanobacterial cultures with minor modifications to the method established by Parikh and Madamwar (2006).

The process involves following steps:

i. *Cell Separation:* The cyanobacterial culture supernatant containing EPS is first separated from the cells. This is achieved by centrifugation at 15,000 g for 40

min at 15°C. After centrifugation, the cell pellet is discarded, and the supernatant containing the EPS is retained.

ii. *Volume Reduction:* The collected supernatant is then concentrated to reduce its volume by approximately 75%. This is accomplished by heating the supernatant on a magnetic stirrer at 60°C for 10-12 h. The evaporation process concentrates the EPS present in the solution.

iii. *EPS Precipitation:* Cold acetone, equal in volume to the concentrated supernatant, is added to induce EPS precipitation. The mixture is kept at 4°C overnight, allowing the EPS to precipitate out of solution.

iv. *Purification by Re-dissolution and Precipitation:* The precipitated EPS is resuspended in Milli-Q water. This re-dissolution step helps remove any non-EPS contaminants. The precipitation with cold acetone is then repeated at least twice to further purify the EPS. Each re-dissolution and re-precipitation cycle enhances the purity of the extracted EPS.

v. *Dialysis:* Following the final precipitation, the crude EPS is further purified by dialysis against Milli-Q water for 20 h at 4°C. Dialysis removes any remaining low molecular weight contaminants present in the EPS solution.

vi. *Freeze-drying:* Finally, the dialyzed EPS solution is subjected to freeze-drying. This process removes the water content, resulting in concentrated, powdered EPS for further analysis or storage.

2.5. Chemical Analysis of Cyanobacterial Biomass and EPS

This section details the chemical analysis methods employed to quantify various components of the cyanobacterial biomass and extracted EPS.

Preparation of sample solution

i. The 100 mg of dry biomass was weight and dissolved in 100 mL Milli Q water making the concentration 1mg mL^{-1}.
ii. Similarly, 100 mg of EPS were taken and dissolved in 100 Milli Q water making the concentration 1 mg mL^{-1}.

2.5.1 Total Saccharide Content

The Anthrone method (Yemm and Willis, 1954) was employed to estimate the total carbohydrate content within the cyanobacterial cultures. Glucose served as the standard for carbohydrate quantification.

Procedure:

i. A 0.2 mL aliquot of cyanobacterial culture was dispensed into test tubes. The volume was then adjusted to 1 mL using ultrapure water (Milli-Q water).

ii. Five milliliters of 0.2% Anthrone reagent prepared in concentrated sulfuric acid (H_2SO_4) was added to each tube, followed by thorough mixing using a vortex mixer.

iii. After cooling the tubes, the mixtures were incubated in a water bath at 90°C (boiling water) for 10 min.

iv. Following incubation, the tubes were cooled to room temperature, and the absorbance was measured spectrophotometrically at 620 nm against a blank.

v. The total carbohydrate content was estimated using the previously generated standard curve prepared with glucose.

2.5.2 Total Protein Content

The protein content of both *M. aeruginosa* and *A. doliolum* cultures was quantified using Lowry's method (Lowry et al., 1951). Bovine Serum Albumin (BSA) served as the standard for calibration.

Procedure:

i. A 0.2 mL aliquot of cyanobacterial culture was added to test tubes, followed by volume adjustment to 1 mL with distilled water.

ii. 5 mL of alkaline copper solution (prepared with 2% sodium carbonate in 0.1 N NaOH, 0.5% $CuSO_4 \cdot 5H_2O$, and 1% potassium sodium tartrate) was added to each tube.

iii. The mixture was incubated for 10 min at 60°C in a water bath.

iv. After incubation, 0.5 mL of 0.1 N Folin-Ciocalteu reagent was added, and the tubes were incubated in the dark for 30 min at room temperature.

v. Following incubation, the developed dark blue color was measured spectrophotometrically at 660 nm absorbance against a blank.

vi. Protein content was determined quantitatively using the previously generated standard protein calibration curve.

2.5.3 Total Amino Acid Content

The amino acid content of both *M. aeruginosa* and *A. doliolum* biomass, and their extracted EPS was quantified by using Ninhydrin method (Ilyas et al. 2020). Leucine was served as the standard for calibration.

Principle

Ninhydrin is a powerful oxidizing agent that decarboxylates the alpha amino acids and yields an intense bluish purple colour which is measured colorimetrically at 570 nm.

Materials

a. Cyanobacteria biomass and EPS solution
b. 8% Ninhydrin reagent
c. 50% ethanol
d. Distilled water

Reagent preparation

a. Ninhydrin reagent (8%)
   4 g of Ninhydrin was dissolved in 50 mL of distilled water.

b. Lecine standard solution

50 mg of Leucine was dissolved in 50 mL of distilled water in volumetric flask.

Procedure:

i. 0.1 ml-1.0 mL of standard amino was pipette out to the test tubes and the volume was adjusted to 4 mL by adding distilled water for standard solution.
ii. For unknown concentration of sample, 0.2 mL of biomass sample and EPS solution was taken in the test tube and similarly, volume was adjusted to 4 mL by distilled water.
iii. 4 mL of distilled was added to the test tube which was used as a blank.
iv. Then 1 mL of Ninhydrin reagent was added to all the test tubes including blank and unknown concentration.
v. Mixed the solution properly by using the vortex mixture.
vi. After covering the mouth of test tube, they were place in the boiling water bath for 15 min.
vii. Then the test tube was kept in the cold water and 1 mL of ethanol was added to each test tube and shaken properly.
viii. The absorbance was recorded at 570 nm in colorimeter.
ix. The amino acid content was quantitatively determined by using the standard protein calibration curve generated.

2.6. Scanning Electron Microscopy (SEM) Imaging

SEM is another effective imaging technique for studying the surface morphology and topography of materials at high resolution. SEM works by scanning a concentrated electron beam across the surface of a specimen and detecting the numerous signals produced by the electron beam's interaction with the material.

Sample preparation

100 mL of *M. aeruginosa* and *A. doliolum* culture was taken in a separate flask, two of which were centrifuge at 6000 g then the supernatant was discarded and the biomass

was dry freeze to obtained powder form of biomass. The other two flask of culture was centrifuged at 15000 g for 40 min at 15°C and the supernatant was further process for EPS extraction as described in section 2.13.

Sample loading

The powder biomass and EPS were subjected to SEM (JSM 6390LV, Tezpur University) to obtained micrograph image of the biomass and EPS.

2.7. Energy Dispersive X-ray (EDX) Spectroscopy

EDAX is an analytical method widely used in combination with scanning electron microscopy (SEM) to determine the elemental composition of materials. The primary premise of EDX is the production of X-rays from a specimen using an electron beam. X-rays are created based on the properties and nature of the elements in the sample.

Sample loading

The powder biomass and EPS obtained for both heavy metals treated and untreated onto *M. aeruginosa* and *A. doliolum* were further subjected to EDX for compound analysis. The sample were evaporated with carbon fiber or rod (carbon coating) and the thickness of the film was kept between 5-20 nm.

2.8. Transmission Electron Microscopy (TEM)

TEM is an effective technology for visualised the interior structure of materials at very high resolution, down to the atomic level. The primary principle of TEM is to record a photographic picture of the electron flux after it passes through a tiny sample of the specimen being studied.

Sample preparation

The 100 mL culture of *M. aeruginosa* and *A. doliolum* was taken in a different flask and four flask each from the culture was treated with 5 mg L^{-1} of Cd^{2+}, Cu^{2+} and Ni^{2+} for 12 h and the two flask of untreated culture were then centrifuge at 6000 g for 10 min after that the supernatant was discarded and the biomass was freeze dried. For

EPS, again 100 mL of culture from the flask, similarly, it was taken in a separate flask and treated with Cd^{2+}, Cu^{2+} and Ni^{2+} for 12 h then it was centrifuge at 15000 g for 40 min at 15°C including the two flask of untreated culture. The biomass was discarded and supernatant was process for isolation of EPS as mentioned in extraction method (Section 2.13).

Sample Loading

The powder biomass of *M. aeruginosa* and *A. doliolum*, and their powder EPS was further analyzed in TEM (TECNAI G2 20 S-TWIN-200KV; Resolution: 2.4A°, Tezpur University) for micrograph image where the powder sample was loaded on the carbon coated copper grid within a thinned (electron transparency) central area (3 mm diameter).

2.9 FTIR Analysis of Biomass and EPS

Sample Preparation:

1. *EPS:*
    a. The extracted EPS was first dissolved in Milli-Q water to create a solution with a concentration of 1 mg mL^{-1}.
    b. This EPS solution was then subjected to a 12-hour treatment with three different heavy metals: Cu^{2+}, Cd^{2+}, and Ni^{2+}. The concentration of each heavy metal was 5 mg L^{-1}.
2. *Cyanobacterial Cells:*
    a. The cyanobacterial culture was centrifuged at 6,000 g for 10 min to separate the cells from the culture medium.
    b. The cell pellet was then washed three times with Milli-Q water to remove any residual culture medium components.

c. After washing, the cyanobacterial cells were re-suspended in Milli-Q water and subsequently treated with the same heavy metals (Cu^{2+}, Cd^{2+}, and Ni^{2+}) at a concentration of 5 mg L^{-1} for 12 h.

d. After the treatment the cyanobacterial cells were centrifuged at 6000 g for 10 min and the biomass pellets was re-suspended in distilled water.

Measurement:

i. Both the treated and untreated samples (EPS and cyanobacterial cells) were analyzed using FTIR spectroscopy.

ii. The instrument employed for this analysis was an IRAffinity-1S spectrophotometer from Shimadzu.

Analysis:

i. FTIR analysis provides information about the functional groups present within a sample based on the characteristic absorption patterns of different chemical bonds.

ii. By comparing the FTIR spectra of treated and untreated samples, researchers can identify potential changes in the functional groups of the EPS and cyanobacterial cells caused by exposure to heavy metals. These changes might indicate interactions between the heavy metals and specific functional groups within the samples.

2.10. Liquid Chromatography Mass Spectrometry

LC-MS is a sophisticated analytical method that separates, identifies, and quantifies chemical components in complicated mixtures. The basic principle behind LC-MS is that Liquid Chromatography (LC) separates the components of a sample depending on their affinity or retention strength during the stationary and mobile phases, and then Mass spectrometry (MS) generates and detects charged ions.

Sample preparation

20 mg of EPS powder from both *M. aeruginosa* and *A. doliolum* were taken in a flask then hydrolyzed using 30 ml of 2M Trifluoroacetic acid (TFA) at 100 °C in water bath till it dries into powder again. Then the hydrolysates was suspended in the same amount of methanol. The suspension was process in LCMS instruments (Thermo Fischer Scientific Pte. Ltd; Q-Exactive Plus Biopharma-High Resolution Orbitrap, IIT Bombay SAIF).

Sample loading

The sample was loaded into the instrument by injecting the liquid sample into the column.

2.11 Adsorption Study of Heavy Metals by Cyanobacterial Biomass and EPS

Materials:

a. Dried cyanobacterial biomass
b. Extracted EPS solution (1 mg mL^{-1})
c. Milli-Q water
d. Heavy metal solutions (Cd^{2+}, $Cu^{2+}$and Ni^{2+}) with varying concentrations (1-10 mg L^{-1})

Procedures:

1. *Biomass Adsorption:*

i. 100 mg of dried cyanobacterial biomass was added to 10 mL of Milli-Q water in glass vials.
ii. The vials were then treated with varying concentrations of heavy metal solutions (Cd^{2+}, Cu^{2+} and Ni^{2+}) ranging from 1 mg L^{-1} to 10 mg L^{-1}.
iii. The vials were agitated on an orbital shaker at 120 rpm for 1 h at room temperature (28 ± 2.0 °C). This shaking step ensures proper mixing and contact between the biomass and the heavy metal solution.

2. *EPS Adsorption:*

i. 10 mL of the EPS solution (1 mg mL^{-1}) was mixed with varying concentrations of heavy metal solutions (Cd^{2+}, Cu^{2+} and Ni^{2+}) similar to the biomass experiment (1-10 mg L^{-1}).
ii. The mixture was incubated for 1 hour to allow for heavy metal adsorption onto the EPS.

3. Sample Preparation for AAS Analysis:

i. *Biomass:* After shaking, the heavy metal concentration remaining in the supernatant (Ce, mg L^{-1}) was directly measured using Atomic Absorption Spectroscopy (AAS). This determines the amount of metal adsorbed by the biomass.
ii. *EPS:* Following the 1-hour incubation, an equal volume of cold ethanol (80% v/v) was added to the EPS-metal mixture to precipitate the EPS. This separation step is necessary because directly analyzing the mixture with AAS would be challenging due to the presence of EPS.
iii. The mixture was then centrifuged at 6,000 g for 10 min to pellet the precipitated EPS.
iv. The supernatant containing the remaining free heavy metal ions was collected and passed through a Whatman filter paper no. 1 to remove any residual EPS particles.
v. Finally, the filtered supernatant was analyzed using AAS (Shimadzu, Model: AA-7000F) to determine the equilibrium concentration (C_e, mg L^{-1}) of heavy metals in the presence of EPS.

Calculations:

1. Amount of Adsorbed Metal (q_e, mg g^{-1}):

The amount of heavy metal adsorbed per unit weight of biomass or EPS at equilibrium (qe, mg g^{-1}) was calculated using Equation (1):

$$q_e = \frac{(C_i - C_e)V}{W} \qquad (1)$$

Where:

C_i (mg L^{-1}) - Initial concentration of the heavy metal solution

C_e (mg L^{-1}) - Equilibrium concentration of the heavy metal in the supernatant (for biomass) or after EPS separation (for EPS)

V (L) - Volume of the solution (10 mL in this case)

W (g) - Amount of dried biomass (0.1 g in this case) or the amount of EPS in 10 mL of the 1 mg ml-1 solution (which can be calculated based on the concentration and volume)

2. Percentage Removal of Heavy Metals:

The percentage removal of heavy metals by the biomass or EPS was calculated using Equation (2):

$$\%\, removal = \left(\frac{(C_i - C_e)}{C_i}\right) \times 100 \qquad (2)$$

Here, C_i and C_e have the same definitions as in Equation (1).

2.12. pH Optimization for Enhanced Heavy Metal Biosorption

Procedure

i. The 100 mg dried biomass was suspended in 100 ml Milli-Q water and 100 mg of EPS also suspended in 100 ml Milli-Q water making 1 mg ml^{-1} EPS solution.

ii. The pH of the solution was adjusted from 2.0 to 9.0 using 0.1N HCl or NaOH for both the biomass and EPS.

iii. After pH adjustment, the solution was treated with Cu^{2+}, $Cd^{2+}$and Ni^{2+} (5 mg L^{-1}) for 1 hour to facilitate biosorption.

iv. After the treatment the biomass suspension was centrifuged at 6000 g for 10 min and the biomass was discarded.

v. Cold ethanol was added to the EPS solution after the treatment to precipitate the EPS and centrifugation at 6000g for 10 min separated the EPS precipitates.

vi. Then the supernatant was filtered with No. 1 Whatman filter paper for a clear solution.

vii. Concentration of heavy metals in the filtrate was determined by Atomic Absorption Spectroscopy (AAS).

2.13. Kinetic Study

Experimental Design:

In this experiment, Cd^{2+}, Cu^{2+} and Ni^{2+} adsorption by cyanobacterial biomass and EPS were investigated, along with the kinetic aspects of this process. For both biomass and EPS, varying concentrations of heavy metals (1-10 mg L^{-1}) were added and the remaining metal content (C_e) was measured after shaking to assess adsorption capacity. A separate experiment was conducted to study the metal removal over time (0-240 min) using AAS analysis following the separation of the biomass/EPS from the solution at different time intervals. The data was then used to calculate adsorption capacity (q_e) and % removal efficiency. Kinetic models were subsequently applied to gain insights into the rate-limiting factors affecting heavy metal uptake by both biomass and EPS.

Procedure:

i. Each test tube contained 100 mg of dried biomass mixed with 10 mL of Milli-Q water.
ii. The mixture was then treated with 10 mL of the heavy metal solution (Cd^{2+}, Cu^{2+} or Ni^{2+}).
iii. For the EPS experiment, the procedure mirrored the biomass experiment, but instead of biomass, 10 mL of the EPS solution (1 mg ml^{-1}) was used.
iv. At each designated time interval (0, 30, 60, 120, 180, and 240 min), samples were collected from the corresponding test tubes.
v. The samples were filtered to separate the biomass or EPS (biosorbent) from the remaining solution.
vi. The filtrate from the biomass experiment was directly analyzed using Atomic Absorption Spectroscopy (AAS) to determine the equilibrium concentration (Ce) of the heavy metals in the solution. This indicates the amount of metal adsorbed by the biomass at that specific time point.
vii. The filtrate from the EPS experiment required additional processing before AAS analysis. Cold ethanol was added to precipitate the EPS, followed by centrifugation (6000 g) to separate the precipitated EPS pellet. Finally, the

remaining supernatant was passed through a filter to remove any residual EPS particles. This filtrate was then analyzed using AAS to determine the Ce of heavy metals in the presence of EPS.

Data Analysis:

The AAS data, representing the C_e of heavy metal ions at different time points, was used to fit well-established kinetic models:

a. Pseudo-first-order model
b. Pseudo-second-order model
c. Intra-particle diffusion model

2.14. Thermodynamic Analysis of Heavy Metal Biosorption Experimental Design

i. A 10 mL solution containing a specific heavy metal (Cu^{2+}, Cd^{2+}, or Ni^{2+}) at a concentration of 5.0 mg L^{-1} was used.
ii. Two separate experiments were conducted:
    a. *Biomass Experiment***:** 100 mg of cyanobacterial dried biomass was added to the heavy metal solution.
    b. *EPS Experiment:* 1 mL of EPS solution (1.0 mg mL^{-1}) was added to the heavy metal solution.
iii. The temperature was varied from 283 K to 332 K (10°C to 60°C) over a period of 1 h. The temperature was monitored using a glass rod mercury thermometer.
iv. After the 1 h incubation at a specific temperature, the samples were centrifuged at 6,000 g for 10 min to separate the biomass or EPS from the solution.
v. The supernatant was then filtered to obtain a clear solution for analysis.
vi. The concentration of remaining heavy metal ions (C_e, mg L-1) in the solution was measured using Atomic Absorption Spectroscopy (AAS).

Thermodynamic Parameter Calculations:

Vant Hoff's equations (SenthilKumar et al. 2011; Sargın and Arslan 2015) were employed to calculate key thermodynamic parameters:

a. Enthalpy (ΔH°): Represents the heat change associated with the biosorption process.

b. Entropy (ΔS°): Represents the change in randomness or disorder during biosorption.

c. Gibbs Free Energy (ΔG°): Indicates the spontaneity of the biosorption reaction under specific conditions.

These parameters provide insights into the energetic favorability and spontaneity of heavy metal removal by the biomass or EPS, highlighting the influence of temperature on the process.

Following Equations (3), (4), and (5) were used to calculate the enthalpy (ΔH°), entropy (ΔS°), and Gibbs free energy (ΔG°):

$$k_C = \frac{q_e}{C_e} \quad (3)$$

$$lnk_C = \frac{\Delta S^\circ}{R} - \frac{\Delta H^\circ}{RT} \quad (4)$$

$$\Delta G^\circ = \Delta H^\circ - T\Delta S^\circ \quad (5)$$

Where qe (mg g^{-1}): Equilibrium concentration of adsorbed heavy metal ions, C_e (mg L^{-1}): Concentration of heavy metal ions remaining in the solution and k_C Equilibrium constant

2.15. Kinetic Models

(i) Pseudo first order Kinetics

The expression below represents the pseudo-first-order rate kinetics (Moussout et al. 2018):

$$q_t = q_e(1 - e^{-k_1 t}) \quad (6)$$

Where, q_e (mg g^{-1}) is the quantity of heavy metals adsorbed at equilibrium, q_t (mg g^{-1}) represents adsorption at time t (min), k_1 (g mg^{-1} min^{-1}) is the rate constant, and n denotes the number of order of reaction. The values of the parameters q_e and k_1 were derived through non-linear curve fitting of time-course data employing equation 6.

(ii) The pseudo second order kinetics

The pseudo-second-order rate kinetics, as proposed by Ho (2000), can be expressed by the following equation:

$$q_t = \frac{{q_e}^2 k_2 t}{q_e k_2 t + 1} \quad (7)$$

Where, k_2 is the pseudo-second-order rate constant (mg g^{-1} min^{-1}). The values of constant k_2 and q_e were calculated from non-linear curve fitting of time-course data using equation 7.

(iii) Intra-particle diffusion

The time course adsorption data were analyzed using the intraparticle diffusion model, introduced by Das et al. (Das et al. 2014).

$$qt = k_d t^{0.5} + \mathrm{I} \quad (8)$$

Where, q_t (mg g^{-1}) is the equilibrium heavy metals sorption at time (t), k_d (mg g^{-1} $min^{1/2}$) represents the intraparticle diffusion rate constant, and I is the intercept. The values of K_d and I were calculated from the non-linear curve fitting of kinetic data employing the above equation.

2.16. Assessment of Interference from Other Metals

An investigation was conducted to assess how the presence of additional heavy metal ions affects the adsorption of Cu^{2+} and Ni^{2+} by cyanobacterial biomass and EPS.

Experimental Design:

i. Binary solutions were prepared containing varying concentrations of Cu^{2+} (1-10 mg L^{-1}) and Ni^{2+} (1-10 mg L^{-1}).

ii. To achieve binary mixtures, a constant concentration of 5 mg L^{-1} of either Cu^{2+} or Ni^{2+} was added to solutions with varying concentrations of the other metal ion (1-10 mg L^{-1}). For instance, for solutions with varying Cu^{2+} concentrations, a fixed concentration of 5 mg L^{-1} Ni^{2+} was considered.

iii. Subsequently, biomass (100 mg) and EPS (10 ml) were added to these binary solutions.

iv. The adsorption of Cu^{2+} in the presence of Ni^{2+} and vice versa was studied for a duration of 1 h at room temperature.

This experiment aimed to determine if the presence of one heavy metal ion (Cu^{2+} or Ni^{2+}) affects the adsorption of the other by the cyanobacterial biomass and EPS.

2.17. Adsorption Models

This section describes three mathematical models commonly used to analyze adsorption processes: Langmuir, Freundlich, and Temkin isotherm models.

(i) The Langmuir Isotherm Model

Developed by Irving Langmuir (1918), this model describes a scenario where adsorption occurs as a single layer on a uniform surface. It assumes no interaction between adsorbed molecules. The Langmuir equation is represented as::

$$q_e = \frac{Q_m k_L C_e}{1+k_L C_e} \qquad (9)$$

where,

q_e (mg g^{-1}): Equilibrium adsorption of heavy metals

C_e (mg L^{-1}): Equilibrium concentration of heavy metals

k_L (L mg^{-1}): Constant related to the free adsorption energy

Q_m (mg g^{-1}): Maximum adsorption potential

The values of Q_m and k_L are determined by fitting experimental data to the Langmuir equation using non-linear curve fitting techniques.

(ii) *The Freundlich Isotherm Model*

The Freundlich model, introduced by Herbert Freundlich in 1907, is an empirical equation used to describe adsorption onto heterogeneous surfaces. This model assumes multilayer adsorption can occur. The Freundlich equation is expressed as:

$$q_e = k_f C_e^{\frac{1}{n}} \qquad (10)$$

Where:

q_e (mg g^{-1}): Amount of solute adsorbed per unit mass of adsorbent at equilibrium

k_f: Freundlich constant related to the adsorption capacity

n: Freundlich exponent indicating adsorption intensity or surface heterogeneity

The values of k_f and n are determined by fitting equilibrium adsorption data to the Freundlich model using non-linear curve fitting.

(iii) The Temkin Isotherm Model

The Temkin isotherm model, proposed by Aharoni and Ungarish (1977), accounts for interactions between the adsorbed molecules and the surface. It assumes the heat of adsorption decreases as the surface coverage increases. This model is suitable for scenarios with non-uniform binding energies on the adsorbent surface. The Temkin isotherm model is represented by the equation below:

$$q_e = \frac{RT}{b_T} \ln (A_T C_e) \qquad (11)$$

Where:

q_e (mg g^{-1}): Amount of solute adsorbed per unit mass of adsorbent at equilibrium

R: Universal gas constant (8.314 J $mol^{-1}K^{-1}$)

T: Absolute temperature (K)

b_T: Temkin isotherm constant related to the heat of adsorption (J mol^{-1})

A_T: Equilibrium binding constant corresponding to the maximum binding energy (L mol^{-1})

C_e: Equilibrium concentration of the solute in the solution (mg L^{-1})

2.18. Potentiometric Titration Sample Preparation:

Sample preparation

a. Cyanobacterial cultures were harvested using a centrifuge during their exponential growth phase.

b. The cells and EPS were treated with 5 mg L^{-1} Cd^{2+}, Cu^{2+} and Ni^{2+} for 60 min.

c. Harvested cells were rinsed with 20 mL of 1.25 mM sodium nitrate ($NaNO_3$) solution to remove any residual growth media components.

d. The washed cells and EPS were suspended in 50 mL of fresh 1.25 mM sodium hydroxide (NaOH) solution.

e. The pH of the suspension was adjusted to a specific value of 11.21 using 0.1 N sodium hydroxide (NaOH). This high pH environment likely promotes deprotonation of acidic groups on the cell surface.

Titration Procedure:

i. The suspension was titrated with a 0.02 M hydrochloric acid (HCl) solution.

ii. The titration was performed by adding small increments (0.1 mL) of the HCl solution to the cell suspension at 1 min intervals.

iii. The pH of the suspension was measured after each HCl addition using a pH meter.

iv. A magnetic stirrer was used to ensure proper mixing of the cell suspension during the titration.

Data Analysis:

Gran's method was employed to determine the equivalence point of the titration. This method involves analyzing the relationship between the volume of titrant added (HCl) and the second derivative of the pH curve. The equivalence point corresponds to the inflection point in the second derivative curve (Wang et al., 2011).

Interpretation:

By analyzing the volume of HCl required to reach the equivalence point, we can estimate the total concentration of acidic functional groups like carboxylic groups on the surface of cyanobacterial cells.

2.19. Desorption

An experiment was conducted to investigate desorption of heavy metals (Cd^{2+}, Cu^{2+} and Ni^{2+}) from cyanobacterial biomass and EPS.

Procedure

i. 100 mg of dried *A. doliolum* biomass and EPS were each exposed to 100 mL of a heavy metal solution (Cd^{2+}, Cu^{2+} or Ni^{2+}) with a concentration of 5 mg L-1.

ii. After a 1h incubation period, the biomass was separated from the solution.

iii. For the EPS, cold ethanol was added to precipitate the EPS from the solution.

iv. The supernatant (remaining solution) and the residues (biomass or precipitated EPS) were collected after separation.

v. An aliquot of 10 mL Milli-Q water was used to wash the biomass/EPS residues containing the adsorbed heavy metals.

vi. The washing process involved continuous shaking for 60 min to facilitate the release of adsorbed metals from the biomass/EPS.

vii. The wash solution (eluent) containing the desorbed heavy metals was separated from the biomass/EPS using centrifugation at 6,000 × g for 10 min.

viii. The amount of heavy metals desorbed from the biomass/EPS was measured using Atomic Absorption Spectroscopy (AAS) analysis of the eluent.

A previously described equation (Pellegrini et al., 2006) was used to calculate the percentage of heavy metals desorbed from the biomass/EPS based on the initial amount of metal adsorbed and the amount recovered in the eluent after washing.

$$Desorption\ \% = \frac{Heavy\ metals\ concentration\ in\ eluent\ (mgL^{-1})}{Heavy\ metals\ removal\ (mg\ L^{-1})} \times 100 \quad (12)$$

SECTION II: LIVE CELLS EXPERIMENTS

2.20. Measurement of Survival and Growth

The impact of heavy metals on cyanobacterial growth was assessed by monitoring changes in optical density (OD) using a UV/VIS spectrophotometer (Systronics-117, India) at a wavelength of 663 nm. 10 mL of cyanobacterial culture were transferred to test tubes and supplemented with varying concentrations (0-100 mg L^{-1}) of the heavy metals cadmium (Cd^{2+}), copper (Cu^{2+}), and nickel (Ni^{2+}). Cultures were incubated for 96 h, with OD measurements taken at 24-hour intervals (0-96 h). Specific growth rate (μd^{-1}) was calculated using the following equation:

$$\text{Specific growth rate } (\mu d^{-1}) = \frac{\ln(n_2 - n_1)}{t_2 - t_1} \quad (13)$$

Where, μ stands for specific growth rate, and n_1 and n_2 are absorbance of culture suspension at the beginning (t_1) and the end (t_2) of the selected time interval.

2.21. Protein Content Determination

The protein content of both the culture of *M. aeruginosa* and *A. doliolum* was quantified using Lowry's method (Lowry et al. 1951) following the same procedure describe in section 2.5.2 Bovine Serum Albumin (BSA) served as the standard for calibration.

2.22. Total Carbohydrates Content

The total carbohydrates content was estimated by following the Anthrone method (Yemm and Willis 1954) as describe in the section 2.5.1 for both the culture of *M. aeruginosa* and *A. doliolum*. The glucose was used as the standard for saccharide quantification.

2.23. Photosynthetic Pigment Quantification

Pigment Extraction:

5 ml of cyanobacterial culture were centrifuged at 10,000 rpm for 20 min to collect the cell pellets. The pellets were then re-suspended in 5 mL of 95% ethanol and incubated overnight at 4°C in the dark. Following incubation, the suspension was centrifuged again, and the resulting supernatant was used for pigment quantification (Mimuro and Fujita, 1977; Kirk and Allen, 1965).

Quantification:

Chlorophyll-a (Chl-a) and Carotenoid (CAR) content were determined spectrophotometrically using a UV/VIS spectrophotometer. Absorbance measurements were taken at specific wavelengths (Chl-a: 665 nm and 649 nm; CAR: 470 nm and 652 nm

Chl-a and CAR concentrations were calculated using the following equations:

$$\text{Chl-a} = 13.7\ A_{665} - 5.76\ A_{649} \quad (14)$$

$$\text{CAR} = (1000\ A_{470} - 0.474\ A_{652})/\ 5.34 \quad (15)$$

2.24. Oxidative Lipid Damage Assessment

The extent of oxidative lipid damage was evaluated by measuring the total content of 2-Thiobarbituric acid reactive substances (TBARS), expressed as a Malondialdehyde (MDA) equivalent using the method described by De Vos and Schat, (1991).

Procedure:

i. Cyanobacterial cultures exposed to heavy metals were harvested by centrifugation at 10,000 rpm for 10 min.
ii. The resulting pellets were treated with 4 mL of a reaction mixture containing 0.25% thiobarbituric acid (TBA) in 10% trichloroacetic acid (TCA) to homogenize the sample.
iii. The homogenate was then incubated at 95°C for 30 min to induce the formation of a TBA-MDA adduct.
iv. To terminate the reaction, the mixture was immediately cooled in an ice bath.
v. Following cooling, the mixture was centrifuged again at 10,000 rpm for 10 min to pellet any cellular debris.
vi. The absorbance of the clear supernatant was measured spectrophotometrically at 532 nm and 600 nm using a UV/VIS spectrophotometer.

MDA Equivalent Calculation:

The MDA equivalent, indicative of TBARS content, was calculated using the following equation:

$$\text{MDA (mM mg}^{-1}\text{ protein)} = (A_{532} - A_{600})/\ 155 \qquad (16)$$

Where, (155 mM^{-1} cm^{-1} is Extinction Co-efficient.)

2.25. Hydrogen Peroxide (H_2O_2) Measurement

The H_2O_2 concentration within cyanobacterial cultures was determined using the method outlined by Okuda et al. (1991) (Okuda et al. 1991).

Procedure:

i. Heavy metal-treated cyanobacterial cultures were centrifuged at 10,000 rpm for 10 min to collect the cell pellets.

ii. The pellets were then resuspended in 5 mL of 50% trichloroacetic acid (TCA) and incubated for 10 min at room temperature.

iii. Following incubation, the suspension was centrifuged again. The supernatant was collected for H_2O_2 measurement, and the cell pellets were discarded.

iv. From the collected supernatant, 1.6 mL was transferred to a new tube and mixed with 0.8 mL of 50% TCA, 0.8 mL of ferrous ammonium sulfate, and 0.4 mL of 2.5 M potassium thiocyanate. The solution was then shaken well.

v. The absorbance of the mixture was measured spectrophotometrically at 480 nm using a UV/VIS spectrophotometer.

vi. The H_2O_2 content was quantitatively estimated using a pre-generated standard curve relating absorbance at 480 nm to known H_2O_2 concentrations.

2.26. Estimation of Superoxide (O_2^-) Radicals

The generation of superoxide radicals (O_2^-) within cyanobacterial cultures was evaluated using the method described by Achary et al. (2012) .

Procedure:

i. 1.0 mL of cyanobacterial culture was mixed with 6.0 mL of a reaction mixture containing:

   a. 50 mM TRIS-HCl buffer (pH 6.4) to maintain a stable pH environment.

   b. 0.2 M NADH (Nicotinamide Adenine Dinucleotide - Reduced) as an electron donor for superoxide generation.

   c. 250 mM sucrose as an osmotic protectant for the cells.

ii. The mixture was then vacuum infiltrated for 15 min to facilitate the entry of reagents into the cyanobacterial cells.

iii. Following infiltration, the mixture was illuminated with artificial light at an intensity of 200 μmol m^{-2} s^{-1} for 24 h to stimulate superoxide production.

iv. During illumination, a characteristic purple colour developed due to the formation of a blue formazan precipitate.

v. After incubation, the absorbance of the blue formazan was measured spectrophotometrically at 530 nm using a UV/VIS spectrophotometer.

Superoxide Radical Quantification:

The O_2^- content was calculated using the following equation:

O_2^- (μmol g^{-1} protein) = (A530 x dilution factor) / (ε x path length x protein content mg/mL)

Where, A_{530} is Absorbance at 530 nm, ε is Extinction coefficient of formazan (12.8 mM^{-1} cm^{-1}), Path length is Cuvette path length (typically 1 cm).

2.27. Hydroxyl Radical (OH−) Activity Assessment

Due to the highly reactive and transient nature of hydroxyl radicals (OH^-), direct measurement within living cells is currently not feasible. However, the method described by Halliwell and Gutteridge (1984)(Halliwell and Gutteridge 1984) can be employed to assess the cellular damage caused by OH^- radical activity.

Procedure:

1. *Sample Preparation:*

    a. Homogenize 10 mL of cyanobacterial culture in a buffer solution containing 10 mM sodium phosphate (pH 7.4) and 15 mM 2-deoxyribose. 2-deoxyribose acts as a substrate for OH- radicals.

b. Centrifuge the homogenate at 12,000 g for 15 min to separate cell debris. Collect the supernatant for further analysis.

2. *OH^- Activity Assessment:*

    a. Take a 0.2 mL aliquot of the collected supernatant and add it to a reaction mixture containing 3 mL of 0.5% thiobarbituric acid (TBA) and 1 mL of glacial acetic acid.

    b. Incubate the reaction mixture at 37°C for 2 h to allow for the formation of a coloured product due to the reaction between TBA and products of OH^- mediated damage to 2-deoxyribose.

3. *Quantification:*

    a. Heat the reaction mixture in a water bath at 100°C for 30 min to further enhance colour development.

    b. Cool the mixture down in an ice bath for 10 min.

    c. Measure the absorbance of the cooled solution using a UV/VIS spectrophotometer at 532 nm. Higher absorbance indicates greater OH- activity (increased damage to 2-deoxyribose).

2.28. Antioxidative Enzyme Assays

2.28.1 Extraction of Antioxidative Enzymes

Growing cyanobacterial cultures were harvested by centrifugation at 10,000 rpm for 10 min. The resulting pellets were resuspended in a lysis buffer containing:

i. 50 mM Potassium Phosphate buffer (pH 7.0) to maintain a stable pH environment.

ii. 1 mM Ethylenediaminetetraacetic acid (EDTA) to chelate metal ions that may interfere with enzyme activity.

iii. 1% (w/v) Polyvinylpyrrolidone (PVP) to prevent protein aggregation during extraction.

The suspension was then sonicated at 350 mA for 2 min under ice-cold conditions to disrupt the cell walls and release the enzymes. The sonicated lysate was centrifuged at 12,000 rpm for 30 min at 4°C. The resulting supernatant containing the extracted antioxidant enzymes was used for further assays.

2.28.2 Estimation of Superoxide Dismutase (SOD)

Assay Principle:

This assay measures SOD activity by monitoring its ability to inhibit the reduction of Nitro Blue Tetrazolium (NBT) (Stewart and Bewley 1980).. NBT is a blue formazan that turns yellow upon reduction. SOD competes with NBT for superoxide radicals, preventing its reduction and color change.

Materials:

a. Enzyme extract (supernatant from Section 2.11.1)
b. Reaction mixture containing:
   50 mM Phosphate buffer (pH 7.8)
   13 mM Methionine
   75 µM NBT
   2 µM Riboflavin
   µM EDTA

Procedure:

i. A reaction mixture was prepared by combining 50 mM phosphate buffer (pH 7.8), 13 mM methionine, 75 µM NBT, 2 µM riboflavin, and 0.1 µM EDTA in a suitable test tube. The final volume was determined based on the number of samples being analyzed.

ii. Enzyme extract (prepared in Section 2.11.1) was added (0.2 mL) to 3 mL of the reaction mixture prepared in step 1. The solution was then mixed gently.

iii. To initiate the reaction, 2 µM riboflavin was added to the mixture, and the tubes were shaken gently to ensure proper mixing. As riboflavin is light-sensitive, this step initiated the generation of superoxide radicals.

iv. The reaction mixture was then incubated under illumination from a minimum 15W fluorescent lamp for 10 min. Light exposure was necessary for superoxide radical generation.

v. After the 10-min incubation, the light source was turned off immediately. To prevent further NBT reduction, the tubes were covered with a black cloth or aluminum foil to block light exposure.

vi. The absorbance of the reaction mixture was measured at 560 nm using a UV/VIS spectrophotometer. Higher absorbance indicated less SOD activity (more NBT reduction).

Unit Definition and Calculation:

One unit (U) of SOD activity was defined as the amount of enzyme extract that inhibited 50% of the initial NBT reduction rate in the absence of the enzyme (Weydert and Cullen 2010). The amount of enzyme extract producing 50% inhibition was estimated from a calibration curve generated using different enzyme extract volumes and plotting the resulting absorbance values.

2.28.3 Catalase (CAT) Activity Assay

Principle:

The activity of catalase (CAT) was determined by its ability to decompose hydrogen peroxide (H_2O_2) into water and oxygen (Jiang and Zhang 2001). This assay measured the rate of H_2O_2 disappearance by monitoring the decrease in absorbance at 240 nm using a UV/VIS spectrophotometer. Hydrogen peroxide has a characteristic absorbance peak at 240 nm, and a decrease in absorbance at this wavelength reflected CAT activity.

Materials:

a. Enzyme extract (supernatant from Section 2.11.1)

b. 50 mM Potassium Phosphate buffer (pH 7.0)

c. 10.5 mM Hydrogen peroxide (H_2O_2)

Procedure:

i. A reaction mixture was prepared by combining 50 mM potassium phosphate buffer (pH 7.0) and 10.5 mM H_2O_2 in a suitable cuvette.

ii. The reaction was initiated by adding 0.2 mL of the enzyme extract (prepared in Section 2.11.1) to the reaction mixture in the cuvette. The solution was then mixed gently.

iii. The initial absorbance of the reaction mixture at 240 nm was measured using a UV/VIS spectrophotometer (A_0).

iv. The reaction mixture was then incubated at room temperature for 2 min.

v. After incubation, the absorbance of the reaction mixture was measured again at 240 nm (A_1).

Calculation of Activity:

The rate of H_2O_2 disappearance, directly proportional to CAT activity, was calculated using the following equation:

$$\text{Activity (U mg}^{-1}\text{ protein min}^{-1}) = [(A_0 - A_1) / (\varepsilon \times t \times v)] \times \text{protein concentration}$$

where:

A_0 = Initial absorbance at 240 nm

A_1 = Final absorbance at 240 nm after incubation

ε = Extinction coefficient of H_2O_2 at 240 nm (39.4 mM^{-1} cm^{-1})

t = Incubation time (min.)

v = Volume of enzyme extract added (mL)

Protein concentration = Amount of protein in the enzyme extract (mg mL^{-1}, determined separately, refer to Section 2.21)

Unit Definition:

One unit (U) of CAT activity was defined as the amount of enzyme that decomposes 1 μmol of H_2O_2 per min under the assay conditions. The final result was expressed in units per milligram of protein (U mg^{-1} protein min^{-1}).

2.28.4 Ascorbate Peroxidase (APX) Activity Assay

Principle:

Ascorbate peroxidase (APX) activity is determined by its ability to catalyze the oxidation of ascorbate (ASC) by hydrogen peroxide (H_2O_2) (Jiang and Zhang, 2001). This assay monitors the decrease in absorbance at 290 nm due to the consumption of ASC using a UV/VIS spectrophotometer. Ascorbate has a characteristic absorbance peak at 290 nm, and its decrease reflects APX activity.

Materials:

a. Enzyme extract (supernatant from Section 2.11.1)

b. 50 mM Potassium Phosphate buffer (pH 7.0)

c. 0.5 mM Ascorbate (ASC)

d. 0.1 mM Hydrogen peroxide (H_2O_2)

Procedure:

i. A reaction mixture was prepared by combining 50 mM potassium phosphate buffer (pH 7.0), 0.5 mM ascorbate (ASC), and 0.1 mM hydrogen peroxide (H_2O_2) in a suitable cuvette. The total volume was adjusted to 1 mL.

ii. The reaction was initiated by adding 0.2 mL of the enzyme extract (prepared in Section 2.11.1) to the reaction mixture in the cuvette. The solution was then mixed gently.

iii. Immediately after adding the enzyme extract, the absorbance of the reaction mixture was measured at 290 nm using a UV/VIS spectrophotometer (initial absorbance, A_0).

iv. The reaction mixture was incubated for 1 min at room temperature.

v. After incubation, the absorbance of the reaction mixture was measured again at 290 nm (final absorbance, A_1).

Calculation of Activity:

APX activity is directly proportional to the rate of ASC disappearance. The activity can be calculated using the following equation:

$$\text{Activity (U mg}^{-1}\text{ protein min}^{-1}) = [(A_0 - A_1) / (\varepsilon \times t \times v)] \times \text{protein concentration}$$

where:

A_0 = Initial absorbance at 290 nm
A_1 = Final absorbance at 290 nm after incubation
ε = Extinction coefficient of ascorbate at 290 nm (2.8 mM^{-1} cm^{-1})
t = Incubation time (min)
v = Volume of enzyme extract added (mL)

Protein concentration = Amount of protein in the enzyme extract (mg mL^{-1}, determined separately, refer to Section 2.21)

Correction for Non-Enzymatic Oxidation:

A blank control lacking the enzyme extract was included in the assay. The decrease in absorbance measured in the blank reflects the non-enzymatic oxidation of ASC by H_2O_2. This value was subtracted from the decrease in absorbance observed in the presence of the enzyme extract to obtain the APX-specific activity.

Unit Definition:

One unit (U) of APX activity is defined as the amount of enzyme that consumes 1 μmol of ascorbate per min under the assay conditions. The final result is expressed in units per milligram of protein (U mg^{-1} protein min^{-1}).

2.28.5 Glutathione Reductase (GR) Activity Assay

Principle:

Glutathione reductase (GR) activity is determined by its ability to oxidize nicotinamide adenine dinucleotide phosphate (NADPH) to nicotinamide adenine dinucleotide phosphate ($NADP^+$) (Schaedle and Bassham 1977). This assay monitors the decrease in absorbance at 340 nm due to NADPH consumption using a UV/VIS spectrophotometer. NADPH has a characteristic absorbance peak at 340 nm, and its decrease reflects GR activity.

Materials:

a. Enzyme extract (supernatant from Section 2.11.1)
b. 0.05 M Tris-HCl buffer (pH 7.5)
c. 0.15 mM NADPH
d. 3 mM $MgCl_2$

Procedure:

i. A standard reaction mixture was prepared by combining 0.05 M Tris-HCl buffer (pH 7.5), 0.15 mM NADPH, and 3 mM $MgCl_2$ in a suitable cuvette. The total volume was adjusted to 1 mL.

ii. The reaction was initiated by adding 0.2 mL of the enzyme extract (prepared in Section 2.11.1) to the reaction mixture in the cuvette. The solution was then mixed gently.

iii. Immediately after adding the enzyme extract, the absorbance of the reaction mixture was measured at 340 nm using a UV/VIS spectrophotometer (initial absorbance, A_0).

iv. The reaction mixture was incubated for 5 min at room temperature.

v. After incubation, the absorbance of the reaction mixture was measured again at 340 nm (final absorbance, A_1).

Calculation of Activity:

GR activity is directly proportional to the rate of NADPH disappearance. The activity can be calculated using the following equation:

$$\text{Activity (U mg}^{-1}\text{ protein min}^{-1}) = [(A_0 - A_1) / (\varepsilon \times t \times v)] \times \text{protein concentration}$$

where:

A_0 = Initial absorbance at 340 nm
A_1 = Final absorbance at 340 nm after incubation
ε = Extinction coefficient of NADPH at 340 nm (6.2 mM^{-1} cm^{-1})
t = Incubation time (min)
v = Volume of enzyme extract added (mL)
Protein concentration = Amount of protein in the enzyme extract (mg mL^{-1}, determined separately, refer to Section 2.21)

Unit Definition:

One unit (U) of GR activity is defined as the amount of enzyme that oxidizes 1 μmol of NADPH per min under the assay conditions. The final result is expressed in units per milligram of protein (U mg^{-1} protein min^{-1}).

CHAPTER 3

RESULTS

SECTION I. BIOSORPTION EXPERIMENTS

3.1. Extra Polymeric Substance (EPS) Extraction

The EPS was extracted from both the *M. aeruginosa* and *A. doliolum* which was obtained in a powder form and stored it under 4°C for further studies and application. Figure 1 provides a visual flowchart outlining the EPS extraction steps.

3.2. Biochemical Content of Cyanobacterial Biomass and Isolated EPS

This study investigated the presence of metal-binding biomolecules in *M. aeruginosa* and *A. doliolum,* focusing on saccharides, proteins, and amino acids. These molecules play a critical role in regulating metal ion concentrations within cells (homeostasis) and have potential applications due to their metal-chelating abilities. The research quantified the content of these biomolecules in both the cellular material (biomass) and the surrounding EPS (extracellular polymeric substances).

The results shown in table 1, revealed a higher abundance of all three compounds in the biomass compared to the EPS for both organisms. *M. aeruginosa* biomass contained 36.5 mg g^{-1} of saccharides, 88.3 mg g^{-1} of proteins, and 18 mg g^{-1} of amino acids, compared to 21.4 mg g^{-1}, 52.2 mg g^{-1}, and 6.8 mg g^{-1} in the EPS, respectively. *A. doliolum* displayed a similar trend, with the biomass containing 42.33 mg g^{-1} of saccharides, 95.5 mg g^{-1} of proteins, and 22.9 mg g^{-1} of amino acids, while the EPS had 21.3 mg g^{-1}, 53.4 mg g^{-1}, and 9.8 mg g^{-1}, respectively. This suggests these biomolecules primarily function in maintaining metal homeostasis within the cells. However, their presence in the EPS indicates a potential role in interacting with and immobilizing metal ions from the environment.

Figure.1. Flowchart diagram of the Extracellular Polymeric Substance (EPS) extraction process from cyanobacterial cultures (*M. aeruginosa* and *A. doliolum*). The purified EPS was freeze-dried and stored at a low temperature (e.g., 4°C) for further analysis or applications.

Table.1. Biochemical Content of *M. aeruginosa* and *A. doliolum* and its Isolated EPS

	Biosorbent			
	M. aeruginosa	*Microcystis* EPS	*A. doliolum*	*Anabaena* EPS
Saccharides (mg g^{-1})	36.5±2.19	21.4±1.39	42.33±1.51	21.3±1.09
Protein (mg g^{-1})	88.3±5.29	52.2±3.18	95.5±6.26	53.4±3.31
Amino acids (mg g^{-1})	18±1.08	6.8±0.46	22.9±1.56	9.8±0.68

3.3. Scanning Electron Microscopy (SEM) Image Analysis

This section analyzes the structure and potential functions of *M. aeruginosa* and *A. doliolum* and EPS (extracellular polymeric substances) isolated from them using Scanning Electron Microscopy (SEM) (Fig. 29).

Microcystis EPS (Figure.1. A-D):

The EPS exhibits strong and well-defined three-dimensional structures. A key feature is the presence of interconnected voids and channels throughout the EPS matrix. This porosity facilitates efficient diffusion and transport of substances within the EPS, crucial for nutrient exchange and waste management within microbial communities. The surface of the EPS appears smooth and glistening, suggesting the presence of specific surface compounds or functional groups contributing to the observed glittering effect. The combination of intricate 3D structures, porous framework, distinct surface properties, and branching arrangements likely contributes to the exceptional metal-binding potential of *Microcystis* EPS.

A. doliolum EPS (Figure.1. E-H):

The EPS displays a solid surface with irregular shapes, resembling a flowery structure. This suggests the presence of specific molecular interactions that are critical for their formation and resilience.

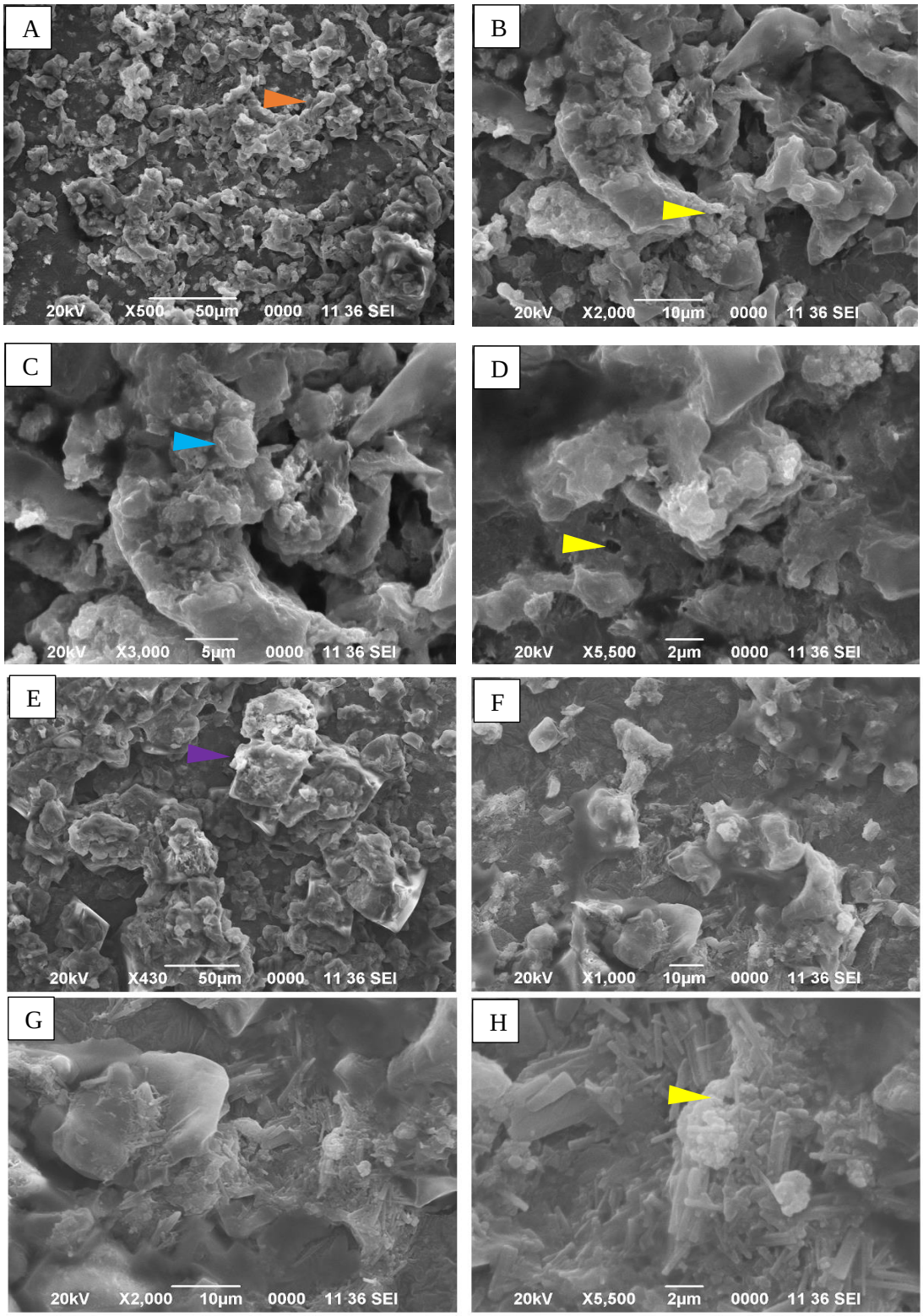

Figure.2. SEM visualization of isolated EPS: (A-D) *Microcystis* EPS and (E-H) *Anabaena* EPS. Key: ▲ Porous structure, ▲ Branched EPS structure, ▲ Glittering surface.

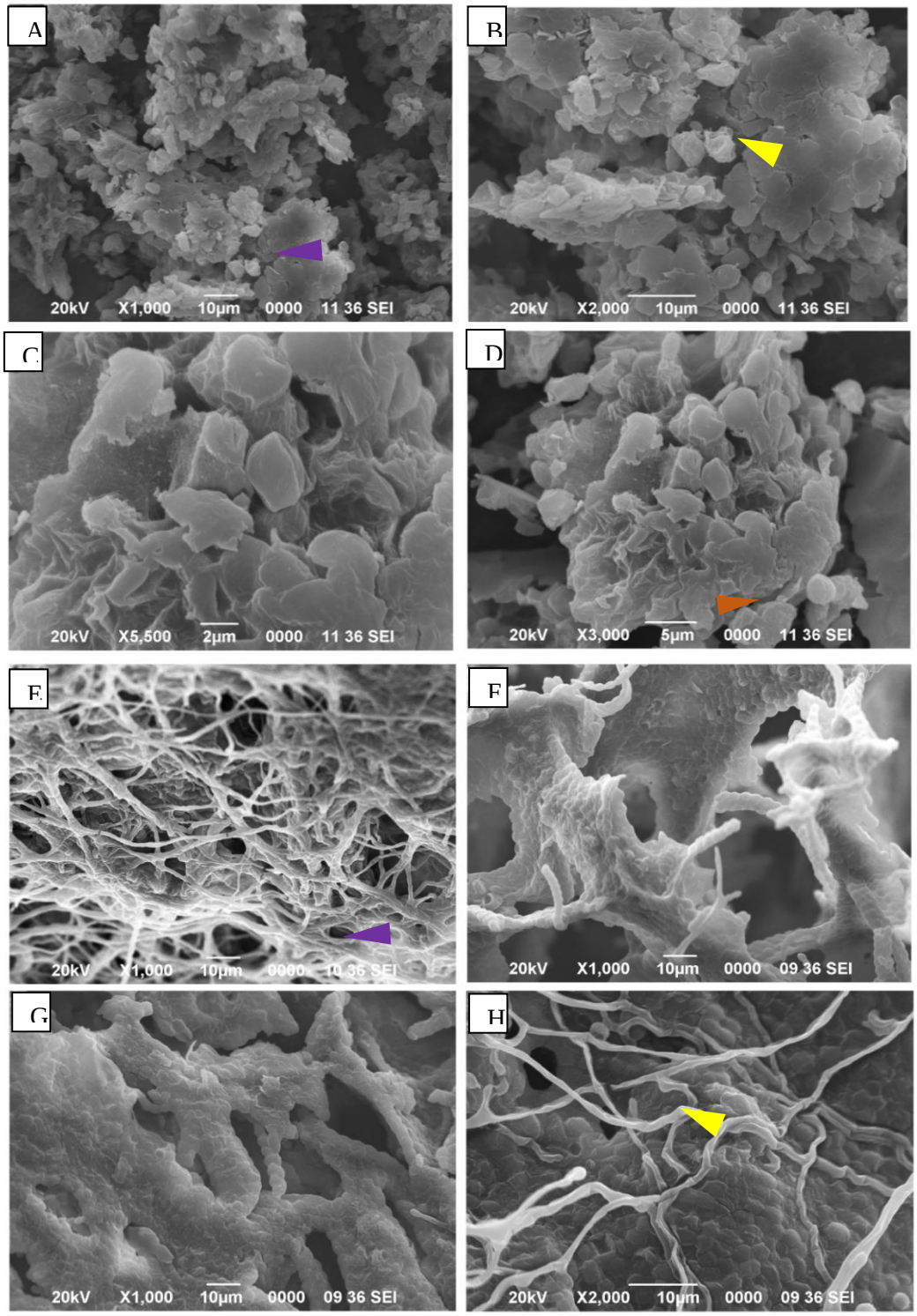

Figure.3. SEM visualization of Native biomass: (A-D) *M. aeruginosa* and (E-H) *A. doliolum*. : ▲ Porous structure, ▲ Tubular structure, ▲ Glittering surface.

Similar to *Microcystis* EPS, porosity is a significant feature within the *A. doliolum* EPS structure. The surface appears smooth and shining, indicating distinct visual properties. This suggests the presence of specific surface compounds or functional groups contributing to the observed glistening effect. The presence of crystalline rod-like structures reveals another important feature of *A. doliolum EPS.* This ordered and repeating atomic arrangement suggests properties like stability and durability, highlighting the complexity and diversity of EPS produced by cyanobacteria.

M. aeruginosa (Figure.2. A-D)

The surface of *M. aeruginosa* displayed robust and consistent 3D structures, reminiscent of flowers or mushrooms. The porous structure was also observed within the surface structures which was a salient feature, indicating interconnected voids and channels across the matrix. The open tubular structures were evident, further enhancing the complex architecture (Baulina 2012). These tubules potentially facilitate the movement of fluids, gases, and even microbial cells within the EPS, contributing to the overall structural robustness of *Microcystis* aggregates. The glittering features were also observed potentially indicating the presence of particular compounds or functional groups on the surface.

A. doliolum (Figure.2. E-H)

The micrograph SEM image of *Anabaena doliolum* shown to have a fibular structure, web-like, and the porous structure are clearly visible and it also display some sporadic structure. The glittering surface is also a salient features of the surface of *A. doliolum* indicating the presence of functional group.

3.4. Elemental Composition of *M. aeruginosa* and *A. doliolum* using EDX

Energy-Dispersive X-ray analysis (EDX) served as a powerful tool to explore the elemental composition of the biomass and EPS isolated from *M. aeruginosa* and *A. doliolum* (Figure 4, 5 and Tables 2, 3). This analysis sheds light on the key elements present and their potential contributions to the overall structure and function of these components.

M. aeruginosa biomass and its EPS:

As expected, carbon (C) and oxygen (O) remained dominant in both biomass (C: 69.32%, O: 28.92%) and EPS (C: 54.29%, O: 39.07%), forming the backbone of essential biomolecules. Interestingly, the biomass displayed a slightly higher abundance of these fundamental elements compared to the EPS. The analysis revealed the presence of several cations and trace elements in both fractions. *Microcystis* biomass contained potassium (K) at 0.37% and magnesium (Mg) at 0.40%, potentially contributing to cellular functions and enzyme activity. Trace elements like iron (Fe) (0.14%) were also detected, possibly playing a role in specific metabolic processes. The EPS of *Microcystis* presented a distinct elemental profile compared to the biomass. Notably, it showed a significantly higher presence of sodium (Na) (9.76%) compared to the biomass (1.39%). This suggests a potential role for Na+ ions in the EPS structure or interactions with the surrounding environment. Additionally, the exclusive presence of copper (Cu^{2+}) and chlorine (Cl) in the EPS hints at their specific functionalities within this extracellular matrix.

A. doliolum biomass and its EPS:

Similar to *Microcystis*, C (61.05%) and O (38.13%) dominated the elemental composition of both *A. doliolum* biomass and EPS (C: 31.39%, O: 38.69%). This dominance reflects the prevalence of organic compounds essential for cellular structure and function. A striking difference between *A. doliolum* and *Microcystis* was the significant amount of nitrogen (N) (24.94%) detected in the EPS. Nitrogen is a crucial element for protein and nucleic acid synthesis, and its presence in the EPS suggests its potential role in specific metabolic processes or interactions occurring within the extracellular matrix. It is remarkable that *A. doliolum* is known for its nitrogen fixation characteristics, while *M. aeruginosa* a non-nitrogen fixing cyanobacteria.

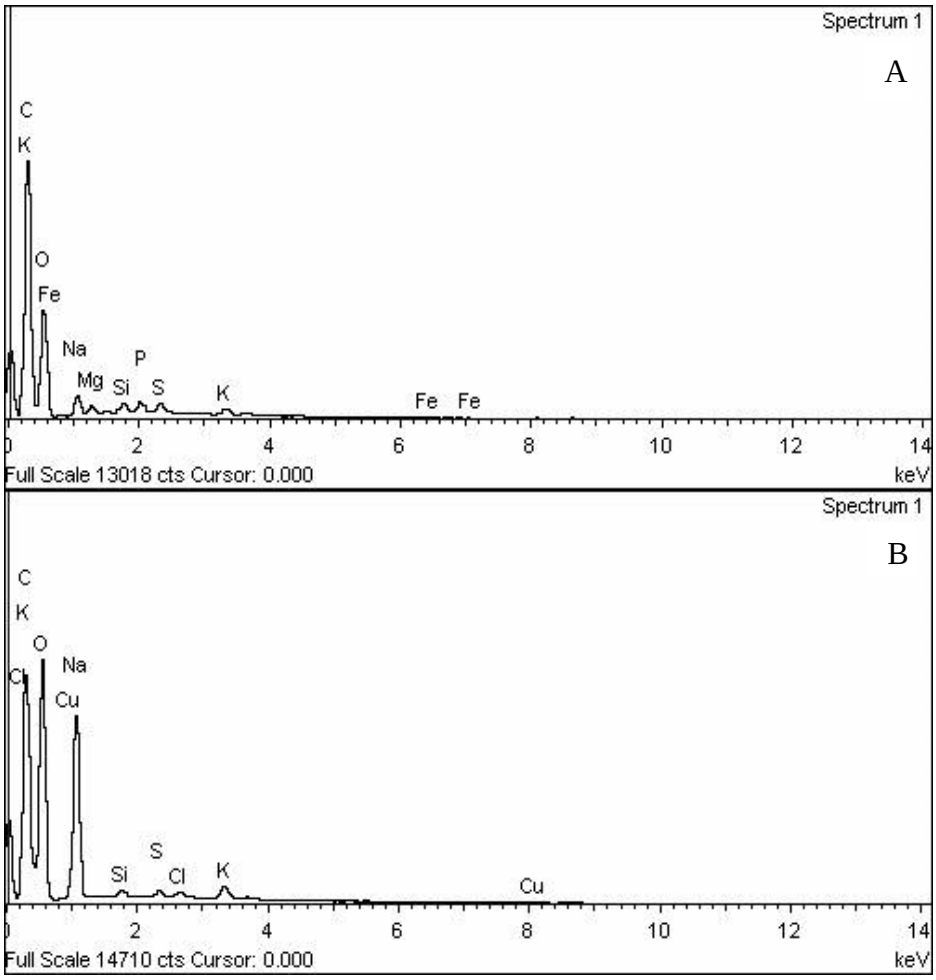

Figure.4. SEM-EDX elemental analysis of *Microcystis* biomass and isolated EPS. (A) *Microcystis* biomass (B) EPS

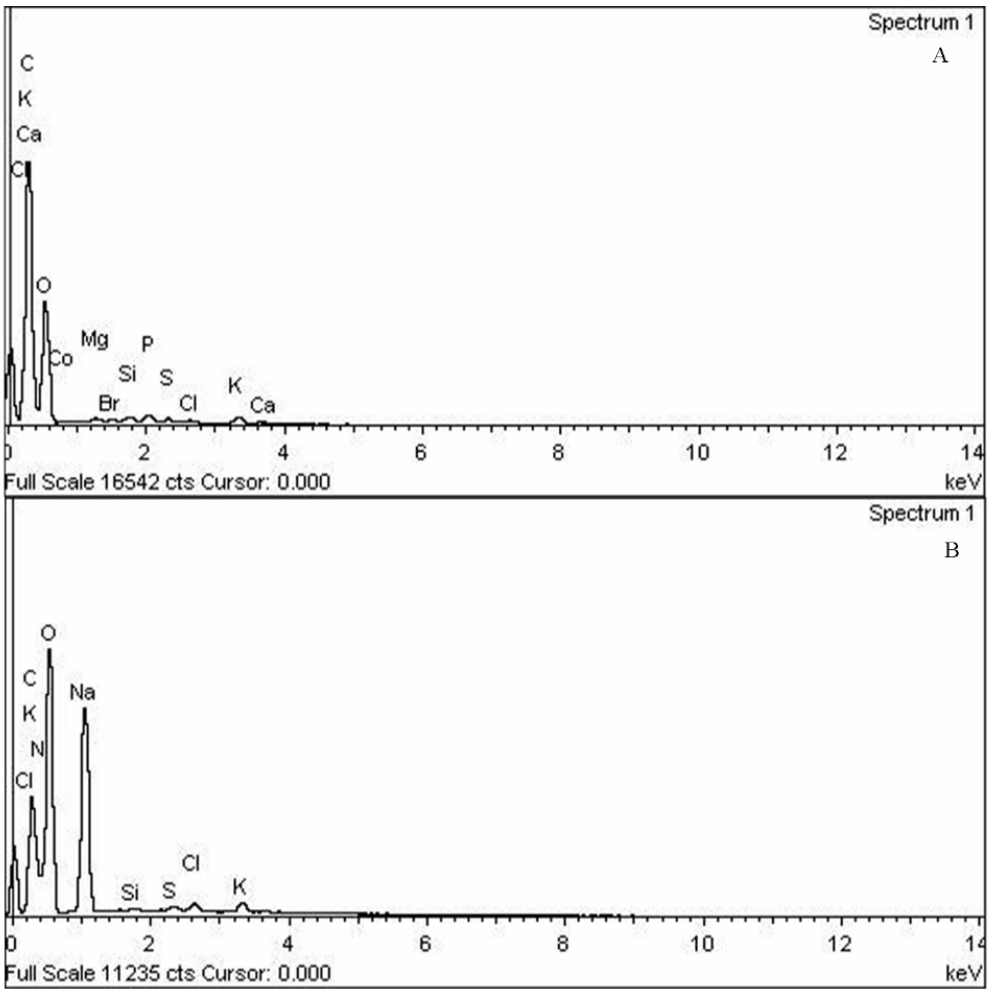

Figure.5. SEM-EDX elemental analysis of *Anabaena* biomass and isolated EPS. (A) *Anabaena* biomass (B) EPS.

The analysis identified various cations and trace elements in *A. doliolum's* biomass and EPS. The biomass contained magnesium (Mg) (0.22%) and silicon (Si) (0.27%), which might contribute to structural stability and enzymatic functions. The EPS displayed a broader spectrum of elements, including phosphorus (P), sulfur (S), chlorine (Cl), potassium (K), and even trace amounts of bromine (Br) and calcium (Ca). The presence of these elements, particularly Na at a considerably higher level (4.75%) compared to the biomass (absent), warrants further investigation into their potential roles within the EPS.

Table 2. Elemental Composition of *Microcystis* Biomass and its EPS Determined by SEM-EDX Analysis

Elements	*Microcystis* Biomass		EPS	
	Weight (%)	Atomic %	Weight (%)	Atomic %
C K	61.97	69.32	45.38	54.29
O K	34.44	28.92	43.50	39.07
Na K	1.39	0.81	9.76	6.10
Mg K	0.40	0.22	-	-
Si K	0.37	0.18	0.23	0.12
P K	0.46	0.20	-	-
S K	0.46	0.19	0.21	0.09
K K	0.37	0.13	0.52	0.19
Fe K	0.14	0.03	-	-
Cl K			0.22	0.09
Cu K			0.19	0.04

Note: Values are presented as both weight percentage and atomic percentage.

Table 3. Elemental Composition of *Anabaena* Biomass and its EPS Determined by SEM-EDX Analysis

Elements	*Anabaena* Biomass		EPS	
	Weight (%)	Atomic %	Weight (%)	Atomic %
C K	53.50	61.05	34.66	43.56
O K	44.51	38.13	49.52	46.72
Mg K	0.22	0.12	-	-
Na K	-	-	13.40	8.80
Si K	0.27	0.13	0.57	0.31
P K	0.42	0.18	-	-
S K	0.21	0.09	0.22	0.10
Cl K	0.17	0.07	0.24	0.10
K K	0.46	0.16	0.54	0.21
Cu K	-	-	0.28	0.07
Zn K	-	-	0.26	0.06
Co K	0.00	0.00	-	-
Br L	0.15	0.03	0.17	0.03
Ca K	0.11	0.04	0.12	0.05

Note: Values are presented as both weight percentage and atomic percentage.

3.5. Surface Image Characterization of EPS Extracted by Transmission Electron Microscopy (TEM)

The TEM image of the heavy metal ions absorbed on the surface of the EPS are given in the figure 6 (*Microcystis* EPS) and figure 7 (*Anabaena* EPS). The entry or accumulation of heavy metal ions into the cell were partially prevented by the presence of EPS envelope because of its binding affinity to heavy metal ions which may leads to metals homeostasis (Baptista and Vasconcelos 2006).

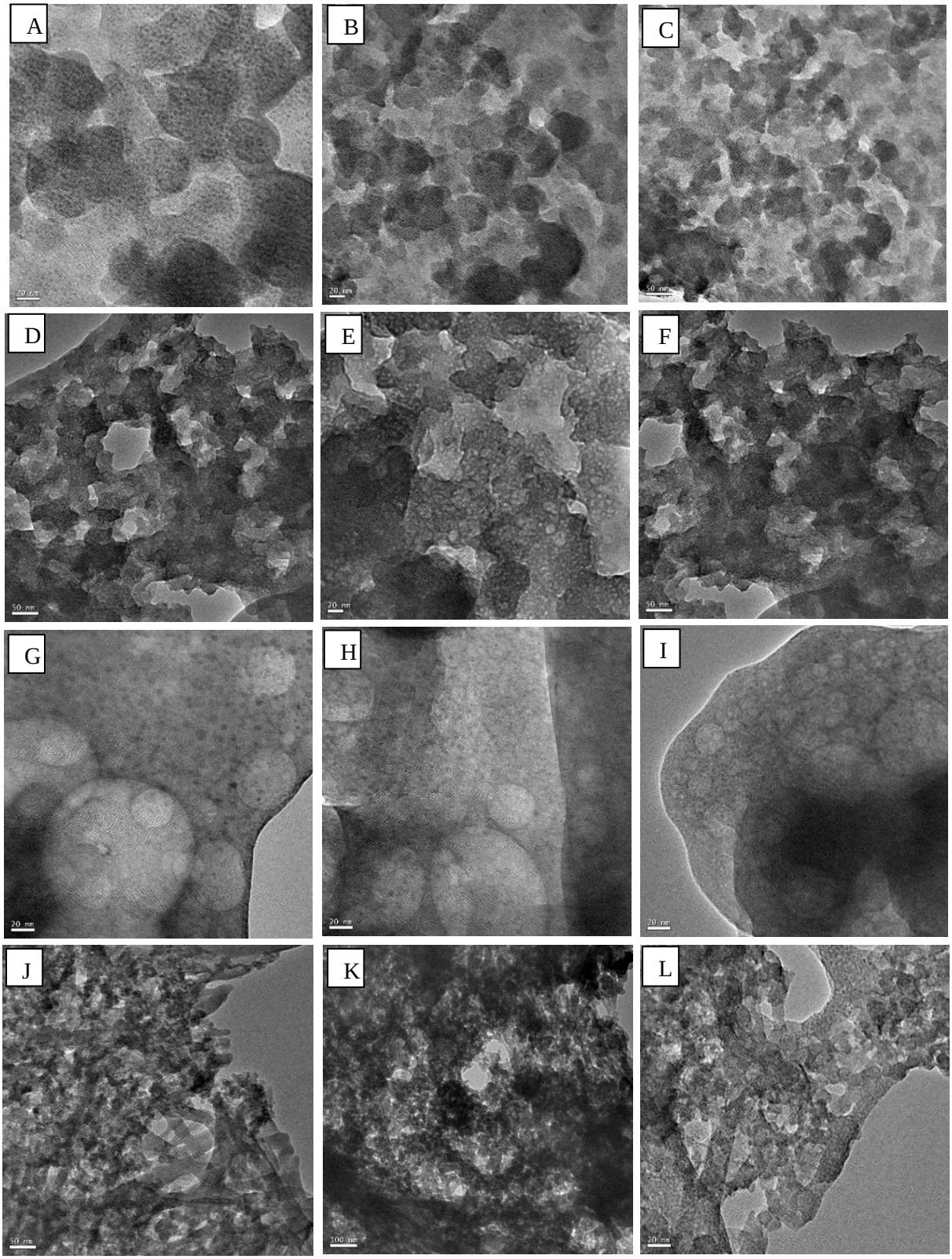

Figure.6. TEM micrograph image of *Microcystis* EPS: (A-C) Untreated, (D-F) Cd^{2+} treated, (G-I) Cu^{2+} treated and (J-L) Ni^{2+} treated.

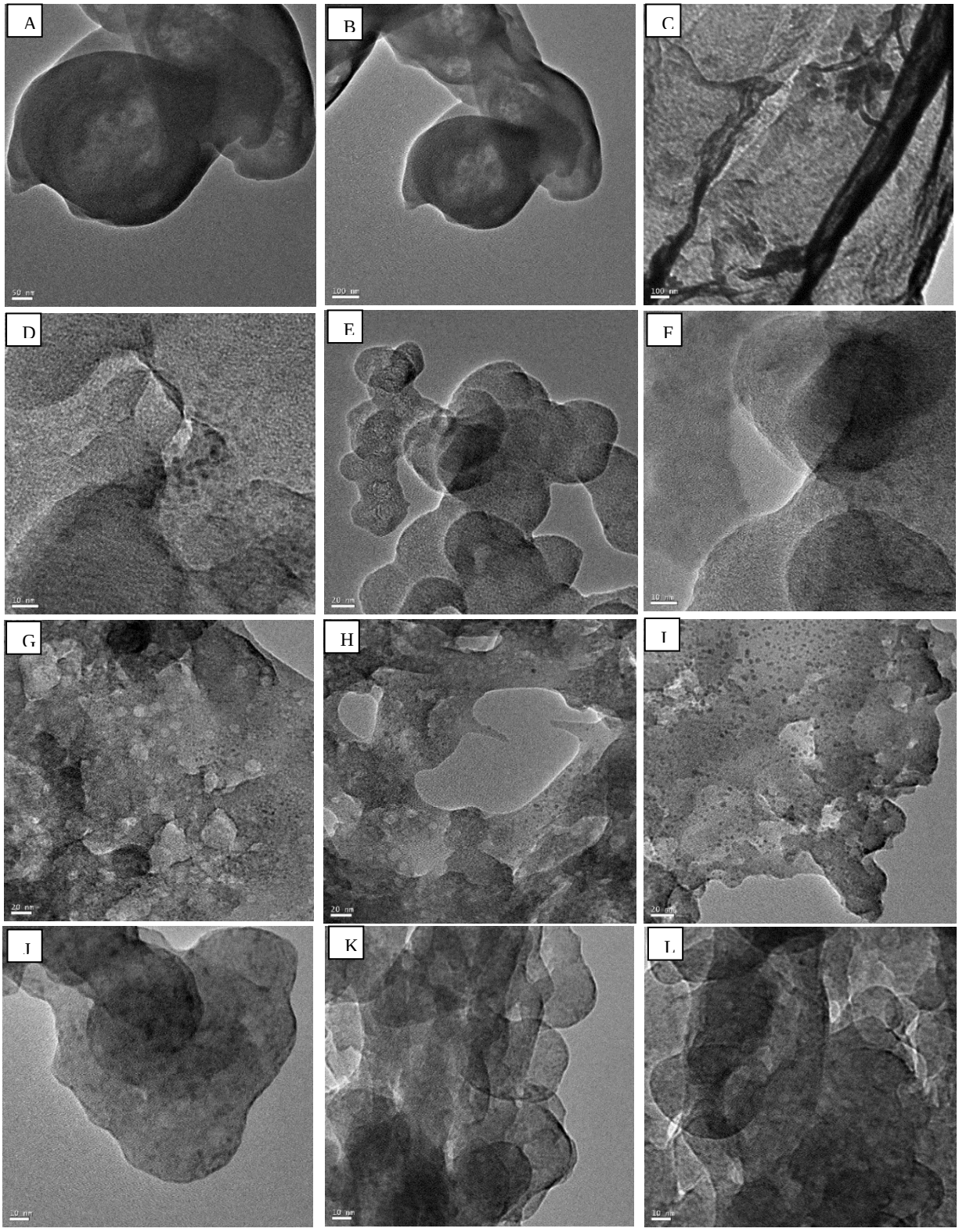

Figure.7. TEM micrograph image of *Anabaena* EPS: (A-C) Untreated, (D-F) Cd^{2+} treated, (G-I) Cu^{2+} treated and (J-L) Ni^{2+} treated.

The micrograph images of EPS from untreated *Microcystis aeruginosa* shows a smooth surface with various small dark spot. The transformation of the surface is clearly visible for Cd^{2+} treated *Microcytis* EPS. The surface was rough and the porous structure of irregular shape and size can be observed. The peculiar transformation in the Cu^{2+} treated in *Microcystis* EPS was the formation of several big and small, spherical or oval shapes. The surface structure of Ni^{2+} treated *Microcystis* EPS show some web-like structure, it has very irregular structure.

The TEM micrograph 2D image of untreated EPS from *Anabaena doliolum* shows wrinkle and robust surface. From the TEM image of Cd^{2+} treated Ana-EPS we can observe the various dark spot which may be the Cd^{2+} ions deposition, one part of surface shows complete dark which may be because of Cd^{2+} ions accumulation. There is no abnormality in the surface can be observe. Cu^{2+} is important micronutrients for all organisms, but the excess amount of Cu^{2+} have caused severe damage (Ma et al. 2009). Cu^{2+} treated *Anabaena* EPS image shows visible ultra-structural change in the surface of EPS. The surface shows to have spiny shape with several porous structures of irregular shape and size. *Anabaena* EPS Ni^{2+} treated also shows the structural change on the EPS surface. A transparent small circular round spot can be observed from the surface which may be the deposition of Ni^{2+} on EPS.

From the TEM image analysis, it has been found that the surface images of both the *Anabaena* EPS and *Microcystis* EPS are not similar. All the heavy metal-treated EPS shows changes in the surface structure differently for each heavy metal treated. The heavy metal-scavenging activity of EPS produced metal precipitation in polymeric aggregates from contaminated environments, followed by metal complexation and chelation.

3.6. Functional Group Identification by FTIR Analysis

In this study, we employed Fourier Transform Infrared (FTIR) spectroscopy to unveil the intricate molecular alterations occurring in *Microcystis* native biomass/EPS during interactions with Cu^{2+}, Cd^{2+} and Ni^{2+} **(**Figure 8**)**. Our FTIR spectra presented distinctive absorption peaks, providing valuable insights into the underlying mechanisms of metal adsorption. At 450.1 cm^{-1}, a peak associated with metal-oxygen

(M-O) bonds, attributed to metal oxides or hydroxides. The peak at 766.2 cm^{-1}, linked to aromatic C-H bending vibrations, exhibited reduced absorption after Cu^{2+}, Cd^{2+} and Ni^{2+} biosorption, suggesting interactions with aromatic structures. This points to the likely binding of Cu^{2+}, Cd^{2+} and Ni^{2+} with aromatic rings through π-electron interactions, causing a decrease in absorption intensity.

Furthermore, the peak at 1220.8 cm^{-1}, corresponding to C-O stretching vibrations (Cheah et al. 2023), exhibited a slight decrease after Cu^{2+}, Cd^{2+} and Ni^{2+} biosorption, indicating coordination of metals with C-O bonds and potential alterations in the electronic environment of associated functional groups. The peak at 1640.3 cm^{-1}, linked to C=O stretching vibrations, displayed lowered absorption, suggesting binding of Cu^{2+}, Cd^{2+} and Ni^{2+} to carbonyl oxygen atoms (Smječanin et al. 2023), potentially impacting electronic and vibrational properties or it might be attributable to N-H bending vibrations linked with protein compounds found in EPS. An unexpected peak at 2348.2 cm^{-1}, related to atmospheric CO_2 stretching vibrations (Tkachenko and Niedzielski 2022), decreased, implying Cu^{2+} and Ni^{2+} interaction with CO_2 on the biomass surface, potentially involving electrostatic forces. Lastly, the peak at 3297.5 cm^{-1}, associated with O-H stretching vibrations in hydroxyl groups (Kavita et al., 2014), decreased after Cu^{2+}, Cd^{2+} and Ni^{2+} biosorption, indicating potential binding to hydroxyl groups and suggesting alterations in hydrogen bonding patterns and electronic properties.

FTIR has also been utilised to identify the molecular interaction of Cu^{2+}, Cd^{2+} and Ni^{2+} with *A. doliolum* biomass and EPS as it provides information on the sample's chemical composition and functional group. Figure 9 shows the various absorption peaks, which provide useful details into the underlying mechanism of metal adsorption onto *A. doliolum* biomass and EPS. The prominent peak at 450.1 cm^{-1} correspond to metal-oxygen (M-O) bond, attributed to metal oxides or hydroxides that's indicates the binding of Cu^{2+} ions to hydroxyl or oxide groups present on the biomass. Metal ions such as Cu^{2+} can create metal-oxygen bonds with hydroxyl or oxide functional groups in biomass, resulting in visible alterations of FTIR spectrum.

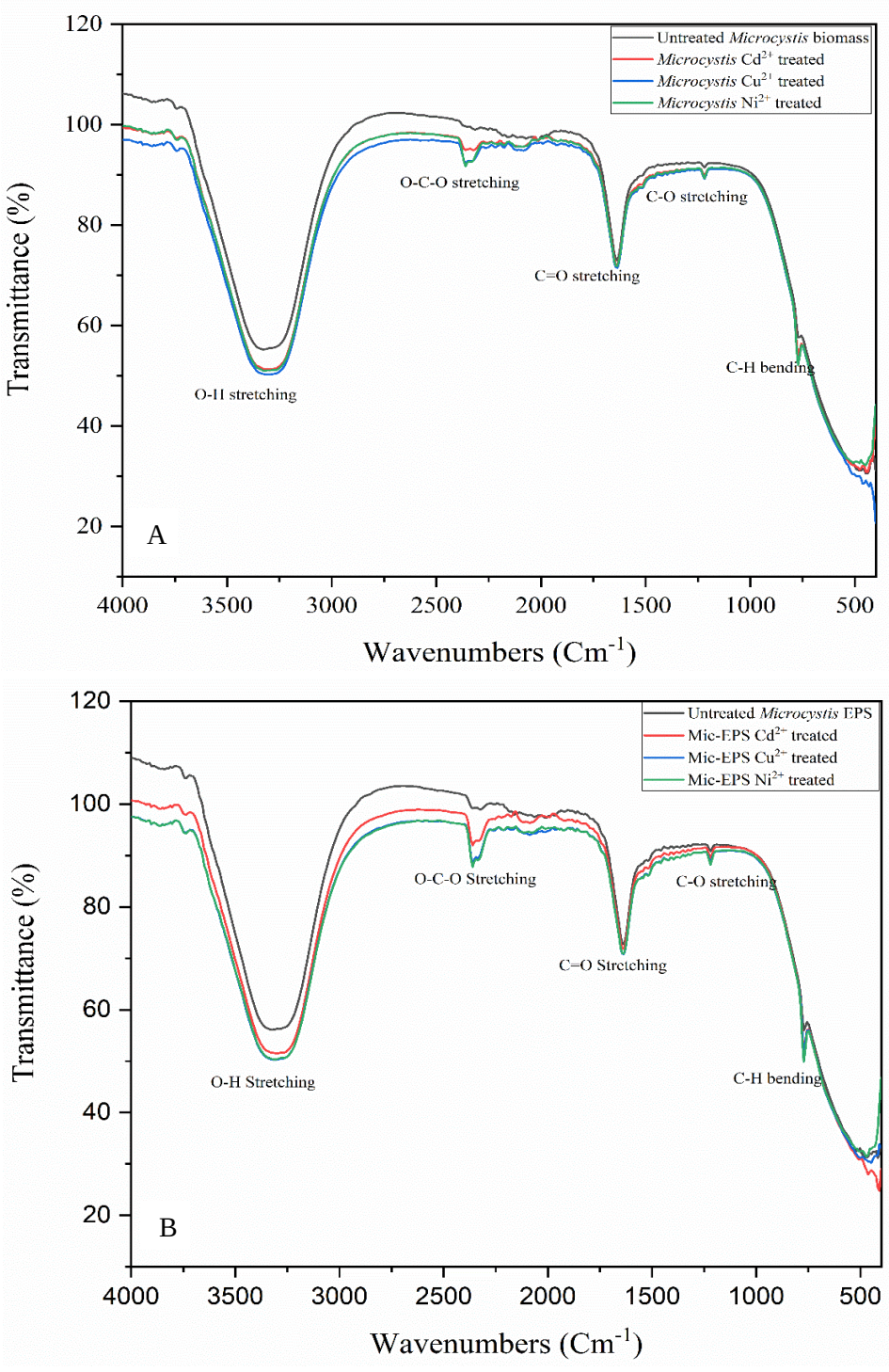

Figure.8. Fourier transform infrared (FTIR) analysis. (A) Comparative spectra of *M. aeruginosa* before and after exposure to Cd^{2+}, Cu^{2+} and Ni^{2+} ions. . (B) Comparative spectra of *M. aeruginosa* extracellular polymeric substances (EPS) before and after exposure to Cd^{2+}, Cu^{2+} and Ni^{2+} ions.

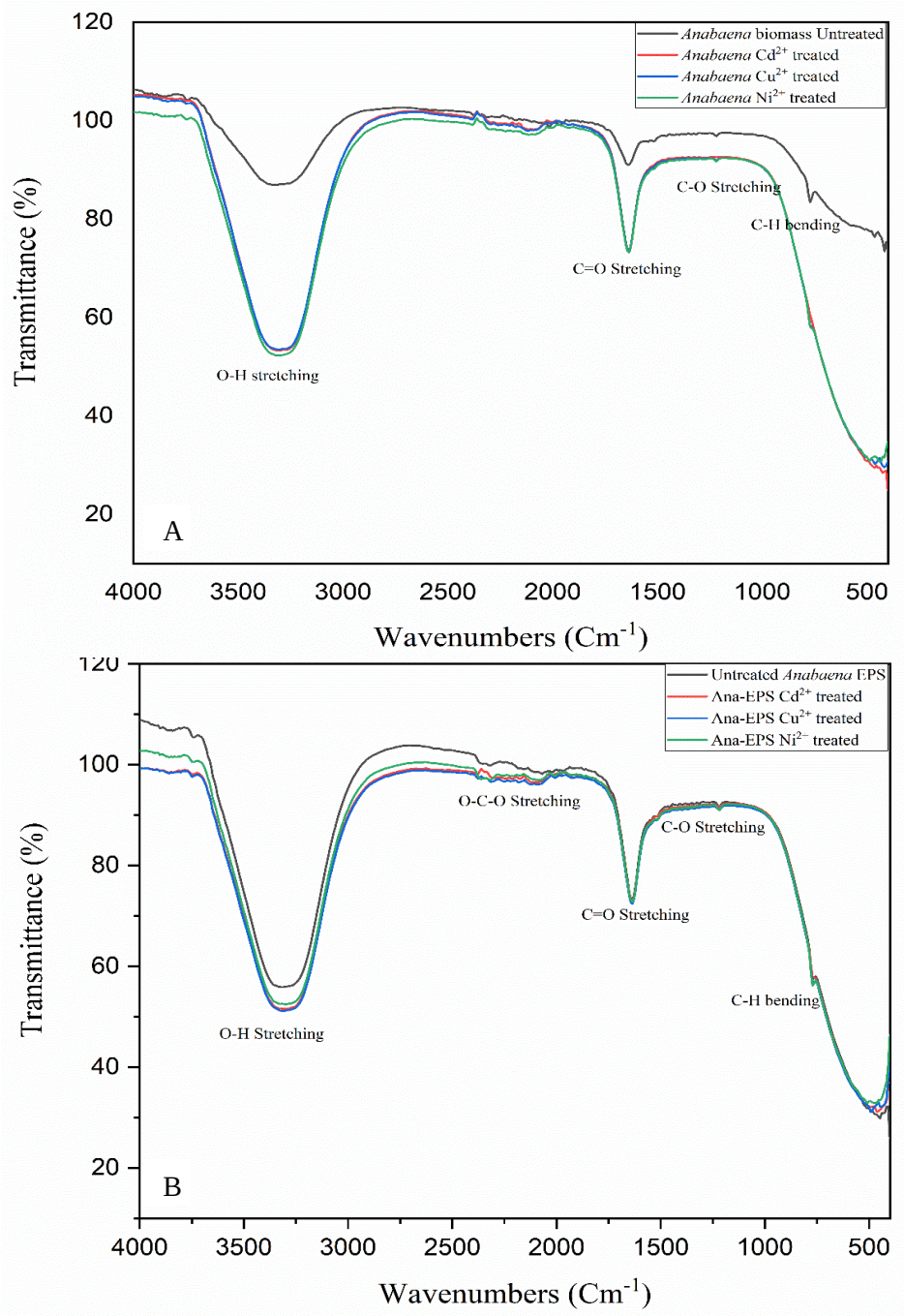

Figure.9. Fourier transform infrared (FTIR) analysis (A) Comparative spectra of *A. doliolum* before and after exposure to Cd^{2+}, Cu^{2+} and Ni^{2+} ions. (B) Comparative spectra of *A. doliolum* extracellular polymeric substances (EPS) before and after exposure to Cd^{2+}, Cu^{2+} and Ni^{2+} ions.

The decreased value in absorbance at this peak indicates a decrease in the strength of M-O bonds caused by metal ion binding to these functional groups. The peak at 766.5 cm^{-1} corresponds to C-H bending vibration, which might be caused by the existence of an aromatic ring in the biomass. After biosorption of Cu^{2+}, Cd^{2+} and Ni^{2+}, there was a significant shift in the spectrum intensity, which suggests that is due to the interaction of metal ions with the aromatic rings in the biomass. Metal ions can attach to aromatic rings via π-electron interactions, resulting in a shift in vibrational characteristics in the spectrum.

The peak at 1220.8 cm^{-1} can be attributed to C-O stretching vibration in the glycosidic linkages of polysaccharide chains. This spectrum reveals the presence of carbohydrate-based components, such as polysaccharides and glycoproteins, which constitute vital extracellular matrix components that have essential functions in microbial biofilms. A sharp peak at 1640.5 cm^{-1} relates to C=O stretching vibrations associated with amide bonds, or it might be attributable to N-H bending vibrations linked with protein compounds found in EPS. The peak at 2348.2 cm^{-1} correspond to O-C-O stretching vibration which is typically associated with absorption of atmospheric carbon dioxide gas (CO_2). A broad spectrum at 3297 cm^{-1} corresponds to O-H stretching which is particularly associated with hydroxyl groups. The presence of hydroxyl groups determines the hydrophilic nature and potential interaction with water and other polar compounds.

3.7. Liquid Chromatography-Mass Spectrometry (LCMS) Compounds Analysis

Liquid Chromatography-Mass Spectrometry (LCMS) analysis offers a powerful tool to examine the intricate composition of EPS (extracellular polymeric substances) isolated from *Microcystis* and *A. doliolum* (Tables 3 and 4). By dissecting these complex mixtures, we can gain valuable insights into the building blocks that define these essential components.

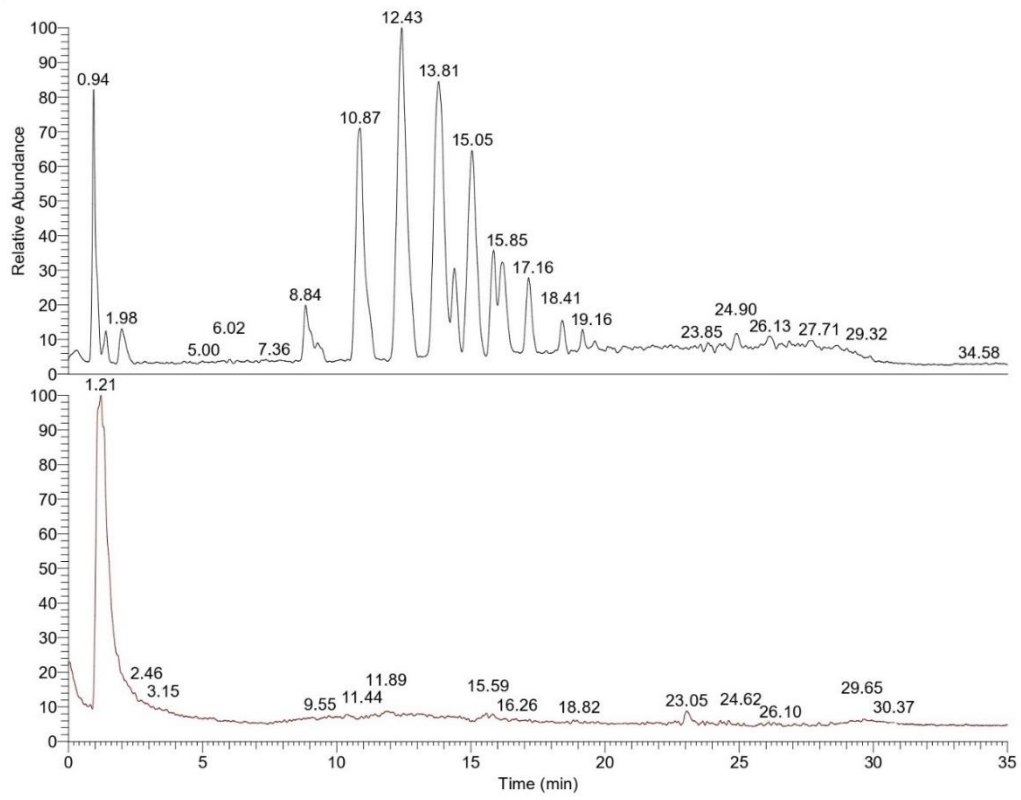

Figure.10. Liquid Chromatography- Mass Spectrometry (LCMS) chromatogram of isolated EPS from *M. aeruginosa*.

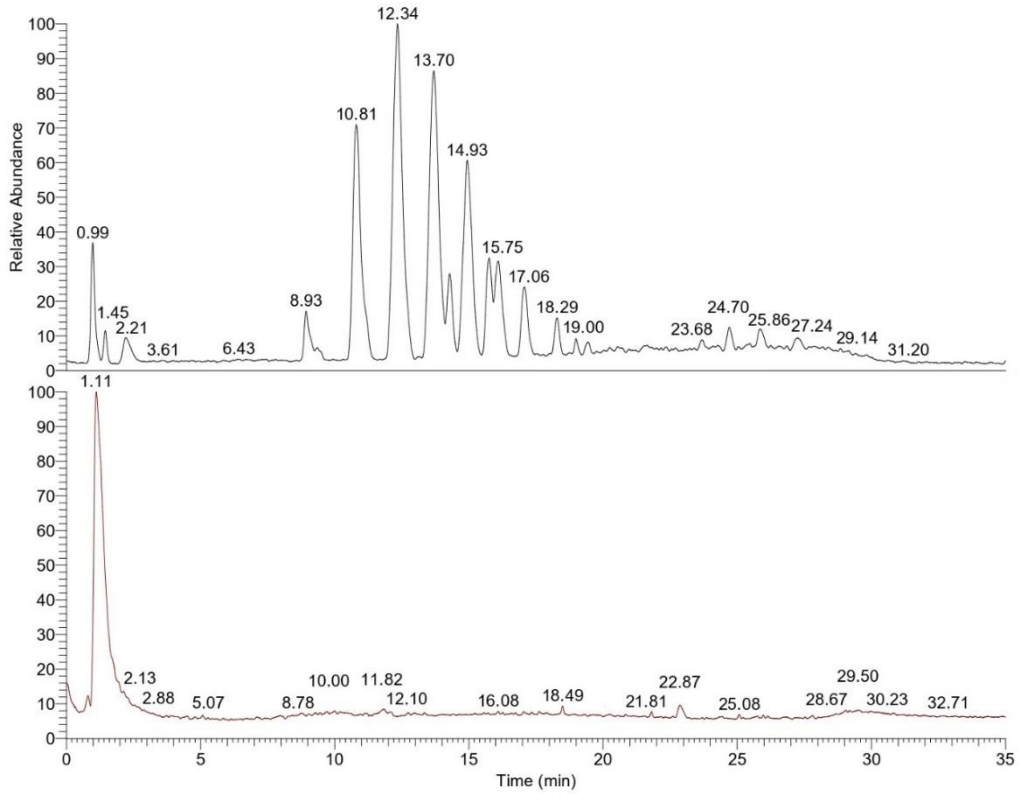

Figure.11. Liquid Chromatography- Mass Spectrometry (LCMS) chromatogram of isolated EPS from *A. doliolum*.

Table 4. LCMS Compound Analysis of *Microcystis* EPS

Compound names	Formula	Annotation delta mass (ppm)	Molecular weight	Retention time (min)
ile-val-val-lys	C_{22} H_{43} N_5 O_5	-4.77	457.32424	13.769
ile-val-val-lys	C_{22} H_{43} N_5 O_5	-4.77	457.32424	14.222
asn-lys-lys	C_{16} H_{32} N_6 O_5	-1.16	388.24297	14.393
Gly-Gly-Arg	C_{10} H_{20} N_6 O_4	-0.69	288.15441	9.396
thr-ala-arg	C_{13} H_{26} N_6 O_5	-1	346.19612	11.276
ile-ile-pro-val	C_{22} H_{40} N_4 O_5	-4.75	440.29778	14.461
DL-Valine	C_5 H_{11} N O_2	1.39	117.07914	0.075
ser-pro	C_8 H_{14} N_2 O_4	-1.07	202.09514	7.98
DL-Valine	C_5 H_{11} N O_2	1.39	117.07914	0.681
DL-Valine	C_5 H_{11} N O_2	1.33	117.07913	1.15
Leucine	C_6 H_{13} N O_2	-0.29	131.09459	1.449
Pro-Leu	C_{11} H_{20} N_2 O_3	-0.83	228.1472	3.078
Leucine	C_6 H_{13} N O_2	-0.29	131.09459	1.106
DL-Proline	C_5 H_9 N O_2	1.24	115.06347	1.057

Table 5. LCMS Compound Analysis of *Anabaena* EPS

Compound names	Calculated Formula	Annotation delta mass (ppm)	Molecular weight	Retention time (min)
thr-ala-arg	C_{13} H_{26} N_6 O_5	-1.17	346.19606	10.781
Gly-Gly-Arg	C_{10} H_{20} N_6 O_4	-0.47	288.15447	9.392
thr-ala-arg	C_{13} H_{26} N_6 O_5	-1.17	346.19606	11.222
Pro-Leu	C_{11} H_{20} N_2 O_3	-0.96	228.14717	3.349
Phenylalanylproline	C_{14} H_{18} N_2 O_3	-0.86	262.13152	5.233
his-glu-glu	C_{16} H_{23} N_5 O_8	-4.09	413.15297	2.63
Val-pro	C_{10} H_{18} N_2 O_3	-0.62	214.13161	1.544
Leucine	C_6 H_{13} N O_2	-0.17	131.09461	1.48
Phe-pro-ala	C_{17} H_{23} N_3 O_4	-1.33	333.16841	5.854
Pro-Pro	C_{10} H_{16} N_2 O_3	-1.09	212.11586	1.394
ALA-PRO	C_8 H_{14} N_2 O_3	-0.45	186.10036	1.315
ser-pro	C_8 H_{14} N_2 O_4	-0.84	202.09519	8.179
MFCD00025555	C_9 H_{18} N_2 O_3	-0.36	202.13167	1.674
asp-gly-lys	C_{12} H_{22} N_4 O_6	-0.92	318.15364	2.111
gly-gly-gly-pro	C_{11} H_{18} N_4 O_5	-0.81	286.12749	1.636
DL-Phenylalanine	C_9 H_{11} N O_2	-0.91	165.07883	2.163
Gly-DL-Phe	C_{11} H_{14} N_2 O_3	-1.06	222.10021	2.833
Pro-Leu	C_{11} H_{20} N_2 O_3	-0.96	228.14717	2.77
gly-pro-pro	C_{12} H_{19} N_3 O_4	-1.12	269.13725	1.353
MFCD00025555	C_9 H_{18} N_2 O_3	-0.36	202.13167	2.589
n-Glycyl-DL-leucine	C_8 H_{16} N_2 O_3	-0.66	188.11597	1.747
glu-pro	C_{10} H_{16} N_2 O_5	-0.72	244.10575	1.303
DL-Proline	C_5 H_9 N O_2	1.24	115.06347	1.067

Microcystis EPS (Table 4)

Dipeptides (2 amino acids linked together) appear to be the most abundant component in *Microcystis* EPS, with examples like ile-val-val-lys and ile-ile-pro-val. Tripeptides (3 amino acids) are also present, as evidenced by thr-ala-arg. Several individual amino acids were identified. Leucine, an essential amino acid crucial for protein synthesis and cellular function, is present. Valine and isoleucine (present within dipeptides) belong to the BCAA group, potentially contributing to stress tolerance in *Microcystis*. The presence of phenylalanine (aromatic, potentially from a degraded protein) in some dipeptides hints at the diverse range of molecules incorporated into the EPS. Serine (part of ser-pro) is a polar amino acid that might contribute to interactions with water molecules and nutrient acquisition. Glycine (present in tripeptides and potentially other structures) is the smallest amino acid and can provide flexibility within the EPS matrix.

A. doliolum EPS (Table 5):

Compared to *Microcystis*, A. doliolum EPS exhibits a greater diversity of identified compounds. This suggests a more complex EPS structure in *A. doliolum*. Histidine (his-glu-glu) introduces a histidine group with an imidazole ring, potentially contributing to metal binding or pH regulation within the EPS. The presence of gly-gly-gly-pro suggests the presence of tetrapeptides (4 amino acids) in *A. doliolum* EPS, adding another layer of complexity compared to *Microcystis*.

The LCMS data from both organisms showed a detailed picture of the EPS composition. *Microcystis* EPS appears to be rich in dipeptides, potentially favoring a more rigid structure. In contrast, *A. doliolum* EPS exhibits a wider variety of molecules, including longer peptides and potentially unique components, suggesting a more intricate and adaptable EPS structure. These variations likely influence the physical properties, interactions with the environment, and overall functions of the EPS in each organism.

Understanding the specific functions of the identified amino acids and their arrangements within the EPS matrix would provide deeper insights into their ecological significance.

3.8. Probing Surface Chemistry of *A. doliolum* with Acid-Base Titration

This study utilized acid-base titration to quantify the surface proton binding sites of *A. doliolum* and *M. aeruginosa* (Figure 12). This technique sheds light on the surface properties of these cells. When cyanobacterial cells were suspended in an acidic solution, surfaces become exposed to an influx of hydrogen ions (H^+). These H^+ ions can interact with functional groups on the cell wall, leading to a process called protonation. Protonation can alter the surface charge of cell, potentially impacting other surface properties as well. Figure 12 likely depicts titration curve obtained during the acid-base titration experiment. As more acid is added to the culture suspension (increasing H^+ concentration), the solution's pH gradually decreases. The initial portion of the curve represents the buffering capacity of the cell surface functional groups as they progressively bind H^+ ions. A plateau or inflection point in the curve could indicate the saturation of these binding sites with H^+ ions, reducing the solution's ability to hold additional acid.

Table.6: Equivalence Point of pH Titration

	Biosorbents			
Heavy metals (mg L-1)	*Miccrocystis aeruginosa*	*Anabaena doliolum*	*Microcytis* EPS	*Anabaena* EPS
0	4.08±0.27	4.10±0.26	3.18±0.23	3.21±0.21
5 (Cd^{2+})	3.23±0.22	3.99±0.25	3.13±0.26	3.16±0.16
5 (Cu^{2+})	3.21±0.20	3.97±0.21	3.12±0.21	3.14±0.20
5 (Ni^{2+})	3.21±0.22	3.91±0.19	3.12±0.25	3.06±0.23

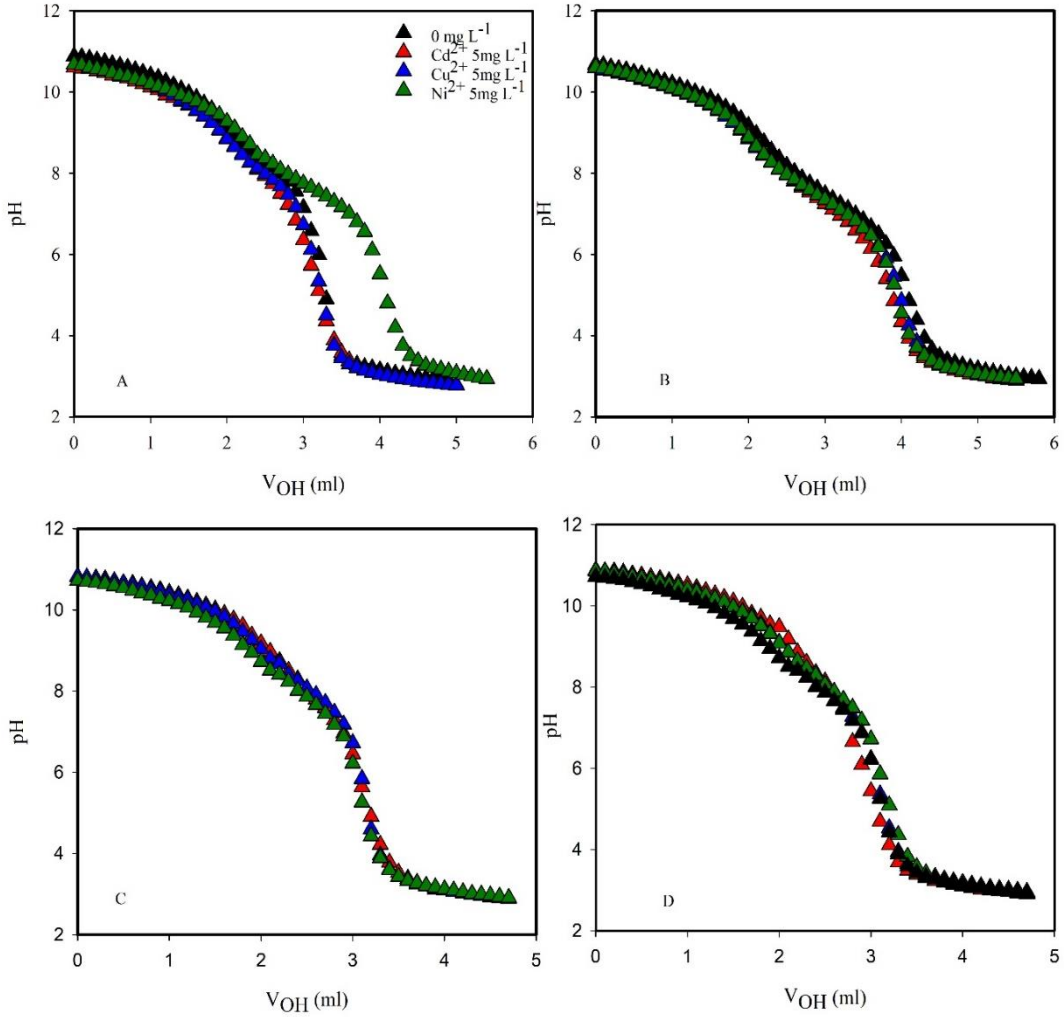

Figure 12. Surface protonation of cyanobacterial biomass and EPS assessed by acid-base titration. (A) *Microcystis* biomass untreated, Cd^{2+}, Cu^{2+} and Ni^{2+} treated, (B) *Anabaena* biomass untreated, Cd^{2+}, Cu^{2+} and Ni^{2+} treated, (C) *Microcystis* -EPS untreated, Cd^{2+}, Cu^{2+} and Ni^{2+} treated and (D) *Anabaena* EPS untreated, Cd^{2+}, Cu^{2+} and Ni^{2+} treated.

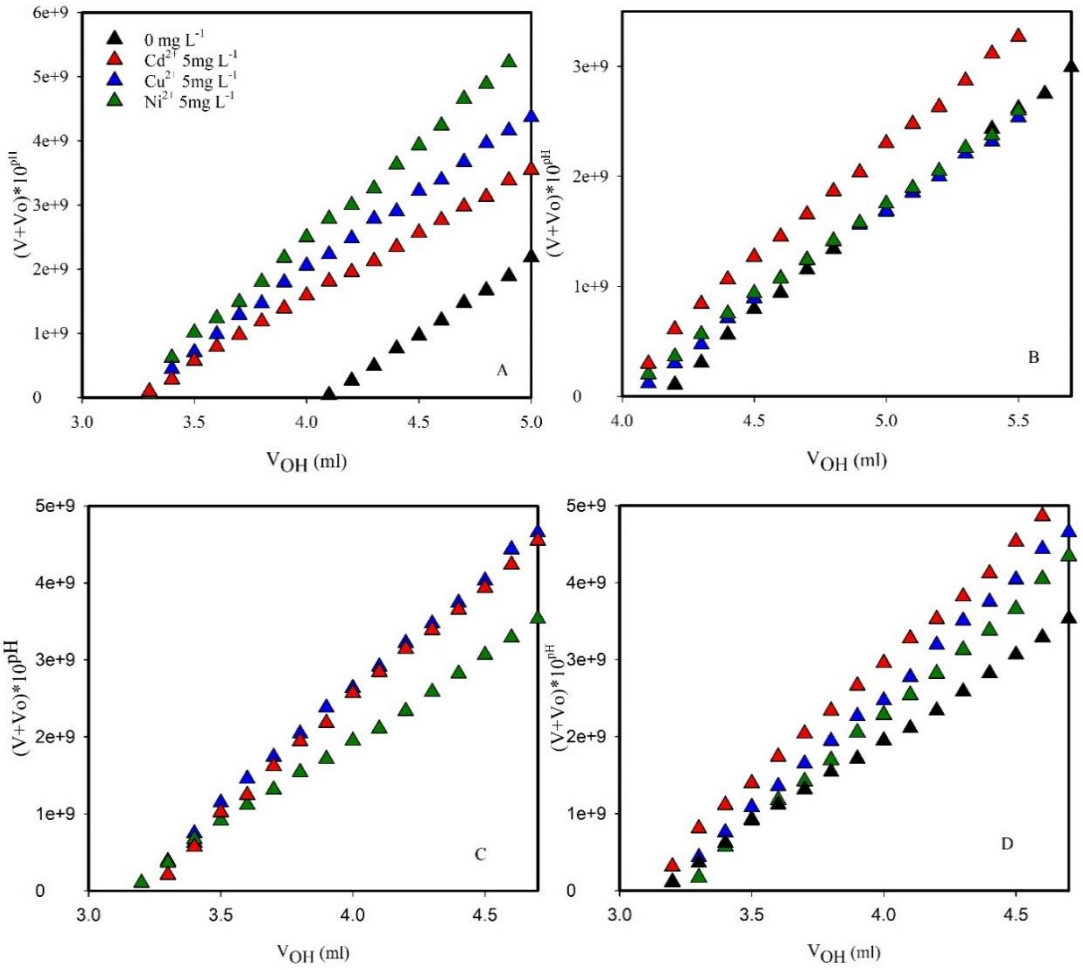

Figure.13. Equivalence point of pH titration for *M. aeruginosa*, *A. doliolum*, and EPS with and without metal treatment. (A) *Microcystis* biomass untreated, Cd^{2+}, Cu^{2+} and Ni^{2+} treated, (B) *Anabaena* biomass untreated, Cd^{2+}, Cu^{2+} and Ni^{2+} treated, (C) *Microcystis* EPS untreated, Cd^{2+}, Cu^{2+} and Ni^{2+} treated and (D) *Anabaena*-EPS untreated, Cd^{2+}, Cu^{2+} and Ni^{2+} treated.

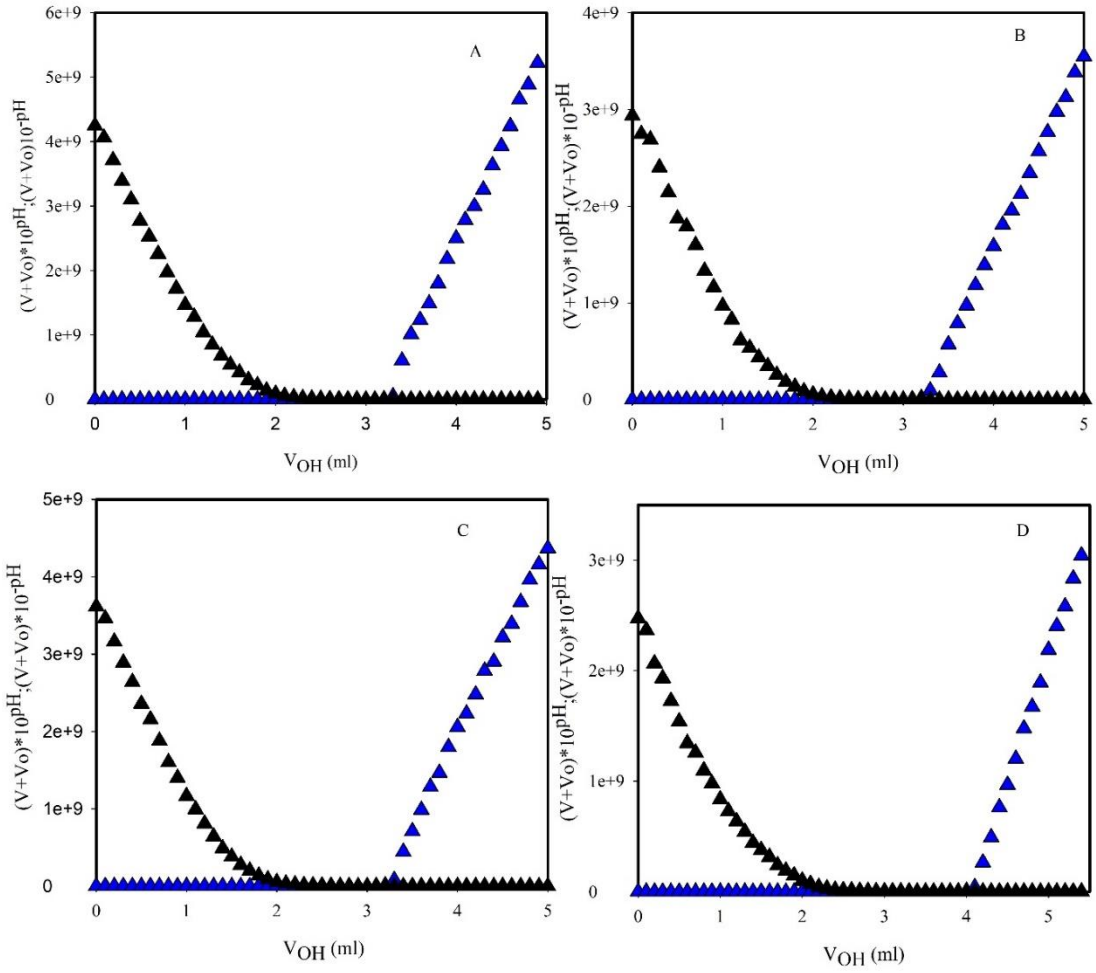

Figure.14. Gran's plot. (A) pH titration of untreated *M. aeruginosa* biomass, (B) pH titration of Cd^{2+} treated biomass (C) pH titration of Cu^{2+} treated biomass, and (D) pH titration of Ni^{2+} treated biomass.

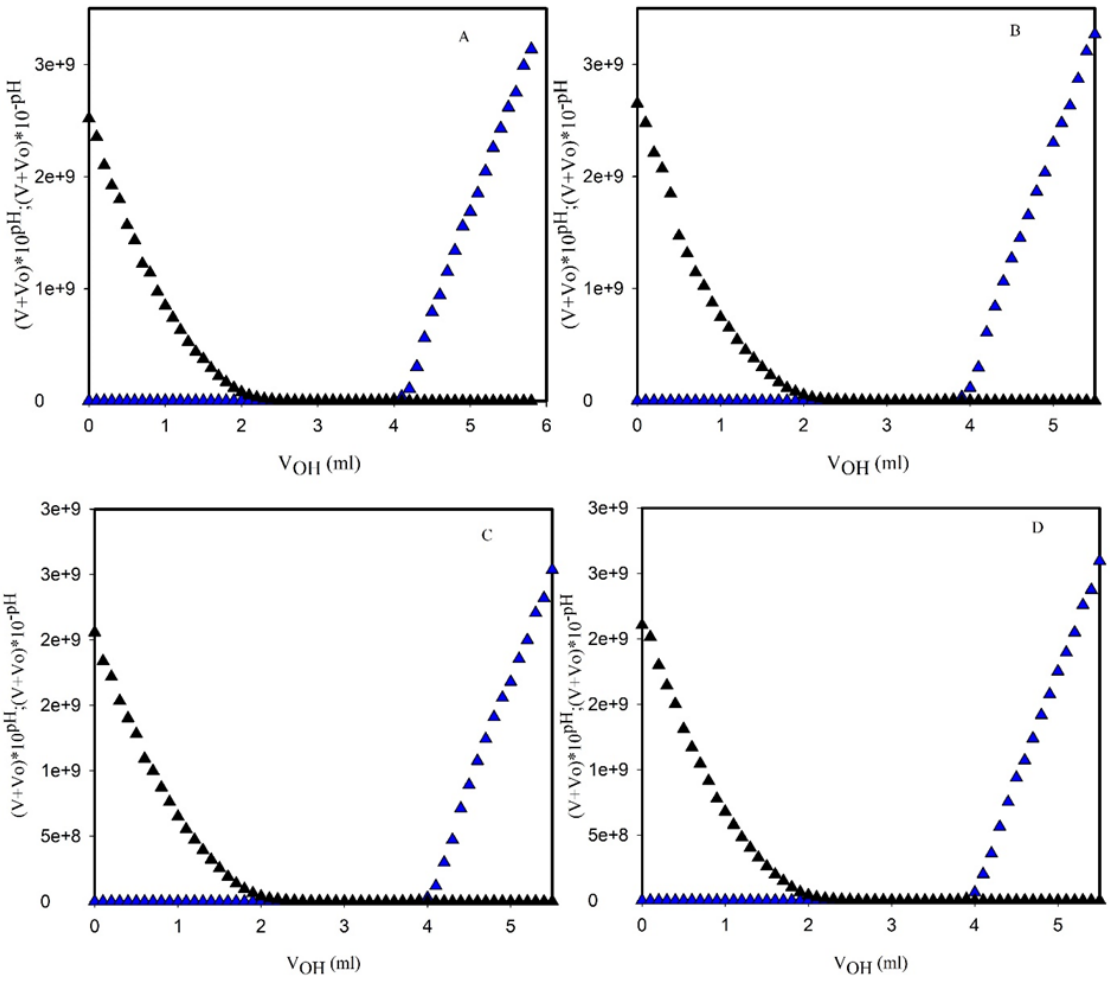

Figure.15. Gran's plot. (A) pH titration of untreated *A. doliolum* biomass, (B) pH titration of Cd^{2+} treated biomass (C) pH titration of Cu^{2+} treated biomass, and (D) pH titration of Ni^{2+} treated biomass.

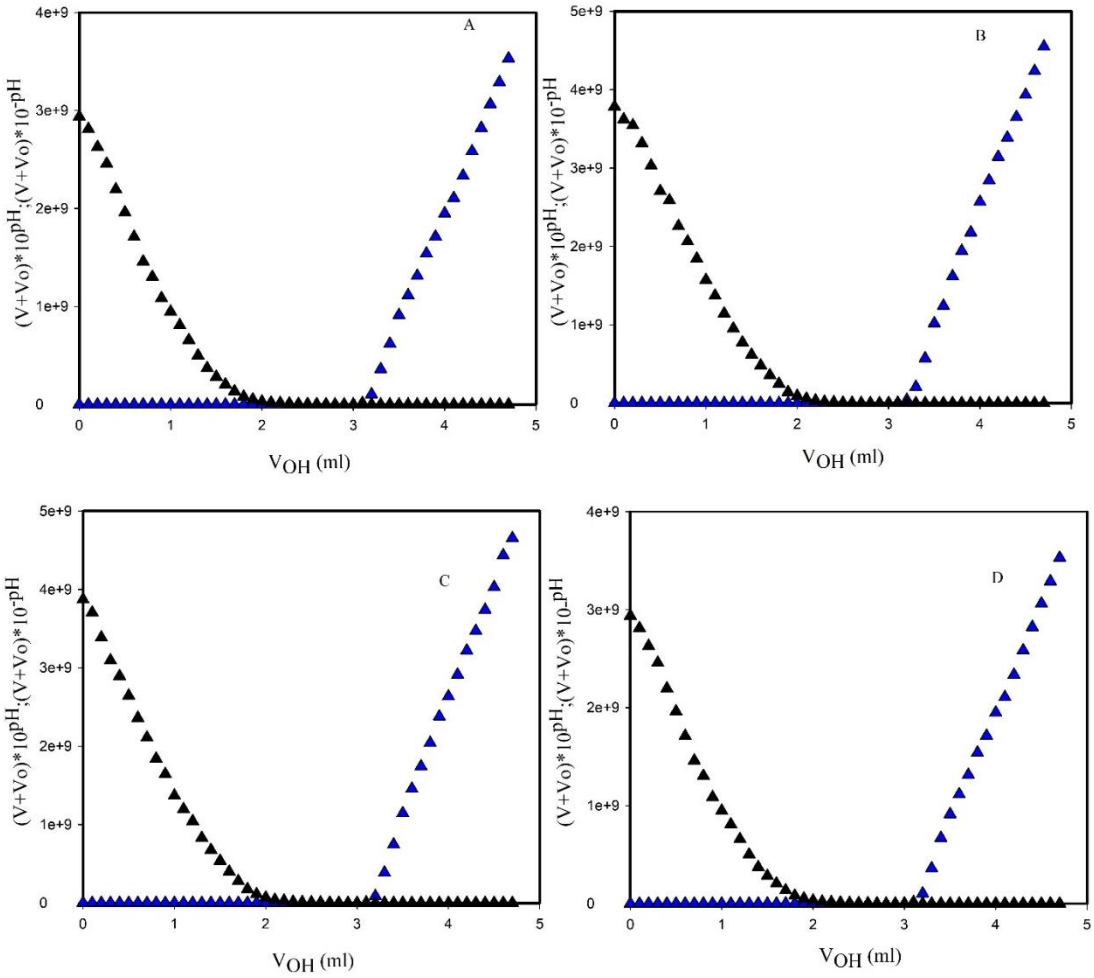

Figure.16. Gran's plot. (A) pH titration of untreated *Microcystis* EPS, (B) pH titration of Cd^{2+} treated EPS (C) pH titration of Cu^{2+} treated EPS, and (D) pH titration of Ni^{2+} treated EPS.

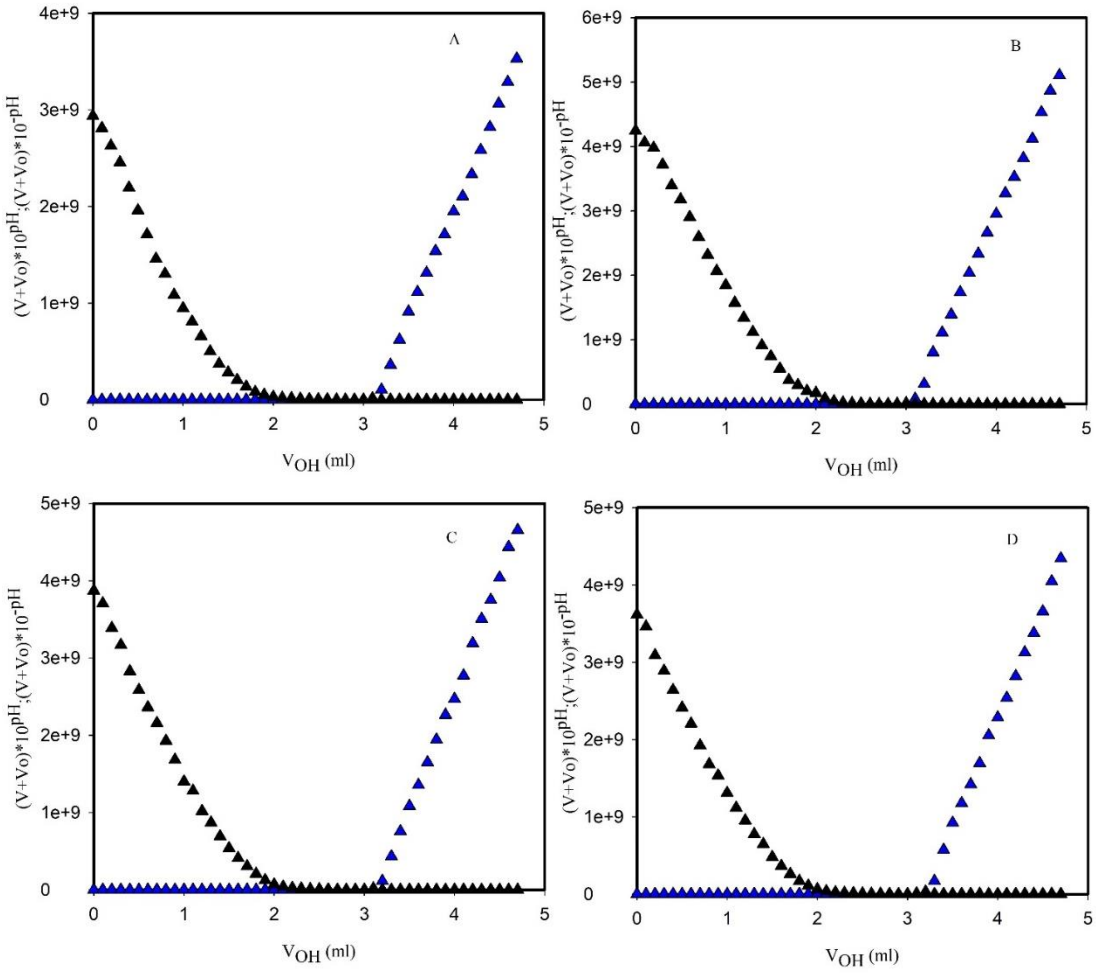

Figure.17. Gran's plot. (A) pH titration of untreated *Anabaena* EPS, (B) pH titration of Cd^{2+} treated EPS (C) pH titration of Cu^{2+} treated EPS, and (D) pH titration of Ni^{2+} treated EPS.

Table 6 and Figure 13 show the equivalence point (the point where all acid is neutralized) during the pH titration of *M. aeruginosa*, *A. doliolum* biomass and their EPS, with and without exposure to Cu^{2+}, Cd^{2+}, and Ni^{2+}. The equivalence point for metal-treated samples is generally lower compared to untreated samples. This suggests that metal binding might alter the surface properties of *A. doliolum*, potentially affecting the availability of functional groups for binding H^+ ions during the titration.

The experiment revealed that metal treatment (Cu^{2+}, Cd^{2+}, and Ni^{2+}) affects the surface properties of *A. doliolum*. This is evident from the changes in the equivalence point observed during the pH titration (Table 6, Fig 13). A lower equivalence point for metal-treated samples suggests alterations in the availability of functional groups for binding protons (H^+). This implies that metal binding might influence the surface charge or overall surface chemistry of biosorbent.

Gran's Plot (Figure 14-17) for *M. aeruginosa, A. doliolum, Microcystis* EPS and *Anabaena* EPS has been utilized for the determination of equivalence point in acid-base titration method which used linear approximation of the relationship between the pH and the titrant volume. On addition to basic graph plots of the pH against the volume of titrant supplied, Gran's plots logarithm of the titrant concentration (or volume) provides accurate measurement. It predicts on the basis that the potential and logarithm of titrant concentration exhibit a linear relationship around the equivalence point. The equivalency point was determined to be the point at which the plot shows a linear part. This linear part corresponds to the region where the change in potential with respect to the logarithm of the titrant concentration is most significant which is generally around the equivalence point.

3.9. Adsorption Studies

3.9.1 pH Optimization

This study investigated how pH influences the removal efficiencies of copper (Cu^{2+}), cadmium (Cd^{2+}), and nickel (Ni^{2+}) by *M. aeruginosa*, *A. doliolum* biomass, and their isolated EPS (extracellular polymeric substances) (Figure 18 and 19). For *M.*

aeruginosa, copper (Cu^{2+}) removal is most efficient (reaching 98%) at a pH of 6.5, but decreases at higher pH. Nickel (Ni^{2+}) removal is less affected by pH, staying relatively constant around 84% across the tested range (pH 2-9). Cadmium (Cd^{2+}) removal shows a unique trend, increasing significantly from 38% at pH 2 to a peak of 81% at pH 7, with a slight decline at even higher pH. *A. doliolum* exhibits a relatively stable copper (Cu^{2+}) removal efficiency across a range of pH values (2 to 9) (Figure 18 B). The removal efficiency remains fairly consistent, ranging from 70% to 76% with some slight fluctuations. This suggests that *A. doliolum* might have a broad range of functional groups or binding sites that can interact with Cu^{2+} ions regardless of the solution's pH within this range (2-9). Nickel (Ni^{2+}) removal by *A. doliolum* follows a somewhat increasing trend with respect to pH. There is a gradual increase in Ni^{2+} removal efficiency from 70% at pH 2 to 78% at pH 7.5, followed by a slight decrease at pH 9 (73%). *A. doliolum* might have functional groups that become more favorable for Ni^{2+} binding at higher pH values (up to pH 7.5). It is possible that at pH 9, a portion of the removed Ni^{2+} precipitates instead of remaining bound to the *A. doliolum*. Cd^{2+} removal efficiency exhibits a significant rise from 20% at pH 2 to a peak of 91% at both pH 7 and 8. This dramatic increase suggests a strong pH dependence on the binding of Cd^{2+} by *A. doliolum*. Cd^{2+} removal efficiency exhibits a significant rise from 20% at pH 2 to a peak of 91% at both pH 7 and 8. This dramatic increase suggests a strong pH dependence on the binding of Cd^{2+} by *A. doliolum*. At lower pH (2-4), some functional groups on *A. doliolum's* surface might be protonated (carrying a positive charge) and repel positively charged Cd^{2+} ions. As the pH increases (reaching 7 and 8), these functional groups may become deprotonated (carrying a negative charge), creating a more favorable electrostatic attraction for Cd^{2+} ions, leading to the observed surge in removal efficiency.

The investigation examined how pH influences metal removal by isolated EPS (extracellular polymeric substances) from *M. aeruginosa* (Figure 19 C) and *A. doliolum* (Figure 19 B). Both EPS displayed impressive initial removal efficiencies for copper (Cu^{2+}) and nickel (Ni^{2+}) at a low pH of 2.0 (around 90% and 80% for *M. aeruginosa* EPS and 80% and 90% for *A. doliolum* EPS, respectively). However, their behaviors diverged at higher pH. For *M. aeruginosa* EPS, Cu^{2+} removal remained stable up to pH 4 but then significantly decreased, suggesting a potential shift in

binding mechanisms or surface properties at higher pH. In contrast, Ni^{2+} removal by *M. aeruginosa* EPS exhibited a steady and consistent increase across the entire pH range (2-8), indicating a robust and pH-independent binding process. Cadmium (Cd^{2+}) removal by *M. aeruginosa* EPS followed a different trend, starting with a low removal rate (50%) at pH 2 and then rising significantly to a peak of 91% at pH 7 before a slight decrease at pH 9.

A. doliolum EPS also showed high initial removal efficiencies for Cu^{2+} and Ni^{2+} at pH 2.0. Unlike *M. aeruginosa* EPS, Cu^{2+} removal by *A. doliolum* EPS steadily increased with increasing pH, reaching a maximum at pH 6.0. This suggests a potential enhancement of binding sites or interactions favorable for Cu^{2+} at higher pH for this specific EPS. Ni^{2+} removal by *A. doliolum* EPS also showed a gradual increase, reaching its peak at a slightly higher pH (7.5) compared to Cu^{2+}. This indicates a progressive improvement in Ni^{2+} binding with increasing pH, but to a lesser extent than Cu^{2+}. Interestingly, Cd^{2+} removal by A. doliolum EPS mirrored the trend observed for M. aeruginosa EPS, starting low (56%) at pH 2 and reaching a maximum removal efficiency of 96% at pH 7 before a slight decrease at even higher pH (pH 9).

Overall, the isolated EPS from both *M. aeruginosa* and *A. doliolum* exhibited distinct pH-dependent removal patterns for Cu^{2+}, Ni^{2+}, and Cd^{2+}. While Ni^{2+} removal showed a more stable and consistent trend across the pH range, Cu^{2+} and Cd^{2+} removal efficiencies were more variable, suggesting a complex interplay between metal speciation, EPS surface properties, and binding mechanisms.

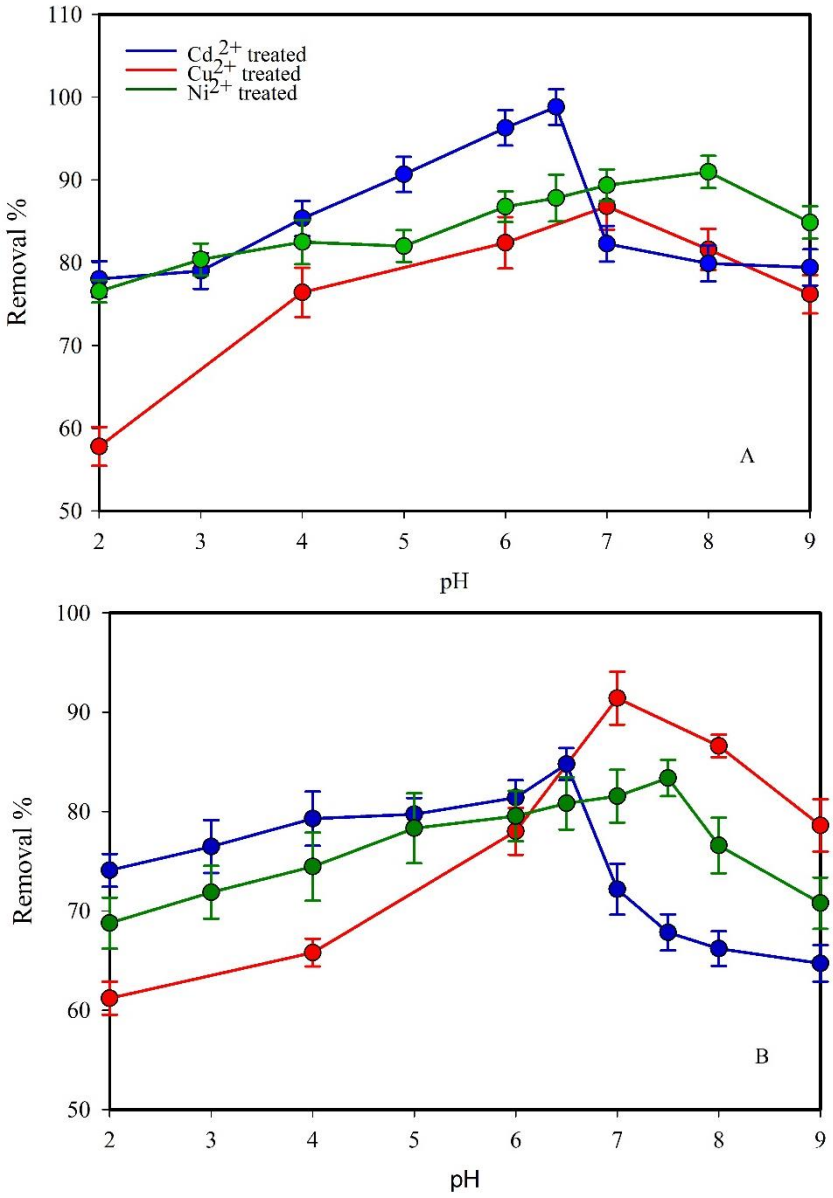

Figure.18. Impact of pH on metal removal efficiency (A) Native biomass of the cyanobacteria *M. aeruginosa* and (B) Native biomass of cyanobacteria *A. doliolum.* The experiments were carried out with an initial concentration of 5 mg L^{-1} for both Ni^{2+} and Cu^{2+}, maintaining a consistent incubation period of 1 h. The values shown represent the mean results from three replicates, accompanied by their corresponding standard deviations (SD).

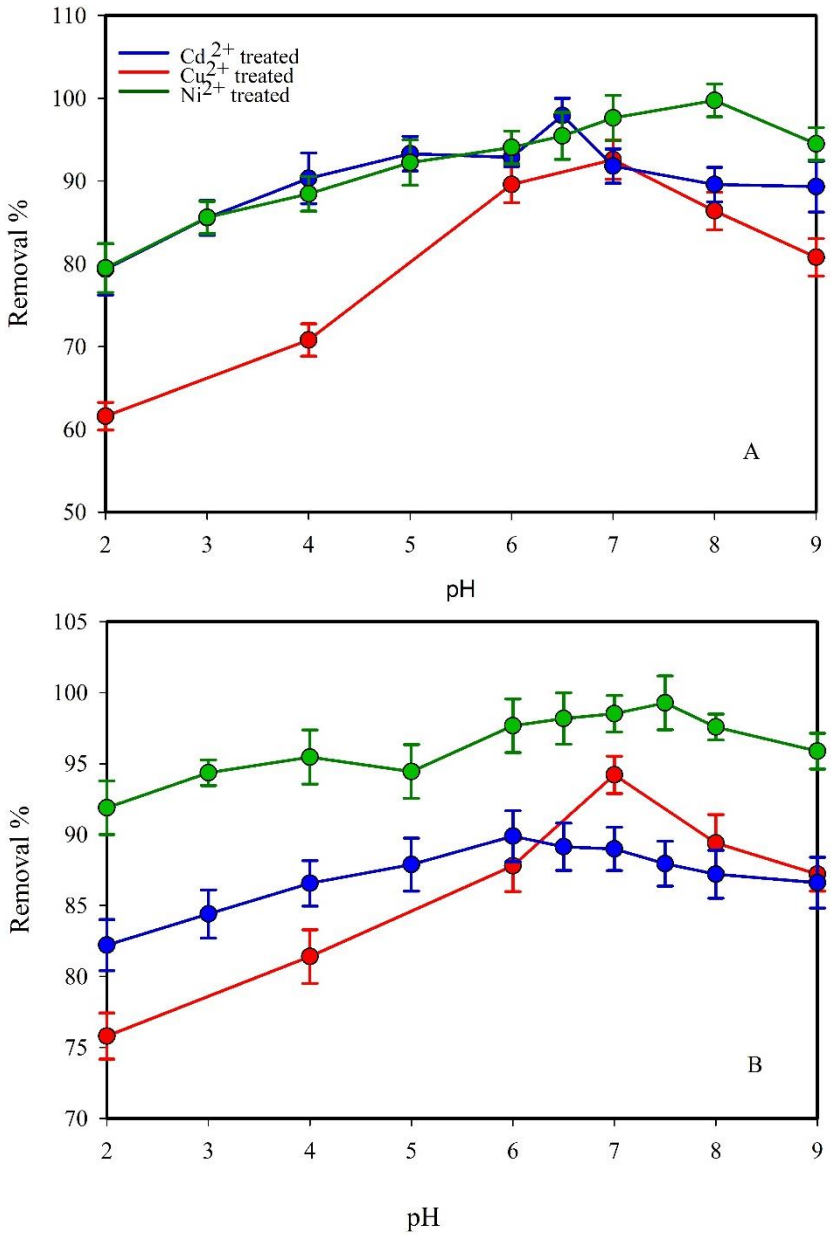

Figure.19. Impact of pH on metal removal efficiency. (A) EPS isolated from *M. aeruginosa* and (B) EPS isolated from *A. doliolum*. The experiments were carried out with an initial concentration of 5 mg L^{-1} for both Ni^{2+} and Cu^{2+}, maintaining a consistent incubation period of 1 h. The values shown represent the mean results from three replicates, accompanied by their corresponding standard deviations (SD).

3.9.2 Kinetic of Biosorption

This section describes the rate of metal uptake by *M. aeruginosa* and *A. doliolum* biomass, along with their isolated EPS (extracellular polymeric substances), through a time course study (Figures 20-23). The data is analyzed using two kinetic models: Pseudo-First-Order (PFO) and Pseudo-Second-Order (PSO). In figures the symbols represent data points and curves represent model predicted curve. We performed the non-linear curve fitting of the experimental data.

Sorption of all three tested metals (Cu^{2+}, Ni^{2+}, Cd^{2+}) was rapid, with over 90% occurring within the first 30-45 min. This suggests a quick initial binding of metal ions to the cell wall, likely through a passive extracellular process. Following the rapid initial uptake, the rate of sorption slowed down. This second phase might represent the active transport of metal ions into the cells.

Table.7. Kinetic Model Comparison for Ni^{2+}, Cu^{2+} and Cd^{2+} Biosorption using Native Biomass of *M. aeruginosa*

Kinetic models	Parameters	Ni^{2+}	Cu^{2+}	Cd^{2+}
Pseudo first order	q_e (mg g^{-1})	0.28±0.02	0.26±0.02	0.18±0.01
	k_1 (min^{-1})	0.16±0.01	0.18±0.01	0.11±0.01
	r^2	0.929	0.939	0.9257
Pseudo second order	q_e (mg g^{-1})	0.28±0.02	0.27±0.01	0.19±0.02
	k_2 (g mg^{-1} min^{-1})	2.22±0.12	3.09±0.19	1.37±0.09
	r^2	0.980	0.971	0.9841
Intraparticular diffusion	k_d (mg g^{-1} $min^{1/2}$)	0.0047±0.0003	0.0033±0.0002	0.0164±0.001
	I	0.096±0.01	0.096±0.01	0.123±0.01
	r^2	0.749	0.732	0.8088

Note: q_e represents equilibrium adsorption capacity, k_1 and k_2 are rate constants, k_d signifies intraparticle diffusion rate constant, and r^2 indicates coefficient of determination.

Figure 20 shows the kinetics of metal sorption by the living biomass of *M. aeruginosa*. Table 7 presents the parameters obtained by fitting the time-course data for *M. aeruginosa* to both Pseudo-First-Order and Pseudo-Second-Order models. The high R-squared (r^2) values (> 0.92) for both models suggest good agreement between the model predictions and the experimental data. However, the Pseudo-Second-Order model exhibited slightly higher R^2 values for all three metals, indicating a potentially better fit for this specific case. Overall, the time course study along with kinetic modeling suggests a two-phase sorption process for heavy metals by *M. aeruginosa*.

Table 8: Kinetic Model Comparison for Ni^{2+}, Cu^{2+} and Cd^{2+} Biosorption using Native Biomass of *A. doliolum*

Kinetic models	Parameters	Ni^{2+}	Cu^{2+}	Cd^{2+}
Pseudo first order	q_e (mg g^{-1})	0.28±0.02	0.27±0.02	0.1793±0.01
	k_1 (min^{-1})	0.17±0.01	0.16±0.01	0.1594±0.02
	r^2	0.9322	0.9100	0.9106
Pseudo second order	q_e (mg g^{-1})	0.29±0.02	0.28±0.018	0.1816±0.01
	k_2 (g mg^{-1} min^{-1})	2.40±0.38	2.20±0.334	2.2154±0.36
	r^2	0.9627	0.9873	0.9847
Intraparticular diffusion	k_d (mg g^{-1} $min^{1/2}$)	0.016±0.001	0.014±0.001	0.0013±0.0001
	I	0.24±0.02	0.2327±0.02	0.1628±0.02
	r^2	0.7242	0.7350	0.7484

Note: q_e represents equilibrium adsorption capacity, k_1 and k_2 are rate constants, k_d signifies intraparticle diffusion rate constant, and r^2 indicates coefficient of determination.

Figures 21, 22, and 23 depict similar trends for metal sorption by native biomass of *A. doliolum*, *M. aeruginosa EPS*, and *A. doliolum EPS*. Tables 8-10 present the results of fitting the time-course data for *A. doliolum* biomass and its isolated EPS,

along with *M. aeruginosa EPS,* to the same kinetic models used for *M. aeruginosa* (Pseudo-First-Order, Pseudo-Second-Order, and Intraparticle Diffusion).

Table 9: Kinetic Model Comparison for Ni^{2+}, Cu^{2+} and Cd^{2+} Biosorption using EPS of *M. aeruginosa*

Kinetic models	Parameters	Ni^{2+}	Cu^{2+}	Cd^{2+}
Pseudo first order	q_e (mg g^{-1})	9.79±0.44	9.49±0.46	7.21±0.59
	k_1 (min^{-1})	0.17±0.01	0.19±0.02	0.12±0.01
	r^2	0.937	0.912	0.9384
Pseudo second order	q_e (mg g^{-1})	9.20±0.46	9.64±0.51	7.45±0.64
	k_2 (g mg^{-1} min^{-1})	0.07±0.01	0.09±0.01	0.04±0.01
	r^2	0.971	0.981	0.9797
Intraparticular diffusion	k_d (mg g^{-1} $min^{1/2}$)	0.36±0.02	0.28±0.01	0.55±0.04
	I	8.59±0.46	8.58±0.52	5.31±0.41
	r^2	0.761	0.742	0.7800

Note: q_e represents equilibrium adsorption capacity, k_1 and k_2 are rate constants, k_d signifies intraparticle diffusion rate constant, and r^2 indicates coefficient of determination.

The R^2 values for both Pseudo-First-Order and Pseudo-Second-Order models remain high (>0.90 for most cases) across all tables, suggesting good agreement between the models and the experimental data. Similar to *M. aeruginosa*, Pseudo-Second-Order models generally exhibit slightly higher R^2 values for *A. doliolum* and EPS, indicating a potentially better fit.

For the *A. doliolum*, the R^2 values for the intraparticle diffusion model are slightly lower (Table 8) compared to the other two models, suggesting it might play a less significant role compared to *M. aeruginosa*.

The R^2 values for the Intraparticle Diffusion model are generally higher for EPS compared to *A. doliolum* and *M. aeruginosa* biomass, suggesting that diffusion within the EPS structure might be a more prominent factor influencing metal uptake Table 9, 10).

Table 10: Kinetic Model Comparison for Ni^{2+}, Cu^{2+} and Cd^{2+} Biosorption using EPS of *A. doliolum*.

Kinetic models	Parameters	Ni^{2+}	Cu^{2+}	Cd^{2+}
Pseudo first order	q_e (mg g^{-1})	9.80±0.60	9.40±0.55	7.1551±0.49
	k_1 (min^{-1})	0.16±0.01	0.14±0.01	0.1334±0.01
	r^2	0.9278	0.9043	0.9270
Pseudo second order	q_e (mg g^{-1})	10.03±0.62	9.69±0.53	7.3515±0.51
	k_2 (g mg^{-1} min^{-1})	0.06±0.004	0.04±0.003	0.0534±0.01
	r^2	0.9791	0.988	0.9835
Intraparticular diffusion	k_d (mg g^{-1} $min^{1/2}$)	0.44±0.03	0.55±0.04	1.7109±0.01
	I	8.33±0.48	7.55±0.47	0.8841±0.05
	r^2	0.7718	0.7733	0.7524

Note: q_e represents equilibrium adsorption capacity, k_1 and k_2 are rate constants, k_d signifies intraparticle diffusion rate constant, and r^2 indicates coefficient of determination.

Overall, the kinetic study suggests a two-phase sorption process for heavy metals by *M. aeruginosa* and *A. doliolum*, and potentially their EPS. The rapid initial phase reflects passive binding, followed by a slower phase that might involve active transport of metals into the cells. The specific contributions of these processes and the role of diffusion within the EPS structure vary depending on the metal and the biosorbent type.

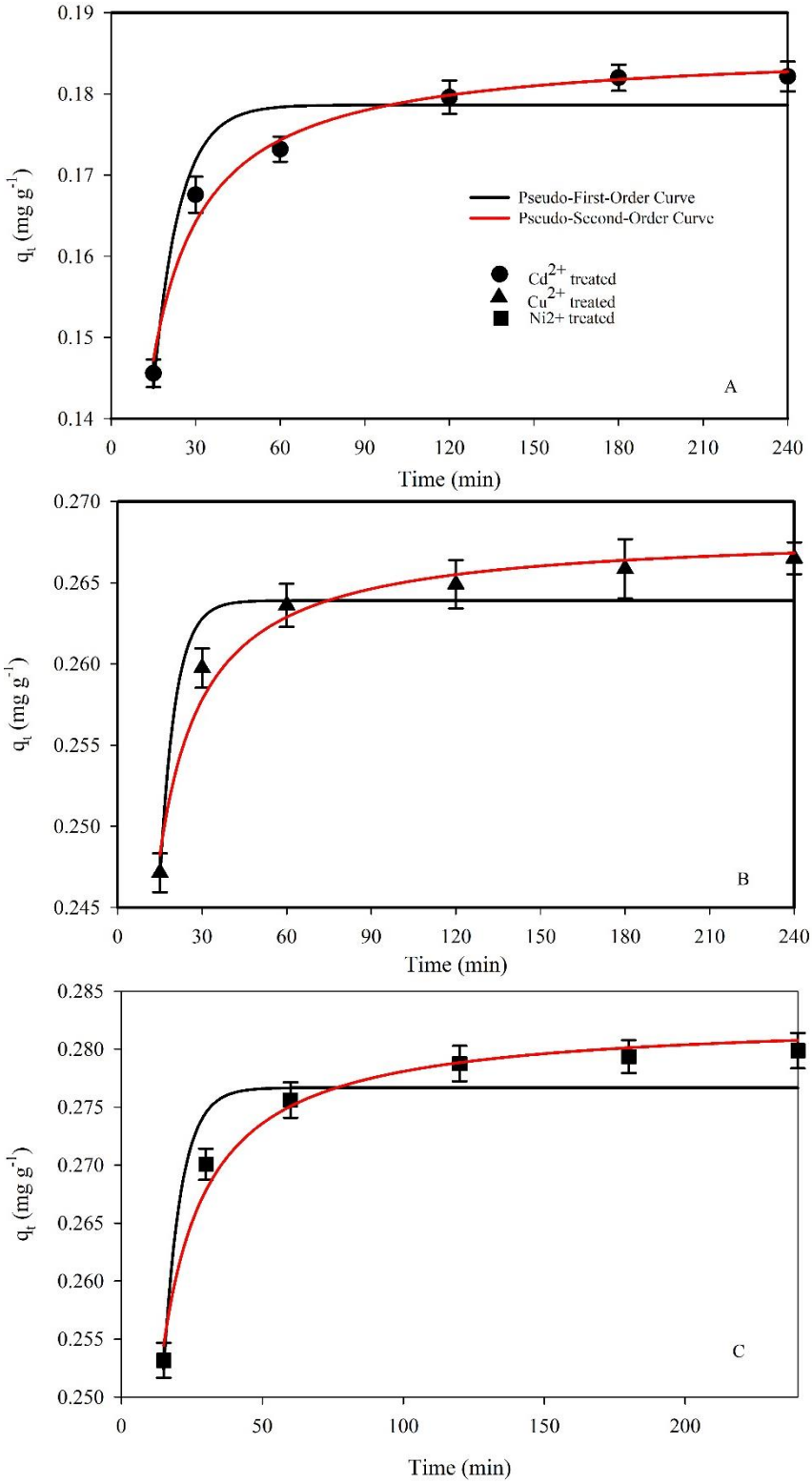

Figure.20. Kinetic profile of metal sorption by living biomass of *M. aeruginosa*. (A) Cd^{2+}, (B) Cu^{2+} and (C) Ni^{2+}. The curves correspond to the predicted values from the PFO and PSO models. Kinetic parameters for each metal can be found in Table 7.

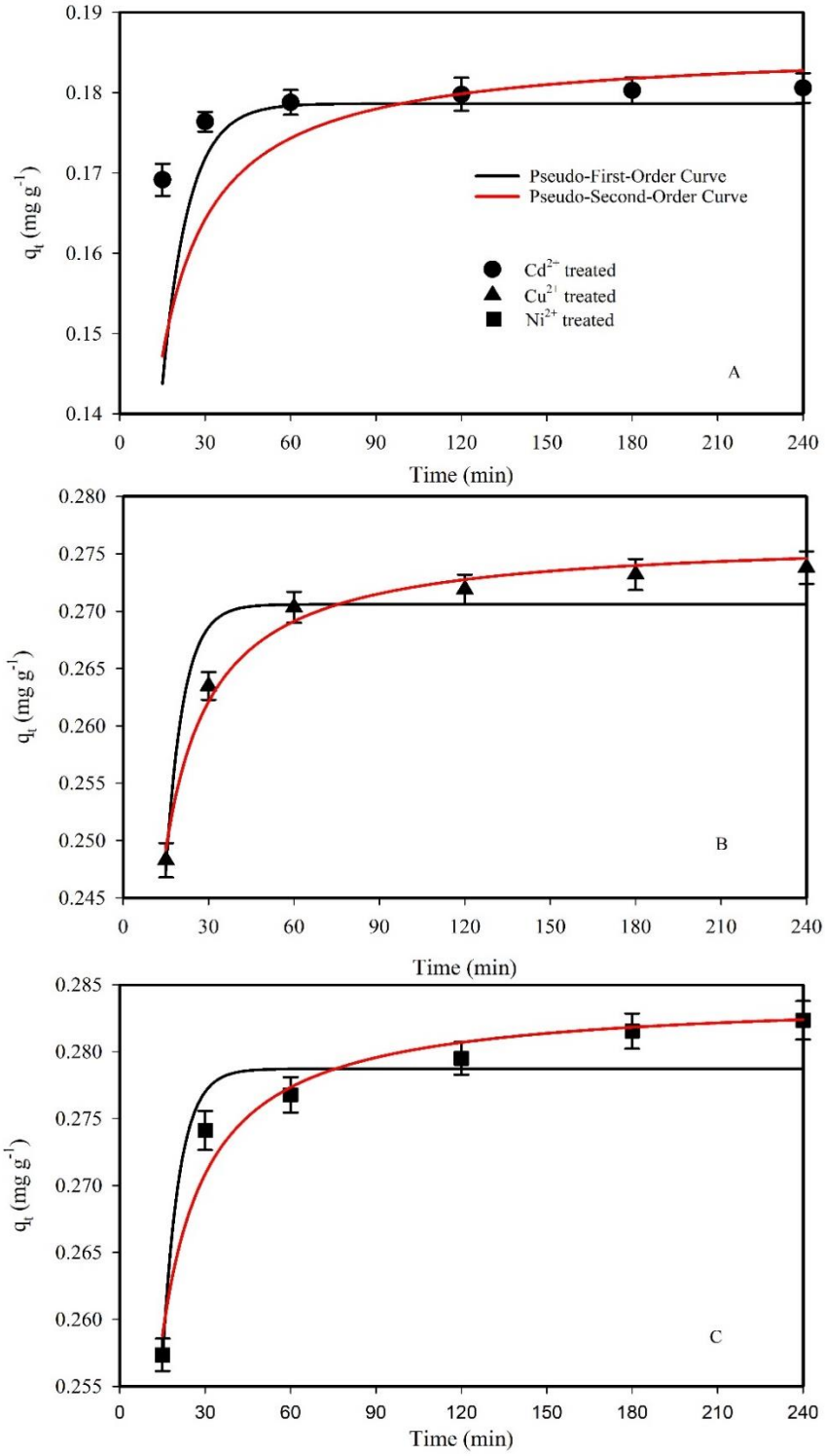

Figure.21. Kinetic profile of metal sorption by living biomass of *A. doliolum* (A) Cd^{2+}, (B) Cu^{2+} and (C) Ni^{2+}.The curves correspond to the predicted values from the PFO and PSO models. Kinetic parameters for each metal can be found in Table 8.

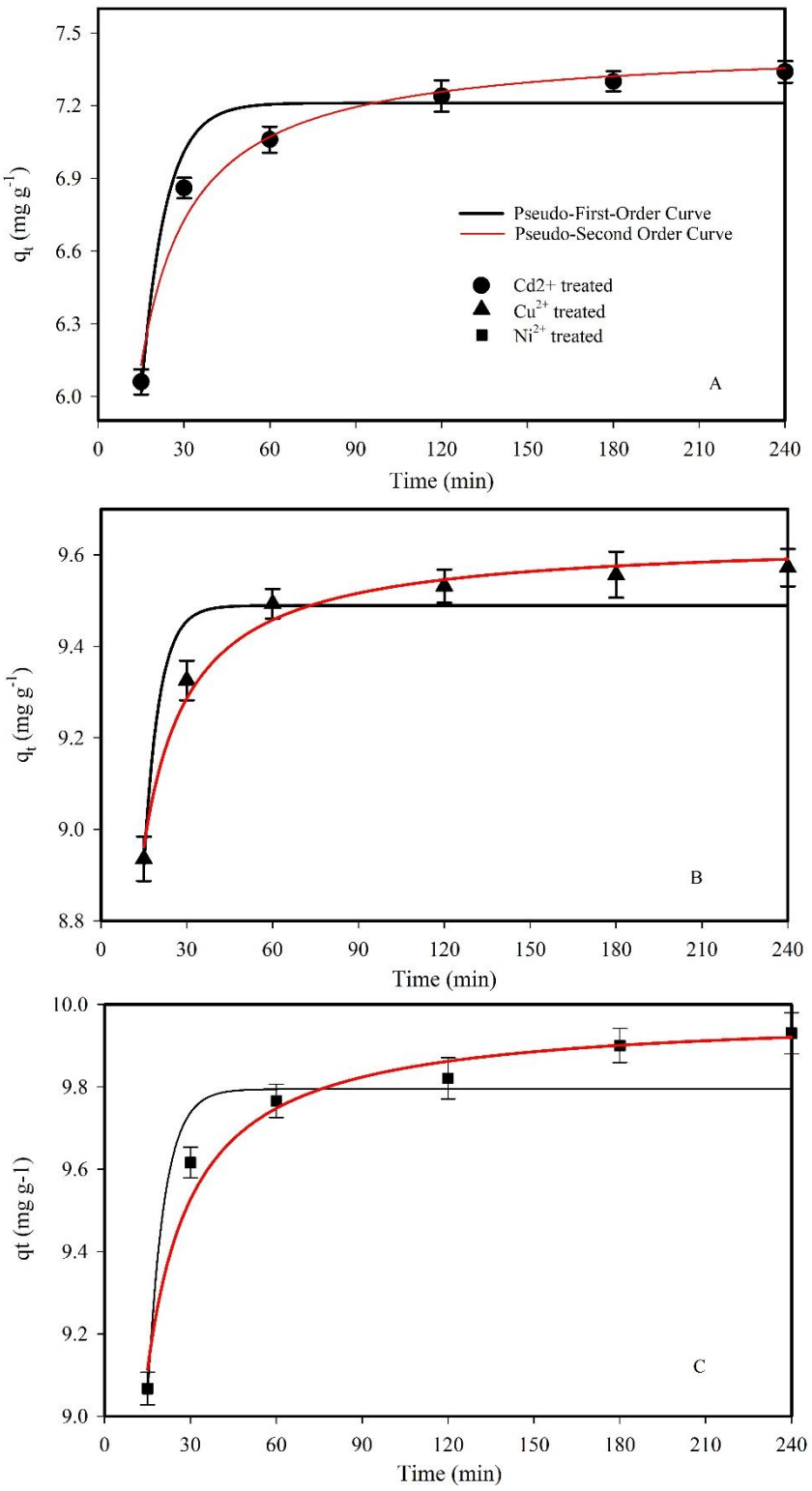

Figure.22. Kinetic profile of metal sorption by isolated EPS of *M. aeruginosa*. The curves represent the predicted sorption trends based on the PFO and PSO. Kinetic parameters for each metal can be found in Table 9.

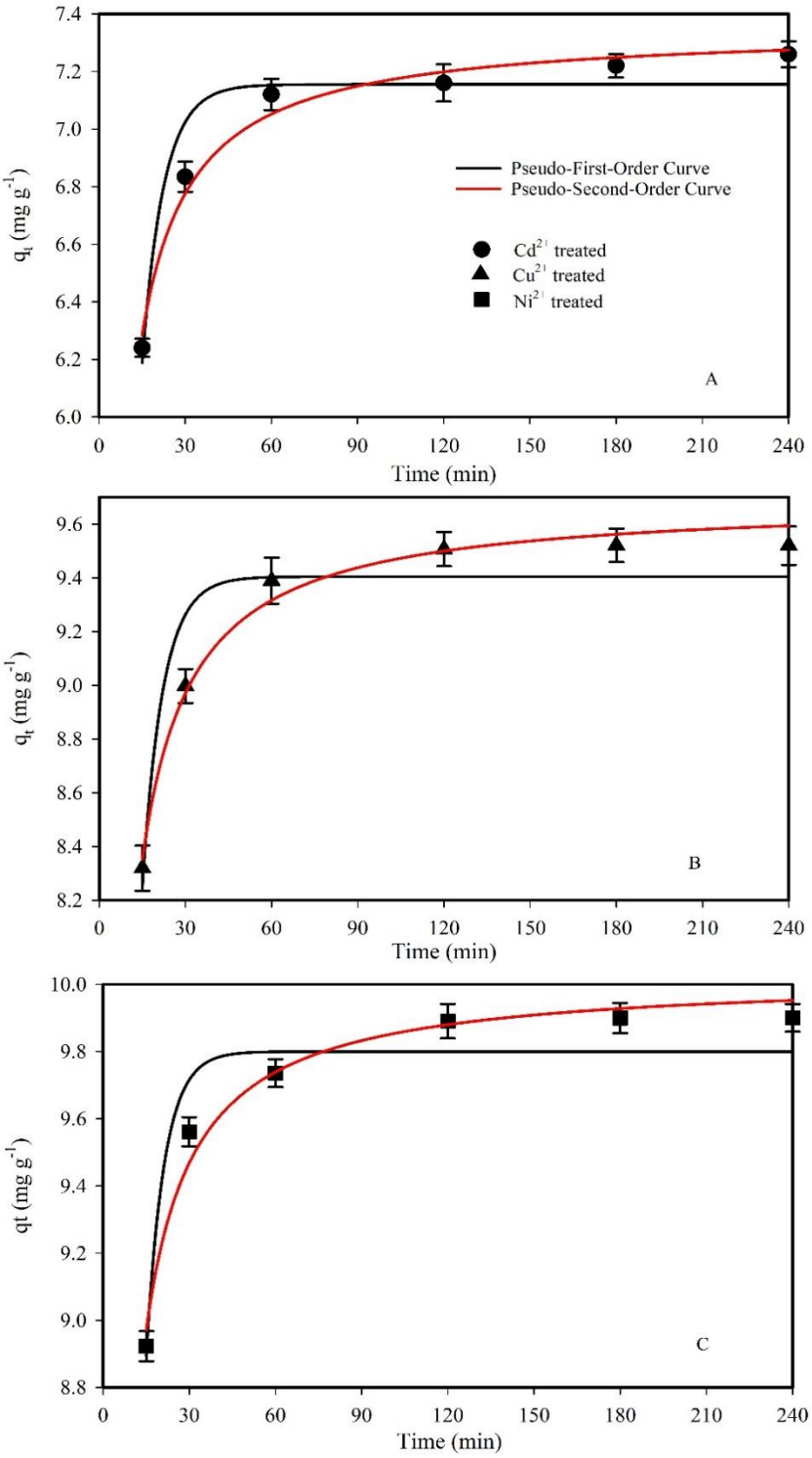

Figure.23. Kinetic profile of metal sorption by isolated EPS of *M. aeruginosa*. The curves represent the predicted sorption trends based on the PFO and PSO. Kinetic parameters for each metal can be found in Table 10.

Intraparticle diffusion analysis:

The figures 24-27 shows the role of intraparticle diffusion in metal sorption by *M. aeruginosa* and *A. doliolum* biomass, along with their isolated EPS, using the intraparticle diffusion model.

The plots of amount of metal sorbed versus the square root of time (t^0.5) exhibit multiple linear portions, appearing as curved lines. This suggests that intraparticle diffusion might not be the sole rate-limiting step for metal uptake.

In case of *M. aeruginosa* (Figure 24, Table 7), the intraparticle diffusion rate constant (k_d) is higher for Ni^{2+} compared to Cu^{2+} and Cd^{2+}, indicating faster diffusion of nickel ions within the biomass. Similar to *M. aeruginosa*, kd values in case of *A. doliolum* biomass follow the trend $Ni^{2+} > Cu^{2+} > Cd^{2+}$, suggesting faster diffusion of nickel (Figure 25, Table 8).

For M. aeruginosa EPS (Figure 26, Table 9), the kd trend remains consistent, with Ni^{2+} exhibiting the highest diffusion rate within the EPS structure. Similar to the other cases, Ni^{2+} displays the fastest diffusion within A. doliolum EPS, as indicated by the highest k_d value (Figure 27, Table 10).

While the intraparticle diffusion model provides insights into the diffusion process, the presence of multiple linear portions in the plots suggests that other mechanisms besides diffusion might also be influencing the rate of metal uptake. These additional mechanisms could involve factors like surface adsorption and pore diffusion within the biomass or EPS structure.

The k_d values (intra-particle diffusion rate constant) **(**Figure 25**)** were found to be higher for Ni^{2+} biosorption than Cu^{2+} and Cd^{2+}, indicating faster diffusion. The plot of the amount of metal sorbed versus the square root of time (I) indicated multiple linear portions (curved line), suggesting that intraparticle diffusion might not be the sole rate-controlling step.

The k_d values (intra-particle diffusion rate constant) (Figure 26) were found to be higher for Ni^{2+} biosorption than Cu^{2+} and Cd^{2+} , indicating faster diffusion onto *Microsystis* EPS. The plot of the amount of metal sorbed versus the square root of time (I) indicated multiple linear portions (curved line), suggesting that intraparticle diffusion might not be the sole rate-controlling step.

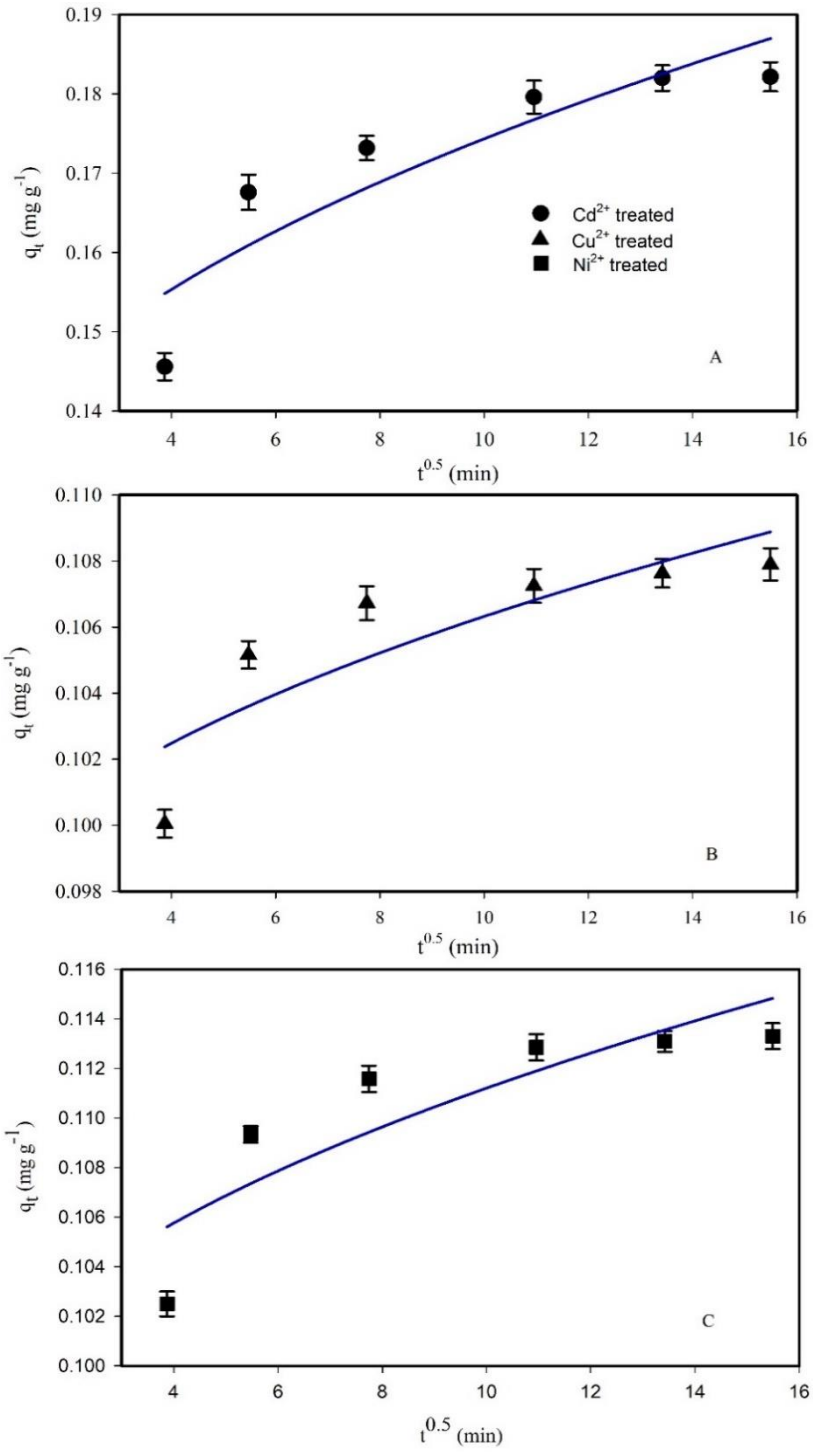

Figure.24. Intraparticle diffusion analysis for metal sorption by *M. aeruginosa* biomass (A) Cd^{2+} biosorption, (B) Cu^{2+} biosorption and (C) Ni^{2+} biosorption. Experimental data points are denoted by symbols, while model predictions are depicted by the corresponding curves.

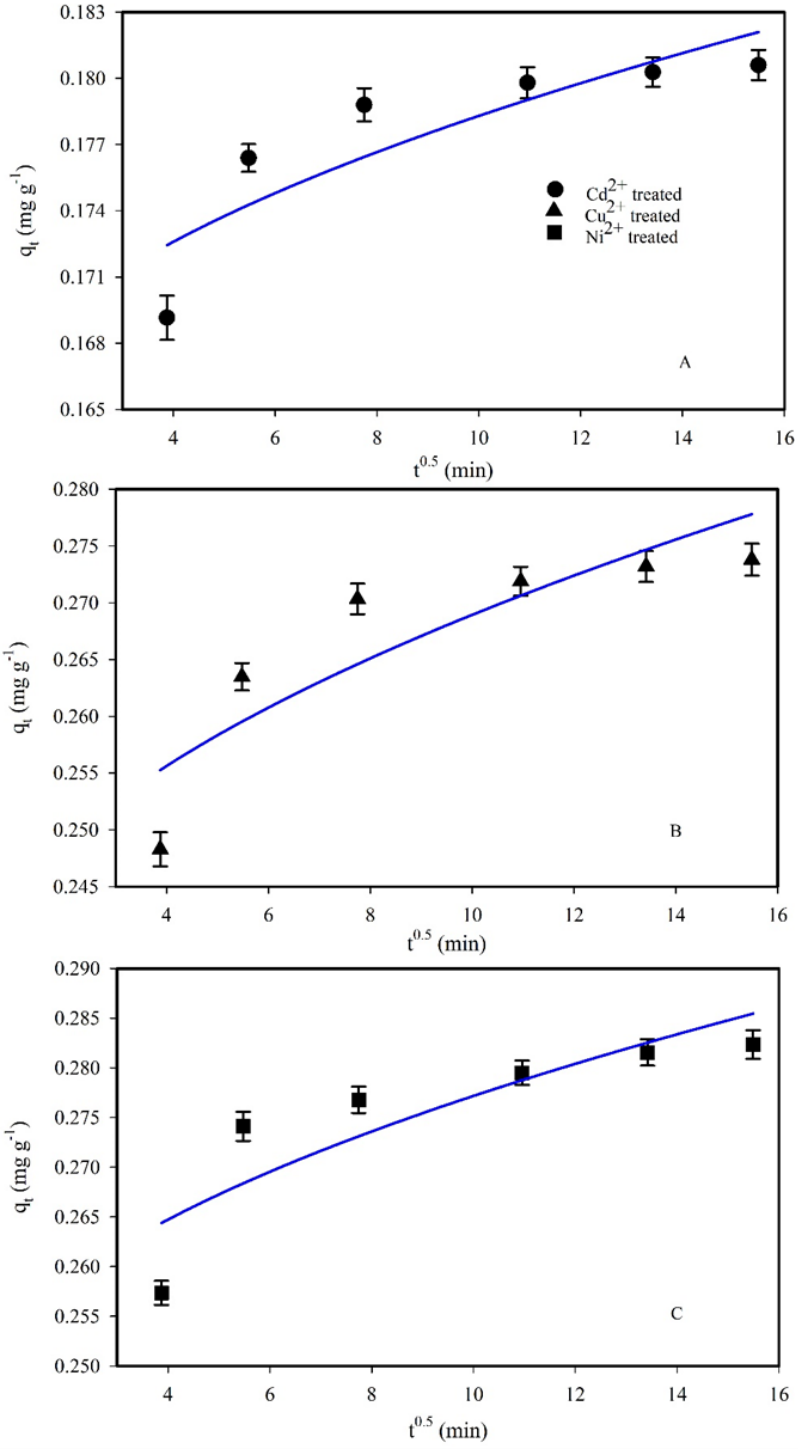

Figure.25. Intraparticle diffusion analysis for metal sorption by *A. doliolum* biomass (A) Cd^{2+} biosorption, (B) Cu^{2+} biosorption and (C) Ni^{2+} biosorption. Experimental data points are denoted by symbols, while model predictions are depicted by the corresponding curves.

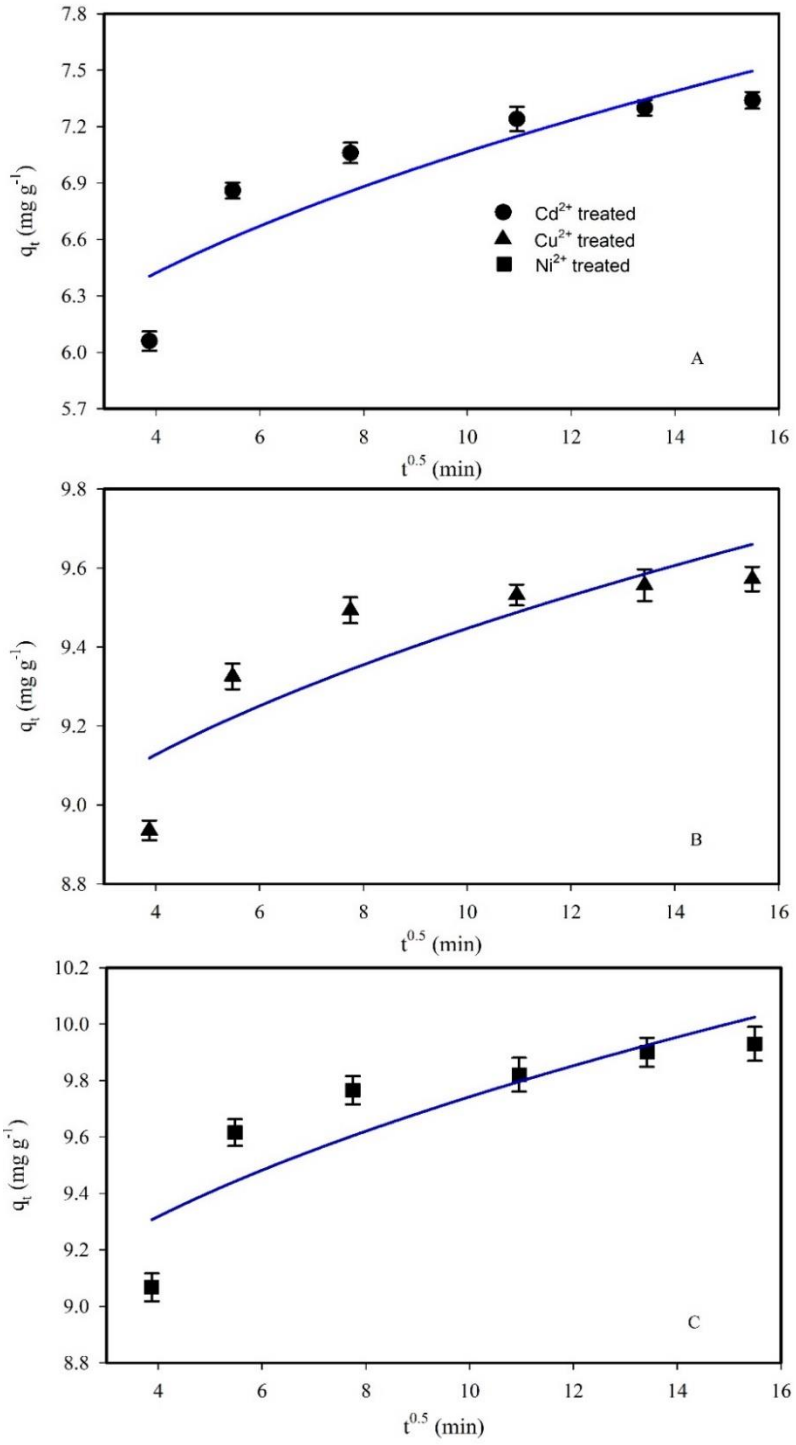

Figure.26. Intraparticle diffusion analysis for metal sorption by isolated EPS of *M. aeruginosa*. (A) Cd^{2+} biosorption, (B) Cu^{2+} biosorption and (C) Ni^{2+} biosorption. Experimental data points are denoted by symbols, while model predictions are depicted by the corresponding curves.

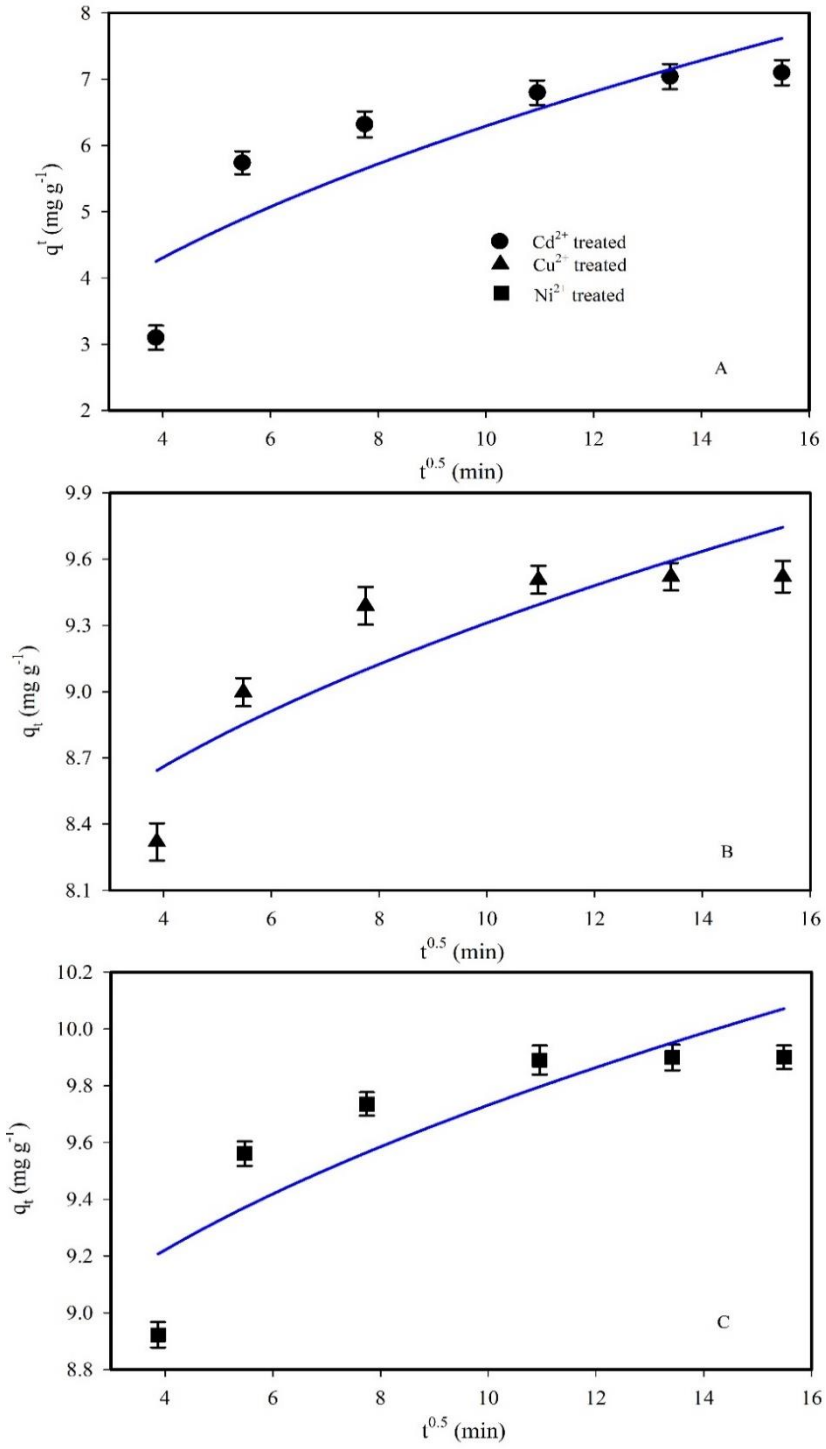

Figure.27. Intraparticle diffusion analysis for metal sorption by isolated EPS of *A. doliolum.* (A) Cd^{2+} biosorption, (B) Cu^{2+} biosorption and (C) Ni^{2+} biosorption. Experimental data points are denoted by symbols, while model predictions are depicted by the corresponding curves.

3.9.3 Thermodynamic Analysis

Experiments were conducted to analyzes the thermodynamic favorability of metal ion adsorption by various biosorbents (*M. aeruginosa*, *A. doliolum* biomass, EPS from *M. aeruginosa* and *A. doliolum*) for Ni^{2+}, Cu^{2+}, and Cd^{2+} ions using the van't Hoff plot.

The van't Hoff plots for each biosorbent-metal ion combination are presented in Figures 28-31. These plots depict the relationship between inverse temperature (1/T) and the natural logarithm of the equilibrium constant (ln kc).

Tables 11-14 summarize the thermodynamic parameters derived from the van't Hoff plots for each biosorbent-metal ion system. These parameters include:

- ΔG^o (Gibbs free energy change): Indicates the spontaneity of the adsorption process.
  - Negative ΔG^o suggests a spontaneous process (favorable).
  - Positive ΔG^o suggests a non-spontaneous process (unfavorable).
- ΔH^o (enthalpy change): Indicates the heat transfer during adsorption.
  - Negative ΔH^o indicates an exothermic process (releases heat).
  - Positive ΔH^o indicates an endothermic process (absorbs heat).
- ΔS^o (entropy change): Indicates the randomness or disorder of the system.
  - Negative ΔS^o suggests a decrease in randomness.
  - Positive ΔS^o suggests an increase in randomness.

The analysis of thermodynamic parameters reveals interesting trends for the biosorption of Ni^{2+}, Cu^{2+}, and Cd^{2+} ions by different biosorbents. The adsorption of all three metals onto the biomass of *M. aeruginosa* and *A. doliolum* was exothermic ($\Delta H^o < 0$), indicating that the process releases heat. However, despite the heat release, the adsorption was nonspontaneous ($\Delta G^o > 0$) under the studied conditions, suggesting the system requires external energy input to favor metal uptake.

In contrast to the biomass, the EPS (Extracellular Polymeric Substances) isolated from *M. aeruginosa* and *A. doliolum* displayed spontaneous ($\Delta G^o < 0$) adsorption for all three metal ions. These processes were also exothermic ($\Delta H^o < 0$) for Ni^{2+} and Cu^{2+}, but interestingly, Cd^{2+} adsorption remained endothermic ($\Delta H^o > 0$) despite being spontaneous.

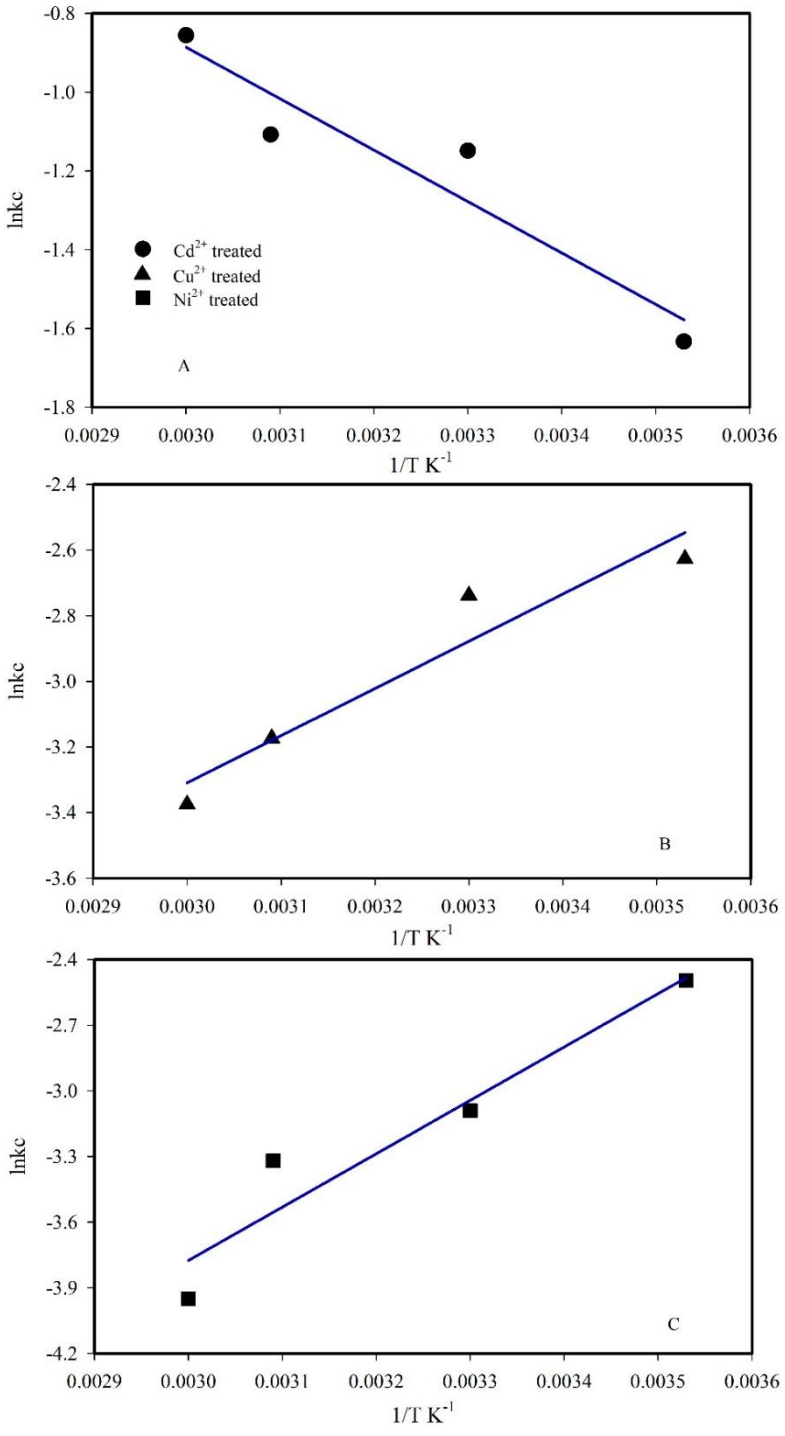

Figure.28. Van't Hoff plot for the biosorption of Ni^{2+} (A), Cu^{2+} (B), and Cd^{2+} (C) ions onto *M. aeruginosa* biomass. The data points represent the experimental values of ln kc at different temperatures. The corresponding thermodynamic parameters (ΔG^{o}, ΔH^{o}, and ΔS^{o}) for each metal ion can be found in Table 11.

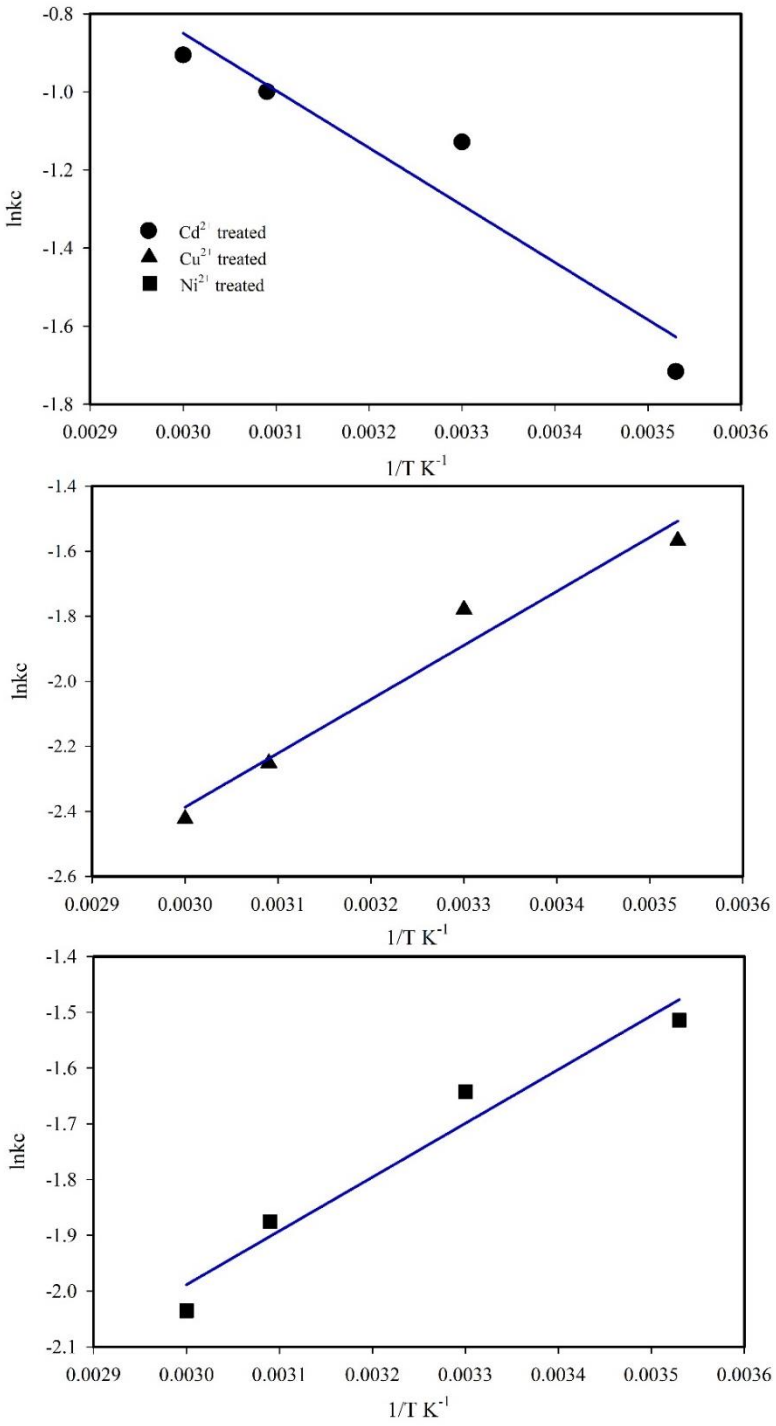

Figure.29. Van't Hoff plot for the biosorption of Ni^{2+} (A), Cu^{2+} (B), and Cd^{2+} (C) ions onto *A. doliolum* biomass. The data points represent the experimental values of ln kc at different temperatures. The corresponding thermodynamic parameters (ΔG^0, ΔH^0, and ΔS^0) for each metal ion can be found in Table 12.

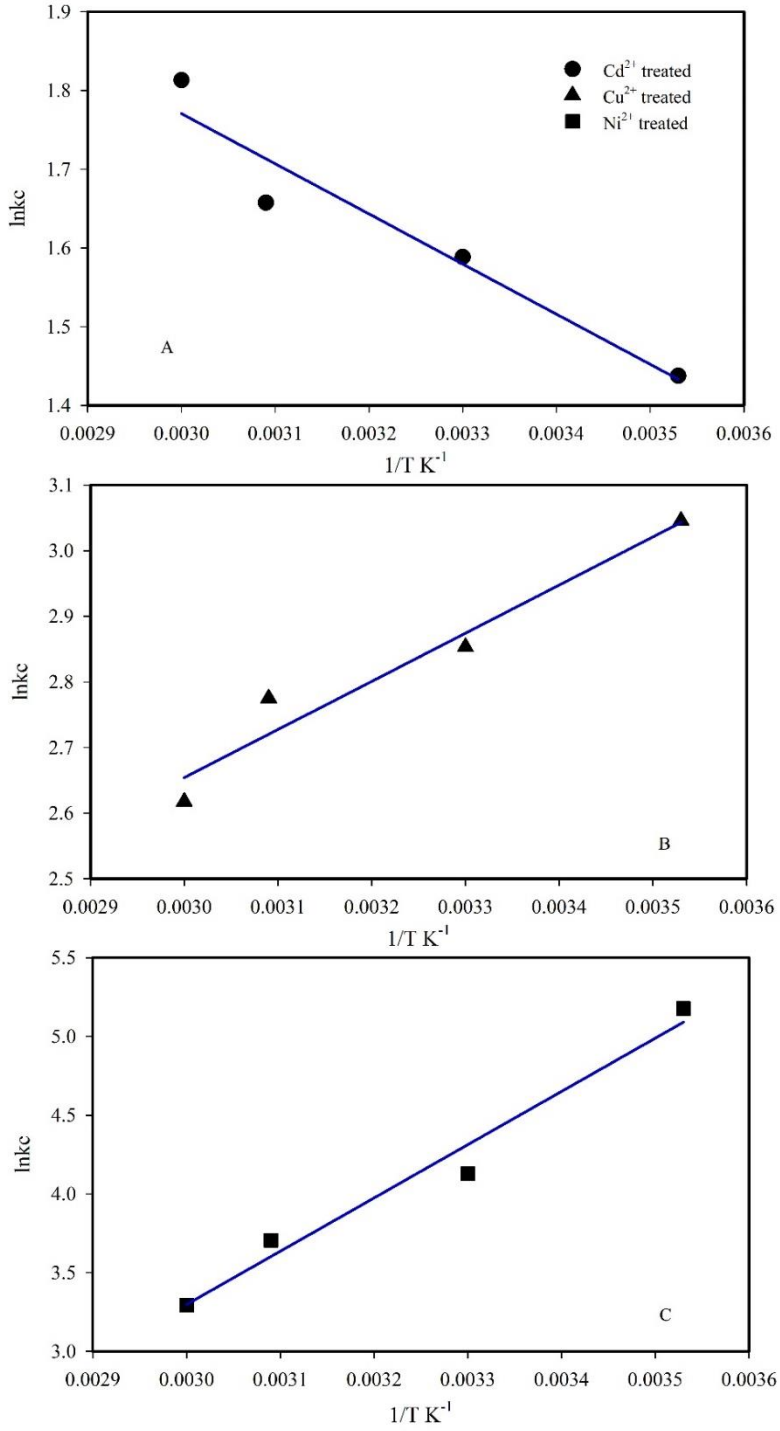

Figure.30. Van't Hoff plot for the biosorption of Ni^{2+} (A), Cu^{2+} (B), and Cd^{2+} (C) ions onto isolated EPS from *M. aeruginosa*. The data points represent the experimental values of ln kc at different temperatures. The corresponding thermodynamic parameters (ΔG^{o}, ΔH^{o}, and ΔS^{o}) for each metal ion can be found in Table 13.

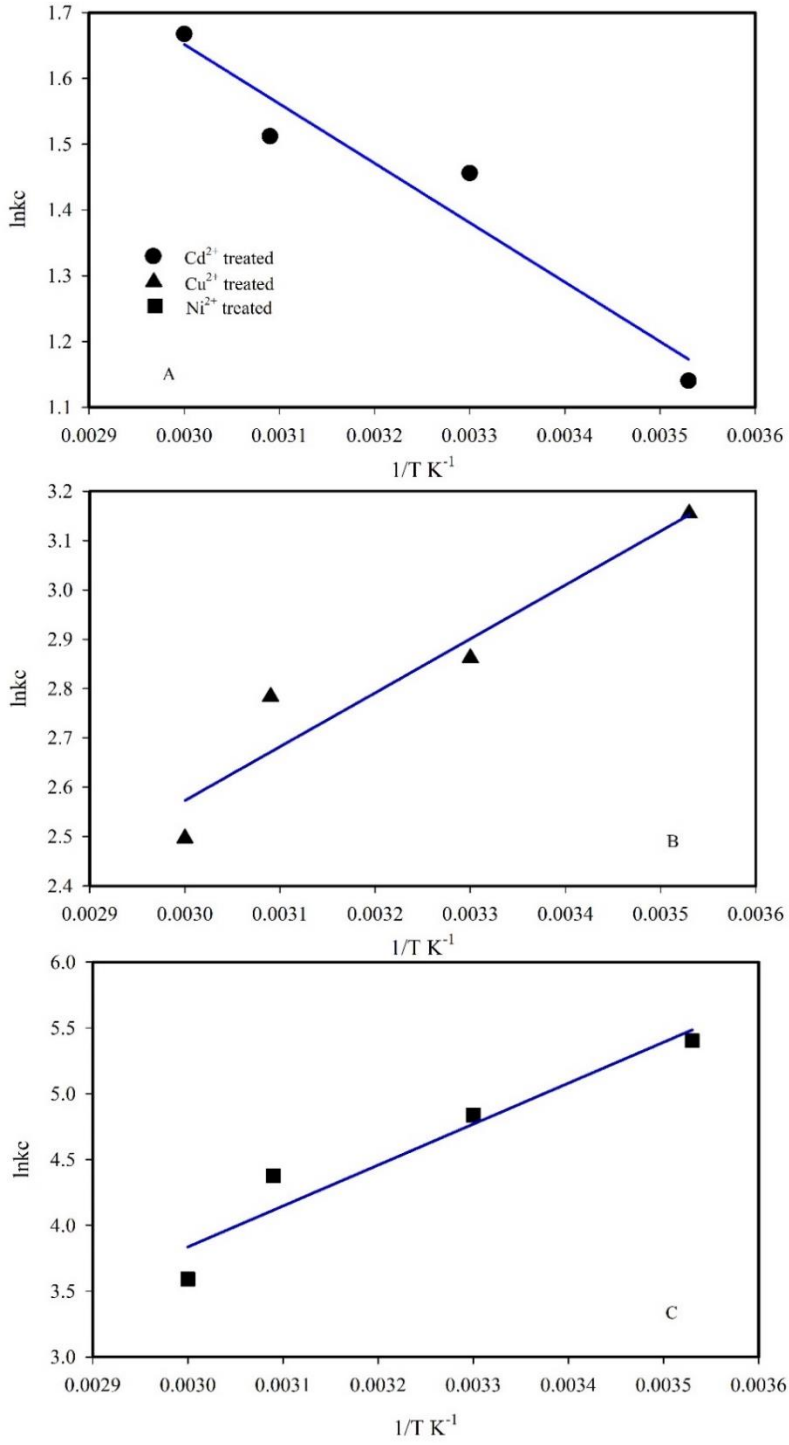

Figure.31. Van't Hoff plot for the biosorption of Ni^{2+} (A), Cu^{2+} (B), and Cd^{2+} (C) ions onto isolated EPS of *A. doliolum*. The data points represent the experimental values of ln kc at different temperatures. The corresponding thermodynamic parameters (ΔG^{o}, ΔH^{o}, and ΔS^{o}) for each metal ion can be found in Table 14.

The results indicate the dependence of biosorption favorability on both the type of biosorbent and the specific metal ion. While *M. aeruginosa* and *A. doliolum* biomass might require further optimization for efficient metal removal, their isolated EPS show promise for spontaneous metal uptake. The endothermic adsorption of Cd^{2+} by EPS suggests a different mechanism compared to Ni^{2+} and Cu^{2+}, warranting further investigation.

Table 11. Thermodynamic Parameters for Ni^2, Cu^{2+} and Cd^{2+} Biosorption onto *M. aeruginosa* Biomass from the Van't Hoff Plot

Metal ions	Model Parameters					
	r^2	Temp (K)	k_c	ΔS^o (kJ mol^{-1})	ΔH^o (kJ mol^{-1})	ΔG^o (kJ mol^{-1})
Ni^{2+}	0.9216	283	0.204	-0.085	-20.39	3.71
		303	0.112			5.41
		323	0.089			7.11
		333	0.048			7.96
Cu^{2+}	0.9165	283	0.178	-0.056	-11.99	3.86
		303	0.160			4.98
		323	0.103			6.10
		333	0.084			6.66
Cd^{2+}	0.9061	283	0.195	0.025	10.93	3.72
		303	0.317			3.21
		323	0.330			2.70
		333	0.425			2.45

Table 12. Thermodynamic Parameters for Ni^2, Cu^{2+} and Cd^{2+} Biosorption onto *A. doliolum* biomass from the Van't Hoff Plot

Metal ions	Model Parameters					
	r^2	Temp (K)	k_c	ΔS^o (kJ mol^{-1})	ΔH^o (kJ mol^{-1})	ΔG^o (kJ mol^{-1})
Ni^{2+}	0.9528	283	0.22	-0.040	-8.04	3.48
		303	0.19			4.29
		323	0.15			5.10
		333	0.13			5.51
Cu^{2+}	0.9614	283	0.21	-0.061	-13.83	3.55
		303	0.17			4.77
		323	0.11			6.0
		333	0.09			6.61
Cd^{2+}	0.9098	283	0.180	0.030	12.27	3.72
		303	0.324			3.21
		323	0.368			2.70
		333	0.404			2.45

Table 13. Thermodynamic Parameters for Ni^{2}, Cu^{2+} and Cd^{2+} Biosorption onto *Microcystis* EPS from the Van't Hoff Plot

	Model Parameters					
Metal ions	r^2	Temp (K)	k_c	ΔS^o (kJ mol^{-1})	ΔH^o (kJ mol^{-1})	ΔG^o (kJ mol^{-1})
Ni^{2+}	0.9761	283	177.2	-0.057	-28.26	-11.99
		303	62.0			-10.85
		323	40.7			-9.70
		333	26.9			-9.12
Cu^{2+}	0.9525	283	21.03	-0.0036	-6.14	-7.35
		303	17.34			-7.31
		323	16.04			-7.24
		333	13.70			-7.17
Cd^{2+}	0.9342	283	3.128	0.31	5.320	-3.37
		303	4.289			-3.99
		323	4.536			-4.60
		333	5.299			-4.91

Table 14. Thermodynamic Parameters for Ni^{2}, Cu^{2+} and Cd^{2+} Biosorption onto *Anabaena* EPS from the Van't Hoff Plot

	Model Parameters					
Metal ions	r^2	Temp (K)	k_c	ΔS^o (kJ mol^{-1})	ΔH^o (kJ mol^{-1})	ΔG^o (kJ mol^{-1})
Ni^{2+}	0.9233	283	222.0	-0.046	-25.98	-12.92
		303	126.0			-11.99
		323	79.45			-11.07
		333	36.29			-10.62
Cu^{2+}	0.9134	283	23.45	-0.006	-9.14	-7.43
		303	17.50			-7.30
		323	16.18			-7.18
		333	12.14			-7.12
Cd^{2+}	0.9339	283	4.211	0.036	7.553	-2.76
		303	4.896			-3.49
		323	5.246			-4.21
		333	6.130			-4.58

3.9.4. Biosorption Quantification

The biosorption of Ni^{2+}, Cu^{2+}, and Cd^{2+} ions by *M. aeruginosa* and A. doliolum biomass, and their respective EPS (Extracellular Polymeric Substances), was investigated using batch equilibrium experiments. The data were analyzed using three isotherm models: Langmuir, Freundlich, and Temkin. The experiment investigated biosorption across a concentration range of 0 to 10 mg L^{-1} for the three metal ions. The data were fitted to the aforementioned isotherm models, presented in Figures 32-35 and Tables 15-18.

Table 15: Langmuir, Freundlich, and Temkin Isotherm Parameters for Biosorption of Ni^{2+}, Cu^{2+}, and Cd^{2+} onto *M. aeruginosa* Biomass

Isotherm models	Model Parameters	Ni^{2+}	Cu^{2+}	Cd^{2+}
Langmuir	q_{max}	2.49±0.14	1.07±0.040	0.74±0.05
	k_L	0.57±0.03	0.57±0.03	1.21±0.06
	r^2	0.9982	0.9894	0.9641
Freundlich	k_F	0.48±0.02	0.37±0.02	0.39±0.03
	1/n	0.87±0.05	0.69±0.04	1.79±0.11
	r^2	0.9995	0.9967	0.9886
Temkin	B_T	0.14±0.01	0.08±0.01	0.12±0.008
	A_T	20.21±1.21	72.53±4.35	27.01±1.91
	r^2	0.8451	0.7522	0.8930

Note: V*alues were determined using non-linear curve fitting techniques in accordance with the Langmuir, Freundlich, and Temkin isotherm. q_{max} (mg g^{-1}); K_L (L mg^{-1}); B_T (J mol_{-1}); A_T (L mol^{-1}).*

Table 16: Langmuir, Freundlich, and Temkin Isotherm Parameters for Biosorption of Ni^{2+}, Cu^{2+}, and Cd^{2+} onto *A. doliolum* Biomass

Isotherm models	Model Parameters	Ni^{2+}	Cu^{2+}	Cd^{2+}
Langmuir	q_{max}	1.62±0.13	1.49±0.11	0.77±0.05
	k_L	0.36±0.03	0.40±0.03	1.63±0.01
	r^2	0.9992	0.9948	0.9840
Freundlich	k_F	0.42±0.03	0.41±0.02	0.48±0.03
	1/n	0.80±0.06	0.77±0.03	1.73±0.12
	r^2	0.9997	0.9989	0.9914
Temkin	B_T	0.13±0.01	0.20±0.01	0.14±0.01
	A_T	21.41±1.46	25.86±1.78	27.40±1.92
	r^2	0.8567	0.8698	0.8603

Note: V*alues were determined using non-linear curve fitting techniques in accordance with the Langmuir, Freundlich, and Temkin isotherm.* q_{max} *(mg* g^{-1}*);* K_L *(L* mg^{-1}*);* B_T *(J* mol_{-1}*);* A_T *(L* mol^{-1}*).*

Table 17: Langmuir, Freundlich, and Temkin Isotherm Parameters for Biosorption of Ni^{2+}, Cu^{2+}, and Cd^{2+} onto *M. aeruginosa* EPS

Isotherm models	Model Parameters	Ni^{2+}	Cu^{2+}	Cd^{2+}
Langmuir	q_{max}	44.81±2.69	37.06±2.22	26.63±1.71
	k_L	3.37±0.17	6.70±0.34	1.48±0.11
	r^2	0.9711	0.9972	0.9966
Freundlich	k_F	51.81±3.11	65.57±3.28	15.60±1.15
	1/n	0.67±0.04	0.67±0.04	1.78±0.14
	r^2	0.9883	0.9984	0.9911
Temkin	B_T	3.16±0.19	4.25±0.24	4.32±0.21
	A_T	545.68±16.37	284.13±11.37	31.77±2.28
	r^2	0.8163	0.8745	0.8932

Note: V*alues were determined using non-linear curve fitting techniques in accordance with the Langmuir, Freundlich, and Temkin isotherm.* q_{max} *(mg* g^{-1}*);* K_L *(L* mg^{-1}*);* B_T *(J* mol_{-1}*);* A_T *(L* mol^{-1}*).*

Table 18: Langmuir, Freundlich, and Temkin Isotherm Parameters for Biosorption of Ni^{2+}, Cu^{2+}, and Cd^{2+} onto *Anabaena* EPS

Isotherm models	Model Parameters	Ni^{2+}	Cu^{2+}	Cd^{2+}
Langmuir	q_{max}	64.37±4.51	42.08±2.73	31.19±2.25
	k_L	2.31±0.16	4.03±0.35	1.32±0.1
	r^2	0.9905	0.9974	0.9861
Freundlich	k_F	71.63±4.36	58.07±3.28	18.01±1.28
	1/n	0.78±0.04	0.70±0.05	1.65±0.12
	r^2	0.9966	0.9985	0.9913
Temkin	B_T	3.94±0.22	3.53±0.26	4.20±0.28
	A_T	263.61±17.13	338.97±22.03	43.00±3.04
	r^2	0.8197	0.7842	0.8964

Note: V*alues were determined using non-linear curve fitting techniques in accordance with the Langmuir, Freundlich, and Temkin isotherm.* q_{max} *(mg* g^{-1}*);* K_L *(L* mg^{-1}*);* B_T *(J* mol_{-1}*);* A_T *(L* mol^{-1}*).*

I. *Langmuir Isotherm:* The Langmuir isotherm assumes monolayer adsorption on a homogeneous surface. This model provided a good fit for most biosorbent-metal ion combinations, with r^2 values exceeding 0.96 in most cases (Tables 15-18). The Langmuir model quantified the maximum adsorption capacity (q_{max}) for each metal ion onto the biosorbents (Tables 15-18). Notably, the q_{max} values were consistently higher for EPS compared to their corresponding biomass, indicating a greater binding capacity for metal ions. For example, the q_{max} for Ni^{2+} adsorption on *M. aeruginosa* EPS was 2.49 mg/g, whereas the biomass only reached 0.74 mg/g (Table 15). This trend was observed for all three metal ions across both types of EPS.

II. *Freundlich Isotherm:* The Freundlich isotherm model describes multilayer adsorption on heterogeneous surfaces. Similar to the Langmuir model, Freundlich isotherm fitting yielded good results with r^2 values exceeding 0.98

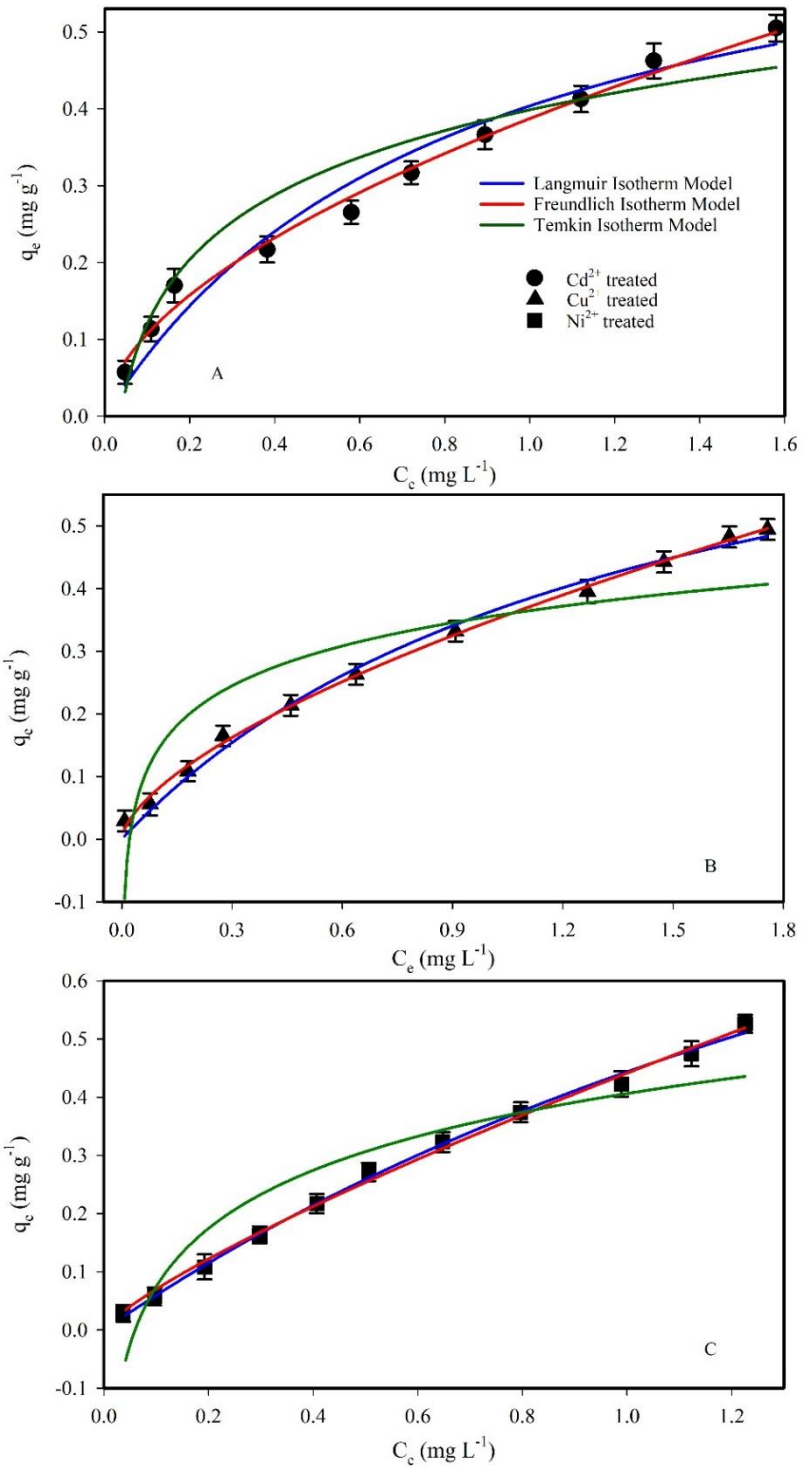

Figure.32. Equilibrium isotherms for the biosorption of Ni^{2+} (A), Cu^{2+} (B), and Cd^{2+} (C) ions onto *M. aeruginosa* biomass. The curves represent the fitting of the Langmuir, Freundlich, and Temkin isotherm models to the experimental data points.

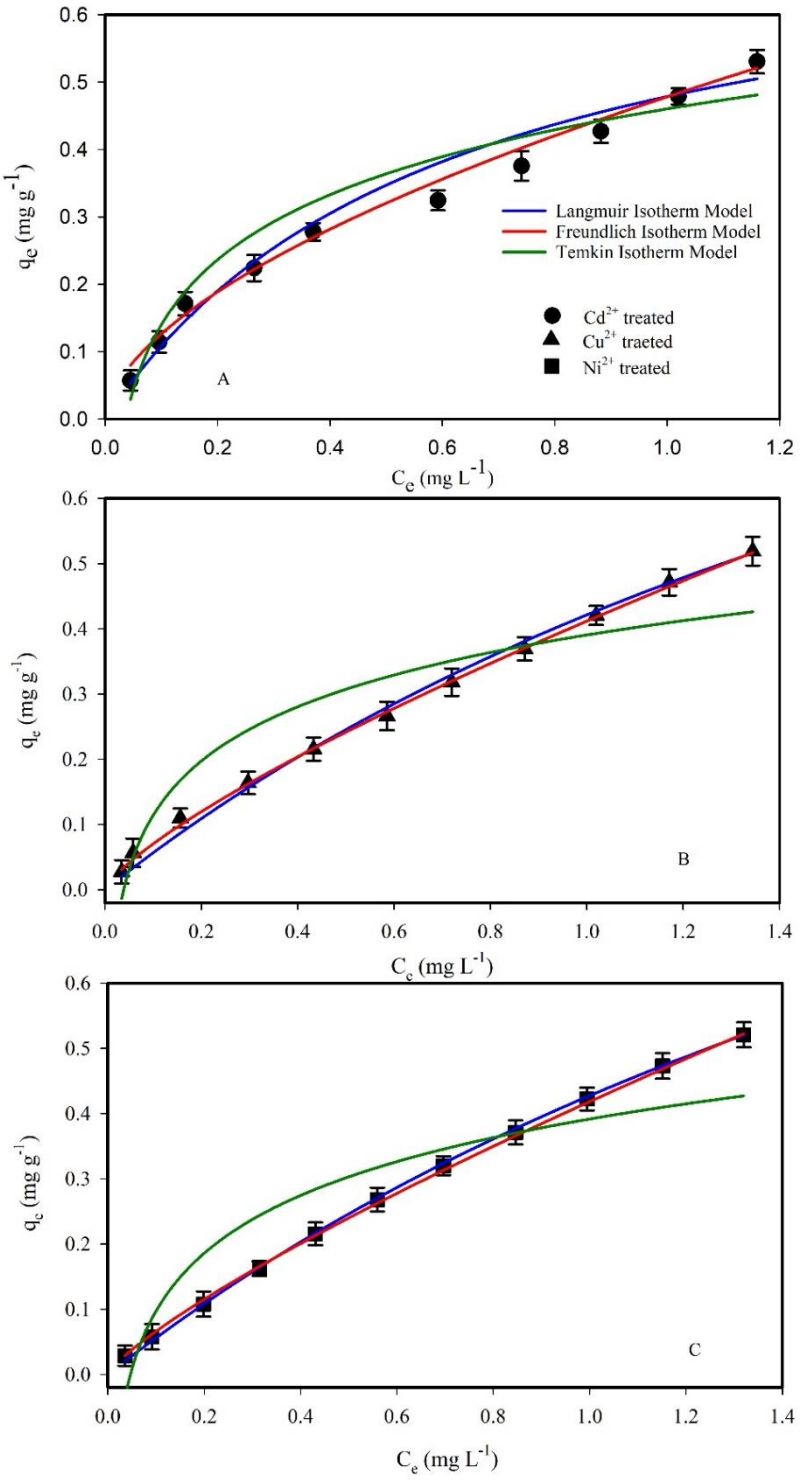

Figure.33. Equilibrium isotherms for the biosorption of Ni^{2+} (A), Cu^{2+} (B), and Cd^{2+} (C) ions onto *A. doliolum* biomass. The curves represent the fitting of the Langmuir, Freundlich, and Temkin isotherm models to the experimental data points.

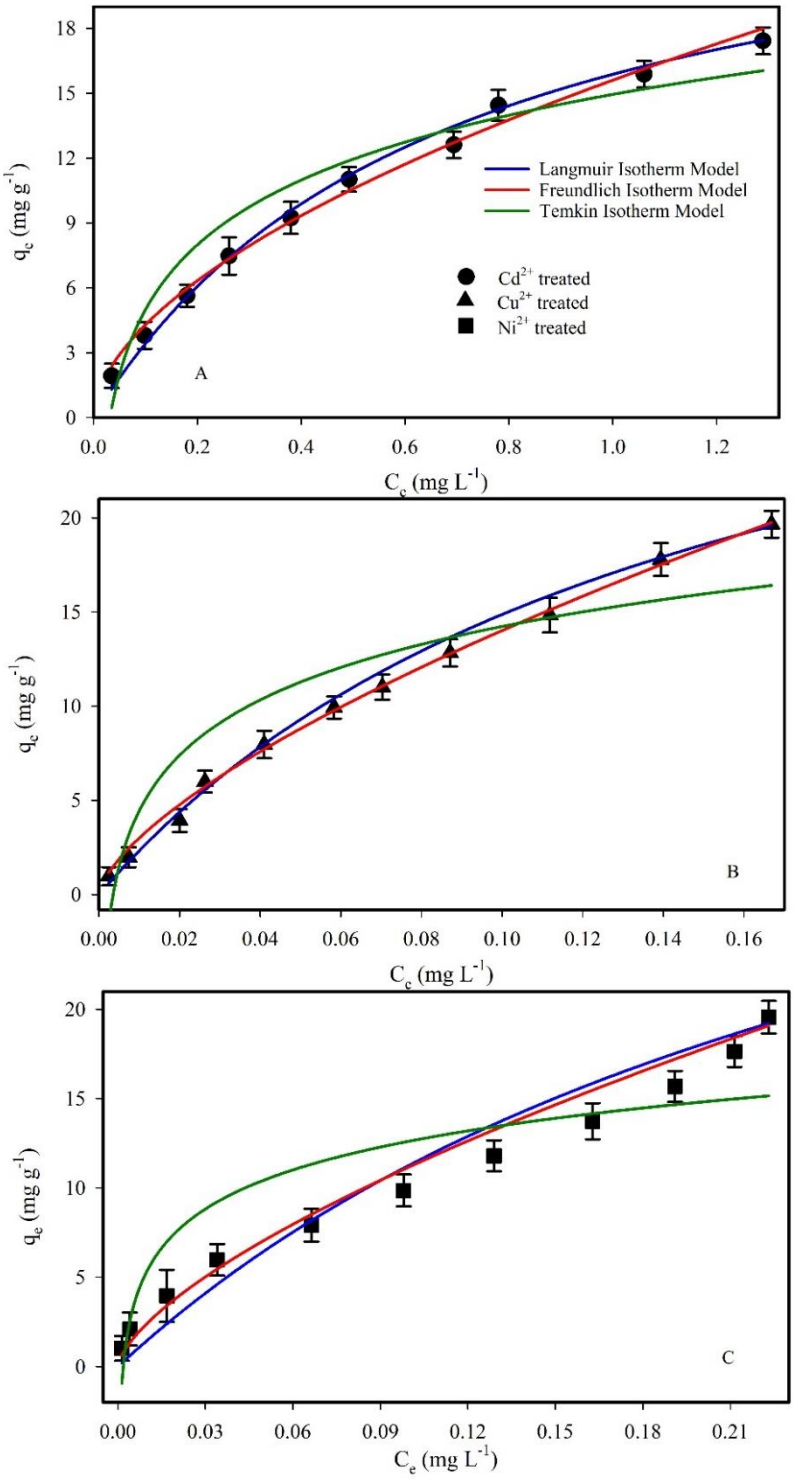

Figure.34. Equilibrium isotherms for the biosorption of Ni^{2+} (A), Cu^{2+} (B), and Cd^{2+} (C) ions onto *M. aeruginosa* EPS. The curves represent the fitting of the Langmuir, Freundlich, and Temkin isotherm models to the experimental data points.

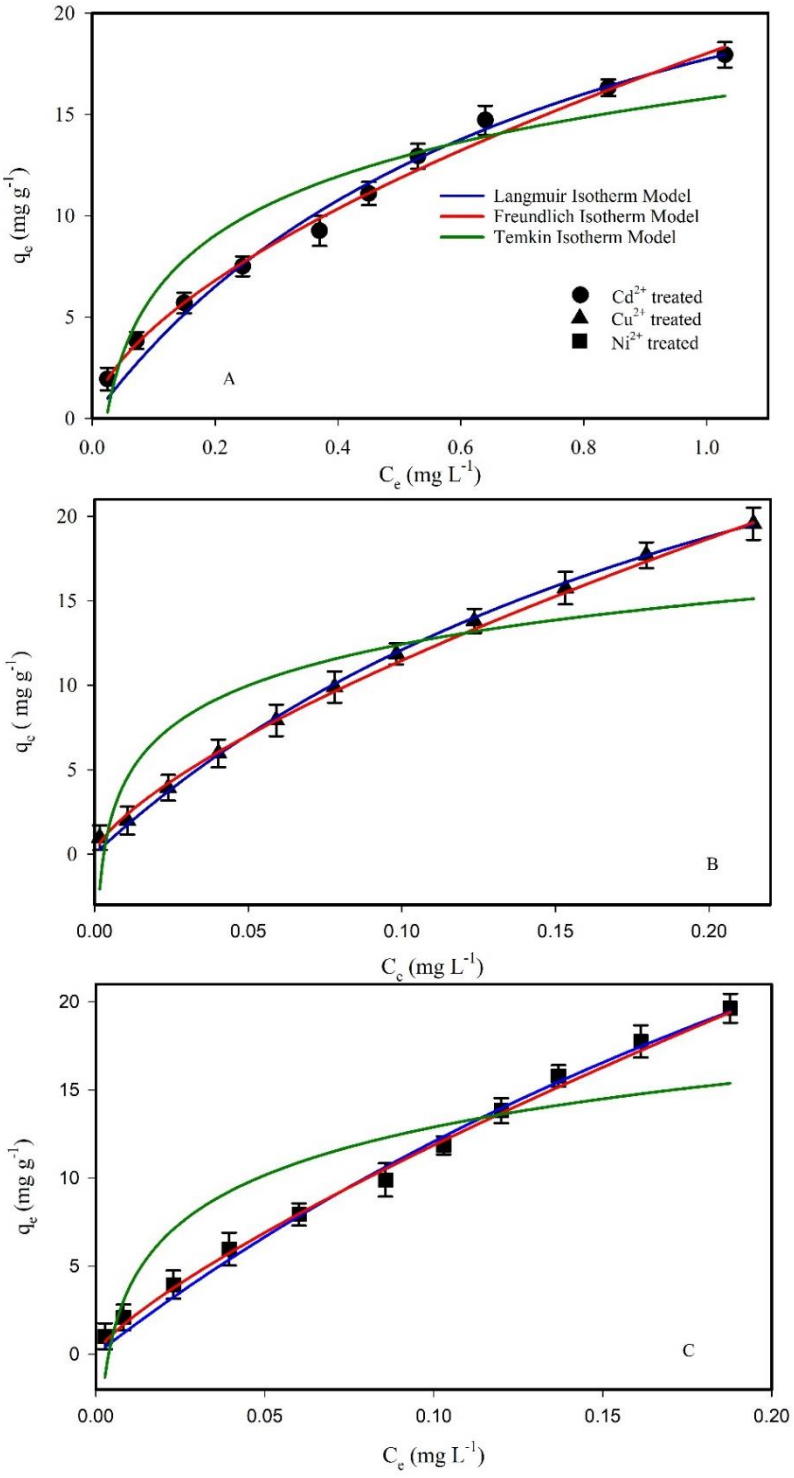

Figure.35. Equilibrium isotherms for the biosorption of Ni^{2+} (A), Cu^{2+} (B), and Cd^{2+} (C) ions onto *A. doliolum* EPS. The curves represent the fitting of the Langmuir, Freundlich, and Temkin isotherm models to the experimental data points.

for most cases (Tables 15-18). The Freundlich constant (k_F) reflects the adsorption intensity, with higher values indicating stronger adsorption. EPS consistently exhibited higher k_F values compared to the biomass for both Cu^{2+} and Ni^{2+} ions, suggesting stronger adsorption onto EPS (Tables 15-16, 17-18). The heterogeneity factor (1/n) close to unity (between 0.67 and 0.87 for most cases) implies favorable biosorption with relatively consistent affinities across binding sites on the biosorbent surface.

III. *Temkin Isotherm:* The Temkin isotherm accounts for the influence of adsorption heat on the process. While the fit of the Temkin model was moderate compared to the other two models (r^2 values ranging from 0.75 to 0.89), it provided insights into the adsorption energetics. The Temkin adsorption constant (AT) reflects the overall force of interaction between the adsorbate (metal ion) and the adsorbent (biosorbent). Interestingly, the AT values were consistently higher for EPS compared to the biomass for all three metals (Tables 15-18). This suggests stronger adsorption forces for metal ions on EPS compared to the biomass.

Overall, the Freundlich isotherm best described the biosorption process for most cases, indicating a heterogeneous surface with multilayer adsorption. The Langmuir isotherm also provided valuable information, particularly the q_{max} values highlighting the superior binding capacity of EPS. The Temkin isotherm, despite a moderate fit, offered insights into the adsorption energetics.

3.9.5. Biosorption of Ni and Cu in binary systems

This section describes the individual and combined biosorption behavior of Ni^{2+} and Cu^{2+} ions using *M. aeruginosa* biomass and EPS (Extracellular Polymeric Substances) derived from the same source. Langmuir, Freundlich, and Temkin isotherm models were employed to analyze the biosorption dynamics. The corresponding model parameters can be found in Tables 19 and 20 for *M. aeruginosa* biomass and EPS, respectively. Figure 36 visually depicts the biosorption isotherms for Cu^{2+} and Ni^{2+} in binary metal systems.

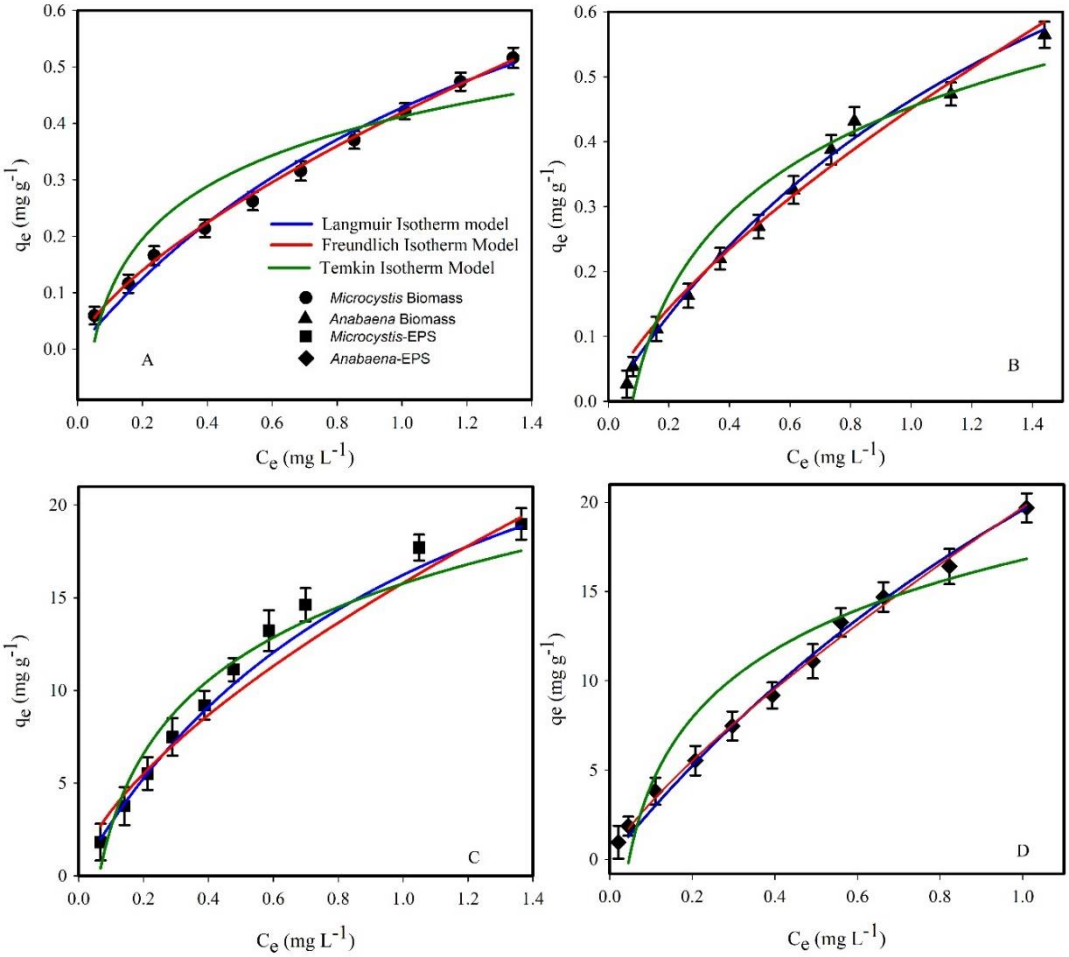

Figure.36. Influence of Ni^{2+} co-existence on Cu^{2+} biosorption. This figure depicts the biosorption behavior of Cu^{2+} ions onto *M. aeruginosa* and *A. doliolum* biomass (A and B) and their respective EPS (C and D) in the presence of co-existing Ni^{2+} ions. The initial concentration of Cu^{2+} varied from 0 to 10 mg L^{-1}, while a constant concentration of Ni^{2+} (5 mg L^{-1}) was introduced in the binary systems. The solid lines represent the fitting of the Langmuir (blue), Freundlich (red), and Temkin (green) isotherm models to the experimental data points (symbols).

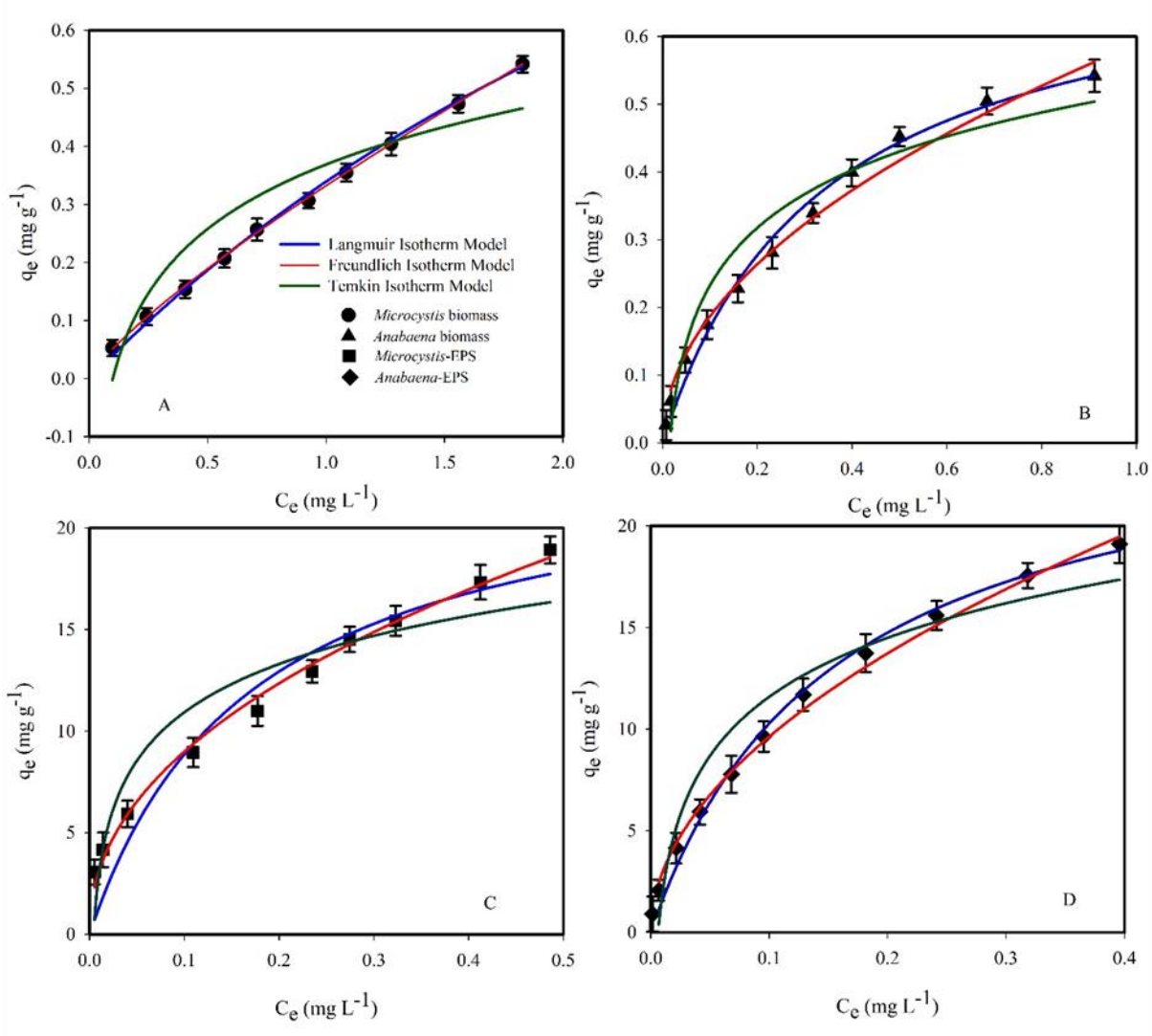

Figure.37. Influence of Cu^{2+} co-existence on Ni^{2+} biosorption. This figure depicts the biosorption behavior of Ni^{2+} ions onto *M. aeruginosa* and *A. doliolum* biomass (A and B) and their respective EPS (C and D) in the presence of co-existing Cu^{2+} ions. The initial concentration of Ni^{2+} varied from 0 to 10 mg L^{-1}, while a constant concentration of Cu^{2+} (5 mg L^{-1}) was introduced in the binary systems. The solid lines represent the fitting of the Langmuir (blue), Freundlich (red), and Temkin (green) isotherm models to the experimental data points (symbols).

M. aeruginosa

The presence of coexisting metal ions significantly impacted the biosorption of both Ni^{2+} and Cu^{2+}. In single metal systems (Tables 18 and 19), the Langmuir isotherm model revealed a higher q_{max} for Ni^{2+} (2.49 mg g^{-1} for *M. aeruginosa* biomass and 44.81 mg g^{-1} for EPS) compared to Cu^{2+} (1.09 mg g^{-1} for biomass and 29.06 mg g^{-1} for EPS) for both biosorbents. This suggests a greater binding capacity for Ni^{2+}.

Introducing a co-existing metal ion resulted in a decrease in the q_{max} for the other metal ion in both biomass and EPS (Tables 19 and 20). For example, *M. aeruginosa* biomass: qmax for Ni^{2+} decreased from 2.49 mg g^{-1} to 1.07 mg g^{-1} with Cu^{2+} co-existence. In case of EPS, the q_{max} for Ni^{2+} decreased from 44.81 mg g^{-1} to 37.06 mg g^{-1} with Cu^{2+} co-existence. This indicates competitive inhibition, where the presence of one metal ion hinders the adsorption of the other due to shared binding sites.

The Freundlich model parameters (k_F) also support this competitive behavior. A decrease in k_F values within the binary systems signifies a compromised biosorption capacity due to competition between metal ions for binding sites (Tables 19 and 20). For instance, in case of *M. aeruginosa* biomass k_F for Ni^{2+} decreased from 0.48 to 0.37 with Cu^{2+} co-existence.

The Temkin isotherm model, though providing a slightly less favorable fit compared to the other two models, showed a similar trend. The decrease in BT values in binary systems suggests reduced binding energies between metal ions and the biosorbent (Tables 19 and 20).

In conclusion, the findings demonstrate competitive adsorption between Ni^{2+} and Cu^{2+} ions for binding sites on both *M. aeruginosa* biomass and EPS. The presence of one metal ion inhibits the adsorption of the other, leading to a decrease in the overall biosorption capacity. The quantitative data from the isotherm models (q_{max} and k_F) provides a clear picture of this competitive effect.

A. doliolum

The same investigation was repeated using *A. doliolum* biomass and EPS (Tables 21 and 22, Figure 37). The results mirrored the observations with *M. aeruginosa*. Co-

existing metal ions significantly affected the biosorption of both Ni^{2+} and Cu^{2+}. Single metal systems displayed a higher q_{max} for Ni^{2+} compared to Cu^{2+} in both biomass and EPS (Tables 21 and 22). For example, in case of *A. doliolum* biomass: q_{max} for Ni^{2+} was 1.62 mg g^{-1} and for Cu^{2+} it was 1.49 mg g^{-1}. Introducing a co-existing metal ion resulted in a decrease in the q_{max} for the other metal ion (Tables 21 and 22), indicating competitive inhibition. The Freundlich model (k_F values) and Temkin model (BT values) further supported the competitive adsorption phenomenon within the binary systems (Tables 21 and 22).

Above results suggested that the presence of co-existing metal ions (Ni^{2+} and Cu^{2+}) significantly affected their individual biosorption onto both *M. aeruginosa* and *A. doliolum* biomass and EPS. Competitive inhibition was observed, where the presence of one metal ion hindered the adsorption of the other. This highlights the importance of considering co-existing contaminants when evaluating biosorption for metal removal from complex environmental samples.

Table 19: Biosorption Isotherm Parameters for Ni^{2+} and Cu^{2+} onto *M. aeruginosa* Biomass (single and binary systems)

Isotherm model	Model parameters	Ni biosorption		Cu biosorption	
		Cu 0.0 (mg L^{-1})	Cu 5.0 (mg L^{-1})	Ni 0.0 (mg L^{-1})	Ni 5.0 (mg L^{-1})
Langmuir	q_{max}	2.49±0.14	1.09±0.05	1.07±0.040	1.82±0.09
	k_L	0.57±0.03	0.65±0.04	0.57±0.03	0.23±0.01
	r^2	0.9982	0.9884	0.9894	0.9984
Freundlich	k_F	0.48±0.02	0.42±0.02	0.37±0.02	0.33±0.02
	1/n	0.87±0.05	0.68±0.05	0.69±0.04	0.81±0.04
	r^2	0.9995	0.9979	0.9967	0.9996
Temkin	B_T	0.14±0.01	0.13±0.01	0.08±0.01	0.16±0.01
	A_T	20.21±1.21	21.27±0.85	72.53±4.35	10.04±0.52
	r^2	0.8451	0.8826	0.7522	0.8876

Note: These parameters were obtained through non-linear curve fitting procedures.

Table 20: Biosorption Isotherm Parameters for Ni^{2+} and Cu^{2+} onto *Microcystis* EPS (Single and Binary Systems)

Isotherm model	Model parameters	Ni biosorption		Cu biosorption	
		Cu 0.0 (mg L^{-1})	Cu 5.0 (mg L^{-1})	Ni 0.0 (mg L^{-1})	Ni 5.0 (mg L^{-1})
Langmuir	q_{max}	44.81±2.69	29.06±1.59	37.06±2.22	38.86±1.98
	k_L	3.37±0.17	3.53±0.17	6.70±0.34	0.92±0.06
	r^2	0.9711	0.9411	0.9972	0.9971
Freundlich	k_F	51.81±3.11	27.22±1.42	65.57±3.28	15.80±0.79
	1/n	0.67±0.04	0.53±0.04	0.67±0.04	0.65±0.04
	r^2	0.9883	0.9818	0.9984	0.9988
Temkin	B_T	3.16±0.19	3.47±0.15	4.25±0.24	5.70±0.27
	A_T	545.68±16.37	221.96±7.54	284.13±11.37	15.91±0.76
	r^2	0.8163	0.8756	0.8745	0.8396

Note: Parameters were calculated by the non-linear curve fitting procedure.

Table 21: Biosorption Isotherm Parameters for Ni^{2+} and Cu^{2+} onto *A. doliolum* Biomass (Single and Binary Systems)

Isotherm model	Model parameters	Ni biosorption		Cu biosorption	
		Cu 0.0 (mg L^{-1})	Cu 5.0 (mg L^{-1})	Ni 0.0 (mg L^{-1})	Ni 5.0 (mg L^{-1})
Langmuir	q_{max}	1.62±0.13	0.74±0.05	1.49±0.11	1.23±0.09
	k_L	0.36±0.03	2.99±0.19	0.40±0.03	0.60±0.04
	r^2	0.9992	0.9915	0.9948	0.9930
Freundlich	k_F	0.42±0.03	0.59±0.03	0.41±0.02	0.45±0.02
	1/n	0.80±0.06	0.49±0.02	0.77±0.03	0.71±0.05
	r^2	0.9997	0.9982	0.9989	0.9949
Temkin	B_T	0.13±0.01	0.12±0.01	0.20±0.01	0.18±0.01
	A_T	21.41±1.46	66.27±4.47	25.86±1.78	12.58±1.02
	r^2	0.8567	0.8396	0.8698	0.8350

Note: These parameters were obtained through non-linear curve fitting procedures.

Table 22: Biosorption Isotherm Parameters for Ni^{2+} and Cu^{2+} onto *A. doliolum* EPS (Single and Binary Systems)

Isotherm model	Model parameters	Ni biosorption		Cu biosorption	
		Cu 0.0 (mg L^{-1})	Cu 5.0 (mg L^{-1})	Ni 0.0 (mg L^{-1})	Ni 5.0 (mg L^{-1})
Langmuir	q_{max}	64.37±4.51	26.13±1.64	42.08±2.73	61.89±3.57
	k_L	2.31±0.16	6.46±0.41	4.03±0.35	0.46±0.03
	r^2	0.9905	0.9929	0.9974	0.9975
Freundlich	k_F	71.63±4.36	31.32±1.93	58.07±3.28	19.72±1.25
	1/n	0.78±0.04	0.51±0.03	0.70±0.05	0.79±0.05
	r^2	0.9966	0.9968	0.9985	0.9983
Temkin	B_T	3.94±0.22	4.20±0.25	3.53±0.26	5.50±0.35
	A_T	263.61±17.13	157.82±9.91	338.97±22.03	21.19±1.33
	r^2	0.8197	0.8325	0.7842	0.8748

Note: Parameters were calculated by the non-linear curve fitting procedure.

3.10. Desorption Study

Experiments were conducted to investigate the reusability and regeneration potential of *M. aeruginosa* and *A. doliolum* biomass, along with their EPS (Extracellular Polymeric Substances), for metal removal. Desorption efficiency is crucial for assessing the cost-effectiveness and recyclability of biosorption systems. De-ionized water was used as the desorbent for Cd^{2+}, Cu^{2+}, and Ni^{2+} ions adsorbed onto the biomass and EPS (Figures 38 and 39).

The results revealed a significantly higher desorption percentage for all three metal ions (Cd^{2+}, Cu^{2+}, and Ni^{2+}) from EPS compared to their respective native biomass

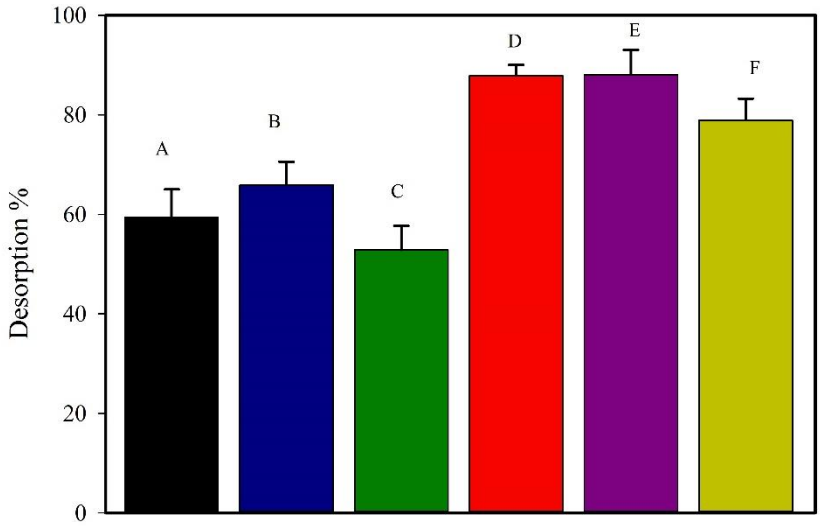

Figure.38. Desorption of Cd^{2+}, Cu^{2+}, and Ni^{2+} from *M. aeruginosa* biomass and EPS. This figure illustrates the desorption efficiency of de-ionized water for Cd^{2+}, Cu^{2+}, and Ni^{2+} ions previously adsorbed onto M. aeruginosa biomass (A-C) and its EPS (D-F). A-C: Depict the desorption percentage of Cd^{2+} (A), Cu^{2+} (B), and Ni^{2+} (C) from M. aeruginosa biomass. D-F: Show the desorption percentage of Cd^{2+} (D), Cu^{2+} (E), and Ni^{2+} (F) from M. aeruginosa EPS.

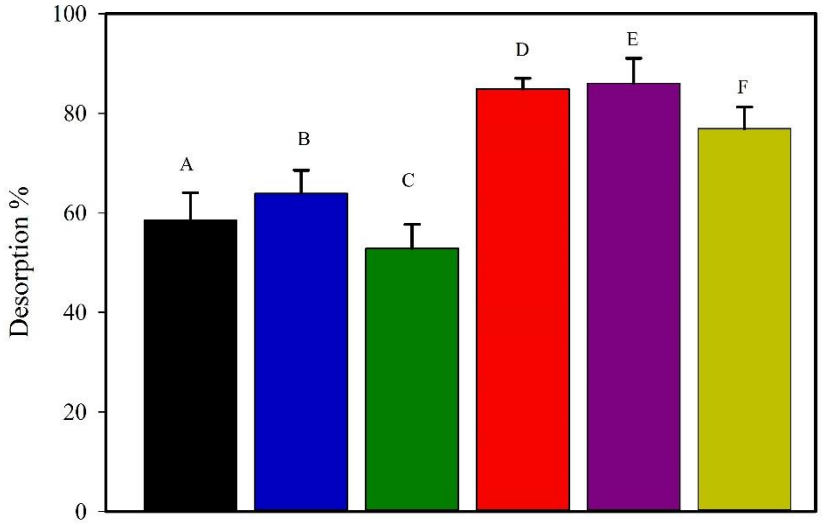

Figure.39. Desorption of Cd^{2+}, Cu^{2+}, and Ni^{2+} from *A. doliolum* biomass and EPS. This figure illustrates the desorption efficiency of de-ionized water for Cd^{2+}, Cu^{2+}, and Ni^{2+} ions previously adsorbed onto *A. doliolum* biomass (A-C) and its EPS (D-F). A-C: Depict the desorption percentage of Cd^{2+} (A), Cu^{2+} (B), and Ni^{2+} (C) from *A. doliolum* biomass. D-F: Show the desorption percentage of Cd^{2+} (D), Cu^{2+} (E), and Ni^{2+} (F) from *A. doliolum* EPS.

(Figures 38 and 39). This suggests that EPS might be a more suitable substrate for metal desorption due to its unique structural and chemical properties.

Desorption efficiency varied across the metal ions. Ni^{2+} consistently exhibited a lower desorption percentage compared to Cu^{2+} and Cd^{2+} on both *M. aeruginosa* and *A. doliolum* biomass, as well as their EPS. This indicates a stronger binding affinity between Ni^{2+} and the biosorbents.

SECTION II: LIVE CELLS EXPERIMENTS

3.11. Growth Pattern and Specific Growth Rate

Figure 40 depicts the growth patterns of *M. aeruginosa* and *A. doliolum*. Both organisms exhibited a lag phase in the first few days (around 5-6 days after inoculation). This was followed by an exponential growth phase between days 10-12 and 30, where their populations rapidly increased. After day 30, they entered a stationary phase, where their growth slowed and cell numbers remained relatively constant. The results suggest that *M. aeruginosa* had a higher growth rate than *A. doliolum* under the given conditions. Interestingly, both species appeared to have similar lag phases. However, during the exponential phase, their growth rates diverged, leading to M. aeruginosa reaching a higher final population density.

The specific growth rate of *M. aeruginosa* treated with copper (Cu^{2+}), nickel (Ni^{2+}), and cadmium (Cd^{2+}) for 96 h is shown in Figure 41. The results reveal that all three heavy metals have a detrimental effect on growth compared to the untreated control (0 µM). As the concentration of heavy metals increases, the specific growth rate of *M. aeruginosa* decreases. Interestingly, low concentrations (0-1.5 µM) of Ni^{2+} and Cu^{2+} resulted in a slight increase in specific growth rate compared to the control. *M. aeruginosa* treated with Cd^{2+} exhibited the strongest inhibition of growth at all concentrations tested, followed by Cu^{2+} and then Ni^{2+}.

Effect of Cu^{2+}, Ni^{2+}, and Cd^{2+} on the specific growth rate of *A. doliolum* (μd^{-1}) is shown in Figure 42. Similar to *M. aeruginosa* (Fig. 41), the specific growth rate of *A. doliolum* treated with copper (Cu^{2+}), nickel (Ni^{2+}), and cadmium (Cd^{2+}) for 96 h shows a general decrease with increasing heavy metal concentration. *A. doliolum* treated with Cd^{2+} exhibited the lowest specific growth rate at all concentrations,

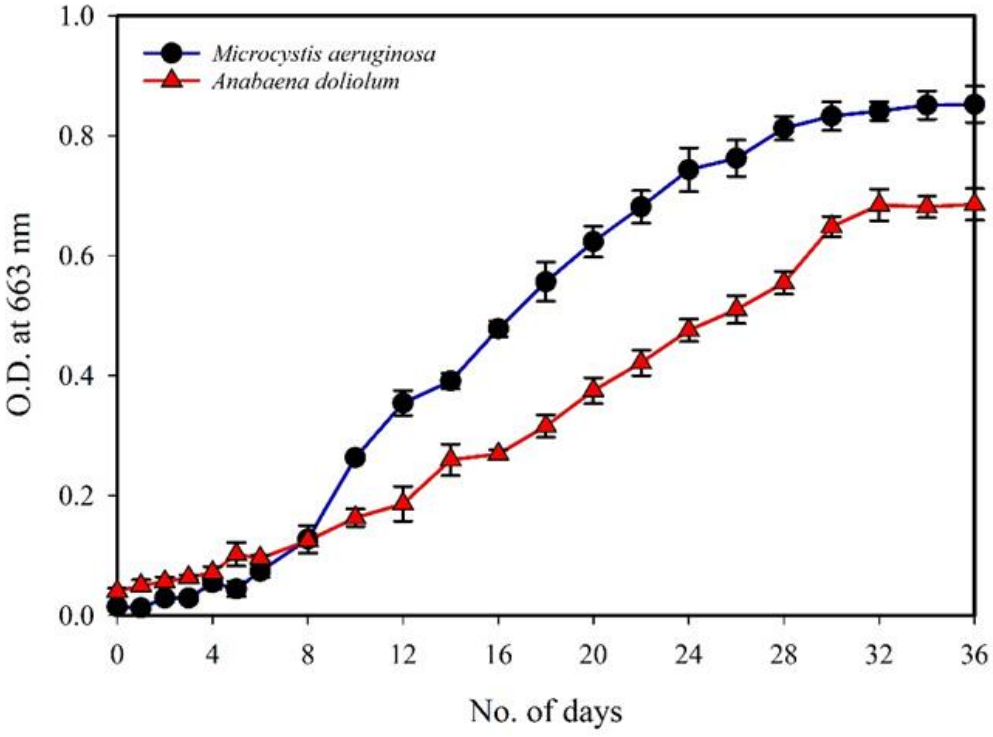

Figure.40. Growth patterns of *M. aeruginosa* and *A. doliolum*. Absorbance of culture at 663 nm was measured every other day to monitor growth over a 36-day period. Error bars represent the standard error of the mean (n=3).

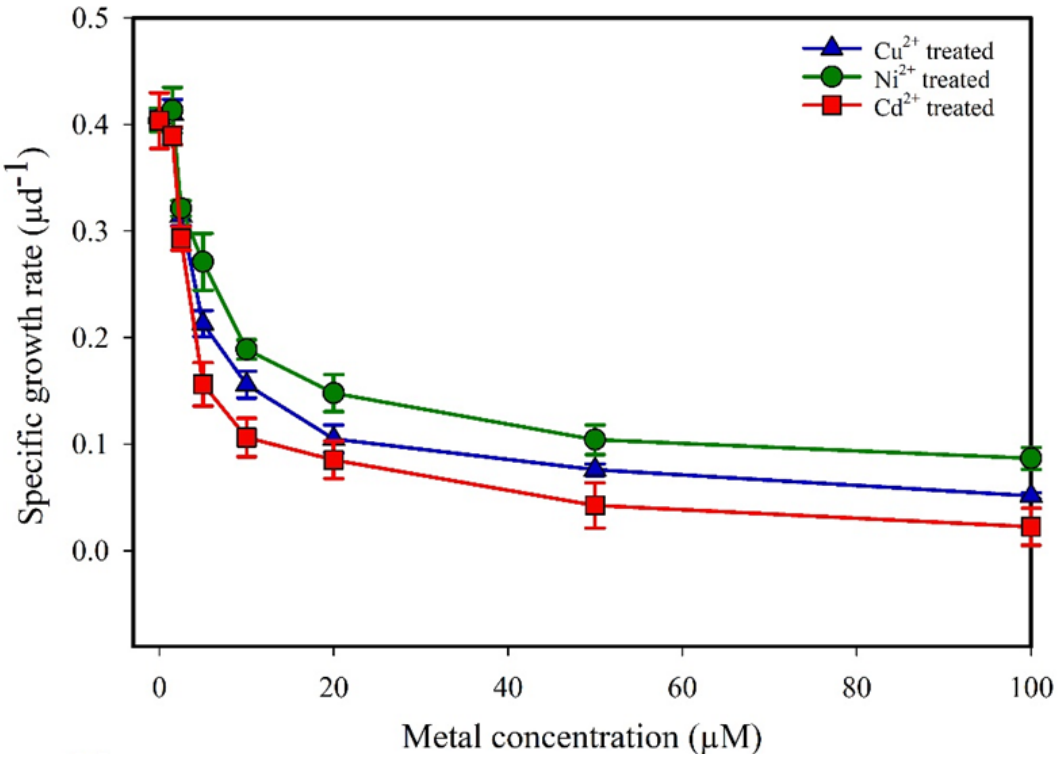

Figure.41. Effect of Cu^{2+}, Ni^{2+}, and Cd^{2+} on the specific growth rate of *M. aeruginosa*. The specific growth rate of *M. aeruginosa* treated with copper (Cu^{2+}), nickel (Ni^{2+}), and cadmium (Cd^{2+}) is shown. Vertical bars represent the standard error of the mean (n=3).

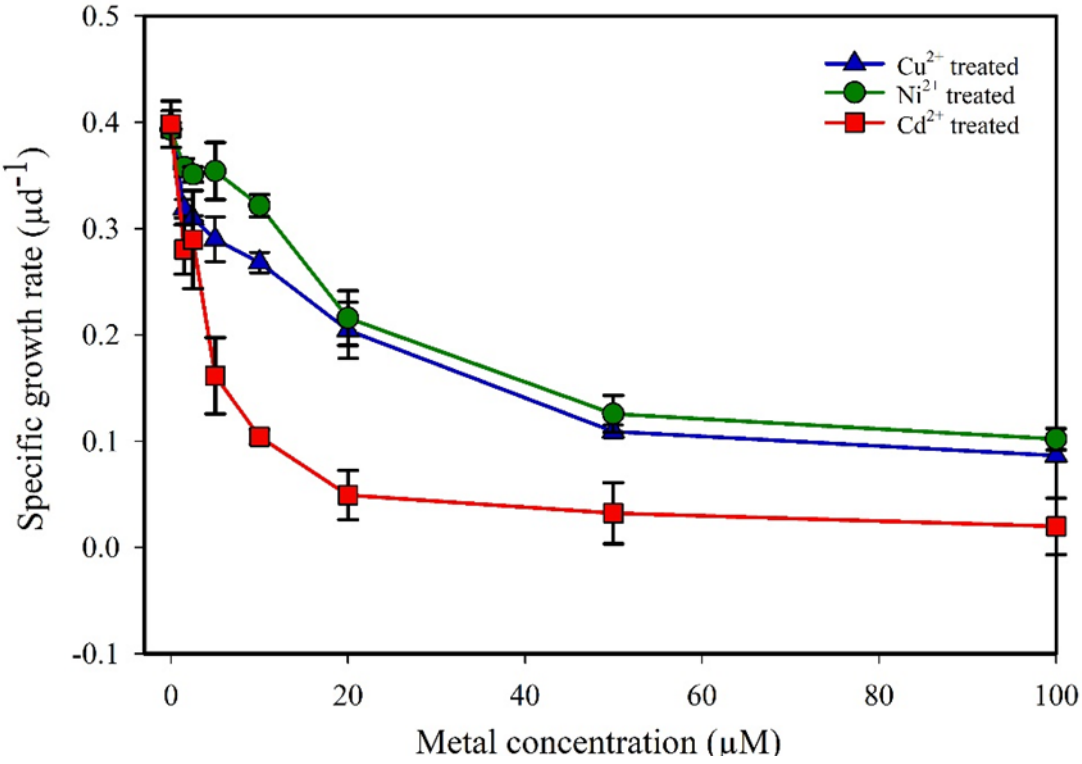

Figure.42. Effect of Cu^{2+}, Ni^{2+}, and Cd^{2+} on the specific growth rate of *A. doliolum*. The specific growth rate of *M. aeruginosa* treated with copper (Cu^{2+}), nickel (Ni^{2+}), and cadmium (Cd^{2+}) is shown. Vertical bars represent the standard error of the mean (n=3).

indicating the strongest inhibition by cadmium. Copper (Cu^{2+}) had a stronger inhibitory effect than nickel (Ni^{2+}) on *A. doliolum* growth.

3.12. Protein Content

Proteins are essential for all organisms, including cyanobacteria, as they play a crucial role in responding to stress. They help cells adapt to changing environmental conditions such as temperature, nutrient availability, light intensity, and various other stressors. Figure 43 illustrates the significant impact of Cu^{2+}, Ni^{2+}, and Cd^{2+} on the protein content of *M. aeruginosa* treated for 96 h. As the concentration of heavy metals in the external medium increases, the total protein content shows a clear decrease. Compared to the untreated control, Cu^{2+} treatment resulted in a 2.7-fold decrease, Ni^{2+} in a 2.2-fold decrease, and Cd^{2+} in the most dramatic decrease of 3.4-fold. These results indicate that Cd^{2+} has the most severe impact on protein content, followed by Cu^{2+} and then Ni^{2+}.

Similar to *M. aeruginosa*, the total protein content of *A. doliolum* treated with Cu^{2+}, Ni^{2+}, and Cd^{2+} for 96 h (Figure 44) also shows a decreasing trend with increasing metal concentration. Compared to the control, Cu^{2+} treatment resulted in a 4.4-fold decrease, Ni^{2+} in a 3.0-fold decrease, and Cd^{2+} in the most significant decrease of 7.9-fold. These results confirm that Cd^{2+} has the strongest inhibitory effect on protein content, followed by Cu^{2+} and then Ni^{2+}.

However, the untreated control group of *A. doliolum* exhibited a higher total protein content compared to untreated *M. aeruginosa*.

3.13. Total Carbohydrates Content

Carbohydrates play a vital role in how cyanobacteria respond to heavy metal stress. They are involved in various processes like energy metabolism, maintaining cell structure, and even detoxifying metals. This allows cyanobacteria to adapt and survive in environments contaminated with heavy metals. Figure 45 demonstrates the significant (P=0.05) impact of Cu^{2+}, Ni^{2+}, and Cd^{2+} on the total carbohydrate content of *M. aeruginosa* treated for 96 h. As the concentration of heavy metals in the

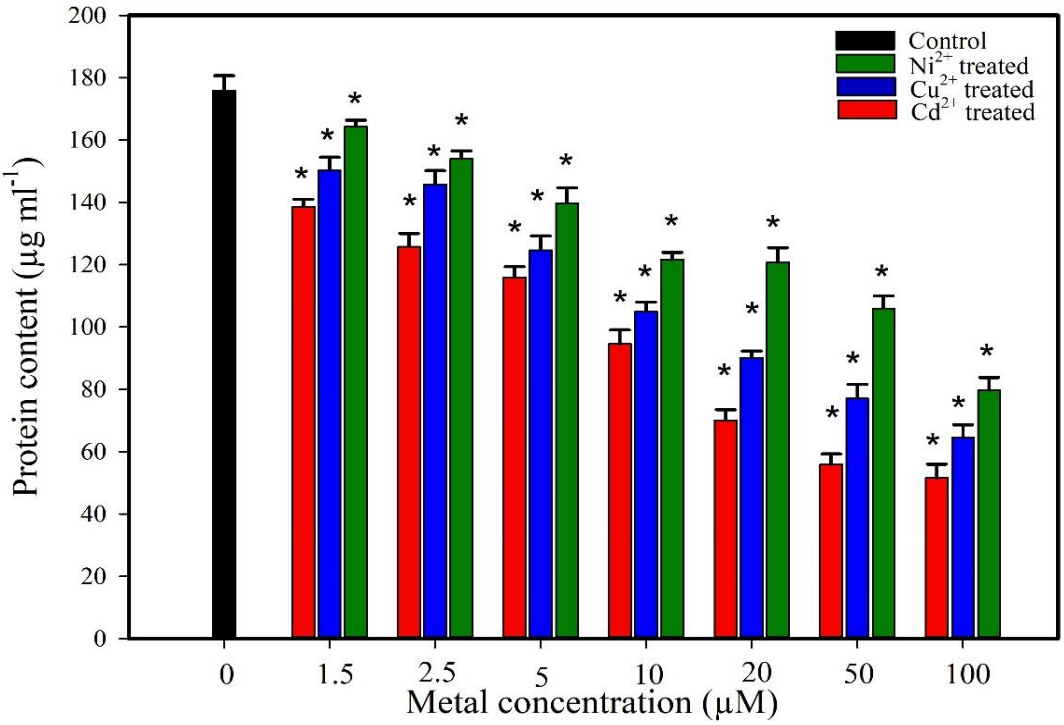

Figure.43. Total protein content (µg ml⁻¹) of *M. aeruginosa* treated with Cu^{2+}, Ni^{2+}, and Cd^{2+} for 96 h. Protein content showed statistically significant differences compared to the untreated control according to a two-tailed Student's T-Test. Asterisks indicate significance level: * (p = 0.05).

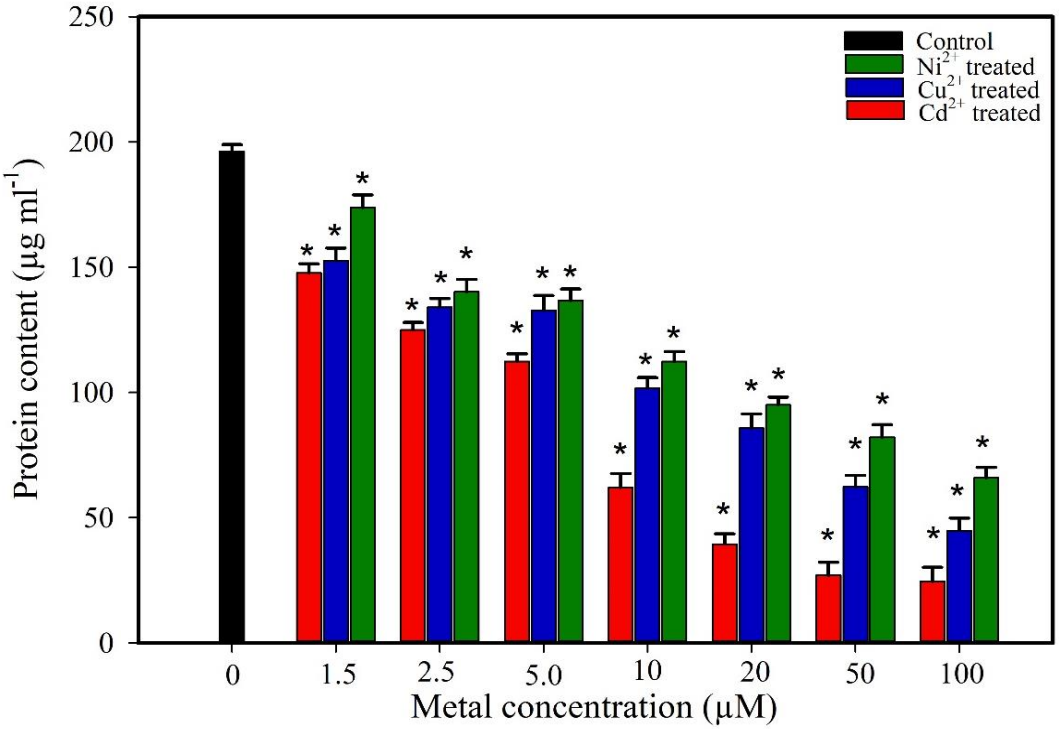

Figure.44. Total protein content (µg ml⁻¹) of *A. doliolum* treated with Cu^{2+}, Ni^{2+}, and Cd^{2+} for 96 h. Total protein content (µg ml⁻¹) of *M. aeruginosa* treated with Cu^{2+}, Ni^{2+}, and Cd^{2+} for 96 h. Protein content showed statistically significant differences compared to the untreated control according to a two-tailed Student's T-Test. Asterisks indicate significance level: * (p = 0.05).

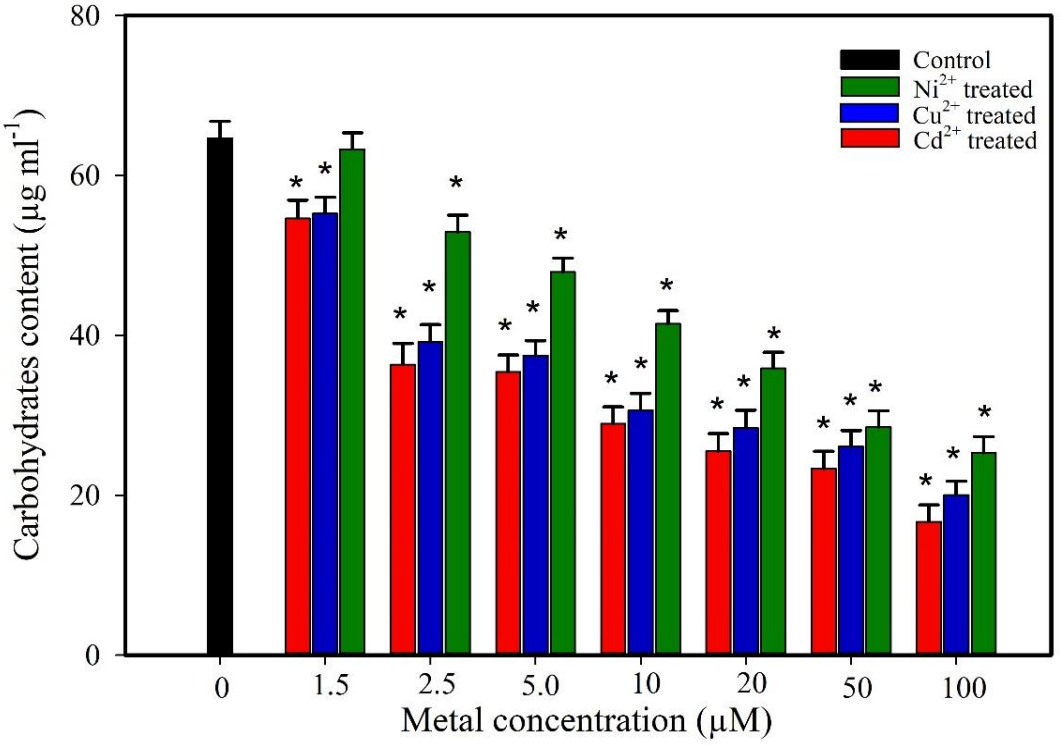

Figure.45. Total carbohydrate content of *M. aeruginosa* treated with Cu^{2+}, Ni^{2+}, and Cd^{2+} for 96 h. Vertical bars represent the standard error of the means (n=3). Total carbohydrate content showed statistically significant differences compared to the untreated control according to a two-tailed Student's T-Test. Asterisks indicate significance level: * (p = 0.05)

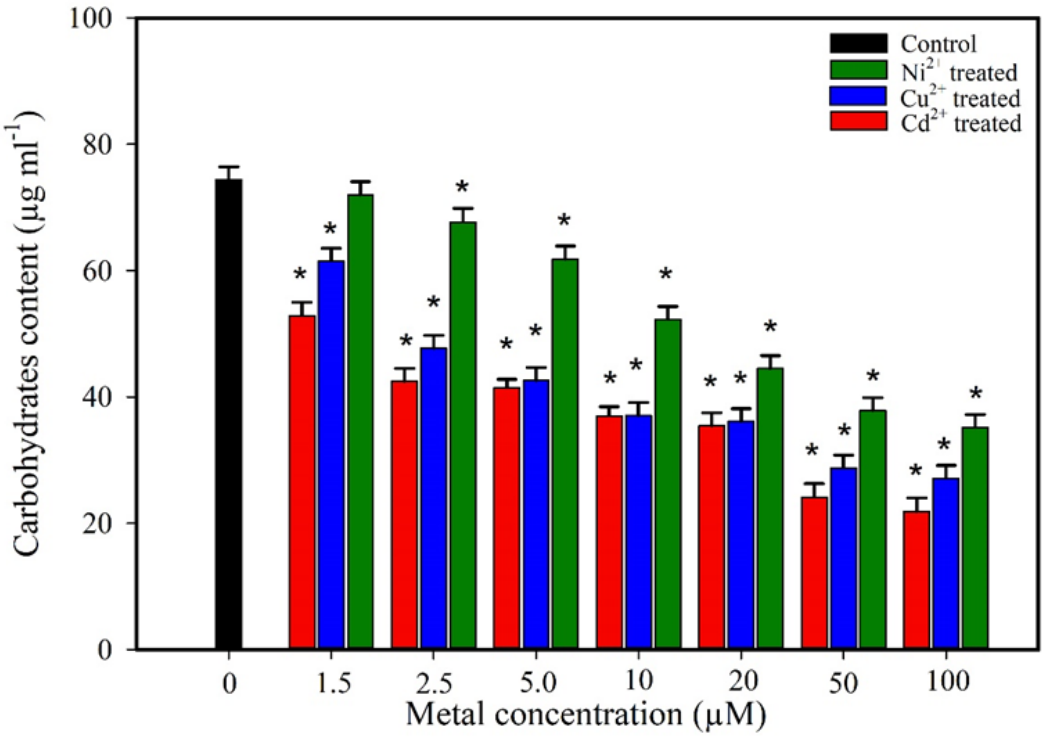

Figure.46. Total carbohydrate content of *A. doliolum* treated with Cu^{2+}, Ni^{2+}, and Cd^{2+} for 96 h. Vertical bars represent the standard error of the means (n=3). Total carbohydrate content showed statistically significant differences compared to the untreated control according to a two-tailed Student's T-Test. Asterisks indicate significance level: * (p = 0.05).

medium increases, the total carbohydrate content shows a clear reduction. Compared to the untreated control, Cu^{2+} treatment resulted in a 3.2-fold decrease, Ni^{2+} in a 2.6-fold decrease, and Cd^{2+} in the most dramatic decrease of 3.8-fold. These results indicate that Cd^{2+} has the strongest inhibitory effect on carbohydrate content, followed by Cu^{2+} and then Ni^{2+}.

Similar to *M. aeruginosa*, the total carbohydrate content of *A. doliolum* treated with Cu^{2+}, Ni^{2+}, and Cd^{2+} for 96 h (Figure 46) also exhibits a decreasing trend with increasing metal concentration in the medium. Compared to the control, Cu^{2+} treatment resulted in a 2.7-fold decrease, Ni^{2+} in a 2.1-fold decrease, and Cd^{2+} in the most significant decrease of 3.3-fold. These results confirm that Cd^{2+} has the strongest inhibitory effect on carbohydrate content, followed by Cu^{2+} and then Ni^{2+}.

Interestingly, untreated *A. doliolum* exhibited a higher total carbohydrate content compared to untreated *M. aeruginosa*.

3.14. Photosynthetic Pigment Content

Photosynthetic pigments, including chlorophylls and carotenoids, are essential components within cyanobacteria that enable them to capture sunlight and convert it into energy. They play a crucial role in light absorption, energy transfer, and protecting cells from excessive light. However, heavy metal stress can significantly impact these pigments, affecting photosynthetic efficiency, pigment biosynthesis, and the mechanisms by which cells respond to oxidative stress and detoxify themselves.

Figure 47 illustrates the impact of Cu^{2+}, Ni^{2+}, and Cd^{2+} treatment on the chlorophyll-a (Chl-a) content of *M. aeruginosa* after 96 h. All three metals caused a reduction in Chl-a content as their concentration increased in the medium. However, Cd^{2+} had the most dramatic effect, with a 64-fold decrease at the highest concentration (5.0 μM) compared to the control. Cu^{2+} and Ni^{2+} treatments resulted in lower but still significant reductions of 3.62-fold and 3.37-fold, respectively. These results indicate that Cd^{2+} has the most severe inhibitory effect on Chl-a content, followed by Cu^{2+} and then Ni^{2+}.

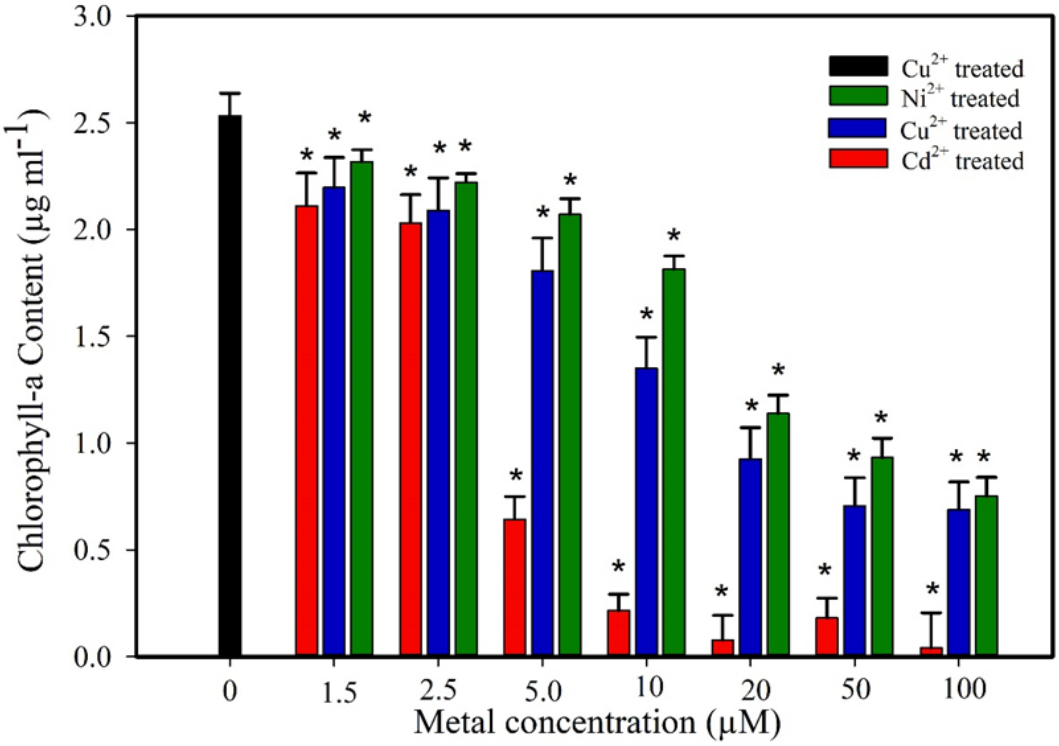

Figure.47. Chlorophyll-a (Chl-a) content of *M. aeruginosa* treated with Cu^{2+}, Ni^{2+}, and Cd^{2+} for 96 h. Vertical bars represent the standard error of the mean (n=3). Total chlorophyll-a content showed statistically significant differences compared to the untreated control according to a two-tailed Student's T-Test. Asterisks indicate significance level: * ($p = 0.05$).

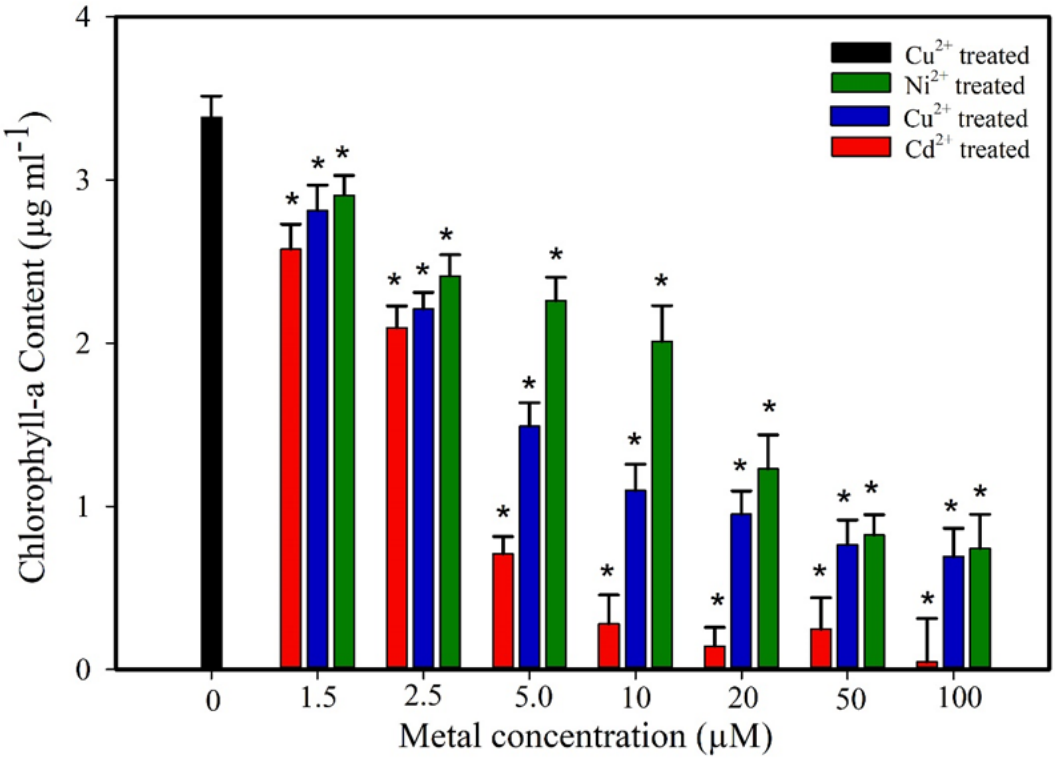

Figure.48. Chlorophyll-a (Chl-a) content of *A. doliolum* treated with Cu^{2+}, Ni^{2+}, and Cd^{2+} for 96 h. Vertical bars represent the standard error of the mean (n=3). Total Chlorophyll-a content showed statistically significant differences compared to the untreated control according to a two-tailed Student's T-Test. Asterisks indicate significance level: * (p = 0.05).

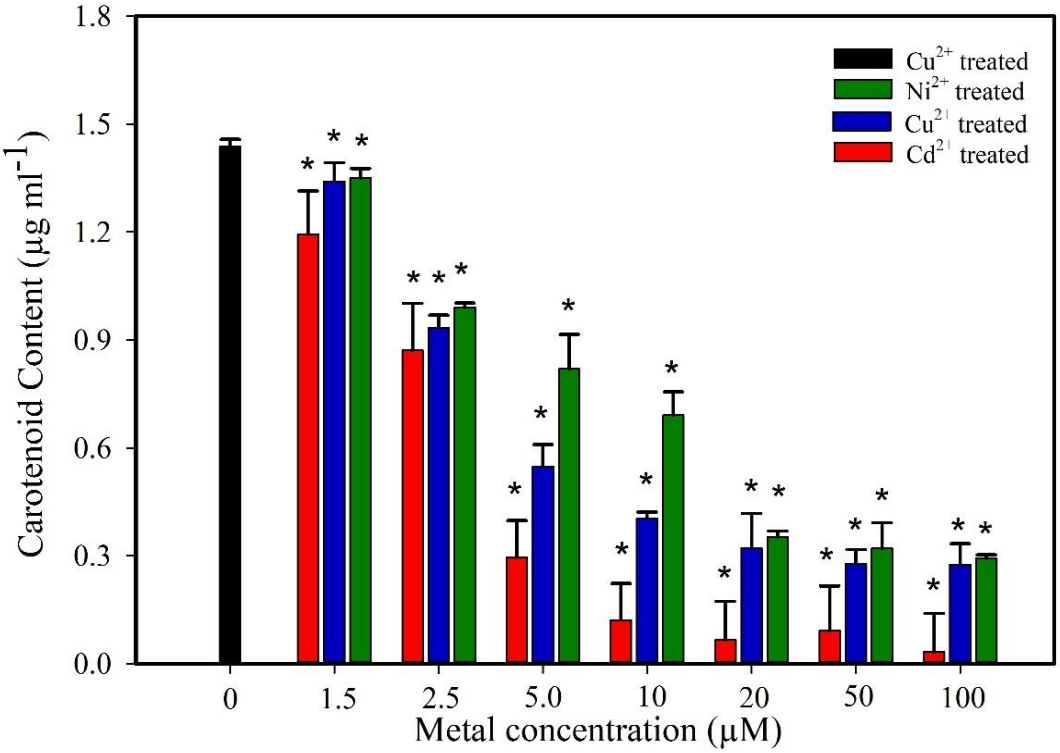

Figure.49. Carotenoid content of *M. aeruginosa* treated with Cu^{2+}, Ni^{2+}, and Cd^{2+} for 96 h. Vertical bars represent the standard error of the mean (n=3). Total carotenoids content showed statistically significant differences compared to the untreated control according to a two-tailed Student's T-Test. Asterisks indicate significance level: * (p = 0.05)

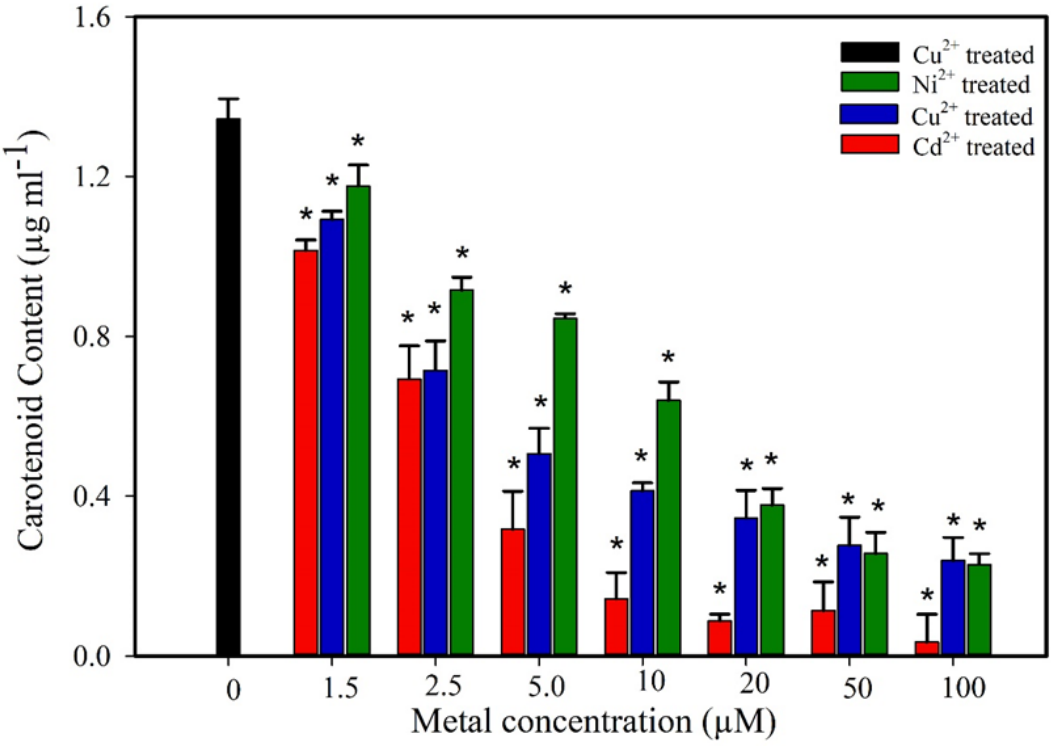

Figure.50. Carotenoid content of *A. doliolum* treated with Cu^{2+}, Ni^{2+}, and Cd^{2+} for 96 h. Vertical bars represent the standard error of the mean (n=3). Total carotenoids content showed statistically significant differences compared to the untreated control according to a two-tailed Student's T-Test. Asterisks indicate significance level: * (p = 0.05).

Similar to *M. aeruginosa*, the chlorophyll-a content of *A. doliolum* treated with Cu^{2+}, Ni^{2+}, and Cd^{2+} for 96 h (Figure 48) also showed a significant decline with increasing metal concentration. Cd^{2+} again displayed the strongest inhibitory effect, causing a 66.4-fold decrease in Chl-a content at the highest concentration compared to the control. Cu^{2+} and Ni^{2+} treatments resulted in reductions of 4.72-fold and 4.56-fold, respectively. These results confirm that Cd^{2+} has the strongest inhibitory effect on Chl-a content in *A. doliolum*, followed by Cu^{2+} and then Ni^{2+}. Figure 49 depicts the impact of Cu^{2+}, Ni^{2+}, and Cd^{2+} treatment on the carotenoid content of *M. aeruginosa* after 96 h. All three metals caused a reduction in carotenoid content as their concentration increased in the medium. Similar to Chl-a, Cd^{2+} had the most significant effect, with a 47.33-fold decrease at the highest concentration compared to the control. Cu^{2+} treatment resulted in a 5.14-fold decrease, while Ni^{2+} showed a less pronounced decrease of 4.73-fold. These results indicate that Cd^{2+} has the strongest inhibitory effect on carotenoid content, followed by Cu^{2+} and then Ni^{2+}. A similar trend was observed for the carotenoid content of *A. doliolum* treated with Cu^{2+}, Ni^{2+}, and Cd^{2+} for 96 h (Figure 50). All three metals caused a reduction in carotenoids; however, Cd^{2+} again exhibited the strongest inhibitory effect, with a 44.6-fold decrease at the highest concentration compared to the control. Cu^{2+} and Ni^{2+} treatments resulted in reductions of 5.7-fold and 5.5-fold, respectively. These results confirm that Cd^{2+} has the strongest inhibitory effect on carotenoid content in *A. doliolum*, followed by Cu^{2+} and then Ni^{2+}.

Chlorophyll-a (Chl-a) appears to be more sensitive to the tested metals (Cu^{2+}, Ni^{2+}, and Cd^{2+}) compared to carotenoids in both *M. aeruginosa* and *A. doliolum*.

3.15. Malondialdehyde (MDA) Content

Malondialdehyde (MDA) is a product of lipid peroxidation, a process that damages cell membranes due to oxidative stress. Measuring MDA content is a common way to assess the level of oxidative stress in cells. Figure 51 shows the impact of Cu^{2+}, Ni^{2+}, and Cd^{2+} treatment on the MDA content of *M. aeruginosa* after 96 h.

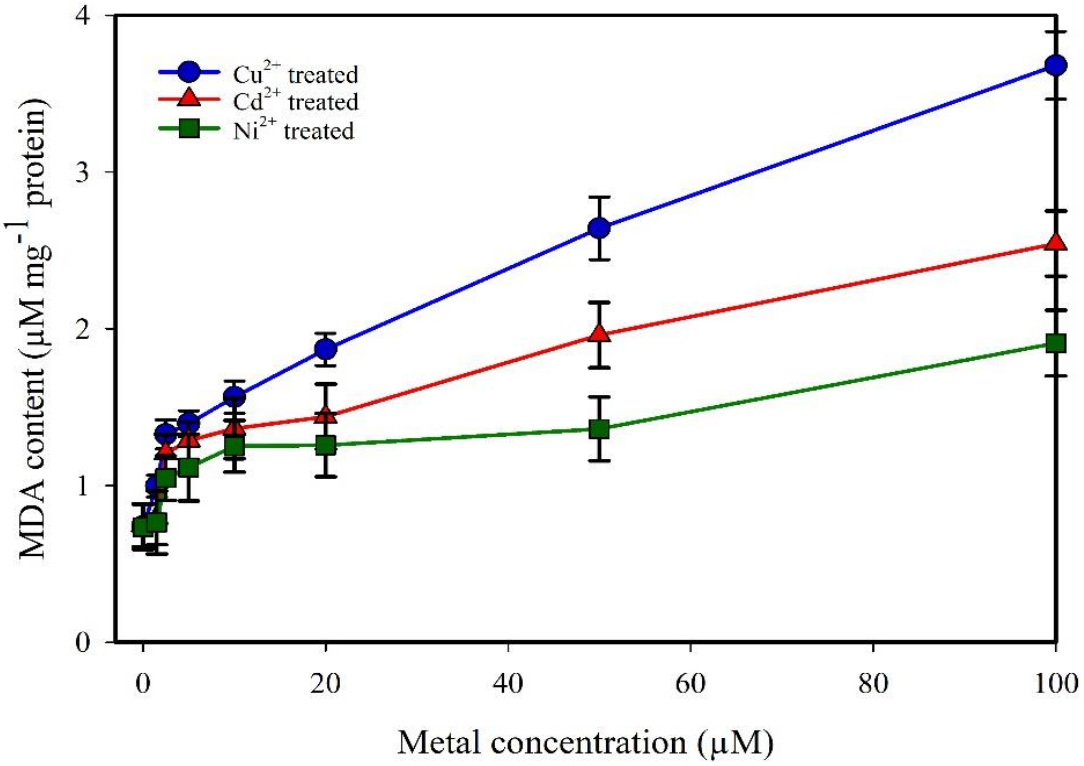

Figure.51. Malondialdehyde (MDA) content of *M. aeruginosa* treated with Cu^{2+}, Ni^{2+}, and Cd^{2+} for 96 h. Vertical bars represent the standard error of the mean (n=3). All treatments with Cu^{2+}, Ni^{2+}, and Cd^{2+} resulted in statistically significant ($P > 0.05$, Two-tailed Student's T-test) increases in MDA content compared to the untreated control.

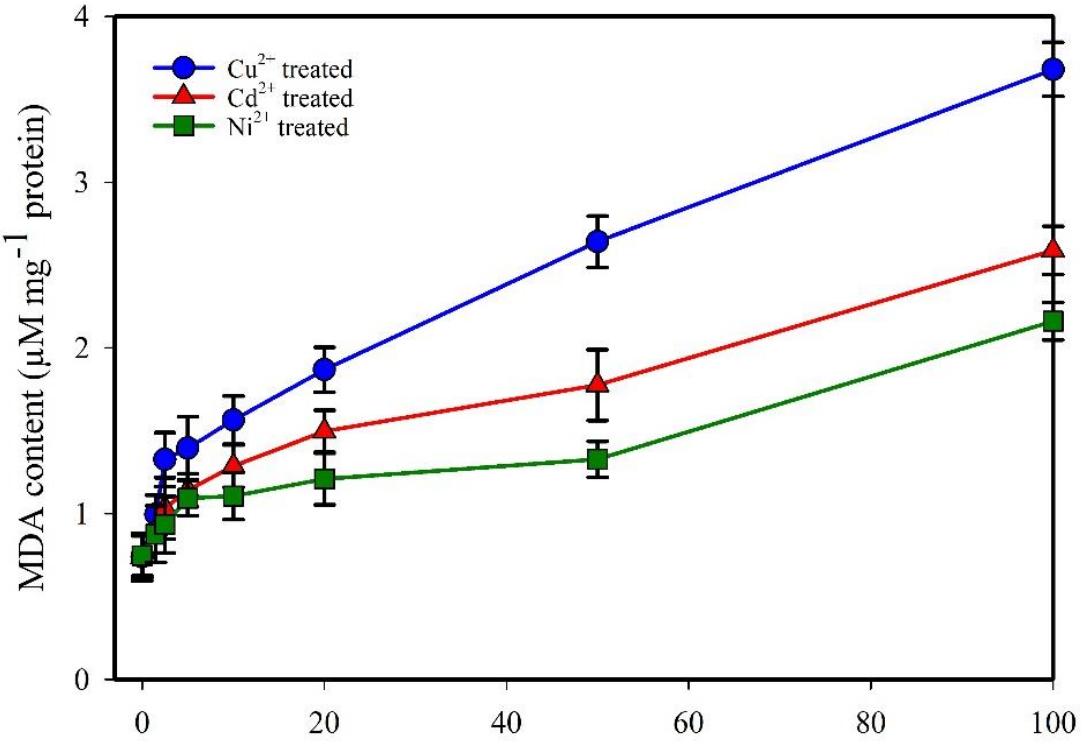

Figure.52. Malondialdehyde (MDA) content of *A. doliolum* treated with Cu^{2+}, Ni^{2+}, and Cd^{2+} for 96 h. Vertical bars represent the standard error of the mean (n=3). All treatments with Cu^{2+}, Ni^{2+}, and Cd^{2+} resulted in statistically significant ($P > 0.05$, Two-tailed Student's T-test) increases in MDA content compared to the untreated control.

As the concentration of heavy metals increases, the MDA content also increases steadily. All treatments with Cu^{2+}, Ni^{2+}, and Cd^{2+} resulted in statistically significant ($P > 0.05$, Two-tailed Student's T-test) increases in MDA content compared to the untreated control. This indicates that all three metals induced oxidative stress in *M. aeruginosa* cells.

Compared to the control, Cd^{2+} treatment resulted in the highest increase in MDA content, with a 4.97-fold increase. Cu^{2+} and Ni^{2+} treatments also caused significant increases of 2.58-fold and 3.38-fold, respectively. These results suggest that Cd^{2+} is the most potent inducer of oxidative stress among the tested metals, followed by Cu^{2+} and then Ni^{2+}.

Similar to *M. aeruginosa*, the MDA content of *A. doliolum* treated with Cu^{2+}, Ni^{2+}, and Cd^{2+} for 96 h (Figure 52) also showed a continuous rise with increasing metal concentration. This indicates a progressive increase in oxidative stress within the cell. Compared to the control, all treatments with Cu^{2+}, Ni^{2+}, and Cd^{2+} caused statistically significant increases ($P > 0.05$, Two-tailed Student's T-test) in MDA content. Compared to the control, Cd^{2+} treatment again resulted in the most significant increase in MDA content, with a 4.97-fold increase. Cu^{2+} and Ni^{2+} treatments caused increases of 2.88-fold and 3.50-fold, respectively. These results confirm that Cd^{2+} is the strongest inducer of oxidative stress in *A. doliolum*, followed by Cu^{2+} and then Ni^{2+}.

3.16. Hydrogen Peroxide (H_2O_2) Level

Hydrogen peroxide (H_2O_2) is a simple molecule consisting of two hydrogen atoms and one oxygen atom. Despite its seeming simplicity, H_2O_2 plays a complex role in cellular biology. It is classified as a reactive oxygen species (ROS). At low concentrations, H_2O_2 acts as a signaling molecule within cells. It can trigger various cellular responses, including gene expression changes, cell growth regulation, and defense mechanisms against pathogens. When H_2O_2 production becomes excessive, it can overwhelm the cell's antioxidant defenses. This leads to a state called oxidative stress, where ROS like H_2O_2 damage various cellular components like proteins, DNA, and membranes,

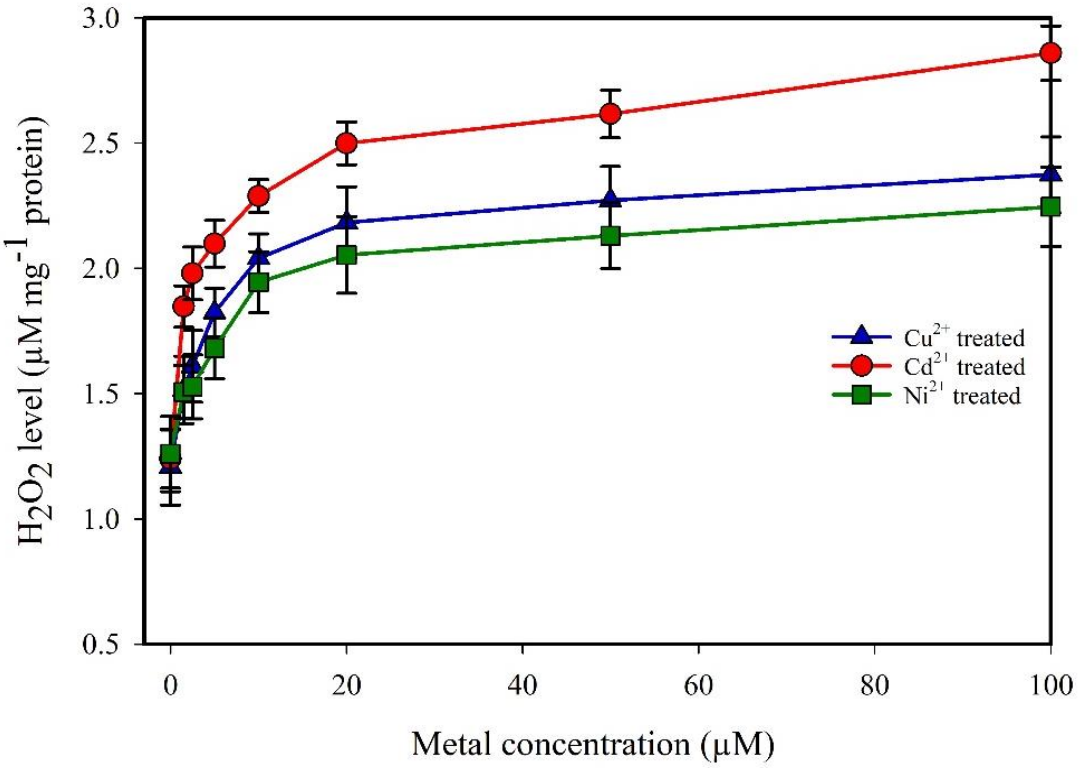

Figure.53. Hydrogen Peroxide (H_2O_2) production in *M. aeruginosa* treated with Cu^{2+}, Ni^{2+}, and Cd^{2+} for 96 h. Vertical bars represent the standard error of the mean (n=3). All treatments with Cu^{2+}, Ni^{2+}, and Cd^{2+} resulted in statistically significant ($P > 0.05$, Two-tailed Student's T-test) increases in H_2O_2 levels compared to the untreated control.

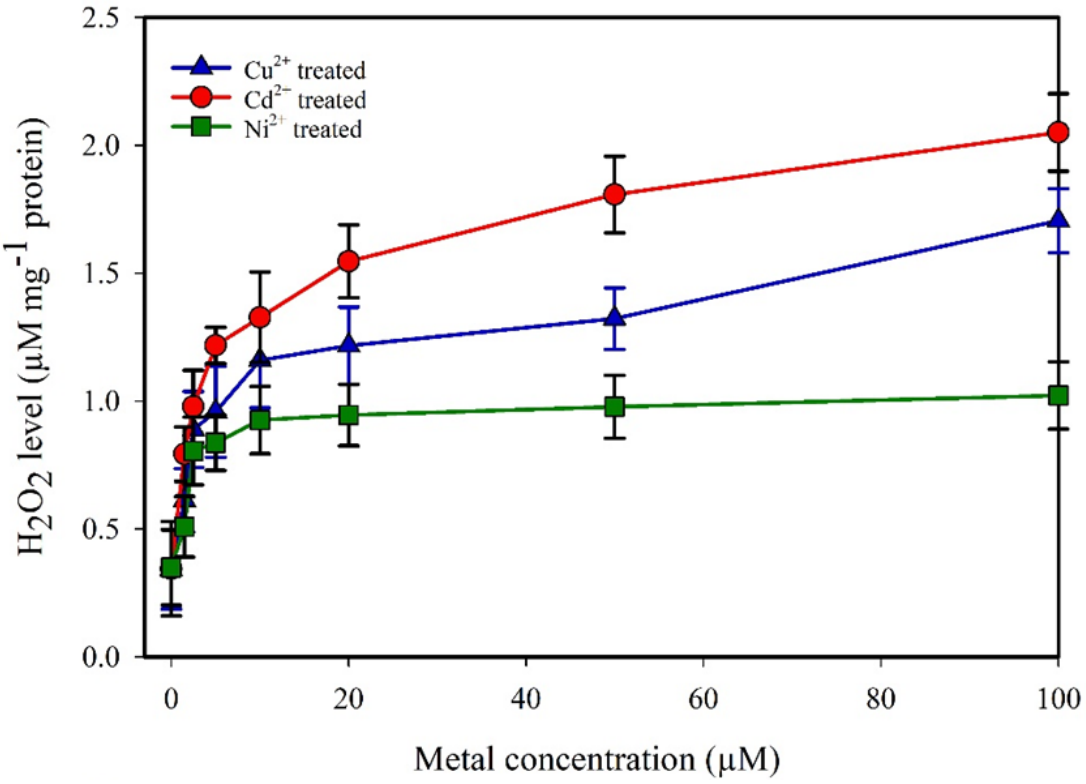

Figure.54. Hydrogen Peroxide (H_2O_2) production in *A. doliolum* treated with Cu^{2+}, Ni^{2+}, and Cd^{2+} for 96 h. Vertical bars represent the standard error of the mean (n=3). All treatments with Cu^{2+}, Ni^{2+}, and Cd^{2+} resulted in statistically significant ($P > 0.05$, Two-tailed Student's T-test) increases in H_2O_2 levels compared to the untreated control.

Figure 53 shows the impact of Cu^{2+}, Ni^{2+}, and Cd^{2+} treatment on the H_2O_2 production in *M. aeruginosa* after 96 h. As the concentration of heavy metals in the medium increases, the H_2O_2 level also increases steadily. This indicates a dose-dependent response, where higher metal concentrations lead to greater oxidative stress. Compared to the control, Cd^{2+} treatment resulted in the highest increase in H_2O_2 level, with a 2.31-fold increase. Cu^{2+} and Ni^{2+} treatments also caused significant increases of 1.96-fold and 1.78-fold, respectively. The vertical bars represent the standard error of the mean (n=3). These results suggest that Cd^{2+} is the most potent inducer of oxidative stress among the tested metals, followed by Cu^{2+} and then Ni^{2+}.

Similar to *M. aeruginosa*, the H_2O_2 level of *A. doliolum* treated with Cu^{2+}, Ni^{2+}, and Cd^{2+} for 96 h (Figure 54) also exhibited a continuous rise with increasing metal concentration. This indicates a progressive increase in oxidative stress within the cells. Notably, *A. doliolum* displayed a higher overall increase in H_2O_2 production compared to *M. aeruginosa*. Compared to the control, Cd^{2+} treatment again resulted in the most significant increase in H_2O_2 level, with a remarkable 5.95-fold increase. Cu^{2+} and Ni^{2+} treatments also caused increases of 5.0-fold and 2.93-fold, respectively. These results confirm that Cd^{2+} is the strongest inducer of oxidative stress in *A. doliolum*, followed by Cu^{2+} and then Ni^{2+}. Interestingly, *A. doliolum* appears to be more sensitive to oxidative stress induced by heavy metals compared to *M. aeruginosa*.

The increases in H_2O_2 production observed in both *M. aeruginosa* and *A. doliolum* treated with Cu^{2+}, Ni^{2+}, and Cd^{2+} were statistically significant ($P > 0.05$) compared to the untreated controls, as determined by a Two Tailed Student's T-test. This statistically significant increase supports the conclusion that these heavy metals induce oxidative stress in these cyanobacteria.

3.17. Superoxide Radicals ($O2^-$)

Superoxide radicals produced in reaction to metal stress can cause oxidative stress and cellular damage in cyanobacteria by interacting with other molecules such lipids, proteins, and nucleic acids. An imbalance between ROS production and antioxidant defence systems can cause oxidative damage, disruption of cellular functioning, and, eventually, cell death. At low concentrations, superoxide radicals can act as signaling

molecules within the cell, participating in processes like immune response activation and wound healing. Oxidative stress occurs when the production of ROS, including superoxide radicals, exceeds the antioxidant defenses of cells.

Figure 55 shows the impact of Cu^{2+}, Ni^{2+}, and Cd^{2+} treatment on the superoxide radical production in *M. aeruginosa* after 96 h. As the concentration of heavy metals in the medium increases, the level of superoxide radicals also increases. This indicates a dose-dependent response, where higher metal concentrations lead to greater oxidative stress. Interestingly, Cu^{2+} treatment resulted in the highest increase in superoxide radical production (2.81-fold) compared to the control, followed by Cd^{2+} (2.25-fold) and Ni^{2+} (1.93-fold). All increases in superoxide radical production compared to the control were statistically significant ($P > 0.05$) as determined by a Two-Tailed Student's T-test. These results suggest that Cu^{2+} may be a more potent inducer of superoxide radical generation in *M. aeruginosa* compared to Cd^{2+} and Ni^{2+} under these conditions.

Similar to *M. aeruginosa*, the superoxide radical level of *A. doliolum* treated with Cu^{2+}, Ni^{2+}, and Cd^{2+} for 96 h (Figure 56) also exhibited a continuous rise with increasing metal concentration. However, *A. doliolum* displayed a generally higher level of superoxide radical production compared to *M. aeruginosa*. In *A. doliolum*, Cu^{2+} again caused the highest increase (5.6-fold) in superoxide radical level compared to the control, followed by Cd^{2+} (4.19-fold) and Ni^{2+} (3.75-fold). All increases in superoxide radical production compared to the control were statistically significant ($P > 0.05$) as determined by a Two-Tailed Student's T-test. These results suggest that Cu^{2+} might be the strongest inducer of superoxide radical generation in *A. doliolum* as well. Interestingly, *A. doliolum* appears to generate higher levels of superoxide radicals overall compared to *M. aeruginosa* when exposed to these heavy metals.

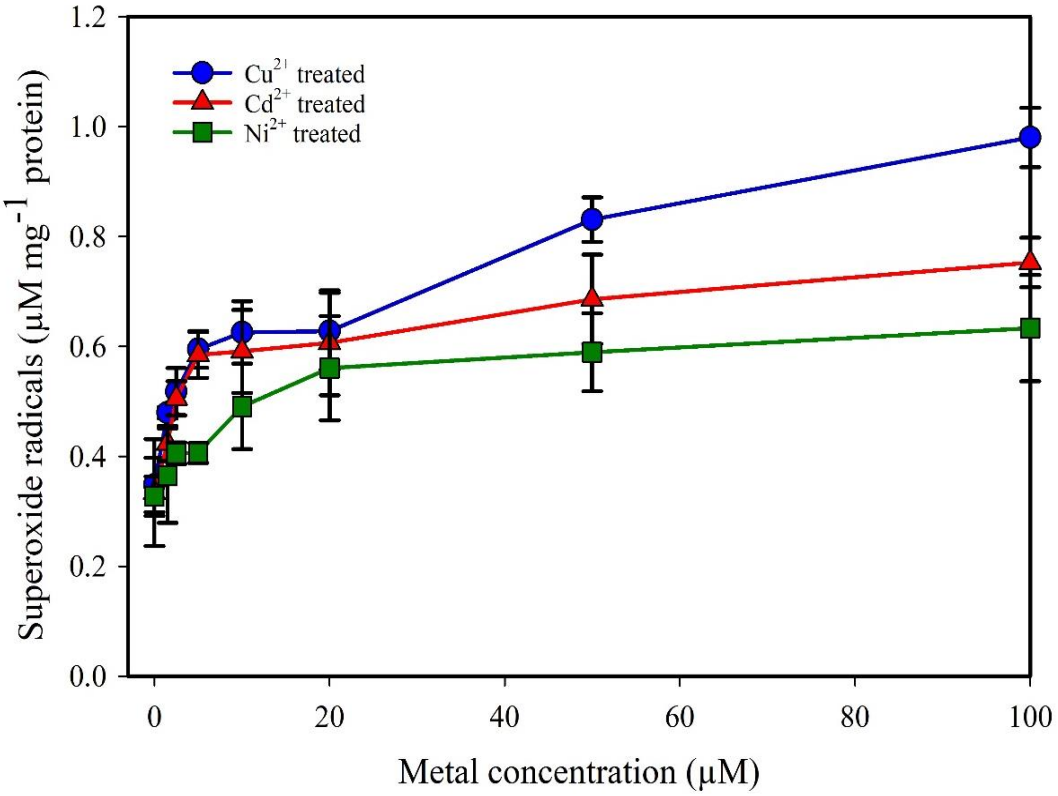

Figure.55. Superoxide radical production in *M. aeruginosa* treated with Cu^{2+}, Ni^{2+}, and Cd^{2+} for 96 h. Vertical bars represent the standard error of the mean (n=3). All treatments with Cu^{2+}, Ni^{2+}, and Cd^{2+} resulted in statistically significant ($P > 0.05$, Two-tailed Student's T-test) increases in O_2^- levels compared to the untreated control.

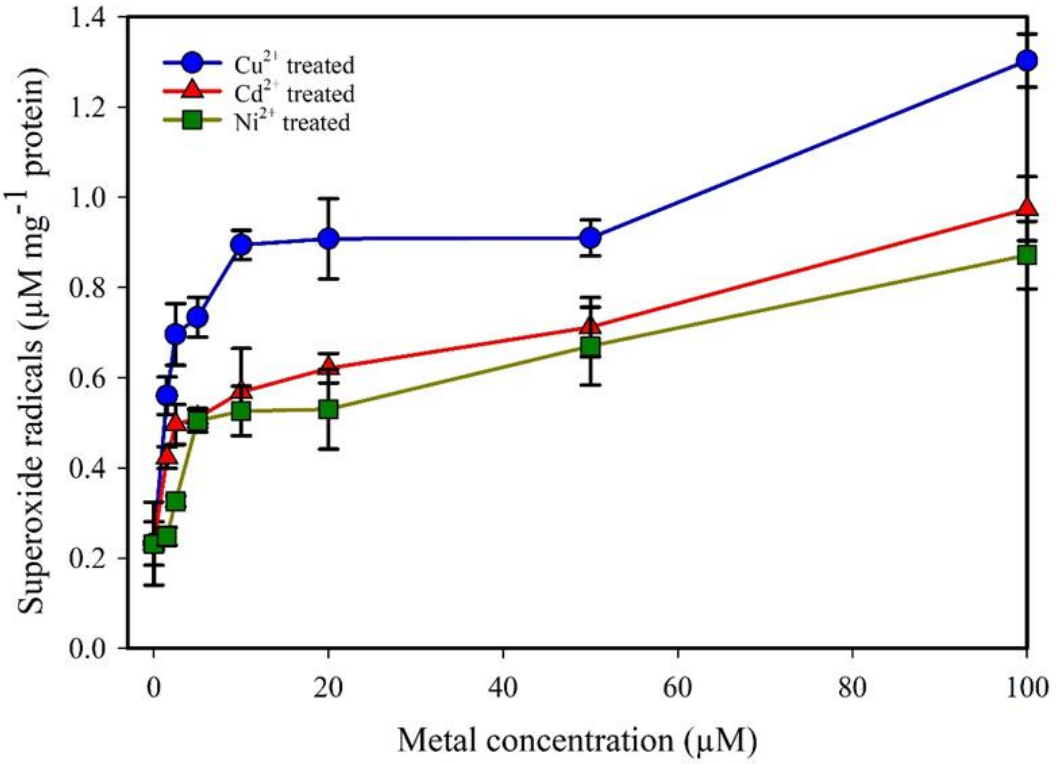

Figure.56. Superoxide radical production in *A. doliolum* treated with Cu^{2+}, Ni^{2+}, and Cd^{2+} for 96 h. Vertical bars represent the standard error of the mean (n=3). All treatments with Cu^{2+}, Ni^{2+}, and Cd^{2+} resulted in statistically significant ($P > 0.05$, Two-tailed Student's T-test) increases in O_2^- levels compared to the untreated control.

3.18. Hydroxyl Radical (OH^-)

Hydroxyl radicals (OH•) are highly reactive molecules and some of the most potent oxidants found within cells. They can damage a wide range of cellular components, including proteins, lipids, and DNA, leading to significant cellular dysfunction and death. Their formation often occurs through the Fenton reaction, where superoxide radicals interact with free iron.

Figures 57 and 58 show the impact of Cu^{2+}, Ni^{2+}, and Cd^{2+} treatment on the hydroxyl radical production in M. aeruginosa and A. doliolum after 96 h, respectively. As observed with superoxide radicals, the level of hydroxyl radicals also increases with increasing heavy metal concentration in both species, indicating a dose-dependent response. *M. aeruginosa* displayed a significant ($P>0.05$; Two Tailed Student's T-Test) increase in hydroxyl radical production compared to the control across all treatments. Cu^{2+} treatment resulted in the highest increase (4.01-fold), followed by Cd^{2+} (3.81-fold) and Ni^{2+} (2.81-fold). These results suggest that Cu^{2+} may be the most potent inducer of hydroxyl radical generation in *M. aeruginosa* under these conditions.

Interestingly, *A. doliolum* displayed a different pattern compared to *M. aeruginosa*. While the hydroxyl radical level still increased with increasing metal concentration, the overall increase was lower. Cu^{2+} again caused the highest increase (2.31-fold) compared to the control, followed by Cd^{2+} (1.57-fold) and Ni^{2+} (0.31-fold). These results suggest that *A. doliolum* may be more efficient at mitigating hydroxyl radical production compared to *M. aeruginosa* when exposed to these heavy metals.

3.19. Estimation of Antioxidant Enzymes Activity

3.19.1. Superoxide Dismutase (SOD) Content

SOD acts as a cellular defense specifically against superoxide radicals. It functions as a catalyst, accelerating the conversion of superoxide radicals into hydrogen peroxide (H_2O_2), a less reactive molecule. Figures 59 and 60 show the impact of Cu^{2+}, Ni^{2+}, and Cd^{2+} treatment on the SOD enzyme activity in *M. aeruginosa* and *A. doliolum* after 96 h, respectively. Interestingly, the results show an increase in SOD activity with increasing heavy metal concentration in both species.

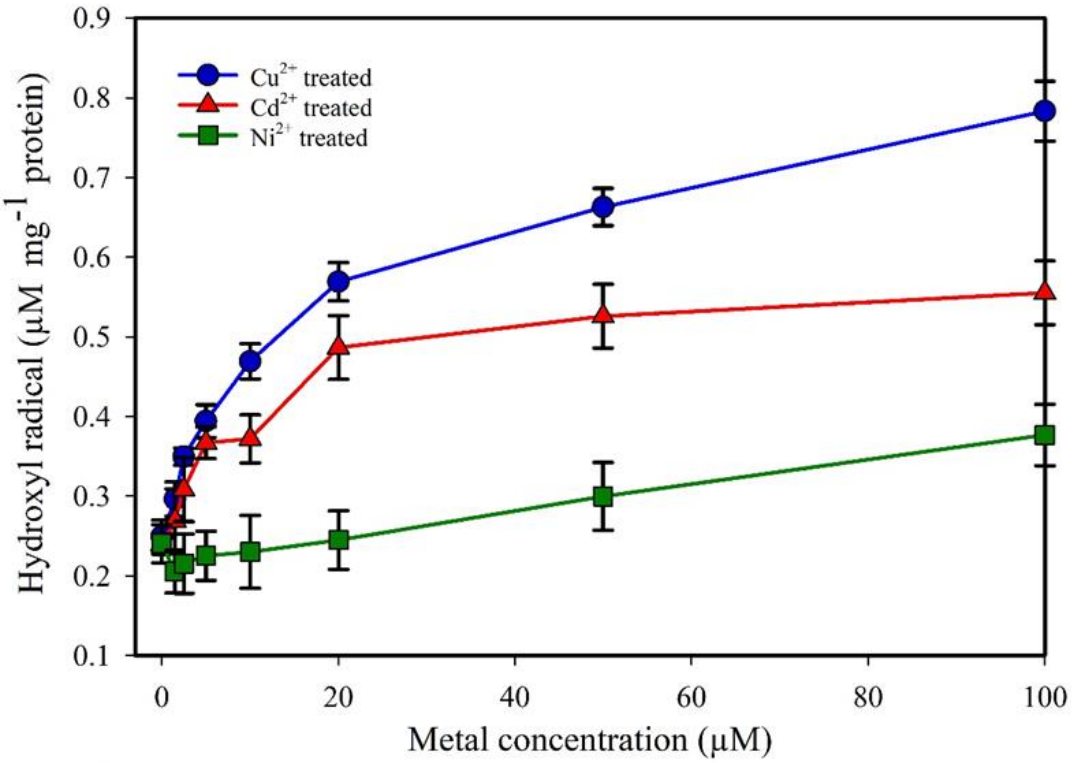

Figure.57. Hydroxyl radical production in *M. aeruginosa* treated with Cu^{2+}, Ni^{2+}, and Cd^{2+} for 96 h. Vertical bars represent the standard error of the mean (n=3). All treatments with Cu^{2+}, Ni^{2+}, and Cd^{2+} resulted in statistically significant ($P > 0.05$, Two-tailed Student's T-test) increases in OH^- levels compared to the untreated control.

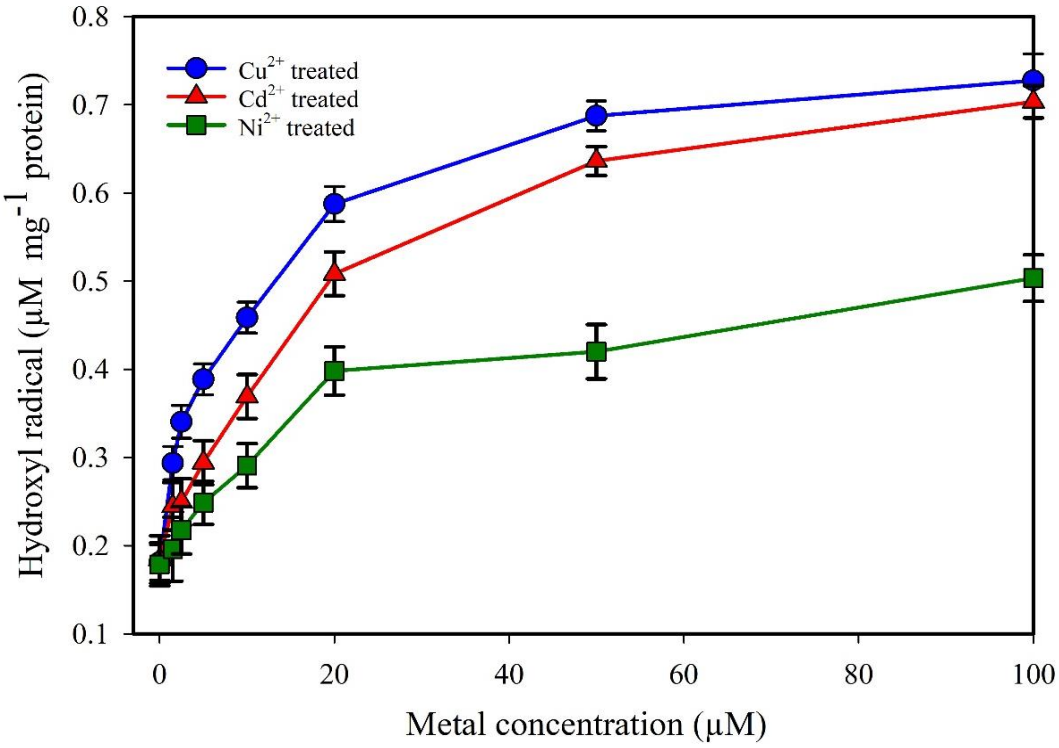

Figure.58. Hydroxyl radical production in *A. doliolum* treated with Cu^{2+}, Ni^{2+}, and Cd^{2+} for 96 h. Vertical bars represent the standard error of the mean (n=3). All treatments with Cu^{2+}, Ni^{2+}, and Cd^{2+} resulted in statistically significant ($P > 0.05$, Two-tailed Student's T-test) increases in OH^- levels compared to the untreated control.

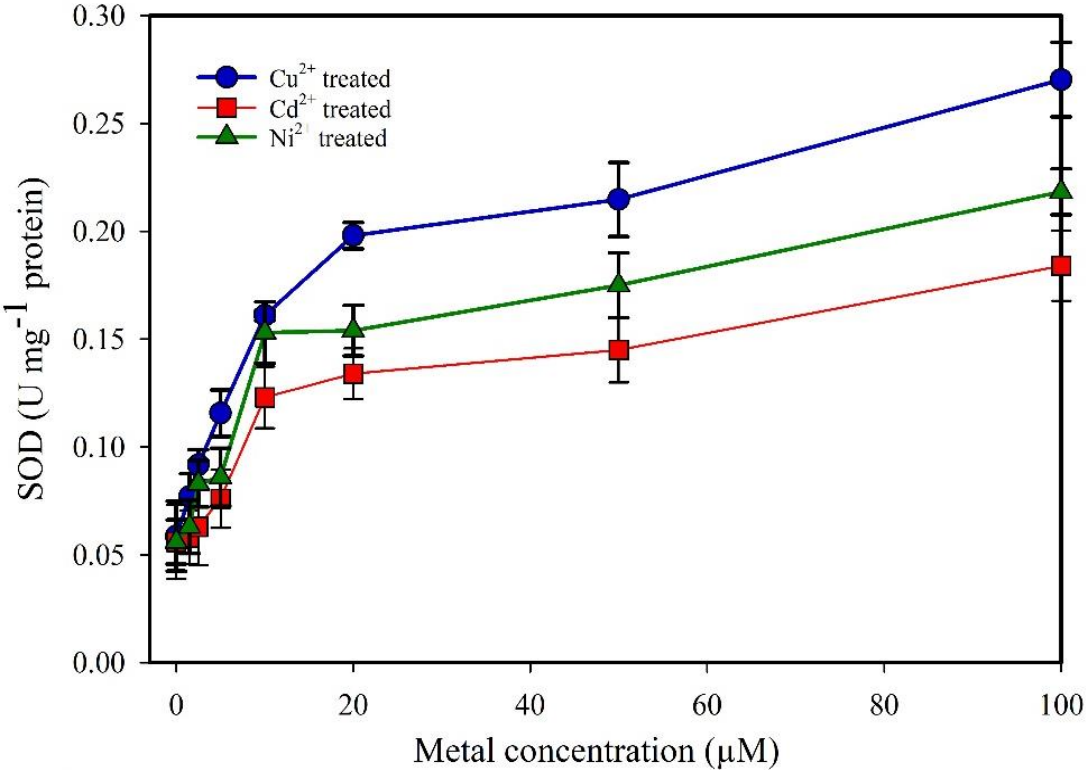

Figure.59. SOD enzyme activity in *M. aeruginosa* treated with Cu^{2+}, Ni^{2+}, and Cd^{2+} for 96 h. Vertical bars represent the standard error of the mean (n=3). All treatments with Cu^{2+}, Ni^{2+}, and Cd^{2+} resulted in statistically significant ($P > 0.05$, Two-tailed Student's T-test) increases in SOD levels compared to the untreated control.

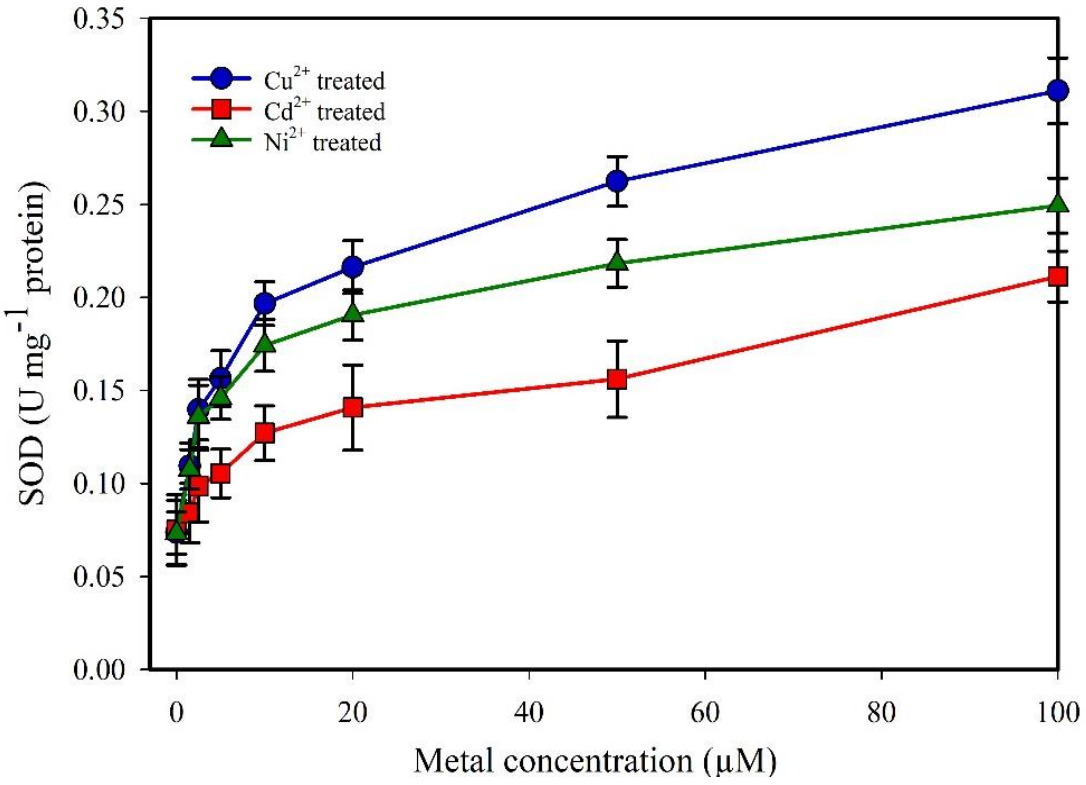

Figure.60. SOD enzyme activity in *A. doliolum* treated with Cu^{2+}, Ni^{2+}, and Cd^{2+} for 96 h. Vertical bars represent the standard error of the mean (n=3). All treatments with Cu^{2+}, Ni^{2+}, and Cd^{2+} resulted in statistically significant ($P > 0.05$, Two-tailed Student's T-test) increases in SOD levels compared to the untreated control.

M. aeruginosa displayed a significant increase in SOD activity compared to the control across all treatments. Cu^{2+} treatment resulted in the highest increase (4.6-fold), followed by Cd^{2+} (3.29-fold) and Ni^{2+} (3.90-fold). All increases in SOD activity compared to the control were statistically significant ($P > 0.05$) as determined by a Two-Tailed Student's T-test. These results suggest that *M. aeruginosa* might be upregulating its SOD activity as a defense mechanism against the increased superoxide radical production caused by heavy metal stress.

A similar pattern of increased SOD activity with increasing metal concentration was observed in *A. doliolum*. Cu^{2+} again caused the highest increase (4.22-fold) compared to the control, followed by Cd^{2+} (3.40-fold) and Ni^{2+} (2.81-fold). All increases in SOD activity compared to the control were statistically significant ($P > 0.05$) as determined by a Two-Tailed Student's T-test. These results suggest that *A. doliolum* also appears to be upregulating its SOD activity in response to heavy metal stress.

3.19.2 Catalase Enzymes (CAT) Activity

Catalase (CAT) is another crucial antioxidant enzyme found in most living organisms, including cyanobacteria. It plays a vital role in cellular defense against oxidative stress by decomposing hydrogen peroxide (H_2O_2), a byproduct of various cellular processes, into water (H_2O) and oxygen (O_2). H_2O_2 itself is less harmful than superoxide radicals, but at high concentrations, it can still contribute to oxidative damage. Catalase helps to maintain a healthy balance of H_2O_2 within cells. Figures 61 and 62 show the impact of Cu^{2+}, Ni^{2+}, and Cd^{2+} treatment on the catalase enzyme activity in *M. aeruginosa* and *A. doliolum* after 96 h, respectively. Similar to the observed increase in SOD activity, both species exhibited a rise in catalase activity with increasing heavy metal concentration.

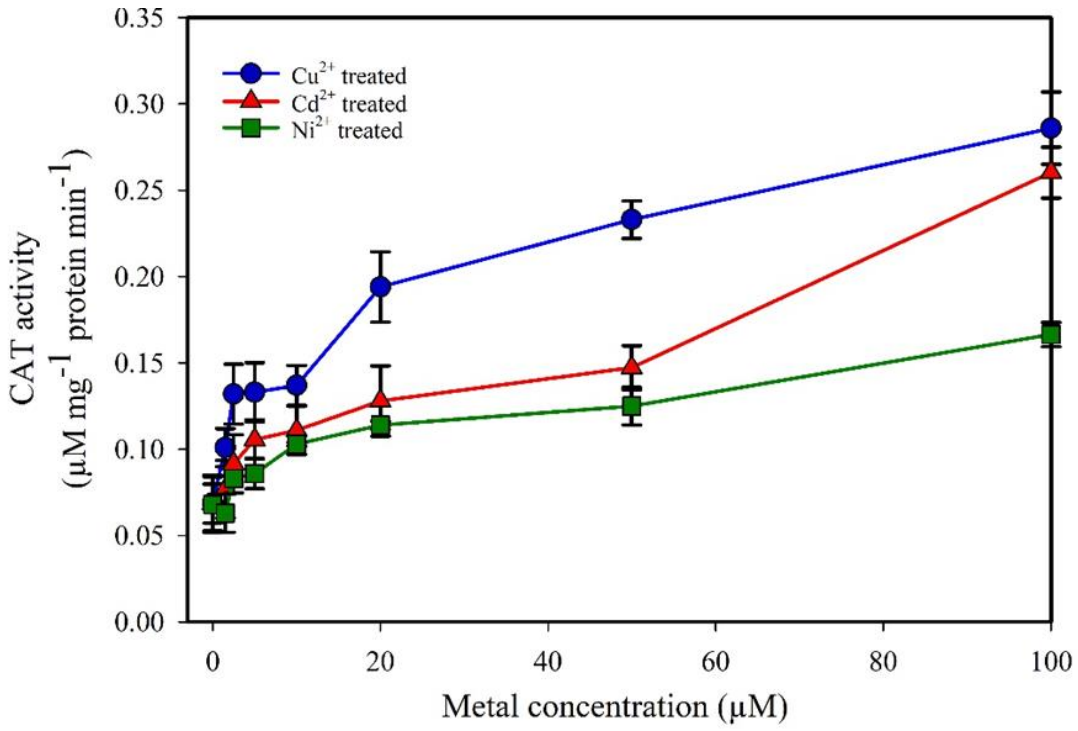

Figure.61. Catalase enzyme activity in *M. aeruginosa* treated with Cu^{2+}, Ni^{2+}, and Cd^{2+} for 96 h. Vertical bars represent the standard error of the mean (n=3). All treatments with Cu^{2+}, Ni^{2+}, and Cd^{2+} resulted in statistically significant ($P > 0.05$, Two-tailed Student's T-test) increases in CAT levels compared to the untreated control.

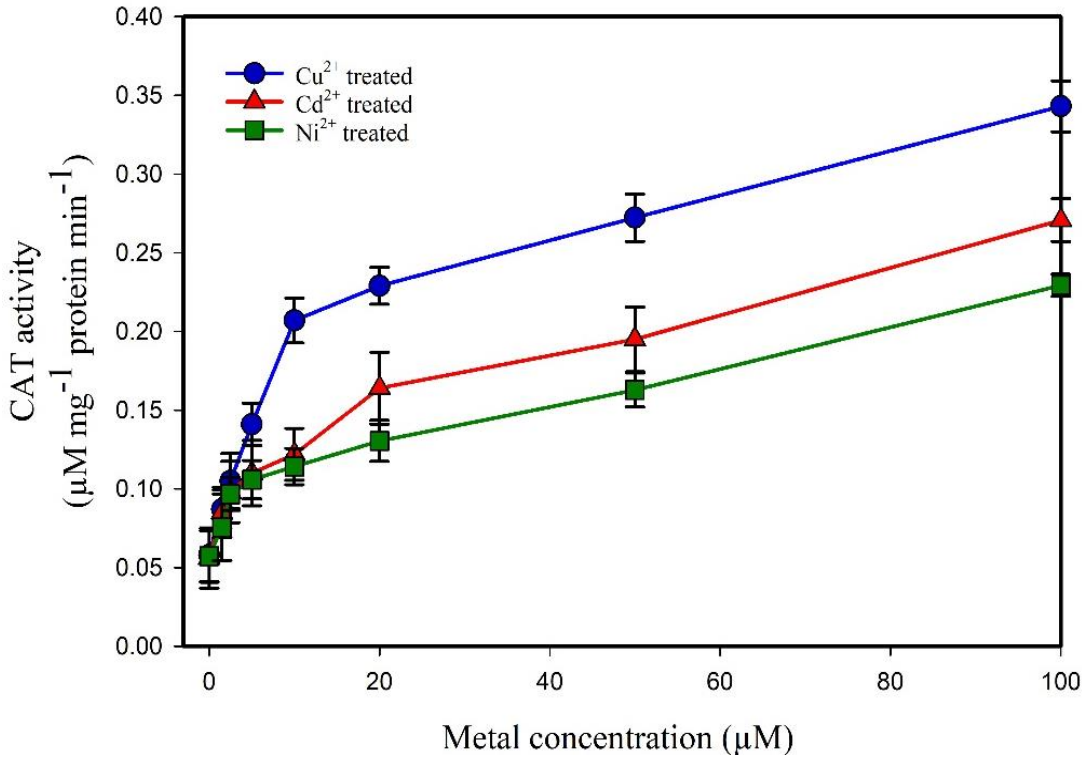

Figure.62. Catalase enzyme activity in *A. doliolum* treated with Cu^{2+}, Ni^{2+}, and Cd^{2+} for 96 h. Vertical bars represent the standard error of the mean (n=3). All treatments with Cu^{2+}, Ni^{2+}, and Cd^{2+} resulted in statistically significant ($P > 0.05$, Two-tailed Student's T-test) increases in CAT levels compared to the untreated control.

M. aeruginosa displayed a significant increase in catalase activity compared to the control across all treatments. Cu^{2+} treatment resulted in the highest increase (4.14-fold), followed by Cd^{2+} (3.79-fold) and Ni^{2+} (2.45-fold). All increases in catalase activity compared to the control were statistically significant ($P > 0.05$) as determined by a Two-Tailed Student's T-test. These results suggest that *M. aeruginosa* might be upregulating its catalase activity as an additional defense mechanism against the elevated H_2O_2 levels generated in response to heavy metal stress.

Interestingly, *A. doliolum* displayed a generally higher level of catalase activity compared to *M. aeruginosa* across all treatments. The catalase activity in *A. doliolum* also increased with increasing metal concentration. Cu^{2+} again caused the highest increase (5.91-fold) compared to the control, followed by Cd^{2+} (4.83-fold) and Ni^{2+} (4.0-fold). All increases in catalase activity compared to the control were statistically significant ($P > 0.05$) as determined by a Two-Tailed Student's T-test. These results suggest that *A. doliolum* might have a more robust antioxidant defense system involving both SOD and catalase compared to *M. aeruginosa*, allowing it to better manage oxidative stress caused by heavy metals.

3.19.3 Ascorbate peroxidase (APX) Activity

Ascorbate peroxidase (APX) is another crucial enzyme in the antioxidant defense system of cyanobacteria and many other organisms. It helps to detoxify hydrogen peroxide (H_2O_2) by catalyzing its reduction to water (H_2O) using ascorbate (vitamin C) as an electron donor. This process helps to protect cells from the damaging effects of H_2O_2-induced oxidative stress.

Figures 63 and 64 show the impact of Cu^{2+}, Ni^{2+}, and Cd^{2+} treatment on the APX enzyme activity in *M. aeruginosa* and *A. doliolum* after 96 h, respectively. Similar to the observed increases in SOD and catalase activity, both species exhibited a rise in APX activity with increasing heavy metal concentration.

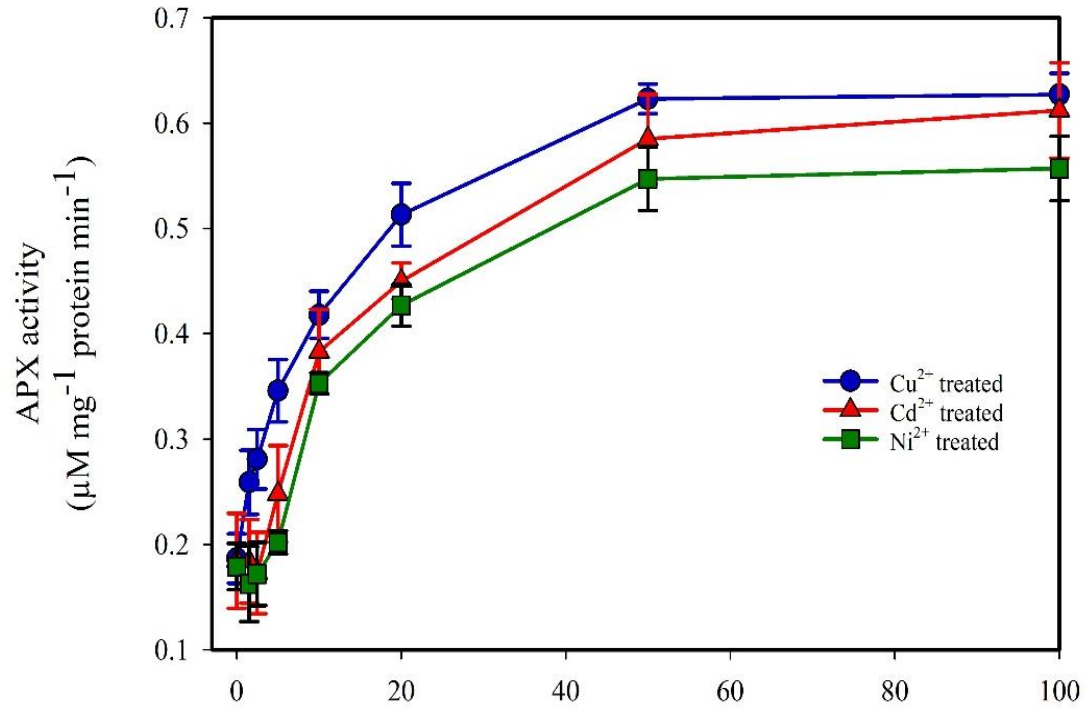

Figure.63. Ascorbate peroxidase (APX) enzyme activity in *M. aeruginosa* treated with Cu^{2+}, Ni^{2+}, and Cd^{2+} for 96 h. Vertical bars represent the standard error of the mean (n=3). All treatments with Cu^{2+}, Ni^{2+}, and Cd^{2+} resulted in statistically significant ($P > 0.05$, Two-tailed Student's T-test) increases in APX levels compared to the untreated control.

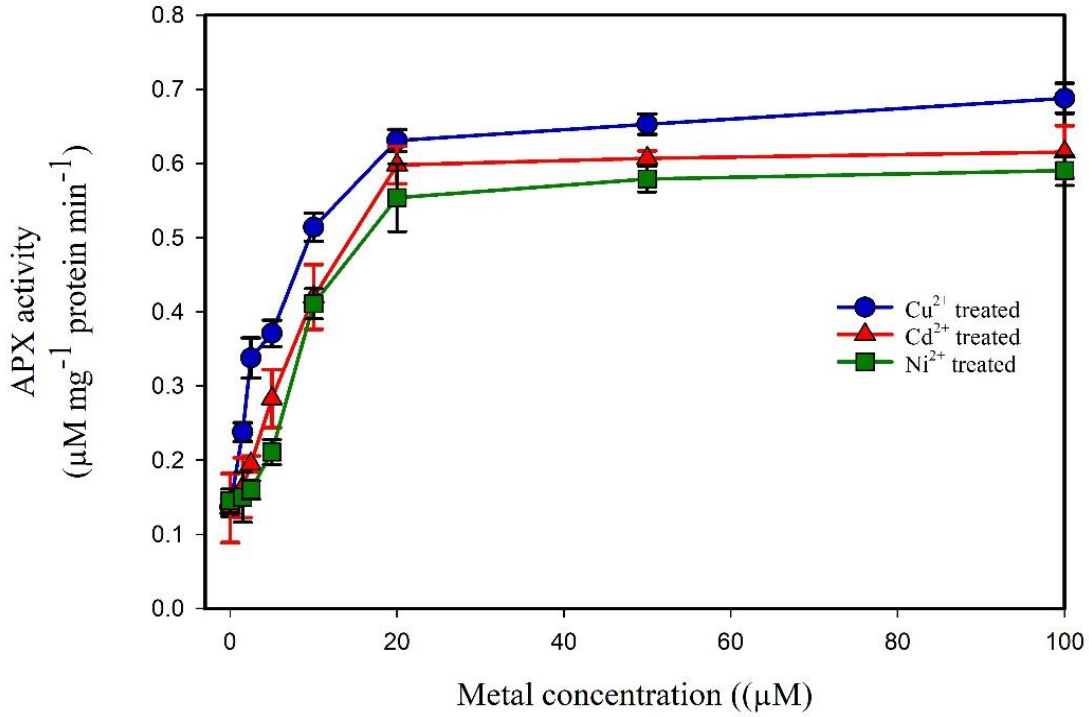

Figure.64. Ascorbate peroxidase (APX) enzyme activity in *A. doliolum* treated with Cu^{2+}, Ni^{2+}, and Cd^{2+} for 96 h. Vertical bars represent the standard error of the mean (n=3). All treatments with Cu^{2+}, Ni^{2+}, and Cd^{2+} resulted in statistically significant (P > 0.05, Two-tailed Student's T-test) increases in APX levels compared to the untreated control.

M. aeruginosa displayed a significant increase in APX activity compared to the control across all treatments. Cu^{2+} treatment resulted in the highest increase (3.36-fold), followed by Cd^{2+} (3.31-fold) and Ni^{2+} (3.11-fold). All increases in APX activity compared to the control were statistically significant ($P > 0.05$) as determined by a Two-Tailed Student's T-test. These results suggest that *M. aeruginosa* might be upregulating its APX activity as part of its antioxidant defense strategy against the elevated H_2O_2 levels generated in response to heavy metal stress.

Interestingly, *A. doliolum* displayed a generally higher level of APX activity compared to *M. aeruginosa* across all treatments. The APX activity in *A. doliolum* also increased with increasing metal concentration. Cu^{2+} again caused the highest increase (5.04-fold) compared to the control, followed by Cd^{2+} (4.54-fold) and Ni^{2+} (4.06-fold). All increases in APX activity compared to the control were statistically significant ($P > 0.05$) as determined by a Two-Tailed Student's T-test. These results suggest that *A. doliolum* might have a more robust antioxidant defense system involving SOD, catalase, and APX compared to *M. aeruginosa*, allowing it to better manage oxidative stress caused by heavy metals.

3.19.4 Glutathione Reductase (GR) Activity

Glutathione reductase (GR) is another important enzyme involved in the cellular antioxidant defense system. It plays a crucial role in maintaining the reduced state of glutathione (GSH), a vital antioxidant molecule. GR catalyzes the conversion of oxidized glutathione (GSSG) back to its reduced form (GSH), allowing GSH to continue its function in scavenging free radicals and protecting cells from oxidative stress.

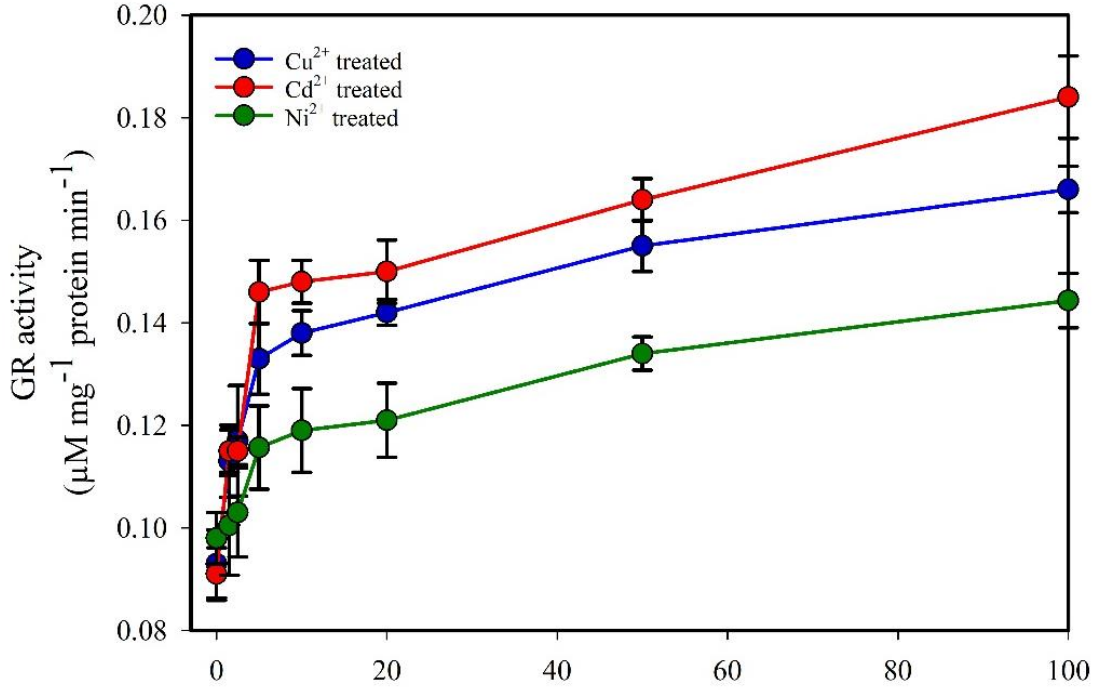

Figure.65. Glutathione reductase (GR) enzyme activity in *M. aeruginosa* treated with Cu^{2+}, Ni^{2+}, and Cd^{2+} for 96 h. Vertical bars represent the standard error of the mean (n=3). All treatments with Cu^{2+}, Ni^{2+}, and Cd^{2+} resulted in statistically significant (P > 0.05, Two-tailed Student's T-test) increases in GR levels compared to the untreated control.

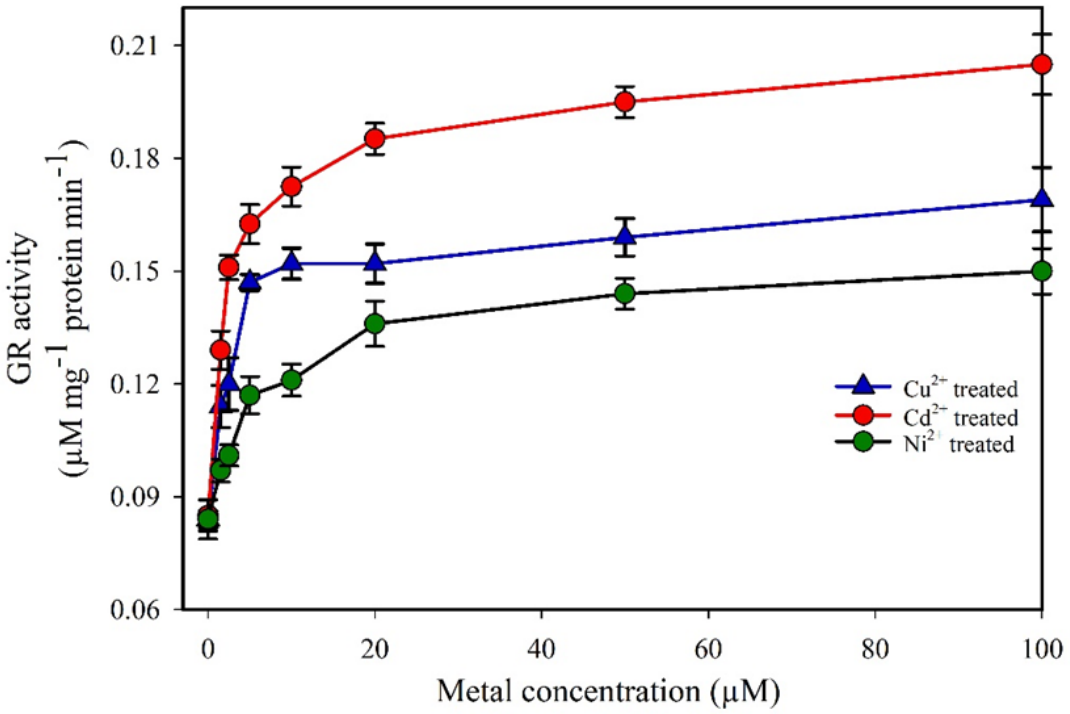

Figure.66. Glutathione reductase (GR) enzyme activity in *A. doliolum* treated with Cu^{2+}, Ni^{2+}, and Cd^{2+} for 96 h. Vertical bars represent the standard error of the mean (n=3). All treatments with Cu^{2+}, Ni^{2+}, and Cd^{2+} resulted in statistically significant (P > 0.05, Two-tailed Student's T-test) increases in GR levels compared to the untreated control.

M. aeruginosa displayed a modest increase in GR activity compared to the control across all treatments. Cd^{2+} treatment resulted in the highest increase (2.02-fold), followed by Cu^{2+} (1.78-fold) and Ni^{2+} (1.47-fold). It is important to note that these increases might not be statistically significant and require further analysis. These results suggest that M. aeruginosa might be upregulating its GR activity to some extent in response to heavy metal stress.

Figures 65 and 66 show the impact of Cu^{2+}, Ni^{2+}, and Cd^{2+} treatment on the GR enzyme activity in *M. aeruginosa* and *A. doliolum* after 96 h, respectively. While both species exhibited an increase in GR activity with increasing heavy metal concentration, the magnitude of the increase was generally lower compared to the observed changes in SOD, catalase, and APX activity. *M. aeruginosa* displayed a modest increase in GR activity compared to the control across all treatments. Cd^{2+} treatment resulted in the highest increase (2.02-fold), followed by Cu^{2+} (1.78-fold) and Ni^{2+} (1.47-fold). These results suggest that *M. aeruginosa* upregulated its GR activity to some extent in response to heavy metal stress, but the level of upregulation was lower compared to other antioxidant enzymes.

Similar to *M. aeruginosa*, *A. doliolum* displayed a moderate increase in GR activity with increasing metal concentration. Cd^{2+} again caused the highest increase (2.41-fold) compared to the control, followed by Cu^{2+} (2.08-fold) and Ni^{2+} (1.78-fold). These results suggest that *A. doliolum* upregulates its GR activity in response to heavy metal stress, but the overall increase is lower compared to the other antioxidant enzymes mentioned previously.

CHAPTER-4

DISCUSSION

SECTION I. BIOSORPTION EXPERIMENTS

Water, the elixir of life, is under siege. The insidious creep of heavy metal contamination threatens this precious resource, posing a dire challenge to human health and ecological well-being. Industrial activities, agricultural practices, and even natural geological processes can all contribute to the accumulation of these toxic elements in our water bodies (Tchounwou et al. 2012; Masindi et al. 2021). Unlike organic pollutants, heavy metals are not readily biodegradable. They persist in the environment, entering the food chain and exerting their detrimental effects at various levels.

Traditional water treatment methods, while effective in removing many contaminants, often fall short when it comes to heavy metals. These methods can be expensive, energy-intensive, and may generate hazardous byproducts (Razzak et al. 2022). The need for innovative, sustainable solutions for heavy metal bioremediation is more pressing than ever.

This thesis ventures into the exciting realm of bioremediation, a burgeoning field that harnesses the remarkable power of living organisms to cleanse contaminated environments. This research has explored the potential of cyanobacteria to cope heavy metal pollution. Cyanobacteria are a diverse group of photosynthetic prokaryotes with a long history on Earth. They play a vital role in aquatic ecosystems and have garnered significant interest in recent years due to their potential applications in various fields, including biofuel production. However, the focus of this research lies in their ability to interact with and remove heavy metals from water.

This study investigated the presence of key biomolecules – saccharides, proteins, and amino acids – within *M. aeruginosa* and *A. doliolum*. These biomolecules play a crucial role in cellular metal homeostasis and potentially contribute to the metal binding properties of cyanobacteria (Ma et al. 2009; Palmer and Franz 2009). The research compared the content of these biomolecules in both the cellular material (biomass) and the surrounding EPS (Extracellular Polymeric Substances) *(*Table 1).

The findings revealed a significantly higher abundance of all three biomolecules (saccharides, proteins, and amino acids) in the biomass compared to the EPS for both *M. aeruginosa* and *A. doliolum.*

Many studies has reported on various biochemical content of different strains of cyanobacteria. Such as Borah et al. (2016) reported the biochemical contents (Lipids, Carbohydrates and Protein) on three species of *Nostoc* and *Cylindrospermum*. From those 6 cyanobacteria species *Cylindrospermum indicum* has shown to have higher biochemical contents i.e. 366.95 mg g^{-1}, 167.73 mg g^{-1} and 10.48 mg g^{-1} of protein, carbohydrates and lipids respectively.

The studies reported by Shankar et al. (2021) on biochemical content of EPS by *Lactobacillus paracasei* shows carbohydrate content of 96.10 mg ml^{-1} and protein content 58.3 mg ml^{-1} depicting higher value for carbohydrates. This suggests that these biomolecules primarily function within the cells to maintain metal homeostasis, regulating the intracellular concentration of metal ions.

Despite the lower abundance in EPS compared to biomass, the presence of all three biomolecules (saccharides, proteins, and amino acids) in the EPS is noteworthy. This indicates a potential role for EPS in interacting with and immobilizing metal ions from the surrounding environment. The functional groups present within these biomolecules, such as carboxyl, phosphate, and amine groups, can form complexes with metal ions, facilitating their binding and potentially contributing to the biosorption capacity of cyanobacteria (Gupta and Diwan 2017). In conclusion, this study demonstrates that *M. aeruginosa* and *A. doliolum* possess a higher abundance of biomolecules – saccharides, proteins, and amino acids – within their biomass compared to the EPS. While these biomolecules primarily function in maintaining cellular metal homeostasis, their presence in the EPS suggests a potential role in metal interaction and immobilization.

Scanning electron microscopy (SEM) analysis revealed a key feature of the EPS structures – their porosity (Derdak et al. 2022). This intricate network of voids and channels throughout the matrix facilitates efficient diffusion and transport of substances within the EPS. This porosity is crucial for nutrient exchange and waste management within microbial aggregates, allowing them to function effectively. Similar porous structures were observed in the EPS produced by Lactobacillus

plantarum and Streptococcus thermophilus (Wang et al. 2015b; Kanamarlapudi and Muddada 2017).

The EPS structures also displayed a distinct smooth and glistening surface, suggesting the presence of specific compounds or functional groups on the exterior that contribute to this glistening effect (Singh et al. 2019). Notably, the EPS exhibited a highly branched morphology, a characteristic shared by EPS produced by *Lactobacillus* strains isolated from cabbage and cucumber (Singh et al. 2016). In contrast to the sheet-like compact morphology reported for EPS isolated from *Lactobacillus plantarum* KF5 (Wang et al. 2010), the *Microcystis* and *Anabaena* EPS structures lacked this specific feature. This absence suggests a unique structural adaptation, potentially tailored to meet the specific ecological and functional needs of these cyanobacteria.

Furthermore, the presence of crystalline rod-like structures within the EPS highlights a level of order and a repeating atomic arrangement associated with crystals (Solmaz et al. 2018). Crystalline features are often linked to properties like stability and durability, suggesting at the complex and diverse nature of the EPS produced by cyanobacteria. While Rani et al. (2017) (Rani et al. 2017)reported a more prominent crystalline structure in the EPS of *Bacillus tequilensis* FR9 compared to its amorphous regions, the EPS analyzed in this study appears to exhibit both crystalline and amorphous domains. This highlights the potential variations in EPS structure even among different microbial strains.

Energy dispersive X-ray spectroscopy (EDX) analysis revealed the elemental composition of both the cyanobacterial biomass and the isolated EPS (Figure 4 and 5, Table 2 and 3). As expected, carbon (C) and oxygen (O) dominated both fractions, reflecting their well-established roles in cellular structures and metabolic processes (Kumar et al. 2019). These elements form the backbone of essential biomolecules like carbohydrates, proteins, lipids, and nucleic acids, critical for maintaining cell integrity and function. Beyond C and O, the presence of silicon (Si) and sulfur (S) in the biomass likely contributes to the structural integrity of cellular components. These elements are also found in biomolecules, further supporting their significance in cellular structure and function (Vašák and Schnabl 2016). Sodium (Na), potassium (K), magnesium (Mg), and iron (Fe) were detected, suggesting their potential involvement in

osmoregulation, ion transport, and various metabolic pathways within the cyanobacteria (Jomova et al. 2022). These elements often act as enzyme cofactors, facilitating vital biochemical reactions in energy metabolism, biosynthesis, and other essential cellular processes. Trace amounts of Mg and Fe were also identified, hinting at potential roles in specific cellular functions and environmental interactions (Siddiqui et al. 2014). The presence of copper (Cu^{2+}) and chlorine (Cl) in the EPS might be attributed to residual elements from the growth media or analytical instruments. Further investigation is needed to confirm their presence and potential roles within the EPS matrix.

The observed differences in elemental composition between the biomass and EPS highlight their distinct functionalities. These elements likely play crucial roles in shaping the structure, properties, and functions of these two cellular components. Interestingly, the presence of sodium (Na) and nitrogen (N) in the EPS suggests their potential involvement in interactions with the surrounding environment or specific metabolic processes within the EPS itself (Sudmalis et al. 2020). Further research into the specific functionalities of these elements within the EPS matrix would provide valuable insights into their significance for the overall ecology of these cyanobacteria.

TEM image analysis were employed to locate heavy metals accumulation on the intracellular region of the EPS and visualize the structural changes to show the different effects of metal toxicity. For *M. aeruginosa* (Figure 6), untreated EPS has a smooth surface with little black patches. When exposed to Cd^{2+}, the surface becomes rough and porous. Cu^{2+} treatment causes the EPS to form spherical or oval shapes, whereas Ni^{2+} treatment produces a web-like structure. The various structural alterations seen in *M. aeruginosa* EPS following treatment with Cd^{2+}, Cu^{2+}, and Ni^{2+} reflect each heavy metal ion's unique chemical characteristics and binding affinities with EPS components.

In this case of *A. doliolum* (Figure 7), untreated EPS exhibits a wrinkled and strong surface. Cd^{2+} treatment causes the deposition of Cd^{2+} ions, which are apparent as black patches, with some regions becoming completely dark due to accumulation. Cu^{2+} treatment forms spiny morphologies and porous structures on the EPS surface, but Ni^{2+} treatment produces translucent circular spots, which might indicate Ni^{2+} deposition. The different structural alterations seen in *Anabaena* EPS after treatment

with Cd^{2+}, Cu^{2+}, and Ni^{2+} reflect each heavy metal ion's unique chemical characteristics and binding affinities with EPS components. These interactions can cause changes in EPS conformation, aggregation, and morphology, resulting in the various surface structures observed in the experimental results (Kim et al. 2007; Mohite et al. 2018).

Fourier-transform infrared spectroscopy (FTIR) analysis provided insights into the diverse functional groups employed by cyanobacteria for binding Cd^{2+}, Cu^{2+}, and Ni^{2+} ions (Figure 8 and 9). These mechanisms include coordination with oxygen atoms, π-electron interactions, and electrostatic forces. Metal ions likely form complexes with oxygen-containing functional groups, such as hydroxyl (-OH), carbonyl (C=O), and ether (C-O) groups, present in both the biomass and EPS (Brady and Duncan, 1994). The presence of metal-oxygen stretching vibrations in the FTIR spectra supports this coordination (Wang et al. 2022). Another potential binding mechanism involves π-electron interactions between metal ions and aromatic rings within the biomass and EPS. These interactions can lead to the formation of π-complexes and alter the electron distribution within the aromatic systems (Oshita and Shimazaki 2022; Corinti et al. 2022). Electrostatic interactions may also play a role. Positively charged metal ions can interact favorably with negatively charged functional groups on the surfaces of biomass and EPS, facilitating adsorption (Zhou and Pang 2018).

Hydrogen bonding with functional groups containing hydrogen atoms (e.g., hydroxyl and amino groups) is another possible binding mechanism. These interactions can contribute to the stabilization of metal ion binding to biomass and EPS surfaces, enhancing adsorption (Reek et al. 2022). Furthermore, metal ions can form complexes with biomolecules like proteins and polysaccharides, which are abundant in both biomass and EPS. This complexation increases the binding affinity of metal ions to these cellular components, promoting adsorption (De La Torre and Pomorski 2024).

The FTIR analysis of EPS functional groups in this study revealed the presence of C=O stretching, C-H stretching, O-H stretching, N-H bending, and C-O stretching vibrations. These functional groups are consistent with those reported by Guo et al. (2016) in their study of activated sludge EPS. Additionally, the findings align with the work of Wang et al. (2012), who identified similar functional groups in the EPS of

Bacillus megaterium TF10, along with additional S-O and P=O stretching vibrations. While these studies identified a broader range of functional groups, the core functionalities observed in our cyanobacteria EPS appear to be well-conserved.

The identification of dipeptides, tripeptides, and individual amino acids within cyanobacterial EPS (Figure 10 and 11, Table 4 and 5) indicates the composition and potential functionalities of these extracellular molecules (Gnoth et al. 2024). Dipeptides and tripeptides may contribute significantly to the structural stability and integrity of the EPS (Santos et al. 2012). However, their functions extend beyond mere scaffolding. These peptides might act as signaling molecules, influencing communication and interactions within the biofilm community (Litz et al. 2011). Additionally, they could serve as a source of nutrients for other microorganisms or even exhibit antibacterial properties, shaping the overall biofilm ecology. The presence of monopeptides like leucine, valine, and isoleucine (branched-chain amino acids, BCAAs) highlights their potential role in protein synthesis and cellular function (Gwin et al. 2020). These amino acids might contribute to stress tolerance and metabolic processes, enhancing the organism's adaptability to environmental challenges. Phenylalanine, an aromatic amino acid, could potentially originate from degraded proteins within the biofilm and contribute to the chemical diversity of the EPS (Zhou et al. 2022). Polar amino acids like serine enable cyanobacteria to interact effectively with water molecules and potentially facilitate nutrient acquisition. This characteristic might enhance the organism's adaptability to its surrounding environment (Ullah et al. 2020). Glycine, the smallest amino acid, could introduce flexibility to the EPS matrix, allowing for structural modifications in response to environmental changes. This dynamic nature of the EPS could be crucial for cyanobacteria to thrive in fluctuating environmental conditions. In contrast to *Microcystis* , the EPS of *Aureococcus doliolum* incorporates histidine, which possesses an imidazole ring with a high affinity for metal ions (Vandenbossche et al. 2015). This allows histidine residues to participate in metal sequestration or detoxification within the EPS matrix. Furthermore, histidine can act as a pH buffer, regulating the acidity or alkalinity of the EPS environment. Maintaining optimal pH conditions is critical for microbial growth and metabolic activity within the biofilm (Ayudhya et al. 2018).

Cyanobacterial cell surfaces include a variety of functional groups, including carboxyl (-COOH), amino (-NH2), hydroxyl (-OH), and phosphate groups (Gonçalves et al. 2015). These groups can operate as proton acceptors or donors, hence increasing the cell surface's buffering capacity (Pokrovsky et al. 2008). In acidic solutions, hydrogen ions (H^+) can interact with functional groups on cell surfaces. Protonation occurs when H^+ ions attach to negatively charged functional groups, such as carboxylate groups, resulting in the creation of protonated species (e.g., $-COOH^+$). Increased pH can cause deprotonation, which releases H^+ ions from functional groups (Nakata 1992). At first, the functional groups on the cell surface can bind H^+ ions, causing a steady fall in pH when acid is introduced. This phase depicts the cell surface's buffering capabilities, with the functional groups acting as proton acceptors to avoid extreme pH shifts (Gao et al. 2016). Adding additional acid raises the concentration of H^+ ions, resulting in saturation of binding sites on the cell surface. At this stage, the cell surface's buffering ability decreases, and the pH may stay rather steady despite further acid input. The saturation point corresponds to the inflection point or plateau on the titration curve. The protonation and deprotonation processes achieve equilibrium when the pH varies during titration. pH changes affect the balance of protonated and deprotonated species on the cell surface, impacting the overall charge and reactivity of the cells. Protonation of functional groups on the cell surface influences the surface charge, hydrophobicity, and reactivity of the cells (Petukh et al. 2013). These surface property changes can have an influence on a variety of cellular functions, including as nutrition intake, metal binding, and interactions with other bacteria and surfaces (Hou et al. 2018). The observed shift in equivalency points during pH titration of metal-treated cyanobacterial biomass and EPS suggests that metal exposure alters surface characteristics, which might have ramifications for environmental interactions and ecosystem function and give useful information on the impact of metal binding on the organism's surface characteristics and overall surface chemistry.

This study found an intricate relationship between pH and the efficiency of copper (Cu^{2+}), cadmium (Cd^{2+}), and nickel (Ni^{2+}) removal by *M. aeruginosa*, *A. doliolum*, and their isolated EPS (Figure 18 and 19). *M. aeruginosa* demonstrated a distinct preference for Cu^{2+} removal at a slightly acidic pH of 6.5 (Figure 18 A). This

efficiency was observed to decrease at higher pH values, suggesting a potential alteration in the surface charge of the biomass or the speciation of Cu^{2+} at increased alkalinity (El-Gendy et al. 2017). In contrast, Ni^{2+} removal remained relatively unaffected by pH, indicating a less pH-dependent binding mechanism for this metal (Schiewer and Patil 2008). A unique trend was observed for Cd^{2+} removal, with a significant increase from acidic to neutral pH (2 to 7), followed by a slight decline at even higher pH. This behavior suggests that functional groups on the *M. aeruginosa* surface become better suited for Cd^{2+} binding at neutral pH values, possibly due to changes in their protonation state (Onufriev and Alexov 2013).

A more stable Cu^{2+} removal efficiency across the entire pH range (2-9) was shown by *A. doliolum* (Fig 18 B). This suggests a wider variety of functional groups or binding sites on the *A. doliolum* surface that can interact with Cu^{2+} ions regardless of the solution's pH within this range. A gradual increase in Ni^{2+} removal by *A. doliolum* was observed with increasing pH, potentially due to the presence of functional groups that become more favorable for Ni^{2+} binding at higher pH values (pH up to 7.5). However, the slight decrease at pH 9 might indicate the precipitation of some removed Ni^{2+} instead of remaining bound to the biomass (Jerroumi et al. 2020). Similar to *M. aeruginosa*, Cd^{2+} removal by *A. doliolum* exhibited a strong pH dependence, with a dramatic rise in efficiency at neutral pH (7 and 8) compared to lower pH. This behavior aligns with the concept of electrostatic interactions, where functional groups become deprotonated at neutral pH, creating favorable attraction for positively charged Cd^{2+} ions (Schiewer and Patil 2008).

Further insights into the complex interplay between pH and metal removal were provided by the investigation of isolated EPS (Figure 19). Both *M. aeruginosa* and *A. doliolum* EPS displayed high initial removal efficiencies for Cu^{2+} and Ni^{2+} at a low pH of 2.0. However, their behaviors diverged at higher pH. *M. aeruginosa* EPS exhibited stable Cu^{2+} removal up to pH 4, followed by a significant decrease. This suggests a potential shift in binding mechanisms or surface properties of the EPS at higher pH. In contrast, Ni^{2+} removal by *M. aeruginosa* EPS increased steadily across the entire pH range, indicating a robust and pH-independent binding process, possibly involving complexation with functional groups within the EPS matrix (Haas et al.

2019; Qasem et al. 2021). Cd^{2+} removal by *M. aeruginosa* EPS mirrored the trend observed for biomass, with a low removal rate at pH 2 and a peak at pH 7.

A. doliolum EPS also showed high initial removal efficiencies for Cu^{2+} and Ni^{2+} at pH 2.0. Unlike *M. aeruginosa* EPS, Cu^{2+} removal by *A. doliolum* EPS steadily increased with increasing pH, reaching a maximum at pH 6.0. This suggests a potential enhancement of binding sites or interactions favorable for Cu^{2+} at higher pH for this specific EPS. Similarly, Ni^{2+} removal by *A. doliolum* EPS showed a gradual increase, reaching its peak at a slightly higher pH (7.5) compared to Cu^{2+}. Interestingly, Cd^{2+} removal by *A. doliolum* EPS mirrored the trend observed for *M. aeruginosa* EPS, suggesting similar underlying mechanisms.

In conclusion, the observed variations in metal removal efficiencies across different pH conditions highlight the complex interplay between metal speciation, EPS surface properties, and binding mechanisms. A more metal-specific response was displayed by *M. aeruginosa*, while *A. doliolum* exhibited broader pH tolerance for Cu^{2+} removal. The isolated EPS of both organisms revealed distinct pH-dependent behaviors, further emphasizing the

This study investigated the rate of metal uptake by M. aeruginosa and A. doliolum biomass, along with their isolated EPS, using a time-course experiment (Figures 20-23). The data is analyzed using two kinetic models: Pseudo-First-Order and Pseudo-Second-Order (Mehta and Gaur 2005; Wang and Guo 2020).

The sorption of all three metals (Cu^{2+}, Ni^{2+}, and Cd^{2+}) was observed to be rapid, with over 90% occurring within the first 30-45 min (Figures 20-23). This rapid initial uptake suggests a rapid binding of metal ions to the cell wall, likely through a passive, extracellular process such as ion exchange or complexation with functional groups on the cell surface (Mehta and Gaur 2005). Following this initial surge, the rate of sorption slowed down. This second phase might represent the active transport of metal ions into the cells (Mehta and Gaur 2005).

Figure 20 depicts the kinetics of metal sorption by live *M. aeruginosa* biomass. Table 7 summarizes the parameters obtained by fitting the time-course data for *M. aeruginosa* to both the Pseudo-First-Order and Pseudo-Second-Order models. The high coefficient of determination (R^2) values (> 0.92) for both models indicate good agreement between the model predictions and the experimental data. However, the

Pseudo-Second-Order model exhibited slightly higher R^2 values for all three metals, suggesting a potentially better fit for this specific case. Overall, the time-course study along with kinetic modelling suggests a two-phase sorption process for heavy metals by *M. aeruginosa*. The first phase likely involves rapid binding to the cell surface, followed by a slower phase that might be attributed to active transport mechanisms.

Figures 21, 22, and 23 depict similar trends for metal sorption by native biomass of *A. doliolum*, *M. aeruginosa* EPS, and *A. doliolum* EPS. Tables 8-10 present the results of fitting the time-course data for these samples to the same kinetic models used for *M. aeruginosa* (Pseudo-First-Order, Pseudo-Second-Order). The R^2 values for both Pseudo-First-Order and Pseudo-Second-Order models remain high (>0.90 for most cases) across all tables, suggesting good agreement between the models and the experimental data. Similar to *M. aeruginosa*, Pseudo-Second-Order models generally exhibit slightly higher R^2 values for *A. doliolum* and EPS, indicating a potentially better fit.

For *A. doliolum*, the R^2 values for the Intraparticle Diffusion model are slightly lower (Table 8) compared to the other two models, suggesting that diffusion within the cell wall might play a less significant role in metal uptake compared to *M. aeruginosa*. In contrast, the R^2 values for the Intraparticle Diffusion model are generally higher for EPS compared to *A. doliolum* and *M. aeruginosa* biomass (Tables 9 and 10). This suggests that diffusion within the EPS structure might be a more prominent factor influencing metal uptake for isolated EPS (Mathivanan et al. 2023).

From the results of this study, it can be concluded that metal sorption involves a two-phase process by *M. aeruginosa* and *A. doliolum*, and potentially their EPS. The rapid initial phase reflects passive binding to the cell surface, followed by a slower phase that might involve active transport of metals into the cells. The specific contributions of these processes and the role of diffusion within the EPS structure vary depending on the metal and the type of biosorbent.

The investigation into the role of intraparticle diffusion using the intraparticle diffusion model yielded interesting insights (Figures 24-27). The plots depicting the amount of metal sorbed versus the square root of time (t^0.5) exhibited multiple linear portions, appearing as curved lines (Figures 24-27). This observation deviates from the linear trend expected for a solely diffusion-controlled process. This suggests that

intraparticle diffusion might not be the sole rate-limiting step for metal uptake by M. aeruginosa, *A. doliolum* biomass, and their isolated EPS (Gora et al. 2022).

Within *M. aeruginosa* (Figure 24), the calculated intraparticle diffusion rate constant (kd) for Ni^{2+} was higher compared to Cu^{2+} and Cd^{2+} (Table 7). This signifies a faster diffusion rate for nickel ions within the *M. aeruginosa* biomass. This trend aligns with the observations for *A. doliolum* biomass (Figure 25), where kd values followed the order $Ni^{2+} > Cu^{2+} > Cd^{2+}$ (Table 8), again indicating the fastest diffusion for nickel.

For both *M. aeruginosa* EPS (Figure 26) and *A. doliolum* EPS (Figure 27), the kd trend remained consistent. The highest kd value was observed for Ni^{2+}, signifying the fastest diffusion rate of nickel ions within the EPS structure (Tables 9 and 10).

While the intraparticle diffusion model offers valuable insights, the presence of multiple linear portions in the plots suggests that other mechanisms besides diffusion might also be influencing the rate of metal uptake. These additional mechanisms could involve surface adsorption on the biomass or EPS or pore diffusion within their structures (Miyar et al. 2021).

This study investigated the thermodynamic favorability of metal adsorption by various biosorbents using the van't Hoff equation (Figures 28-31). The biosorbents investigated include *M. aeruginosa* biomass, *A. doliolum* biomass, EPS (Extracellular Polymeric Substances) from *M. aeruginosa*, and EPS from *A. doliolum*. The metals studied are Ni^{2+}, Cu^{2+}, and Cd^{2+}.

Figures 28-31 depict the van't Hoff plots for each biosorbent-metal ion combination. These plots reveal the relationship between inverse temperature (1/T) and the natural logarithm of the equilibrium constant (ln kc). The adsorption of all three metals onto the biomass of *M. aeruginosa* and *A. doliolum* was found to be exothermic ($\Delta H^{o} < 0$), indicating that the process releases heat. However, despite the heat release, the adsorption was nonspontaneous ($\Delta G^{o} > 0$) under the studied conditions. This suggests that the system requires external energy input to overcome an energetic barrier and favor metal uptake (Decherchi and Cavalli 2020). In contrast to the biomass, the EPS isolated from *M. aeruginosa* and *A. doliolum* displayed spontaneous ($\Delta G^{o} < 0$) adsorption for all three metal ions. These processes were also exothermic ($\Delta H^{o} < 0$) for Ni^{2+} and Cu^{2+}, suggesting heat release during adsorption.

Interestingly, Cd^{2+} adsorption onto EPS remained endothermic ($\Delta H^0 > 0$) despite being spontaneous. This observation suggests a unique mechanism for Cd^{2+} uptake compared to Ni^{2+} and Cu^{2+}, warranting further investigation. It can be concluded that, the dependence of biosorption favorability depends on both the type of biosorbent and the specific metal ion. While *M. aeruginosa* and *A. doliolum* biomass might require further optimization for efficient metal removal under the studied conditions, their isolated EPS show promise for spontaneous metal uptake.

This study employed batch equilibrium experiments to understand the mechanisms by which *M. aeruginosa* and *A. doliolum* biomass, along with their isolated EPS, sequester metal ions (Ni^{2+}, Cu^{2+}, and Cd^{2+}) (ranging from 0 to 10 mg L^{-1}). To gain a comprehensive understanding of the adsorption process, the data were analyzed using three isotherm models: Langmuir, Freundlich, and Temkin (Figures 32-35, Tables 15-18).

The Langmuir isotherm, which presupposes a scenario where metal ions form a single, uniform layer (monolayer) on the biosorbent surface (A.O 2012), effectively described the biosorption process for most combinations of biosorbents and metal ions examined in this study. This is evidenced by the high r^2 values exceeding 0.96 in many cases (Tables 15-18). The Langmuir model's strength lies in its ability to quantify the maximum adsorption capacity (q_{max}) for each metal ion onto the specific biosorbents (Tables 15-18). Notably, the q_{max} values consistently favored EPS over their corresponding biomass, signifying a superior metal binding capacity of the EPS fraction. This trend held true for all three metal ions across both EPS types, suggesting a potentially greater abundance of functional groups or more favorable binding sites within the EPS structure for metal complexation (Reference).

The Freundlich isotherm model, which describes multilayer adsorption on heterogeneous surfaces (Araújo et al. 2018), yielded good results with r^2 values exceeding 0.98 for most cases (Tables 15-18), similar to the Langmuir model. The Freundlich constant (k_F) reflects the adsorption intensity, with higher values indicating stronger adsorption. Interestingly, EPS consistently exhibited higher k_F values compared to the biomass for both Cu^{2+} and Ni^{2+} ions, suggesting a stronger affinity of EPS for these metal ions (Tables 14-15, 16-17). The heterogeneity factor (1/n) close to unity (ranging from 0.67 to 0.87 for most cases) implies favorable biosorption with

relatively consistent binding site affinities across the biosorbent surface (Reference). This suggests that both homogeneous and heterogeneous adsorption mechanisms might be at play, with EPS potentially offering a wider range of binding sites with varying affinities for different metal ions.

The Temkin isotherm model takes into account the influence of adsorption heat on the process (Chu 2021). While the fit of the Temkin model was moderate compared to the other two models (r^2 values ranging from 0.75 to 0.89), it provided valuable insights into the energetics of adsorption. The Temkin adsorption constant (A_T) reflects the overall force of interaction between the metal ion (adsorbate) and the biosorbent (adsorbent). Interestingly, the AT values were consistently higher for EPS compared to the biomass for all three metals (Tables 15-18). This observation suggests stronger adsorption forces for metal ions on EPS compared to the biomass, potentially due to the presence of functional groups within the EPS that can participate in stronger ionic or covalent interactions with the metals (Kiefer and Höll 2001).

By employing a combination of isotherm models, this study offers a multifaceted perspective on the mechanisms governing metal uptake by cyanobacteria and their EPS. The Freundlich isotherm emerged as the most suitable model for describing the overall biosorption process, indicating a heterogeneous surface with multilayer adsorption. The Langmuir isotherm provided valuable information on the superior metal binding capacity of EPS compared to biomass. The Temkin isotherm, despite a moderate fit, shed light on the adsorption energetics, revealing stronger adsorption forces for metals on EPS. This comprehensive analysis suggests that a combination of factors, including the presence of functional groups within the EPS, the heterogeneity of the biosorbent surface, and the interplay between adsorption forces, contribute to the remarkable metal uptake capabilities of cyanobacteria and their EPS.

This study evaluated the potential of *M. aeruginosa* and *A. doliolum* for heavy metal removal from aqueous solutions, comparing their performance to various other adsorbents (Table 4.1). Sorption capacity, often expressed in milligrams of metal adsorbed per gram of biosorbent (mg/g), reflects the maximum amount of metal a particular biosorbent can bind under specific experimental conditions. In this study, *M. aeruginosa* exhibited a remarkable sorption capacity for three examined metal ions,

exceeding or comparable to several other adsorbents (Table 4.1). This indicates a high affinity of *M. aeruginosa* for metal ions and its potential to remove significant quantities of metal ions from a solution.

Table 4.1. Comparative Heavy Metal Sorption Capacities of *Microcystis aeruginosa*, *Anabaena doliolum* and other adsorbent.

	Adsorbent	Heavy metals	Concentration range (mg L^{-1})	Adsorption capacity (mg g^{-1})	Removal (%)	Reference
1	*Microcystis aeruginosa*	Ni	1-10	2.49	88.84	Current study
		Cu		1.07	85.48	
		Cd		0.74	82.5	
2	*Anabaena doliolum*	Ni	1-10	1.62	85.10	Current study
		Cu		1.49	86.94	
		Cd		0.77	82.90	
3	*Cupriavidus necator GX_5*	Cd	5–200	18.59	86	(Li et al. 2023)
4	*Peudomonas putida*	Cu	n/d	6.6	n/d	(Pardo et al. 2003)
		Cd		8.0		
5	*Pseudomonas spp*	Ni	50-400	57.43	n/d	(Ansari and Malik 2007)
		Cd		56.19		
6	*Trichoderma harzianum*	Cd	50-800	243.90	n/d	(Mushtaq et al. 2022)
		Cu		133.33		
7	*T. longibrachiatum*	Cd	50-800	204.08	n/d	(Mushtaq et al. 2022)

		Cu		121.95		
8	*T. reesei*	Cd	50-800	256.41	n/d	(Mushtaq et al. 2022)
		Cu		161.29		
9	*T. atrobrunneum*	Cd	50-800	344.83	n/d	(Mushtaq et al. 2022)
		Cu		312.50		
10	*T. citrinoviride*	Cd	50-800	263.16	n/d	(Mushtaq et al. 2022)
		Cu		188.68		
11	*Posidonia oceanica*	Cd	30-250	30.22	n/d	(Boulaiche et al. 2019)
		Cu		43.90		
		Ni		41.02		
12	*Microcystis aeruginosa*	Cd	5-25	n/d	92.00	(Zeng et al. 2022)
		Cu			83.24	
		Ni			88.67	
13	*Chara aculeolata*	Cd	1-400	23.0	95	(Sooksawat et al. 2016)
14	*Nitella opaca*	Cd	1-400	20.5	91	(Sooksawat et al. 2016)
15	*Cystoseira indicia*	Cu	25-300	59.52		(Akbari et al. 2015)
16	*Eucheuma denticulatum*	Cu	25-200	66.23	66.95	(Rahman and Sathasivam 2016)
17	*Scenedesmus quadricauda*	Cd	n/d	135.1	66.0	(Mirghaffari et al. 2015)

18	*Ulva lactuca*	Cu	5-80	64.5	n/d	(Ibrahim et al. 2016)
		Cd		62.5		
19	*Chlorella minutissima UTEX2341*	Cd	n/d	303.03	74.34	(Yang et al. 2015)
		Cu		16.16	83.60	
20	*Chlorella sp*	Cd	n/d	15.5	92.45	(Shen et al. 2018)
21	*Scenedesmus sp.*	Cd	20-120	128	83	(Waqar et al. 2023)
22	*Pichia pastoris*	Cu	20-100			(Chen et al. 2021)
	Cell			16.13	21.2	
	Cell wall			11.53	20.7	
	Cell membrane			10.97	18.5	
23	Coconut husk	Cu	100-500	443.0	88.6	(Malik et al. 2017)
		Ni		404.5	80.9	
23	*Gloeothece magna*	Cd	0.3-1	0.45	n/d	(Mohammed 2012)
24	*Anabaena doliolum* Ind1	Cd	0.5-2	52.59	68.6	(Goswami et al. 2015)
25	Synechocystis sp. PCC 6803	Cd	4.0	17.712	65.508	(Shen et al. 2021)
26	Activated Carbon	Cd	30-200	178.5	86.00	(Karnib et al. 2014)
		Ni		400	90.00	
27	Chitin nanofibrils (Polysaccharides)	Cd	n/d	330.15	n/d	(Liu et al. 2013)
		Ni		134.72		

		Cu		141.08		
28	Hydrocolloid liquid-core capsules	Ni	1000	65	n/d	(Nussinovitch and Dagan 2015)
		Cd		197		
		Cu		219		
29	Aqueous sodium alginate solution	Cu	100-1000	167.1		(Wang et al. 2016)
		Cd		179.0		
30	*Microcytis*	Ni	1-50	100	n/d	(Pradhan et al. 2007)
31	Chitosan/sporopollenin microcapsules	Cu	2-12	85	n/d	(Sargın and Arslan 2015)
		Cd		87		
		Ni		34		
32	*Bacillus thuringiensis* strain OSM29	Cd	25-150	59.17	87.8	(Oves et al. 2013)
		Cu		39.84	91.8	
		Ni		43.13	94.6	
33	Acinetobacter sp. FM4 (Bacteria)	Cu	50-400	83	n/d	(Masood and Malik 2015)
		Ni		47		
34	Maghemite Nanoparticles	Cd	2-250	Cd 19.72	8.4	(Akhbarizadeh et al. 2014)
		Cu		Cu 24.44	88.2	
		Ni		Ni 22.99	15.7	
35	Cyanospira capsulata	Cu	200-400	115	n/d	(De Philippis et al. 2007)

36	Nostoc PCC7936	Cu	200-400	85	n/d	(De Philippis et al. 2007)

Removal efficiency, typically expressed as a percentage, signifies the proportion of metal ions eliminated from the solution by the biosorbent. In this study, both *M. aeruginosa* and *A. doliolum* achieved high removal efficiencies for all three metals (Ni^{2+}, Cu^{2+}, and Cd^{2+}), exceeding 82% in most cases. This implies that a large fraction of the initial metal concentration was sequestered by the cyanobacteria, effectively reducing the free metal ions remaining in the solution.

Although sorption capacity provides a benchmark for the intrinsic metal binding ability of a biosorbent, a high sorption capacity doesn't necessarily guarantee high removal efficiency. A high removal efficiency can be achieved even with a moderate sorption capacity if a sufficient amount of biosorbent is used relative to the metal concentration.

While this study provides valuable insights, some limitations need to be addressed in future research. The current study employed a specific concentration range (1-10 mg/L) for metal ions. Investigating the sorption behavior percent remove at higher metal concentrations would provide a more comprehensive understanding of the biosorption process.

This study investigated the heavy metal sorption capacities and removal efficiencies of EPS isolated from *M. aeruginosa* and *A. doliolum*. The results are compared to various other microorganisms and EPS reported in the literature to understand the potential of EPS for heavy metal bioremediation (Table 4.2).

A striking observation is the significantly higher sorption capacities of both *M. aeruginosa* EPS (Ni^{2+}: 44.81 mg/g, Cu^{2+}: 37.06 mg/g) and *A. doliolum* EPS (Ni^{2+}: 64.37 mg/g, Cu^{2+}: 42.08 mg/g) compared to their whole cell counterparts (Table 4.1). This suggests that EPS plays a crucial role in metal sequestration, potentially due to a higher concentration of functional groups like carboxyl, phosphate, and amine groups within the EPS matrix (Rizvi and Khan 2019). These functional groups can interact

with metal ions through various mechanisms, leading to stronger and more efficient metal binding compared to the cell wall of the whole organism.

Similar to the whole cell data (Table 4.1), both *M. aeruginosa* EPS and *A. doliolum* EPS achieved exceptionally high removal efficiencies for all three metals (Ni^{2+}, Cu^{2+}, and Cd^{2+}), exceeding 96% in most cases (Table 4.2). This emphasizes the effectiveness of EPS in removing a large fraction of the metal ions from the solution, highlighting its potential for practical applications. The sorption capacities of *M. aeruginosa* EPS and *A. doliolum* EPS surpass those of several bacterial EPS reported in the literature, such as *Mucilaginibacter rubeus* (Cu^{2+}: 92.57 mg/g) (Li et al. 2022) and *Rhodococcus opacus* (Cd^{2+}: 46.73 mg/g) (Dobrowolski et al. 2019). This indicates a potentially stronger metal binding ability of cyanobacterial EPS. Further, *M. aeruginosa* EPS displayed comparable sorption capacities for Ni^{2+} and Cu^{2+} to some fungi like *Athelia rolfsii* (Cu^{2+}: 103.09 mg/g) (Li et al. 2016) and *Alteromonas* sp. JL2810 (Ni^{2+}: 226.3 mg/g) (Zhang et al. 2017). This suggests that cyanobacterial EPS can be a viable alternative to other well-established biosorbents for metal removal. The sorption capacities of *M. aeruginosa* EPS and *A. doliolum* EPS are significantly higher than those of soil (Cu^{2+}: 13.5 mg/g, Cd^{2+}: 14.1 mg/g) (Wu et al. 2021). This highlights the potential advantage of using EPS-based bioremediation strategies.

While this study provides valuable insights, further research is needed to explore the mechanisms behind the superior metal binding capacity of cyanobacterial EPS. Understanding the specific functional groups involved and their interactions with different metal ions would be crucial for optimizing EPS-based bioremediation strategies. Additionally, investigating the regeneration potential of EPS after metal uptake would be essential for developing sustainable and cost-effective applications.
This study investigated the biosorption behavior of Ni^{2+} and Cu^{2+} ions using *M. aeruginosa* and *A. doliolum* biomass and their corresponding EPS. The Langmuir, Freundlich, and Temkin isotherm models were employed to analyze the competitive adsorption phenomena.

Table 4.2. Comparative Heavy Metal Sorption Capacities of *Microcystis* EPS, Anabaena EPS and other Microorganisms EPS.

	EPS	Heavy metals	Concentration range (mg L^{-1})	Adsorption capacity (mg g^{-1})	Removal (%)	Reference
1	*Microcystis aeruginosa*	Ni	1-10	44.81	99.73	Current study
		Cu		37.06	99.49	
		Cd		26.63	96.5	
2.	*Anabaena doilolum*	Ni	1-10	64.37	99.77	Current study
		Cu		42.08	99.56	
		Cd		31.19	97.5	
3	*Mucilaginibacter rubeus*	Cu	5-100		92.57	(Li et al. 2022)
		Au			81.11	
4	*Athelia rolfsii*	Cd	400-550	116.28		(Li et al. 2016)
		Cu		103.09		
5	*Rhodococcus opacus*	Cd	1000	46.73	30	(Dobrowolski et al. 2019)
6	*Rhodobacter sphaeroides* KMS24	Cu	72.60	28.23	90.31	(Panwichian et al. 2011)
		Cd	1.23	0.48	91.38	
7	*Cloacibacterium normanense*	Ni		0.01	85	(Nouha et al. 2016)
		Cu		0.07	40	
8	*Alteromonas sp. JL2810* (Marine bacteria)	Cu	40-400	140.8		(Zhang et al. 2017)
		Ni		226.3		

9	Anammox granular sludge	Cu		36.1		(Pagliaccia et al. 2022)
		Ni		48.2		
10	*B. licheniformis* NSPA5,	Cu	1000	0.943		(Shameer 2016)
	B. cereus NSPA8			0.945		
	B. subtilis NSPA13			0.928		
11	*Bacillus sp.* MC3B-22	Cd	10-100	97		(Camacho-Chab et al. 2018)
	Microbacterium sp. MC3B-10			141		
12	*Bacillus cereus* KMS3-1	Cd	50	1.19	29.3	(Mathivanan et al. 2023)
13	*Wangia profunda* (SM-A87))	Cu	0-400	128.21		(Zhou et al. 2012)
		Cd		116.28		
14	*Lactobacillus fermentum* 6b	Cd	200-1200	714.286	81.8	(Kermanshahi et al. 2023)
15	*Arthrobacter ps-5*	Cu		169.15		(Shuhong et al. 2014)
16	Soil	Cu	10-80	13.5		(Wu et al. 2021)
		Cd		14.1		
17	*Agrobacterium tumefaciens* F2	Cu		97.09	94.4	(Cui et al. 2020)
		Ni		51.28	77.9	
18	*Aspergillus fumigatus*	Cu		40.0	76.3	(Yin et al. 2011)
		Cd		85.5	81.2	

The presence of co-existing metal ions significantly impacted the sorption of both Ni^{2+} and Cu^{2+} by *M. aeruginosa* (Figure 36). Single metal systems, as revealed by the Langmuir isotherm, displayed a higher maximum adsorption capacity (q_{max}) for Ni^{2+} compared to Cu^{2+} for both biomass and EPS. This suggests a preferential binding of *M. aeruginosa* towards Ni^{2+} ions. Interestingly, the introduction of a co-existing metal ion led to a decrease in the q_{max} for the other metal in both biomass and EPS. For example, the q_{max} for Ni^{2+} on *M. aeruginosa* biomass decreased from 2.49 mg g^{-1} to 1.07 mg g^{-1} with Cu^{2+} co-existence. This competitive inhibition phenomenon arises when both metal ions compete for the same binding sites on the biosorbent, hindering each other's adsorption (Kaewsarn et al. 2001; El-Naas et al. 2007). The Freundlich model parameters (k_F) corroborated this competitive behavior. A decrease in kF values within the binary systems signifies a compromised biosorption capacity due to competition between metal ions, aligning with previous findings (Ma and Tobin 2003). While the Temkin isotherm provided a slightly less favorable fit, it also displayed a similar trend, with decreased B_T values suggesting reduced binding energies between metal ions and the biosorbent in binary systems.

The investigation using *A. doliolum* biomass and EPS yielded results mirroring those observed with *M. aeruginosa* (Figure 60). Single metal systems displayed a higher q_{max} for Ni^{2+} compared to Cu^{2+}, indicating a preferential sorption of Ni^{2+}. The introduction of a co-existing metal ion resulted in a decrease in the q_{max} for the other metal, signifying competitive inhibition. The Freundlich (k_F values) and Temkin (BT values) models further supported this competitive adsorption phenomenon within the binary systems. Several studies have reported competitive adsoption phenomenon within binary system (Vilar et al. 2008; Sulaymon et al. 2013; Suzaki et al. 2017; Mahamadi 2019).

The findings of this study highlight the importance of considering co-existing contaminants when evaluating biosorption for metal removal from real-world environmental samples. The presence of multiple metal ions can significantly affect their individual adsorption behavior due to competitive interactions at the binding sites on the biosorbent (Sulaymon et al. 2013; Kakaei et al. 2021). This emphasizes the need for further research to understand the complex interplay between various metal ions and biosorbents in environmentally relevant settings with diverse metal mixtures.

This study evaluated the reusability and regeneration potential of *M. aeruginosa* and *A. doliolum* biomass, along with their EPS, for metal removal using Milli-Q water as the desorbent. Desorption efficiency is a crucial factor for assessing the economic viability and environmental sustainability of biosorption technologies (Zhou et al. 2023).

The findings revealed a significant challenge – a generally low desorption efficiency for all three metal ions (Cd^{2+}, Cu^{2+}, and Ni^{2+}) using Milli-Q water, particularly for Ni^{2+}. This suggests that metal ions, especially Ni^{2+}, form strong bonds with the functional groups on the biomass and EPS, potentially hindering their release with a weak desorbent like deionized water (Mellis et al. 2017). This aligns with previous studies. For instance, (Jalali et al. 2023) reported limited desorption of Cu^{2+} and Cd^{2+} from soil of two sites i.e. agriculture and greenhouse using Milli-Q water, highlighting the need for stronger desorbing agents.

An interesting observation was the significantly higher desorption efficiency for all metals from EPS compared to their corresponding biomass counterparts. This suggests that the unique structural and chemical properties of EPS, rich in functional groups like carboxyl, phosphate, and amine groups (Li et al. 2021), might facilitate weaker interactions with metal ions compared to the biomass. This could allow for easier metal release using a weak desorbent like Milli-Q water. The study by (Yu et al. 2022) supports this hypothesis, demonstrating a higher desorption efficiency for Cu^{2+} from EPS based biosorbents compared to raw biomass, possibly due to the weaker ionic interactions between Cu^{2+} and the alginate functional groups.

While this study provides valuable insights, some limitations need to be addressed. Firstly, Milli-Q water might not be the most effective desorbent for all metal-biosorbent combinations. Exploring stronger desorbing agents, such as acids, alkalis, or chelating agents, is crucial for optimizing desorption efficiency (Akpomie et al. 2015). Secondly, the potential environmental impact of using stronger desorbents needs to be carefully considered. Identifying eco-friendly desorbents or developing regeneration techniques that minimize desorbent requirements are important areas for future research.

SECTION II: LIVE CELLS EXPERIMENTS

This study investigated the influence of heavy metals (Cu^{2+}, Ni^{2+}, and Cd^{2+}) on the growth patterns and specific growth rates of *M. aeruginosa* and *A. doliolum*. Both *M. aeruginosa* and *A. doliolum* displayed typical growth patterns with distinct lag, exponential, and stationary phases as observed in Figure 40. This aligns with previous studies on cyanobacterial growth dynamics (Sánchez-Bayo et al. 2020). Interestingly, *M. aeruginosa* exhibited a higher growth rate compared to *A. doliolum* under the given conditions, reaching a higher final cell density. This suggests a potential difference in their intrinsic growth capacities.

The impact of heavy metals on growth is evident in Figures 41 and 42. All three metals (Cu^{2+}, Ni^{2+}, and Cd^{2+}) exhibited a dose-dependent inhibitory effect on the specific growth rate of both *M. aeruginosa* and *A. doliolum*. This is consistent with prior research, where heavy metals have been shown to disrupt various cellular processes, hindering growth and proliferation in cyanobacteria (Wang et al. 2015a; Facey et al. 2022). Notably, cadmium (Cd^{2+}) displayed the strongest inhibitory effect on the growth of both species at all concentrations tested. This suggests that Cd^{2+} might be particularly toxic to these cyanobacteria, potentially due to its interference with essential metabolic pathways (Rzymski et al. 2014).

An interesting observation was the slight increase in specific growth rate for *M. aeruginosa* treated with low concentrations (0-1.5 μM) of Ni^{2+} and Cu^{2+} compared to the control (Figure 41). This stimulating effect, where low doses of a stressor can stimulate growth, has been reported for some cyanobacteria exposed to certain metals (Fan et al. 2019). The underlying mechanisms for this phenomenon are not fully understood, but it might be related to response, where low doses trigger defense mechanisms that enhance cellular tolerance to higher stress levels (Huertas et al. 2014). While both *M. aeruginosa* and *A. doliolum* displayed a general decrease in growth rate with increasing metal concentrations, some species-specific differences were observed. Cadmium (Cd^{2+}) exhibited the strongest inhibition for both species, but *A. doliolum* appeared more sensitive to Cu^{2+} compared to Ni^{2+}, whereas the opposite trend was seen for *M. aeruginosa*. These variations highlight the potential for differential metal tolerance mechanisms in these cyanobacterial species.

This study investigated the impact of heavy metals (Cu^{2+}, Ni^{2+}, and Cd^{2+}) on the protein and carbohydrate content of *M. aeruginosa* and *A. doliolum*. Proteins and carbohydrates are essential biomolecules that play critical roles in stress response and cellular function in cyanobacteria (Javed and Usmani 2015). The findings (Figures 43 and 44) reveal a significant decrease in protein content for both *M. aeruginosa* and *A. doliolum* following exposure to all three heavy metals (Cu^{2+}, Ni^{2+}, and Cd^{2+}) in a dose-dependent manner. This aligns with previous research, where heavy metals have been shown to disrupt protein synthesis and degradation pathways in cyanobacteria (John et al. 2008). Interestingly, cadmium (Cd^{2+}) consistently exhibited the most severe reduction in protein content for both species compared to Cu^{2+} and Ni^{2+}. This suggests that Cd^{2+} might be particularly potent in hindering protein synthesis or accelerating protein degradation within these cyanobacteria. An interesting observation was the higher baseline protein content in untreated *A. doliolum* compared to untreated *M. aeruginosa*. This difference could be due to inherent variations in protein allocation patterns between the two species (Baracho and Lombardi 2023).

Similar to protein content, the total carbohydrate content of both *M. aeruginosa* and *A. doliolum* displayed a decreasing trend with increasing heavy metal concentration (Figures 45 and 46). This suggests that these cyanobacteria might be utilizing carbohydrates as an energy source to cope with the stress imposed by heavy metals. Carbohydrates can be broken down to provide energy for various cellular processes, potentially aiding in metal detoxification or stress tolerance mechanisms (Jacques et al. 2019). Once again, Cd^{2+} exposure led to the most significant reduction in carbohydrate content for both species, suggesting a potentially higher energy demand associated with Cd^{2+} stress response. Similar to protein content, untreated *A. doliolum* exhibited a higher total carbohydrate content compared to untreated *M. aeruginosa*. This might indicate a baseline difference in how these species allocate resources for energy storage. *A. doliolum* might maintain a larger carbohydrate reserve under the control conditions used in this experiment. Similar results has been reported by Ghorbani et al (2022) for carbohydrates content of *Nostoc* sp. N27P72 and *Nostoc* sp. FB71 treated with Cu^{2+}, Cr^{2+} and Ni^{2+}.

This study examined the impact of heavy metals (Cu^{2+}, Ni^{2+}, and Cd^{2+}) on the content of chlorophyll-a (Chl-a) and carotenoids, essential photosynthetic pigments in

M. aeruginosa and *A. doliolum*. Photosynthetic pigments play a vital role in light absorption, energy transfer, and protecting cells from excessive light damage (Simkin et al. 2022). Understanding how heavy metals affect these pigments is crucial as it can significantly influence the photosynthetic efficiency and overall health of cyanobacteria. The findings (Figures 47-50) reveal a clear dose-dependent decrease in both Chl-a and carotenoid content for both *M. aeruginosa* and *A. doliolum* following exposure to all three heavy metals. This aligns with previous research demonstrating that heavy metals can disrupt pigment biosynthesis pathways and damage chloroplast structures, hindering photosynthesis in cyanobacteria (Yadav et al. 2020; Thevarajah et al. 2023). Interestingly, cadmium (Cd^{2+}) consistently exhibited the highest reduction in both Chl-a and carotenoid content compared to Cu^{2+} and Ni^{2+} for both species. This suggests that Cd^{2+} might be particularly potent in inhibiting pigment biosynthesis or causing severe damage to the photosynthetic apparatus. Another noteworthy observation is the higher sensitivity of Chl-a compared to carotenoids in both *M. aeruginosa* and *A. doliolum*. This could be due to the specific roles of these pigments. Chlorophyll-a is directly involved in the light reactions of photosynthesis, making it potentially more vulnerable to disruptions caused by heavy metals. Carotenoids, on the other hand, have a secondary role in light absorption and also function in protecting cells from photooxidative stress (Polívka and Frank 2010; Zakar et al. 2016). While the overall trends were similar, some minor variations were observed between *M. aeruginosa* and *A. doliolum*. The decrease in pigment content appeared slightly more pronounced in *A. doliolum* compared to *M. aeruginosa* for both Chl-a and carotenoids at the highest metal concentrations. This suggests potential differences in their susceptibility to pigment degradation under heavy metal stress. Different studies has shown the reduction of photosynthetic pigments both Chlorophyll-a and carotenoids as the effect of heavy metal treatment. For example, Cd^{2+} and Zn^{2+} treatment on Durum Wheat reported by Paunov et al. (2018) and Pb^{2+} and Cu^{2+} treatment on *Citrus aurantium* L reported by Giannakoula et al. (2021) shows the negative impacts of heavy metals on photosynthetic pigments.

This study investigated the impact of heavy metals (Cu^{2+}, Ni^{2+}, and Cd^{2+}) on oxidative stress markers in *M. aeruginosa* and *A. doliolum*. Oxidative stress occurs when the production of reactive oxygen species (ROS) overwhelms the cellular

antioxidant defense system, leading to potential damage to biomolecules and cellular structures (Vatansever et al. 2013; Rezayian et al. 2019). Understanding the differential effects of heavy metals on ROS production and oxidative stress is crucial for assessing their overall toxicity to cyanobacteria.

The findings demonstrate that Cd^{2+} exposure resulted in the highest increase in MDA content (Figures 51 and 52), a marker of lipid peroxidation, for both *M. aeruginosa* and *A. doliolum*. This suggests that Cd^{2+} might be particularly effective in inducing oxidative stress and damaging cell membranes in these cyanobacteria. Previous studies explain the potential mechanisms by which Cd^{2+} can trigger these effects, including disruption of antioxidant systems, mitochondrial dysfunction, and enhanced ROS production (Khan et al. 2022). Similarly, the increase in MDA content in response to heavy metals was also reported by Choudhary et al. (2007) on cyanobacterium *Spirulina platensis*-S5.

Interestingly, Cu^{2+} emerged as the most potent inducer of H_2O_2 and OH^- production in both *M. aeruginosa* and *A. dolioum* (Figures 53-58). Previous studies link this phenomenon to ability of Cu^{2+} to undergo redox cycling and participate in Fenton-like reactions, leading to the generation of highly reactive hydroxyl radicals (OH^-) from H_2O_2 (Perez-Benito 2001; Festa and Thiele 2011). While Cu^{2+} induced the highest levels of O_2^- compared to Cd^{2+} and Ni^{2+} (Figures 55 and 56), the potential contribution of various factors, including mitochondrial dysfunction and cellular responses to metal-induced stress cannot be ruled out (Li et al. 2018a; Sun et al. 2022). It is important to note that the study did not report significant species-specific differences in the generation of ROS or oxidative stress markers.

This study investigated the impact of heavy metals (Cu^{2+}, Ni^{2+}, and Cd^{2+}) on the activity of various antioxidant enzymes (Superoxide Dismutase (SOD), Catalase (CAT), Ascorbate Peroxidase (APX), and Glutathione Reductase (GR)) in *M. aeruginosa* and *A. doliolum*. Antioxidant enzymes are a vital cellular defense system that protects organisms from the damaging effects of oxidative stress (Singh et al. 2023). Oxidative stress arises from an imbalance between the production of reactive oxygen species (ROS) and the cell's capacity to detoxify them (Hong et al. 2024). When ROS production overwhelms the antioxidant defense system, it can lead to cellular dysfunction, growth inhibition, and even cell death (Latifi et al. 2009).

Antioxidant enzymes function by scavenging ROS or facilitating their conversion into less harmful molecules. SOD, for instance, catalyzes the dismutation of superoxide radicals (O_2^-) into hydrogen peroxide (H_2O_2), a less reactive species. CAT further decomposes H_2O_2 into water (H_2O) and oxygen (O_2). APX specifically detoxifies H_2O_2 using ascorbate (vitamin C) as an electron donor. GR regenerates the reduced form of glutathione (GSH), a vital antioxidant molecule that plays a key role in various detoxification processes (Forman et al. 2009). By working together, these enzymes help to maintain cellular redox homeostasis and protect against oxidative stress.

The findings (Figures 59-66) revealed an increase in the activity of all four key antioxidant enzymes (SOD, CAT, APX and GR) for both *M. aeruginosa* and *A. doliolum* following exposure to all three heavy metals. This suggests that these cyanobacteria activate their antioxidant defense systems in response to the elevated ROS production caused by heavy metal stress (Cassier-Chauvat and Chauvat 2014). The observed increase in enzyme activity was statistically significant ($p > 0.05$) for most treatments, indicating a robust cellular response. While all metals induced enzyme activity, Cu^{2+} consistently caused the most significant increase in SOD, CAT, and APX activity in both species (Figures 59-54). This might be due to Cu^{2+}'s tendency to undergo redox cycling and participate in Fenton reactions, leading to a more pronounced generation of ROS compared to Cd^{2+} and Ni^{2+} (Maret 2016; Khalil et al. 2016).

A. doliolum generally exhibited a higher basal level and a greater increase in the activity of SOD, CAT, and APX compared to *M. aeruginosa* across all treatments (Figures 59-64). This suggests that *A. doliolum* might possess a more robust constitutive and inducible antioxidant defense system, potentially contributing to its better tolerance towards heavy metal-induced oxidative stress. The response of GR activity to heavy metal exposure was less pronounced compared to other antioxidant enzymes (Figures 65 and 66). Both *M. aeruginosa* and *A. doliolum* displayed a modest increase in GR activity with increasing metal concentration, but the magnitude of the increase was lower. This suggests that the regulation of GR activity might be less sensitive to heavy metal stress compared to SOD, CAT, and APX in these cyanobacteria.

The SOD enzyme activity of *Clitoria ternatea* L also shown to increase comparing to control in response to Mercury (Hg) treatment was reported by Priya et al. (2014). The studies reported by Zhang et al. (2007) have shown that heavy metal (Pb^{2+}, Cd^{2+}, and Hg^{2+}) stress also increases the activity of antioxidant enzymes, such as catalase CAT and APX. For example, in *Kandelia candel* and *Bruguiera gymnorrhiza* plants, CAT activity increases in the leaves at higher stress levels, but remains unchanged in *B. gymnorrhiza* leaves. The study reported by Wang et al. (2004) in *Brassica juncea* roots, SOD and APX enzymes were increases with the increase in Cu^{2+} concentration but interestingly, CAT enzyme activity shown to decreases from the control. These findings highlight the conserved role of antioxidant enzyme upregulation as a defense mechanism against heavy metal-induced oxidative stress in various cyanobacteria species.

SUMMARY

This thesis describes the exciting potential of cyanobacteria, particularly *Microcystis aeruginosa* and *Anabaena doliolum*, to act as biosorbents against heavy metal contamination in water. The research employs a bioremediation approach, investigating the effectiveness of both live cyanobacteria (biomass) and their Exopolysaccharides (EPS), in removing harmful heavy metals (Cd^{2+}, Cu^{2+}, and Ni^{2+}) from water.

The study goes beyond just establishing their efficacy; it precisely dissects the underlying mechanisms governing this metal removal process. By understanding these mechanisms, we can optimize bioremediation strategies for real-world application. Additionally, the research sheds light on the impact of metal exposure on the cyanobacteria themselves, analyzing their tolerance mechanisms and response to the cellular stress caused by these heavy metals.

The research confirms that both *M. aeruginosa* and *A. doliolum*, in their biomass and EPS forms, possess the remarkable ability to remove Cu^{2+}, Ni^{2+}, and Cd^{2+} ions from water. Interestingly, the study goes a step further by quantifying this ability. By measuring the amount of metal adsorbed by each type of material, the research showed that EPS exhibited a higher metal adsorption capacity compared to biomass. This suggests that EPS could potentially be a more efficient bioremediation tool, capable of removing larger quantities of heavy metals from contaminated water bodies.

The study showed a fascinating interplay between the cyanobacteria and the metals at a molecular level. Metal adsorption by biomass is exothermic (releases heat) but unfavorable (requires external energy input) for the process to occur efficiently. This suggests that the cyanobacteria themselves may need to expend energy to facilitate metal binding onto their cell walls. In contrast, EPS adsorption demonstrates favorability (spontaneous) for all metals except Cd^{2+} (endothermic - absorbs heat). This implies that for most metals, the interaction between the EPS and the metal ions is energetically favorable, happening readily without any external energy input. However, Cd^{2+} seems to require the EPS to invest some energy in the binding process.

To understand the interaction between the metals and the EPS binding sites, the study employs Langmuir and Freundlich isotherm models. These models depict a complex mechanisms between the metal ions and the EPS. The results suggest that both even and uneven binding sites are likely present on the EPS surface. This allows for the adsorption of multiple layers of metal ions, creating a more robust and efficient metal removal system.

Metal removal efficiency is not a static value; it varies with the pH of the external medium for both biomass and EPS. M. aeruginosa exhibits peak Cu^{2+} removal at a specific pH of 6.5, while Cd^{2+} removal increases steadily up to pH 7. *A. doliolum* displays an unchanged Cu^{2+} removal across various pH levels, with a gradual rise in Ni^{2+} removal as the pH increases. Interestingly, Cd^{2+} removal in *A. doliolum* increased at higher pH (7-8). Understanding this pH influence allows for bioremediation strategies to be optimized for different water environments. For example, if a water body has a naturally low pH, utilizing M. aeruginosa might be more effective for Cu^{2+} removal.

The study sheds light on the two-phase process of metal uptake by cyanobacteria. The first rapid phase involves a passive interaction – the metal ions bind to the cell wall of the cyanobacteria through weak physical forces like electrostatic interactions. This initial binding happens very quickly, with the study indicating over 90% of total uptake can be achieved within a mere 30-45 min. This rapid initial phase can be likened to a quick screening process where the metal ions get loosely attached to the cyanobacteria. The second phase is a slower process, which may involve the active transport of metals into the cells, potentially for detoxification purposes. This suggests that the cyanobacteria might have specific mechanisms to transport the accumulate metals inside their cells, possibly to isolate them from their cellular machinery and minimize potential damage. Diffusion plays a more prominent role in EPS compared to whole cells. This highlights a potential difference in the mechanisms employed by these two bioremediation tools. EPS, with its porous structure, might allow for easier diffusion of metal ions compared to the more complex cell wall of the whole cyanobacteria.

The study demonstrates that the presence of one metal reduces the adsorption of another metal on EPS. This phenomenon can be likened to a competition for limited

binding sites on the EPS surface. The study suggests that specific binding sites exist on the EPS for these metals, and when one metal occupies these sites, there is less binding sites available for others. This finding necessitates consideration of co-existing contaminants when designing bioremediation strategies using EPS. If a water source is known to be polluted with multiple heavy metals, a pre-treatment step to remove some of the metals or a combination of different bioremediation techniques might be necessary to achieve optimal overall removal efficiency.

EPS desorbs a higher percentage of adsorbed metals compared to biomass, suggesting that it can be more easily regenerated and reused for metal removal. This reusability aspect strengthens the case for EPS as a sustainable bioremediation tool.

The study showed that all three metals (Cd^{2+}, Cu^{2+}, and Ni^{2+}) inhibit the growth of both cyanobacteria species. They achieve this by reducing essential cellular components like protein, carbohydrate, chlorophyll-a, and carotenoid content. The severity of this inhibition varies by metal, with Cd^{2+} showed highest toxicity, followed by Cu^{2+} and Ni^{2+}. Metal exposure throws the cyanobacteria into a state of oxidative stress, evident by the increased production of free radicals (MDA, H_2O_2, and O_2^-) within their cells. These free radicals are highly reactive and can damage cellular components like proteins, lipids, and DNA if not effectively neutralized. Once again, Cd^{2+} emerges as the most potent stressor, followed by Cu^{2+} and Ni^{2+}. Interestingly, *A. doliolum* appears to be more susceptible to oxidative stress compared to M. aeruginosa. This suggests that *M. aeruginosa* might have more robust antioxidant defense mechanisms in place to combat the free radicals generated by metal exposure.

In response to metal-induced oxidative stress, both cyanobacteria species upregulate antioxidant enzymes (SOD, catalase, and APX). These enzymes act as antioxidants, scavenging and neutralizing the free radicals before they can cause significant damage. The study reveals that *A. doliolum* has a generally higher basal activity of these enzymes compared to *M. aeruginosa*. However, *A. doliolum* also shows a stronger increase in catalase and APX activity in response to heavy metals, suggesting a more inducible antioxidant defense system. This inducible response allows *A. doliolum* to potentially adapt and survive in environments with higher metal contamination over time.

Further studies could investigate:

- The biosorption potential of other cyanobacteria species and explore their metal selectivity.
- The synergistic effects of combining different cyanobacteria strains or EPS with other bioremediation techniques.
- The long-term impact of metal exposure on the cyanobacteria, including potential genetic adaptations.
- The development of large-scale bioremediation systems utilizing cyanobacteria or EPS for real-world application.

REFERENCES

A. Abid B, M. BrbootI M, M. Al-ShuwaikI N (2011) Removal of Heavy Metals Using Chemicals Precipitation. ETJ 29:595–612. https://doi.org/10.30684/etj.29.3.15

Afroze S, Sen TK (2018) A Review on Heavy Metal Ions and Dye Adsorption from Water by Agricultural Solid Waste Adsorbents. Water Air Soil Pollut 229:225. https://doi.org/10.1007/s11270-018-3869-z

Aftab KU, Ahmad IZ (2013) Alterations in Antioxidative Defense System of Anabaena Variabilis in the Presence of Heavy Metals. APCBEE Procedia 5:491–496. https://doi.org/10.1016/j.apcbee.2013.05.083

Agarwal P, Soni R, Kaur P, et al (2022) Cyanobacteria as a Promising Alternative for Sustainable Environment: Synthesis of Biofuel and Biodegradable Plastics. Front Microbiol 13:939347. https://doi.org/10.3389/fmicb.2022.939347

Agbemafle R, Elsie Aggo S, Akutey O, Bentum JK (2019) Heavy Metal Concentrations in Leachates and Crops Grown Around Waste Dumpsites in Sekondi-Takoradi in the Western Region of Ghana. Research J of Environmental Toxicology 14:16–25. https://doi.org/10.3923/rjet.2020.16.25

Aharoni C, Ungarish M (1977) Kinetics of activated chemisorption. Part 2.—Theoretical models. J Chem Soc, Faraday Trans 1 73:456. https://doi.org/10.1039/f19777300456

Akbari M, Hallajisani A, Keshtkar AR, et al (2015) Equilibrium and kinetic study and modeling of Cu(II) and Co(II) synergistic biosorption from Cu(II)-Co(II) single and binary mixtures on brown algae C. indica. Journal of Environmental Chemical Engineering 3:140–149. https://doi.org/10.1016/j.jece.2014.11.004

Akhbarizadeh R, Shayestefar MR, Darezereshki E (2014) Competitive Removal of Metals from Wastewater by Maghemite Nanoparticles: A Comparison Between Simulated Wastewater and AMD. Mine Water Environ 33:89–96. https://doi.org/10.1007/s10230-013-0255-3

Akpomie KG, Dawodu FA, Adebowale KO (2015) Mechanism on the sorption of heavy metals from binary-solution by a low cost montmorillonite and its desorption potential. Alexandria Engineering Journal 54:757–767. https://doi.org/10.1016/j.aej.2015.03.025

Aksu Z, Kutsal T (1990) A comparative study for biosorption characteristics of heavy metal ions with *C. vulgaris*. Environmental Technology 11:979–987. https://doi.org/10.1080/09593339009384950

Al-Amin A, Parvin F, Chakraborty J, Kim Y-I (2021) Cyanobacteria mediated heavy metal removal: a review on mechanism, biosynthesis, and removal capability. Environmental Technology Reviews 10:44–57. https://doi.org/10.1080/21622515.2020.1869323

Alengebawy A, Abdelkhalek ST, Qureshi SR, Wang M-Q (2021) Heavy Metals and Pesticides Toxicity in Agricultural Soil and Plants: Ecological Risks and Human Health Implications. Toxics 9:42. https://doi.org/10.3390/toxics9030042

Al-Homaidan AA, Al-Qahtani HS, Al-Ghanayem AA, et al (2018) Potential use of green algae as a biosorbent for hexavalent chromium removal from aqueous solutions. Saudi Journal of Biological Sciences 25:1733–1738. https://doi.org/10.1016/j.sjbs.2018.07.011

Ali AAH (2023) Overview of the vital roles of macro minerals in the human body. Journal of Trace Elements and Minerals 4:100076. https://doi.org/10.1016/j.jtemin.2023.100076

Ali H, Khan E (2018) Bioaccumulation of non-essential hazardous heavy metals and metalloids in freshwater fish. Risk to human health. Environ Chem Lett 16:903–917. https://doi.org/10.1007/s10311-018-0734-7

Ali H, Khan E, Ilahi I (2019) Environmental Chemistry and Ecotoxicology of Hazardous Heavy Metals: Environmental Persistence, Toxicity, and Bioaccumulation. Journal of Chemistry 2019:1–14. https://doi.org/10.1155/2019/6730305

Ali Redha A (2020) Removal of heavy metals from aqueous media by biosorption. Arab Journal of Basic and Applied Sciences 27:183–193. https://doi.org/10.1080/25765299.2020.1756177

Al-Juboori RA, Bakly S, Bowtell L, et al (2022) Innovative capacitive deionization-degaussing approach for improving adsorption/desorption for macadamia nutshell biochar. Journal of Water Process Engineering 47:102786. https://doi.org/10.1016/j.jwpe.2022.102786

Alotaibi BS, Khan M, Shamim S (2021) Unraveling the Underlying Heavy Metal Detoxification Mechanisms of Bacillus Species. Microorganisms 9:1628. https://doi.org/10.3390/microorganisms9081628

Amiard J, Amiardtriquet C, Barka S, et al (2006) Metallothioneins in aquatic invertebrates: Their role in metal detoxification and their use as biomarkers. Aquatic Toxicology 76:160–202. https://doi.org/10.1016/j.aquatox.2005.08.015

Anand U, Dey S, Parial D, et al (2023) Algae and bacteria consortia for wastewater decontamination and transformation into biodiesel, bioethanol, biohydrogen,

biofertilizers and animal feed: a review. Environ Chem Lett 21:1585–1609. https://doi.org/10.1007/s10311-023-01562-w

Angelin J, Kavitha M (2020) Exopolysaccharides from probiotic bacteria and their health potential. International Journal of Biological Macromolecules 162:853–865. https://doi.org/10.1016/j.ijbiomac.2020.06.190

Ansari MI, Malik A (2007) Biosorption of nickel and cadmium by metal resistant bacterial isolates from agricultural soil irrigated with industrial wastewater. Bioresource Technology 98:3149–3153. https://doi.org/10.1016/j.biortech.2006.10.008

A.O D (2012) Langmuir, Freundlich, Temkin and Dubinin–Radushkevich Isotherms Studies of Equilibrium Sorption of Zn 2+ Unto Phosphoric Acid Modified Rice Husk. IOSRJAC 3:38–45. https://doi.org/10.9790/5736-0313845

Aquino E, Barbieri C, Oller Nascimento CA (2011) Engineering Bacteria for Bioremediation. In: Carpi A (ed) Progress in Molecular and Environmental Bioengineering - From Analysis and Modeling to Technology Applications. InTech

Araújo CST, Almeida ILS, Rezende HC, et al (2018) Elucidation of mechanism involved in adsorption of Pb(II) onto lobeira fruit (Solanum lycocarpum) using Langmuir, Freundlich and Temkin isotherms. Microchemical Journal 137:348–354. https://doi.org/10.1016/j.microc.2017.11.009

Arif N, Yadav V, Singh S, et al (2016) Influence of High and Low Levels of Plant-Beneficial Heavy Metal Ions on Plant Growth and Development. Front Environ Sci 4:. https://doi.org/10.3389/fenvs.2016.00069

Asada K (2006) Production and Scavenging of Reactive Oxygen Species in Chloroplasts and Their Functions. Plant Physiology 141:391–396. https://doi.org/10.1104/pp.106.082040

Ayawei N, Ebelegi AN, Wankasi D (2017) Modelling and Interpretation of Adsorption Isotherms. Journal of Chemistry 2017:1–11. https://doi.org/10.1155/2017/3039817

Babiak W, Krzemińska I (2021) Extracellular Polymeric Substances (EPS) as Microalgal Bioproducts: A Review of Factors Affecting EPS Synthesis and Application in Flocculation Processes. Energies 14:4007. https://doi.org/10.3390/en14134007

Baptista MS, Vasconcelos MT (2006) Cyanobacteria Metal Interactions: Requirements, Toxicity, and Ecological Implications. Critical Reviews in Microbiology 32:127–137. https://doi.org/10.1080/10408410600822934

Baracho DH, Lombardi AT (2023) Study of the growth and biochemical composition of 20 species of cyanobacteria cultured in cylindrical photobioreactors. Microb Cell Fact 22:36. https://doi.org/10.1186/s12934-023-02035-z

Barakat MA (2011) New trends in removing heavy metals from industrial wastewater. Arabian Journal of Chemistry 4:361–377. https://doi.org/10.1016/j.arabjc.2010.07.019

Bashir K, Nagasaka S, Itai RN, et al (2007) Expression and enzyme activity of glutathione reductase is upregulated by Fe-deficiency in graminaceous plants. Plant Mol Biol 65:277–284. https://doi.org/10.1007/s11103-007-9216-1

Baulina OI (2012) Ultrastructural Plasticity of Cyanobacteria. Springer Berlin Heidelberg, Berlin, Heidelberg

Bayuo J, Abukari MA, Pelig-Ba KB (2020) Desorption of chromium (VI) and lead (II) ions and regeneration of the exhausted adsorbent. Appl Water Sci 10:171. https://doi.org/10.1007/s13201-020-01250-y

Benalia MC, Youcef L, Bouaziz MG, et al (2022) Removal of Heavy Metals from Industrial Wastewater by Chemical Precipitation: Mechanisms and Sludge Characterization. Arab J Sci Eng 47:5587–5599. https://doi.org/10.1007/s13369-021-05525-7

Bird AJ (2015) Cellular sensing and transport of metal ions: implications in micronutrient homeostasis. The Journal of Nutritional Biochemistry 26:1103–1115. https://doi.org/10.1016/j.jnutbio.2015.08.002

Blaby-Haas CE, Merchant SS (2012) The ins and outs of algal metal transport. Biochimica et Biophysica Acta (BBA) - Molecular Cell Research 1823:1531–1552. https://doi.org/10.1016/j.bbamcr.2012.04.010

Blanco P, Hernando-Amado S, Reales-Calderon J, et al (2016) Bacterial Multidrug Efflux Pumps: Much More Than Antibiotic Resistance Determinants. Microorganisms 4:14. https://doi.org/10.3390/microorganisms4010014

Bloch K, Ghosh S (2022) Cyanobacteria mediated toxic metal removal as complementary and alternative wastewater treatment strategy. In: Integrated Environmental Technologies for Wastewater Treatment and Sustainable Development. Elsevier, pp 533–548

Boonchai R, Kaewsuk J, Seo G (2015) Effect of nutrient starvation on nutrient uptake and extracellular polymeric substance for microalgae cultivation and separation. Desalination and Water Treatment 55:360–367. https://doi.org/10.1080/19443994.2014.939501

Borah D, Kennedy B, Gopalakrishnan S, et al (2020) Bioremediation and Biomass Production with the Green Microalga Chlorococcum humicola and Textile Mill

Effluent (TE). Proc Natl Acad Sci, India, Sect B Biol Sci 90:415–423. https://doi.org/10.1007/s40011-019-01112-x

Borah D, Vimala N and Thajuddin N (2016). Biochemical composition and chemotaxonomy of cyanobacteria isolated from Assam, North-East India. Phykos 46 (2): 33-45 (2016).

Boulaiche W, Belhamdi B, Hamdi B, Trari M (2019) Kinetic and equilibrium studies of biosorption of M(II) (M = Cu, Pb, Ni, Zn and Cd) onto seaweed Posidonia oceanica fibers. Appl Water Sci 9:173. https://doi.org/10.1007/s13201-019-1062-1

Bowers K, Srai SKS (2018) The trafficking of metal ion transporters of the Zrt- and Irt-like protein family. Traffic 19:813–822. https://doi.org/10.1111/tra.12602

Bozzi AT, Gaudet R (2021) Molecular Mechanism of Nramp-Family Transition Metal Transport. Journal of Molecular Biology 433:166991. https://doi.org/10.1016/j.jmb.2021.166991

Breitenbach R, Gerrits R, Dementyeva P, et al (2022) The role of extracellular polymeric substances of fungal biofilms in mineral attachment and weathering. npj Mater Degrad 6:42. https://doi.org/10.1038/s41529-022-00253-1

Briffa J, Sinagra E, Blundell R (2020) Heavy metal pollution in the environment and their toxicological effects on humans. Heliyon 6:e04691. https://doi.org/10.1016/j.heliyon.2020.e04691

Brown PA, Gill SA, Allen SJ (2000) Metal removal from wastewater using peat. Water Research 34:3907–3916. https://doi.org/10.1016/S0043-1354(00)00152-4

Bullen JC, Saleesongsom S, Gallagher K, Weiss DJ (2021) A Revised Pseudo-Second-Order Kinetic Model for Adsorption, Sensitive to Changes in Adsorbate and Adsorbent Concentrations. Langmuir 37:3189–3201. https://doi.org/10.1021/acs.langmuir.1c00142

Burford N, Eelman M, Groom K (2005) Identification of complexes containing glutathione with As(III), Sb(III), Cd(II), Hg(II), Tl(I), Pb(II) or Bi(III) by electrospray ionization mass spectrometry. Journal of Inorganic Biochemistry 99:1992–1997. https://doi.org/10.1016/j.jinorgbio.2005.06.019

Caccamo A, Vega De Luna F, Wahni K, et al (2023) Ascorbate Peroxidase 2 (APX2) of Chlamydomonas Binds Copper and Modulates the Copper Insertion into Plastocyanin. Antioxidants 12:1946. https://doi.org/10.3390/antiox12111946

Camacho-Chab J, Castañeda-Chávez M, Chan-Bacab M, et al (2018) Biosorption of Cadmium by Non-Toxic Extracellular Polymeric Substances (EPS)

Synthesized by Bacteria from Marine Intertidal Biofilms. IJERPH 15:314. https://doi.org/10.3390/ijerph15020314

Carpenè E, Andreani G, Isani G (2007) Metallothionein functions and structural characteristics. Journal of Trace Elements in Medicine and Biology 21:35–39. https://doi.org/10.1016/j.jtemb.2007.09.011

Cassier-Chauvat C, Chauvat F (2014) Responses to Oxidative and Heavy Metal Stresses in Cyanobacteria: Recent Advances. IJMS 16:871–886. https://doi.org/10.3390/ijms16010871

Cavalca L, Corsini A, Zaccheo P, et al (2013) Microbial Transformations of Arsenic: Perspectives for Biological Removal of Arsenic from Water. Future Microbiol 8:753–768. https://doi.org/10.2217/fmb.13.38

Chang J, Zhang H, Cheng H, et al (2020) Spent Ganoderma lucidum substrate derived biochar as a new bio-adsorbent for Pb2+/Cd2+ removal in water. Chemosphere 241:125121. https://doi.org/10.1016/j.chemosphere.2019.125121

Cheah C, Cheow YL, Ting ASY (2023) Pre-Treatment of Exopolymeric Substances from Bacillus cereus for Metal Removal as a Novel Strategy to Enhance Metal Biosorption. Water Air Soil Pollut 234:121. https://doi.org/10.1007/s11270-023-06150-w

Chen X, Hossain MF, Duan C, et al (2022) Isotherm models for adsorption of heavy metals from water - A review. Chemosphere 307:135545. https://doi.org/10.1016/j.chemosphere.2022.135545

Chen X, Tian Z, Cheng H, et al (2021) Adsorption process and mechanism of heavy metal ions by different components of cells, using yeast (*Pichia pastoris*) and Cu^{2+} as biosorption models. RSC Adv 11:17080–17091. https://doi.org/10.1039/D0RA09744F

Choudhary M, Jetley UK, Abash Khan M, et al (2007) Effect of heavy metal stress on proline, malondialdehyde, and superoxide dismutase activity in the cyanobacterium Spirulina platensis-S5. Ecotoxicology and Environmental Safety 66:204–209. https://doi.org/10.1016/j.ecoenv.2006.02.002

Chu KH (2021) Revisiting the Temkin Isotherm: Dimensional Inconsistency and Approximate Forms. Ind Eng Chem Res 60:13140–13147. https://doi.org/10.1021/acs.iecr.1c01788

Chu KH, Hashim MA, Bashiri H, et al (2023) The Flory–Huggins Isotherm and Water Contaminant Adsorption: Debunking Some Modeling Fallacies. Ind Eng Chem Res 62:1121–1131. https://doi.org/10.1021/acs.iecr.2c03799

Chu W-L, Phang S-M (2019) Biosorption of Heavy Metals and Dyes from Industrial Effluents by Microalgae. In: Alam MdA, Wang Z (eds) Microalgae

Biotechnology for Development of Biofuel and Wastewater Treatment. Springer Singapore, Singapore, pp 599–634

Chuah TG, Jumasiah A, Azni I, et al (2005) Rice husk as a potentially low-cost biosorbent for heavy metal and dye removal: an overview. Desalination 175:305–316. https://doi.org/10.1016/j.desal.2004.10.014

Chugh M, Kumar L, Shah MP, Bharadvaja N (2022) Algal Bioremediation of heavy metals: An insight into removal mechanisms, recovery of by-products, challenges, and future opportunities. Energy Nexus 7:100129. https://doi.org/10.1016/j.nexus.2022.100129

Ciani M, Adessi A (2023) Cyanoremediation and phyconanotechnology: cyanobacteria for metal biosorption toward a circular economy. Front Microbiol 14:1166612. https://doi.org/10.3389/fmicb.2023.1166612

Collins MP, Forgac M (2020) Regulation and function of V-ATPases in physiology and disease. Biochimica et Biophysica Acta (BBA) - Biomembranes 1862:183341. https://doi.org/10.1016/j.bbamem.2020.183341

Concórdio-Reis P, Reis MAM, Freitas F (2020) Biosorption of Heavy Metals by the Bacterial Exopolysaccharide FucoPol. Applied Sciences 10:6708. https://doi.org/10.3390/app10196708

Corinti D, Maccelli A, Chiavarino B, et al (2022) Cation-π Interactions between a Noble Metal and a Polyfunctional Aromatic Ligand: Ag^{+} (benzylamine). Chemistry A European J 28:e202200300. https://doi.org/10.1002/chem.202200300

Cosgrove WJ, Loucks DP (2015) Water management: Current and future challenges and research directions. Water Resources Research 51:4823–4839. https://doi.org/10.1002/2014WR016869

Costa OYA, Raaijmakers JM, Kuramae EE (2018) Microbial Extracellular Polymeric Substances: Ecological Function and Impact on Soil Aggregation. Front Microbiol 9:1636. https://doi.org/10.3389/fmicb.2018.01636

Cui D, Tan C, Deng H, et al (2020a) Biosorption Mechanism of Aqueous Pb^{2+}, Cd^{2+}, and Ni^{2+} Ions on Extracellular Polymeric Substances (EPS). Archaea 2020:1–9. https://doi.org/10.1155/2020/8891543

Cui J-Q, He Q-S, Liu M-H, et al (2020b) Comparative Study on Different Remediation Strategies Applied in Petroleum-Contaminated Soils. IJERPH 17:1606. https://doi.org/10.3390/ijerph17051606

Das B, Mondal NK, Bhaumik R, Roy P (2014) Insight into adsorption equilibrium, kinetics and thermodynamics of lead onto alluvial soil. Int J Environ Sci Technol 11:1101–1114. https://doi.org/10.1007/s13762-013-0279-z

De Caroli M, Furini A, DalCorso G, et al (2020) Endomembrane Reorganization Induced by Heavy Metals. Plants 9:482. https://doi.org/10.3390/plants9040482

De La Torre M, Pomorski A (2024) Investigation of metal ion binding biomolecules one molecule at a time. Front Chem 12:1378447. https://doi.org/10.3389/fchem.2024.1378447

De Philippis R (1998) Exocellular polysaccharides from cyanobacteria and their possible applications. FEMS Microbiology Reviews 22:151–175. https://doi.org/10.1016/S0168-6445(98)00012-6

De Philippis R, Colica G, Micheletti E (2011) Exopolysaccharide-producing cyanobacteria in heavy metal removal from water: molecular basis and practical applicability of the biosorption process. Appl Microbiol Biotechnol 92:697–708. https://doi.org/10.1007/s00253-011-3601-z

De Philippis R, Paperi R, Sili C (2007) Heavy metal sorption by released polysaccharides and whole cultures of two exopolysaccharide-producing cyanobacteria. Biodegradation 18:181–187. https://doi.org/10.1007/s10532-006-9053-y

De Vos CHR, Schat H (1991) Free radicals and heavy metal tolerance. In: Rozema J, Verkleij JAC (eds) Ecological responses to environmental stresses. Springer Netherlands, Dordrecht, pp 22–31

Decherchi S, Cavalli A (2020) Thermodynamics and Kinetics of Drug-Target Binding by Molecular Simulation. Chem Rev 120:12788–12833. https://doi.org/10.1021/acs.chemrev.0c00534

Derdak R, Sakoui S, Pop OL, et al (2022) Screening, optimization and characterization of exopolysaccharides produced by novel strains isolated from Moroccan raw donkey milk. Food Chemistry: X 14:100305. https://doi.org/10.1016/j.fochx.2022.100305

Dey S, Veerendra GTN, Phani Manoj AV, Anjaneya Babu PSS (2023) Performances of plant leaf biosorbents for biosorption of phosphorous from synthetic water. Cleaner Materials 8:100191. https://doi.org/10.1016/j.clema.2023.100191

Dhir B (2021) Role of transporters of copper, manganese, zinc, and nickel in plants exposed to heavy metal stress. In: Metal and Nutrient Transporters in Abiotic Stress. Elsevier, pp 145–168

Dixon C, Wilken LR (2018) Green microalgae biomolecule separations and recovery. Bioresour Bioprocess 5:14. https://doi.org/10.1186/s40643-018-0199-3

Dobrowolski R, Krzyszczak A, Dobrzyńska J, et al (2019) Extracellular polymeric substances immobilized on microspheres for removal of heavy metals from aqueous environment. Biochemical Engineering Journal 143:202–211. https://doi.org/10.1016/j.bej.2019.01.004

Domozych DS, Ciancia M, Fangel JU, et al (2012) The Cell Walls of Green Algae: A Journey through Evolution and Diversity. Front Plant Sci 3:. https://doi.org/10.3389/fpls.2012.00082

Drewniak L, Sklodowska A (2013) Arsenic-transforming microbes and their role in biomining processes. Environ Sci Pollut Res 20:7728–7739. https://doi.org/10.1007/s11356-012-1449-0

Duan Z, Tan X, Zhang D, Parajuli K (2020) Development of thermal treatment for the extraction of extracellular polymeric substances from *Microcystis* : Evaluating extraction efficiency and cell integrity. Algal Research 48:101879. https://doi.org/10.1016/j.algal.2020.101879

Dubey S, Shri M, Gupta A, et al (2018) Toxicity and detoxification of heavy metals during plant growth and metabolism. Environ Chem Lett 16:1169–1192. https://doi.org/10.1007/s10311-018-0741-8

Duffus JH (2002) "Heavy metals" a meaningless term? (IUPAC Technical Report). Pure and Applied Chemistry 74:793–807. https://doi.org/10.1351/pac200274050793

El-Gendy MMAA, Ten NM, Ibrahim HAE-H, Abd El-Baky DH (2017) Heavy Metals Biosorption from Aqueous Solution by Endophytic *Drechslera hawaiiensis* of *Morus alba* L. Derived from Heavy Metals Habitats. Mycobiology 45:73–83. https://doi.org/10.5941/MYCO.2017.45.2.73

El-Naas MH, Al-Rub FA, Ashour I, Al Marzouqi M (2007) Effect of competitive interference on the biosorption of lead(II) by Chlorella vulgaris. Chemical Engineering and Processing: Process Intensification 46:1391–1399. https://doi.org/10.1016/j.cep.2006.11.003

Etxeberria E, Pozueta-Romero J, Gonzalez P (2012) In and out of the plant storage vacuole. Plant Science 190:52–61. https://doi.org/10.1016/j.plantsci.2012.03.010

Facey JA, Violi JP, King JJ, et al (2022) The Influence of Micronutrient Trace Metals on *Microcystis aeruginosa* Growth and Toxin Production. Toxins 14:812. https://doi.org/10.3390/toxins14110812

Fan G, Bao M, Wang B, et al (2019) Inhibitory Effects of Cu2O/SiO2 on the Growth of *Microcystis aeruginosa* and Its Mechanism. Nanomaterials 9:1669. https://doi.org/10.3390/nano9121669

Festa RA, Thiele DJ (2011) Copper: An essential metal in biology. Current Biology 21:R877–R883. https://doi.org/10.1016/j.cub.2011.09.040

Forman HJ, Zhang H, Rinna A (2009) Glutathione: Overview of its protective roles, measurement, and biosynthesis. Molecular Aspects of Medicine 30:1–12. https://doi.org/10.1016/j.mam.2008.08.006

Foulkes EC (2000) Transport of Toxic Heavy Metals Across Cell Membranes. Proc Soc Exp Biol Med 223:234–240. https://doi.org/10.1046/j.1525-1373.2000.22334.x

Foyer CH, Hanke G (2022) ROS production and signalling in chloroplasts: cornerstones and evolving concepts. The Plant Journal 111:642–661. https://doi.org/10.1111/tpj.15856

Foyer CH, Noctor G (2011) Ascorbate and Glutathione: The Heart of the Redox Hub. Plant Physiol 155:2–18. https://doi.org/10.1104/pp.110.167569

Freundlich H (1907) Über die Adsorption in Lösungen. Zeitschrift für Physikalische Chemie 57U:385–470. https://doi.org/10.1515/zpch-1907-5723

Fu F, Wang Q (2011) Removal of heavy metal ions from wastewaters: A review. Journal of Environmental Management 92:407–418. https://doi.org/10.1016/j.jenvman.2010.11.011

Fujii J, Homma T, Osaki T (2022) Superoxide Radicals in the Execution of Cell Death. Antioxidants 11:501. https://doi.org/10.3390/antiox11030501

Gao J-F, Si C-Y, Li H-Y (2016) Role of functional groups on protonated de-oiled soybean involved in triclosan biosorption from aqueous solution. RSC Adv 6:67319–67330. https://doi.org/10.1039/C6RA06702F

Ghorbani E, Nowruzi B, Nezhadali M, Hekmat A (2022) Metal removal capability of two cyanobacterial species in autotrophic and mixotrophic mode of nutrition. BMC Microbiol 22:58. https://doi.org/10.1186/s12866-022-02471-8

Giannakoula A, Therios I, Chatzissavvidis C (2021) Effect of Lead and Copper on Photosynthetic Apparatus in Citrus (Citrus aurantium L.) Plants. The Role of Antioxidants in Oxidative Damage as a Response to Heavy Metal Stress. Plants 10:155. https://doi.org/10.3390/plants10010155

Gill RA, Ahmar S, Ali B, et al (2021) The Role of Membrane Transporters in Plant Growth and Development, and Abiotic Stress Tolerance. IJMS 22:12792. https://doi.org/10.3390/ijms222312792

Girma G (2015) Microbial Bioremediation of some Heavy Metals in Soils: An updated review. Egyptian Academic Journal of Biological Sciences, G Microbiology 7:29–45. https://doi.org/10.21608/eajbsg.2015.16483

Gnoth K, Bär JW, Rosche F, et al (2024) Contribution of amino acids in the active site of dipeptidyl peptidase 4 to the catalytic action of the enzyme. PLoS ONE 19:e0289239. https://doi.org/10.1371/journal.pone.0289239

Gonçalves AL, Ferreira C, Loureiro JA, et al (2015) Surface physicochemical properties of selected single and mixed cultures of microalgae and

cyanobacteria and their relationship with sedimentation kinetics. Bioresour Bioprocess 2:21. https://doi.org/10.1186/s40643-015-0051-y

Gora EH, Saldana SG, Casper LM, et al (2022) Effect of Exhausted Coffee Ground Particle Size on Metal Ion Adsorption Rates and Capacities. ACS Omega 7:38600–38612. https://doi.org/10.1021/acsomega.2c04058

Goswami S, Syiem MB, Pakshirajan K (2015) Cadmium removal by *Anabaena doliolum* Ind1 isolated from a coal mining area in Meghalaya, India: associated structural and physiological alterations. Environmental Engineering Research 20:41–50. https://doi.org/10.4491/eer.2014.059

Guo X, Wang X, Liu J (2016) Composition analysis of fractions of extracellular polymeric substances from an activated sludge culture and identification of dominant forces affecting microbial aggregation. Sci Rep 6:28391. https://doi.org/10.1038/srep28391

Gupta P, Diwan B (2017) Bacterial Exopolysaccharide mediated heavy metal removal: A Review on biosynthesis, mechanism and remediation strategies. Biotechnology Reports 13:58–71. https://doi.org/10.1016/j.btre.2016.12.006

Gwin JA, Church DD, Wolfe RR, et al (2020) Muscle Protein Synthesis and Whole-Body Protein Turnover Responses to Ingesting Essential Amino Acids, Intact Protein, and Protein-Containing Mixed Meals with Considerations for Energy Deficit. Nutrients 12:2457. https://doi.org/10.3390/nu12082457

Gybina AA, Prohaska JR (2008) Copper deficiency results in AMP-activated protein kinase activation and acetylCoA carboxylase phosphorylation in rat cerebellum. Brain Research 1204:69–76. https://doi.org/10.1016/j.brainres.2008.01.087

Haas S, Boschi V, Grannas A (2019) Metal sorption studies biased by filtration of insoluble metal oxides and hydroxides. Science of The Total Environment 646:1433–1439. https://doi.org/10.1016/j.scitotenv.2018.07.419

Hajiagha MN, Kafil HS (2023) Efflux pumps and microbial biofilm formation. Infection, Genetics and Evolution 112:105459. https://doi.org/10.1016/j.meegid.2023.105459

Halliwell B (2006) Reactive Species and Antioxidants. Redox Biology Is a Fundamental Theme of Aerobic Life. Plant Physiology 141:312–322. https://doi.org/10.1104/pp.106.077073

Halliwell B, Gutteridge JMC (1984) Oxygen toxicity, oxygen radicals, transition metals and disease. Biochemical Journal 219:1–14. https://doi.org/10.1042/bj2190001

Hamidi M, Okoro OV, Ianiri G, et al (2023) Exopolysaccharide from the yeast Papiliotrema terrestris PT22AV for skin wound healing. Journal of Advanced Research 46:61–74. https://doi.org/10.1016/j.jare.2022.06.012

Harshavardhan VT, Wu T-M, Hong C-Y (2017) Glutathione Reductase and Abiotic Stress Tolerance in Plants. In: Hossain MA, Mostofa MG, Diaz-Vivancos P, et al. (eds) Glutathione in Plant Growth, Development, and Stress Tolerance. Springer International Publishing, Cham, pp 265–286

Hasani A, Madhi M, Gholizadeh P, et al (2019) Metal nanoparticles and consequences on multi-drug resistant bacteria: reviving their role. SN Appl Sci 1:360. https://doi.org/10.1007/s42452-019-0344-4

Hasanuzzaman M, Bhuyan MHMB, Anee TI, et al (2019) Regulation of Ascorbate-Glutathione Pathway in Mitigating Oxidative Damage in Plants under Abiotic Stress. Antioxidants 8:384. https://doi.org/10.3390/antiox8090384

Hasyimah NAR, Furusawa G, Amirul AA (2021) Biosorption of a dye and heavy metals using dead cells of filamentous bacterium, Aureispira sp. CCB-QB1. Int J Environ Sci Technol 18:1627–1636. https://doi.org/10.1007/s13762-020-02918-3

He F, Shi Y-J, Li J-L, et al (2022) Genome-wide analysis and expression profiling of Cation/H+ exchanger (CAX) family genes reveal likely functions in cadmium stress responses in poplar. International Journal of Biological Macromolecules 204:76–88. https://doi.org/10.1016/j.ijbiomac.2022.01.202

He G, Qin L, Tian W, et al (2020) Heavy Metal Transporters-Associated Proteins in Solanum tuberosum: Genome-Wide Identification, Comprehensive Gene Feature, Evolution and Expression Analysis. Genes 11:1269. https://doi.org/10.3390/genes11111269

He L, Wang S, Liu M, et al (2023) Transport and transformation of atmospheric metals in ecosystems: A review. Journal of Hazardous Materials Advances 9:100218. https://doi.org/10.1016/j.hazadv.2022.100218

Heck DE, Shakarjian M, Kim HD, et al (2010) Mechanisms of oxidant generation by catalase. Annals of the New York Academy of Sciences 1203:120–125. https://doi.org/10.1111/j.1749-6632.2010.05603.x

Hegazy GE, Soliman NA, Ossman ME, et al (2023) Isotherm and kinetic studies of cadmium biosorption and its adsorption behaviour in multi-metals solution using dead and immobilized archaeal cells. Sci Rep 13:2550. https://doi.org/10.1038/s41598-023-29456-5

Ho Y (2000) The kinetics of sorption of divalent metal ions onto sphagnum moss peat. Water Research 34:735–742. https://doi.org/10.1016/S0043-1354(99)00232-8

Hoiczyk E, Hansel A (2000) Cyanobacterial Cell Walls: News from an Unusual Prokaryotic Envelope. J Bacteriol 182:1191–1199. https://doi.org/10.1128/JB.182.5.1191-1199.2000

Hong Y, Boiti A, Vallone D, Foulkes NS (2024) Reactive Oxygen Species Signaling and Oxidative Stress: Transcriptional Regulation and Evolution. Antioxidants 13:312. https://doi.org/10.3390/antiox13030312

Hou D, Yang T, Tang J, Li S (2018) Reactive force-field molecular dynamics study on graphene oxide reinforced cement composite: functional group de-protonation, interfacial bonding and strengthening mechanism. Phys Chem Chem Phys 20:8773–8789. https://doi.org/10.1039/C8CP00006A

Hu Q, Zhang Z (2019) Application of Dubinin–Radushkevich isotherm model at the solid/solution interface: A theoretical analysis. Journal of Molecular Liquids 277:646–648. https://doi.org/10.1016/j.molliq.2019.01.005

Huang F, Dang Z, Guo C-L, et al (2013) Biosorption of Cd(II) by live and dead cells of Bacillus cereus RC-1 isolated from cadmium-contaminated soil. Colloids and Surfaces B: Biointerfaces 107:11–18. https://doi.org/10.1016/j.colsurfb.2013.01.062

Huang L, Jin Y, Zhou D, et al (2022) A Review of the Role of Extracellular Polymeric Substances (EPS) in Wastewater Treatment Systems. IJERPH 19:12191. https://doi.org/10.3390/ijerph191912191

Huertas M, López-Maury L, Giner-Lamia J, et al (2014) Metals in Cyanobacteria: Analysis of the Copper, Nickel, Cobalt and Arsenic Homeostasis Mechanisms. Life 4:865–886. https://doi.org/10.3390/life4040865

Ibrahim WM, Hassan AF, Azab YA (2016) Biosorption of toxic heavy metals from aqueous solution by *Ulva lactuca* activated carbon. Egyptian Journal of Basic and Applied Sciences 3:241–249. https://doi.org/10.1016/j.ejbas.2016.07.005

Ighalo JO, Adeniyi AG (2020) Adsorption of pollutants by plant bark derived adsorbents: An empirical review. Journal of Water Process Engineering 35:101228. https://doi.org/10.1016/j.jwpe.2020.101228

Ilyas N, Mumtaz K, Akhtar N, et al (2020) Exopolysaccharides Producing Bacteria for the Amelioration of Drought Stress in Wheat. Sustainability 12:8876. https://doi.org/10.3390/su12218876

Isarankura-Na-Ayudhya P, Thippakorn C, Pannengpetch S, et al (2018) Metal complexation by histidine-rich peptides confers protective roles against cadmium stress in *Escherichia coli* as revealed by proteomics analysis. PeerJ 6:e5245. https://doi.org/10.7717/peerj.5245

Jacques A, Chaaya N, Beecher K, et al (2019) The impact of sugar consumption on stress driven, emotional and addictive behaviors. Neuroscience and

Biobehavioral Reviews 103:178–199. https://doi.org/10.1016/j.neubiorev.2019.05.021

Jain R, Raghukumar S, Tharanathan R, Bhosle NB (2005) Extracellular Polysaccharide Production by Thraustochytrid Protists. Mar Biotechnol 7:184–192. https://doi.org/10.1007/s10126-004-4025-x

Jain S, Muneer S, Guerriero G, et al (2018) Tracing the role of plant proteins in the response to metal toxicity: a comprehensive review. Plant Signaling and Behavior 13:e1507401. https://doi.org/10.1080/15592324.2018.1507401

Jalali M, Bahramian Ragheb S, Moharami S (2023) Mono and Competitive Adsorption-Desorption of Cd, Co, Cu, and Zn in Ten Agricultural and Greenhouse Soils. Soil and Sediment Contamination: An International Journal 1–24. https://doi.org/10.1080/15320383.2023.2283121

Javanbakht V, Alavi SA, Zilouei H (2014) Mechanisms of heavy metal removal using microorganisms as biosorbent. Water Science and Technology 69:1775–1787. https://doi.org/10.2166/wst.2013.718

Javed M, Usmani N (2015) Stress response of biomolecules (carbohydrate, protein and lipid profiles) in fish Channa punctatus inhabiting river polluted by Thermal Power Plant effluent. Saudi Journal of Biological Sciences 22:237–242. https://doi.org/10.1016/j.sjbs.2014.09.021

Jeng S-S, Chen Y-H (2022) Association of Zinc with Anemia. Nutrients 14:4918. https://doi.org/10.3390/nu14224918

Jerroumi S, Amarine M, Nour H, et al (2020) Removal of nickel through sulfide precipitation and characterization of electroplating wastewater sludge. Water Quality Research Journal 55:345–357. https://doi.org/10.2166/wqrj.2020.116

Jiang M, Zhang J (2001) Effect of Abscisic Acid on Active Oxygen Species, Antioxidative Defence System and Oxidative Damage in Leaves of Maize Seedlings. Plant and Cell Physiology 42:1265–1273. https://doi.org/10.1093/pcp/pce162

Jiao Y, Cody GD, Harding AK, et al (2010) Characterization of Extracellular Polymeric Substances from Acidophilic Microbial Biofilms. Appl Environ Microbiol 76:2916–2922. https://doi.org/10.1128/AEM.02289-09

John R, Ahmad P, Gadgil K, Sharma S (2008) Effect of cadmium and lead on growth, biochemical parameters and uptake in Lemna polyrrhizaL. Plant Soil Environ 54:262–270. https://doi.org/10.17221/2787-PSE

Jomova K, Makova M, Alomar SY, et al (2022) Essential metals in health and disease. Chemico-Biological Interactions 367:110173. https://doi.org/10.1016/j.cbi.2022.110173

Juan CA, Pérez De La Lastra JM, Plou FJ, Pérez-Lebeña E (2021) The Chemistry of Reactive Oxygen Species (ROS) Revisited: Outlining Their Role in Biological Macromolecules (DNA, Lipids and Proteins) and Induced Pathologies. IJMS 22:4642. https://doi.org/10.3390/ijms22094642

Kaewsarn P, Yu Q, Ma W (2001) Interference of Co-ions in Biosorption of Cu^{2+} by Biosorbent from Marine Alga *Durvillaea potatorum*. Environmental Engineering Science 18:99–104. https://doi.org/10.1089/10928750151132294

Kakaei S, Sattarzadeh Khameneh E, Monji Boveiri A (2021) Effect of ionic radius on Ti IV), Zr IV), and Hf IV) adsorption by RB biomass. RPE. https://doi.org/10.22034/rpe.2021.297939.1035

Kalam S, Abu-Khamsin SA, Kamal MS, Patil S (2021) Surfactant Adsorption Isotherms: A Review. ACS Omega 6:32342–32348. https://doi.org/10.1021/acsomega.1c04661

Kamath Miyar H, Pai A, Goveas LC (2021) Adsorption of Malachite Green by extracellular polymeric substance of Lysinibacillus sp. SS1: kinetics and isotherms. Heliyon 7:e07169. https://doi.org/10.1016/j.heliyon.2021.e07169

Kanamarlapudi SLRK, Chintalpudi VK, Muddada S (2018) Application of Biosorption for Removal of Heavy Metals from Wastewater. In: Derco J, Vrana B (eds) Biosorption. InTech

Kanamarlapudi SLRK, Muddada S (2017) Characterization of Exopolysaccharide Produced by *Streptococcus thermophilus* CC30. BioMed Research International 2017:1–11. https://doi.org/10.1155/2017/4201809

Karnib M, Kabbani A, Holail H, Olama Z (2014) Heavy Metals Removal Using Activated Carbon, Silica and Silica Activated Carbon Composite. Energy Procedia 50:113–120. https://doi.org/10.1016/j.egypro.2014.06.014

Karyotou K, Donaldson RP (2005) Ascorbate peroxidase, a scavenger of hydrogen peroxide in glyoxysomal membranes. Archives of Biochemistry and Biophysics 434:248–257. https://doi.org/10.1016/j.abb.2004.11.003

Kato A, Takatani N, Use K, et al (2015) Identification of a Cyanobacterial RND-Type Efflux System Involved in Export of Free Fatty Acids. Plant Cell Physiol 56:2467–2477. https://doi.org/10.1093/pcp/pcv150

Kawaguchi T, Decho AW (2000) Biochemical Characterization of Cyanobacterial Extracellular Polymers (EPS) from Modern Marine Stromatolites (Bahamas). Preparative Biochemistry and Biotechnology 30:321–330. https://doi.org/10.1080/10826060008544971

Kerkhove E, Pennemans V, Swennen Q (2013) Cadmium, Effect on Transport Across Cell Membranes. In: Kretsinger RH, Uversky VN, Permyakov EA (eds)

Encyclopedia of Metalloproteins. Springer New York, New York, NY, pp 378–382

Kermanshahi RK, Ahed Khaniki GJ, Goudarzi L (2023) Biosorption of Cd+2 and Pb+2 by Exopolysaccharide Extracted from Lactobacillus fermentum 6b; Adsorption Isotherm and Kinetic Studies. ijph. https://doi.org/10.18502/ijph.v52i3.12145

Khalil MMH, Shahat A, Radwan A, El-Shahat MF (2016) Colorimetric determination of Cu(II) ions in biological samples using metal-organic framework as scaffold. Sensors and Actuators B: Chemical 233:272–280. https://doi.org/10.1016/j.snb.2016.04.079

Khan Z, Elahi A, Bukhari DA, Rehman A (2022) Cadmium sources, toxicity, resistance and removal by microorganisms-A potential strategy for cadmium eradication. Journal of Saudi Chemical Society 26:101569. https://doi.org/10.1016/j.jscs.2022.101569

Kiefer R, Höll WH (2001) Sorption of Heavy Metals onto Selective Ion-Exchange Resins with Aminophosphonate Functional Groups. Ind Eng Chem Res 40:4570–4576. https://doi.org/10.1021/ie0101821

Kim J-J, Kim Y-S, Kumar V (2019) Heavy metal toxicity: An update of chelating therapeutic strategies. Journal of Trace Elements in Medicine and Biology 54:226–231. https://doi.org/10.1016/j.jtemb.2019.05.003

Kim SU, Cheong YH, Seo DC, et al (2007) Characterisation of heavy metal tolerance and biosorption capacity of bacterium strain CPB4 (Bacillus spp.). Water Science and Technology 55:105–111. https://doi.org/10.2166/wst.2007.007

Kirkman HN, Rolfo M, Ferraris AM, Gaetani GF (1999) Mechanisms of Protection of Catalase by NADPH. Journal of Biological Chemistry 274:13908–13914. https://doi.org/10.1074/jbc.274.20.13908

Koller M, Saleh HM (2018) Introductory Chapter: Introducing Heavy Metals. In: Saleh HE-DM, Aglan RF (eds) Heavy Metals. InTech

Kozuleva MA, Ivanov BN, Vetoshkina DV, Borisova-Mubarakshina MM (2020) Minimizing an Electron Flow to Molecular Oxygen in Photosynthetic Electron Transfer Chain: An Evolutionary View. Front Plant Sci 11:211. https://doi.org/10.3389/fpls.2020.00211

Kröger N, Poulsen N (2008) Diatoms—From Cell Wall Biogenesis to Nanotechnology. Annu Rev Genet 42:83–107. https://doi.org/10.1146/annurev.genet.41.110306.130109

Kumar M, Kumar M, Pandey A, Thakur IS (2019) Genomic analysis of carbon dioxide sequestering bacterium for exopolysaccharides production. Sci Rep 9:4270. https://doi.org/10.1038/s41598-019-41052-0

Langmuir I (1918) THE ADSORPTION OF GASES ON PLANE SURFACES OF GLASS, MICA AND PLATINUM. J Am Chem Soc 40:1361–1403. https://doi.org/10.1021/ja02242a004

Lata S, Singh PK, Samadder SR (2015) Regeneration of adsorbents and recovery of heavy metals: a review. Int J Environ Sci Technol 12:1461–1478. https://doi.org/10.1007/s13762-014-0714-9

Latifi A, Ruiz M, Zhang C-C (2009) Oxidative stress in cyanobacteria. FEMS Microbiol Rev 33:258–278. https://doi.org/10.1111/j.1574-6976.2008.00134.x

Lawson PS, Sterritt RM, Lester JN (1984) Adsorption and complexation mechanisms of heavy metal uptake in activated sludge. J Chem Technol Biotechnol 34:253–262. https://doi.org/10.1002/jctb.280340405

Lee Chang KJ, Nichols CM, Blackburn SI, et al (2014) Comparison of Thraustochytrids Aurantiochytrium sp., Schizochytrium sp., Thraustochytrium sp., and Ulkenia sp. for Production of Biodiesel, Long-Chain Omega-3 Oils, and Exopolysaccharide. Mar Biotechnol 16:396–411. https://doi.org/10.1007/s10126-014-9560-5

Leong YK, Chang J-S (2020) Bioremediation of heavy metals using microalgae: Recent advances and mechanisms. Bioresource Technology 303:122886. https://doi.org/10.1016/j.biortech.2020.122886

Li H, Wei M, Min W, et al (2016) Removal of heavy metal Ions in aqueous solution by Exopolysaccharides from Athelia rolfsii. Biocatalysis and Agricultural Biotechnology 6:28–32. https://doi.org/10.1016/j.bcab.2016.01.013

Li J, Huang X, Hou Z, Ding T (2022) Sorption of diclofenac by polystyrene microplastics: Kinetics, isotherms and particle size effects. Chemosphere 290:133311. https://doi.org/10.1016/j.chemosphere.2021.133311

Li L, Yang ZW, Qiu Y, Wang Y (2024) Phosphorus Adsorbed by Hydrochloric Acid Desorption–Activated Red Mud Adsorbents: A Molecular Dynamics Study

Li W, Zhou P, Zhang J, et al (2018a) Generation of reactive oxygen species by promoting the Cu(II)/Cu(I) redox cycle with reducing agents in aerobic aqueous solution. Water Science and Technology 78:1390–1399. https://doi.org/10.2166/wst.2018.416

Li X, Xiao Q, Shao Q, et al (2023) Adsorption of Cd (II) by a novel living and non-living Cupriavidus necator GX_5: optimization, equilibrium and kinetic studies. BMC Chemistry 17:54. https://doi.org/10.1186/s13065-023-00977-4

Li X, Zhang D, Sheng F, Qing H (2018b) Adsorption characteristics of Copper (II), Zinc (II) and Mercury (II) by four kinds of immobilized fungi residues. Ecotoxicology and Environmental Safety 147:357–366. https://doi.org/10.1016/j.ecoenv.2017.08.058

Li Y, Xin M, Xie D, et al (2021) Variation in Extracellular Polymeric Substances from *Enterobacter* sp. and Their Pb $^{2+}$ Adsorption Behaviors. ACS Omega 6:9617–9628. https://doi.org/10.1021/acsomega.1c00185

Lismont, Revenco, Fransen (2019) Peroxisomal Hydrogen Peroxide Metabolism and Signaling in Health and Disease. IJMS 20:3673. https://doi.org/10.3390/ijms20153673

Litz C, Helfmann S, Gerhardt S, Andrade SLA (2011) Structure of GlnK1, a signalling protein from *Archaeoglobus fulgidus*. Acta Crystallogr F Struct Biol Cryst Commun 67:178–181. https://doi.org/10.1107/S1744309110047482

Liu D, Zhu Y, Li Z, et al (2013) Chitin nanofibrils for rapid and efficient removal of metal ions from water system. Carbohydrate Polymers 98:483–489. https://doi.org/10.1016/j.carbpol.2013.06.015

Lowry OliverH, Rosebrough NiraJ, Farr AL, Randall RoseJ (1951) PROTEIN MEASUREMENT WITH THE FOLIN PHENOL REAGENT. Journal of Biological Chemistry 193:265–275. https://doi.org/10.1016/S0021-9258(19)52451-6

Ma W, Tobin JM (2003) Development of multimetal binding model and application to binary metal biosorption onto peat biomass. Water Research 37:3967–3977. https://doi.org/10.1016/S0043-1354(03)00290-2

Ma Z, Jacobsen FE, Giedroc DP (2009) Coordination Chemistry of Bacterial Metal Transport and Sensing. Chem Rev 109:4644–4681. https://doi.org/10.1021/cr900077w

Mahamadi C (2019) On the dominance of Pb during competitive biosorption from multi-metal systems: A review. Cogent Environmental Science 5:1635335. https://doi.org/10.1080/23311843.2019.1635335

Malik B, Kaur Sandhu K (2023) Occurrence and impact of heavy metals on environment. Materials Today: Proceedings S2214785323004078. https://doi.org/10.1016/j.matpr.2023.01.317

Malik R, Dahiya S, Lata S (2017) An experimental and quantum chemical study of removal of utmostly quantified heavy metals in wastewater using coconut husk: A novel approach to mechanism. International Journal of Biological Macromolecules 98:139–149. https://doi.org/10.1016/j.ijbiomac.2017.01.100

Mallampati SR, Mitoma Y, Okuda T, et al (2013) Total immobilization of soil heavy metals with nano-Fe/Ca/CaO dispersion mixtures. Environ Chem Lett 11:119–125. https://doi.org/10.1007/s10311-012-0384-0

Mandal SK, Singh RP, Patel V (2011) Isolation and Characterization of Exopolysaccharide Secreted by a Toxic Dinoflagellate, Amphidinium carterae

Hulburt 1957 and Its Probable Role in Harmful Algal Blooms (HABs). Microb Ecol 62:518–527. https://doi.org/10.1007/s00248-011-9852-5

Maret W (2016) The Metals in the Biological Periodic System of the Elements: Concepts and Conjectures. IJMS 17:66. https://doi.org/10.3390/ijms17010066

Martinoia E, Massonneau A, Frangne N (2000) Transport Processes of Solutes across the Vacuolar Membrane of Higher Plants. Plant and Cell Physiology 41:1175–1186. https://doi.org/10.1093/pcp/pcd059

Marvasi M, Visscher PT, Casillas Martinez L (2010) Exopolymeric substances (EPS) from Bacillus subtilis : polymers and genes encoding their synthesis: EPS from Bacillus subtilis. FEMS Microbiology Letters 313:1–9. https://doi.org/10.1111/j.1574-6968.2010.02085.x

Masindi V, Mkhonza P, Tekere M (2021) Sources of Heavy Metals Pollution. In: Inamuddin, Ahamed MI, Lichtfouse E, Altalhi T (eds) Remediation of Heavy Metals. Springer International Publishing, Cham, pp 419–454

Masood F, Malik A (2015) Single and Multi-Component Adsorption of Metal Ions by *Acinetobacter* sp. FM4. Separation Science and Technology 50:892–900. https://doi.org/10.1080/01496395.2014.969378

Mathivanan K, Uthaya Chandirika J, Srinivasan R, et al (2023) Exopolymeric substances production by Bacillus cereus KMS3-1 enhanced its biosorption efficiency in removing Cd2+ and Pb2+ in single and binary metal mixtures. Environmental Research 228:115917. https://doi.org/10.1016/j.envres.2023.115917

Meez E, Rahdar A, Kyzas GZ (2021) Sawdust for the Removal of Heavy Metals from Water: A Review. Molecules 26:4318. https://doi.org/10.3390/molecules26144318

Mehta SK, Gaur JP (2005) Use of Algae for Removing Heavy Metal Ions From Wastewater: Progress and Prospects. Critical Reviews in Biotechnology 25:113–152. https://doi.org/10.1080/07388550500248571

Mellis EV, Casagrande JC, Soares MR (2017) Nickel adsorption and desorption in an acric oxisol as a function of pH, ionic strength and incubation time. Ciênc agrotec 41:32–41. https://doi.org/10.1590/1413-70542017411020116

Melnikov F, Geohagen BC, Gavin T, et al (2020) Application of the hard and soft, acids and bases (HSAB) theory as a method to predict cumulative neurotoxicity. NeuroToxicology 79:95–103. https://doi.org/10.1016/j.neuro.2020.04.009

Mirghaffari N, Moeini E, Farhadian O (2015) Biosorption of Cd and Pb ions from aqueous solutions by biomass of the green microalga, Scenedesmus

quadricauda. J Appl Phycol 27:311–320. https://doi.org/10.1007/s10811-014-0345-z

Mitra GN (2015) Definitions of Heavy Metals, Essential and Beneficial Plant Nutrients. In: Regulation of Nutrient Uptake by Plants. Springer India, New Delhi, pp 87–89

Mohammed AS, Kapri A, Goel R (2011) Heavy Metal Pollution: Source, Impact, and Remedies. In: Khan MS, Zaidi A, Goel R, Musarrat J (eds) Biomanagement of Metal-Contaminated Soils. Springer Netherlands, Dordrecht, pp 1–28

Mohammed RR (2012) Removal of Heavy Metals from Waste Water Using Black Teawaste. Arab J Sci Eng 37:1505–1520. https://doi.org/10.1007/s13369-012-0264-8

Mohan Murali Achary V, Jena S, Panda KK, Panda BB (2008) Aluminium induced oxidative stress and DNA damage in root cells of Allium cepa L. Ecotoxicology and Environmental Safety 70:300–310. https://doi.org/10.1016/j.ecoenv.2007.10.022

Mohite BV, Koli SH, Patil SV (2018) Heavy Metal Stress and Its Consequences on Exopolysaccharide (EPS)-Producing Pantoea agglomerans. Appl Biochem Biotechnol 186:199–216. https://doi.org/10.1007/s12010-018-2727-1

Morales-Barrera L, Flores-Ortiz CM, Cristiani-Urbina E (2020) Single and Binary Equilibrium Studies for Ni2+ and Zn2+ Biosorption onto Lemna gibba from Aqueous Solutions. Processes 8:1089. https://doi.org/10.3390/pr8091089

Mota R, Pereira SB, Meazzini M, et al (2015) Differential proteomes of the cyanobacterium Cyanothece sp. CCY 0110 upon exposure to heavy metals. Data in Brief 4:152–158. https://doi.org/10.1016/j.dib.2015.04.015

Moussout H, Ahlafi H, Aazza M, Maghat H (2018) Critical of linear and nonlinear equations of pseudo-first order and pseudo-second order kinetic models. Karbala International Journal of Modern Science 4:244–254. https://doi.org/10.1016/j.kijoms.2018.04.001

Mushtaq S, Bareen FE, Tayyeb A (2022) Equilibrium kinetics and thermodynamic studies on biosorption of heavy metals by metal-resistant strains of Trichoderma isolated from tannery solid waste. Environ Sci Pollut Res 30:10925–10954. https://doi.org/10.1007/s11356-022-22860-w

Nakata H (1992) Protonation susceptibility of functional groups: A new parameter for interpreting chemical ionization mass spectra of bifunctional organic compounds. Org Mass Spectrom 27:686–688. https://doi.org/10.1002/oms.1210270607

Napolitano G, Fasciolo G, Venditti P (2021) Mitochondrial Management of Reactive Oxygen Species. Antioxidants 10:1824. https://doi.org/10.3390/antiox10111824

Nickisch R, De Vos WM, Meier MAR, Baig MI (2023) Removal of Transition-Metal Ions by Metal-Complexing Polythiosemicarbazone Membranes. ACS Appl Polym Mater 5:7240–7251. https://doi.org/10.1021/acsapm.3c01192

Nimbalkar PR, Khedkar MA, Parulekar RS, et al (2018) Role of Trace Elements as Cofactor: An Efficient Strategy toward Enhanced Biobutanol Production. ACS Sustainable Chem Eng 6:9304–9313. https://doi.org/10.1021/acssuschemeng.8b01611

Nnaji ND, Onyeaka H, Miri T, Ugwa C (2023) Bioaccumulation for heavy metal removal: a review. SN Appl Sci 5:125. https://doi.org/10.1007/s42452-023-05351-6

Nouha K, Kumar RS, Tyagi RD (2016) Heavy metals removal from wastewater using extracellular polymeric substances produced by Cloacibacterium normanense in wastewater sludge supplemented with crude glycerol and study of extracellular polymeric substances extraction by different methods. Bioresource Technology 212:120–129. https://doi.org/10.1016/j.biortech.2016.04.021

Nové M, Kincses A, Molnár J, et al (2020) The Role of Efflux Pumps and Environmental pH in Bacterial Multidrug Resistance. In Vivo 34:65–71. https://doi.org/10.21873/invivo.11746

Nowicka B (2022) Heavy metal–induced stress in eukaryotic algae—mechanisms of heavy metal toxicity and tolerance with particular emphasis on oxidative stress in exposed cells and the role of antioxidant response. Environ Sci Pollut Res 29:16860–16911. https://doi.org/10.1007/s11356-021-18419-w

Nussinovitch A, Dagan O (2015) Hydrocolloid liquid-core capsules for the removal of heavy-metal cations from water. Journal of Hazardous Materials 299:122–131. https://doi.org/10.1016/j.jhazmat.2015.06.013

Nyiramigisha P, Komariah, Sajidan (2021) Harmful Impacts of Heavy Metal Contamination in the Soil and Crops Grown Around Dumpsites. RAS 9:271–282. https://doi.org/10.7831/ras.9.0_271

Okajima MK, Bamba T, Kaneso Y, et al (2008) Supergiant Ampholytic Sugar Chains with Imbalanced Charge Ratio Form Saline Ultra-absorbent Hydrogels. Macromolecules 41:4061–4064. https://doi.org/10.1021/ma800307w

Okuda T, Matsuda Y, Yamanaka A, Sagisaka S (1991) Abrupt Increase in the Level of Hydrogen Peroxide in Leaves of Winter Wheat Is Caused by Cold Treatment. Plant Physiol 97:1265–1267. https://doi.org/10.1104/pp.97.3.1265

Oleńska E, Małek W, Kotowska U, et al (2021) Exopolysaccharide Carbohydrate Structure and Biofilm Formation by Rhizobium leguminosarum bv. trifolii Strains Inhabiting Nodules of Trifoliumrepens Growing on an Old Zn–Pb–Cd-Polluted Waste Heap Area. IJMS 22:2808. https://doi.org/10.3390/ijms22062808

Onufriev AV, Alexov E (2013) Protonation and pK changes in protein–ligand binding. Quart Rev Biophys 46:181–209. https://doi.org/10.1017/S0033583513000024

Op De Beeck M, Persson P, Tunlid A (2021) Fungal extracellular polymeric substance matrices – Highly specialized microenvironments that allow fungi to control soil organic matter decomposition reactions. Soil Biology and Biochemistry 159:108304. https://doi.org/10.1016/j.soilbio.2021.108304

Oshita H, Shimazaki Y (2022) π–π Stacking Interaction of Metal Phenoxyl Radical Complexes. Molecules 27:1135. https://doi.org/10.3390/molecules27031135

Osińska-Jaroszuk M, Jarosz-Wilkołazka A, Jaroszuk-Ściseł J, et al (2015) Extracellular polysaccharides from Ascomycota and Basidiomycota: production conditions, biochemical characteristics, and biological properties. World J Microbiol Biotechnol 31:1823–1844. https://doi.org/10.1007/s11274-015-1937-8

Oves M, Khan MS, Zaidi A (2013) Biosorption of heavy metals by Bacillus thuringiensis strain OSM29 originating from industrial effluent contaminated north Indian soil. Saudi Journal of Biological Sciences 20:121–129. https://doi.org/10.1016/j.sjbs.2012.11.006

Pagliaccia B, Carretti E, Severi M, et al (2022) Heavy metal biosorption by Extracellular Polymeric Substances (EPS) recovered from anammox granular sludge. Journal of Hazardous Materials 424:126661. https://doi.org/10.1016/j.jhazmat.2021.126661

Pagnanelli F, Toro L, Vegliò F (2002) Olive mill solid residues as heavy metal sorbent material: a preliminary study. Waste Management 22:901–907. https://doi.org/10.1016/S0956-053X(02)00086-7

Pal A, Paul AK (2008) Microbial extracellular polymeric substances: central elements in heavy metal bioremediation. Indian J Microbiol 48:49–64. https://doi.org/10.1007/s12088-008-0006-5

Palmer AE, Franz KJ (2009) Introduction to "Cellular Metal Homeostasis and Trafficking." Chem Rev 109:4533–4535. https://doi.org/10.1021/cr900293t

Pandey S, Dubey SK, Kashyap AK, Jain BP (2022) Cyanobacteria-mediated heavy metal and xenobiotics bioremediation. In: Cyanobacterial Lifestyle and its Applications in Biotechnology. Elsevier, pp 335–350

Panwichian S, Kantachote D, Wittayaweerasak B, Mallavarapu M (2011) Removal of heavy metals by exopolymeric substances produced by resistant purple nonsulfur bacteria isolated from contaminated shrimp ponds. Electro Journal of Biotech 14:. https://doi.org/10.2225/vol14-issue4-fulltext-2

Pardo R, Herguedas M, Barrado E, Vega M (2003) Biosorption of cadmium, copper, lead and zinc by inactive biomass of Pseudomonas Putida. Anal Bioanal Chem 376:26–32. https://doi.org/10.1007/s00216-003-1843-z

Parikh A, Madamwar D (2006) Partial characterization of extracellular polysaccharides from cyanobacteria. Bioresource Technology 97:1822–1827. https://doi.org/10.1016/j.biortech.2005.09.008

Park D, Yun Y-S, Park JM (2010) The past, present, and future trends of biosorption. Biotechnol Bioproc E 15:86–102. https://doi.org/10.1007/s12257-009-0199-4

Pasricha S, Mathur V, Garg A, et al (2021) Molecular mechanisms underlying heavy metal uptake, translocation and tolerance in hyperaccumulators-an analysis. Environmental Challenges 4:100197. https://doi.org/10.1016/j.envc.2021.100197

Patel H (2021) Review on solvent desorption study from exhausted adsorbent. Journal of Saudi Chemical Society 25:101302. https://doi.org/10.1016/j.jscs.2021.101302

Paulsen IT, Jr. MHS (1997) A Novel Family of Ubiquitous Heavy Metal Ion Transport Proteins. Journal of Membrane Biology 156:99–103. https://doi.org/10.1007/s002329900192

Paunov M, Koleva L, Vassilev A, et al (2018) Effects of Different Metals on Photosynthesis: Cadmium and Zinc Affect Chlorophyll Fluorescence in Durum Wheat. IJMS 19:787. https://doi.org/10.3390/ijms19030787

Perez-Benito JF (2001) Copper(II)-Catalyzed Decomposition of Hydrogen Peroxide: Catalyst Activation by Halide Ions. Monatshefte für Chemie/Chemical Monthly 132:1477–1492. https://doi.org/10.1007/s007060170004

Petukh M, Stefl S, Alexov E (2013) The Role of Protonation States in Ligand-Receptor Recognition and Binding. CPD 19:4182–4190. https://doi.org/10.2174/1381612811319230004

Pilon M, Ravet K, Tapken W (2011) The biogenesis and physiological function of chloroplast superoxide dismutases. Biochimica et Biophysica Acta (BBA) - Bioenergetics 1807:989–998. https://doi.org/10.1016/j.bbabio.2010.11.002

Pino GH, Souza De Mesquita LM, Torem ML, Saavedra Pinto GA (2006) Biosorption of cadmium by green coconut shell powder. Minerals Engineering 19:380–387. https://doi.org/10.1016/j.mineng.2005.12.003

Pinto E, Sigaud-kutner TCS, Leitão MAS, et al (2003) HEAVY METAL–INDUCED OXIDATIVE STRESS IN ALGAE [1]. Journal of Phycology 39:1008–1018. https://doi.org/10.1111/j.0022-3646.2003.02-193.x

Pizzagalli MD, Bensimon A, Superti-Furga G (2021) A guide to plasma membrane solute carrier proteins. The FEBS Journal 288:2784–2835. https://doi.org/10.1111/febs.15531

Plazinski W, Dziuba J, Rudzinski W (2013) Modeling of sorption kinetics: the pseudo-second order equation and the sorbate intraparticle diffusivity. Adsorption 19:1055–1064. https://doi.org/10.1007/s10450-013-9529-0

Pokrovsky OS, Martinez RE, Golubev SV, et al (2008) Adsorption of metals and protons on Gloeocapsa sp. cyanobacteria: A surface speciation approach. Applied Geochemistry 23:2574–2588. https://doi.org/10.1016/j.apgeochem.2008.05.007

Polívka T, Frank HA (2010) Molecular Factors Controlling Photosynthetic Light Harvesting by Carotenoids. Acc Chem Res 43:1125–1134. https://doi.org/10.1021/ar100030m

Popper ZA, Ralet M-C, Domozych DS (2014) Plant and algal cell walls: diversity and functionality. Annals of Botany 114:1043–1048. https://doi.org/10.1093/aob/mcu214

Pradhan B, Bhuyan PP, Nayak R, et al (2022) Microalgal Phycoremediation: A Glimpse into a Sustainable Environment. Toxics 10:525. https://doi.org/10.3390/toxics10090525

Pradhan S, Singh S, Rai LC (2007) Characterization of various functional groups present in the capsule of *Microcystis* and study of their role in biosorption of Fe, Ni and Cr. Bioresource Technology 98:595–601. https://doi.org/10.1016/j.biortech.2006.02.041

Priya AK, Gnanasekaran L, Dutta K, et al (2022) Biosorption of heavy metals by microorganisms: Evaluation of different underlying mechanisms. Chemosphere 307:135957. https://doi.org/10.1016/j.chemosphere.2022.135957

Priya M, Balakrishnan V, Lakshmi AK, et al (2014) Mercury Induced Oxidative Stress of Antioxidants in *Clitoria ternatea* L. ILNS 23:1–8. https://doi.org/10.56431/p-5331fs

Puckett CA, Ernst RJ, Barton JK (2010) Exploring the cellular accumulation of metal complexes. Dalton Trans 39:1159–1170. https://doi.org/10.1039/B922209J

Qasem NAA, Mohammed RH, Lawal DU (2021) Removal of heavy metal ions from wastewater: a comprehensive and critical review. npj Clean Water 4:36. https://doi.org/10.1038/s41545-021-00127-0

Radzymińska-Lenarcik E, Kwiatkowska-Marks S, Kościuszko A (2022) Transport of Heavy Metals Pb(II), Zn(II), and Cd(II) Ions across CTA Polymer Membranes Containing Alkyl-Triazole as Ions Carrier. Membranes 12:1068. https://doi.org/10.3390/membranes12111068

Rahbar Saadat Y, Yari Khosroushahi A, Pourghassem Gargari B (2021) Yeast exopolysaccharides and their physiological functions. Folia Microbiol 66:171–182. https://doi.org/10.1007/s12223-021-00856-2

Rahman MdS, Sathasivam KV (2016) Heavy metal biosorption potential of a Malaysian Rhodophyte (Eucheuma denticulatum) from aqueous solutions. Int J Environ Sci Technol 13:1973–1988. https://doi.org/10.1007/s13762-016-1022-3

Raj V, Chauhan MS, Pal SL (2022) Potential of sugarcane bagasse in remediation of heavy metals: A review. Chemosphere 307:135825. https://doi.org/10.1016/j.chemosphere.2022.135825

Raji Z, Karim A, Karam A, Khalloufi S (2023) Adsorption of Heavy Metals: Mechanisms, Kinetics, and Applications of Various Adsorbents in Wastewater Remediation—A Review. Waste 1:775–805. https://doi.org/10.3390/waste1030046

Rama Jyothi N (2021) Heavy Metal Sources and Their Effects on Human Health. In: Khaled Nazal M, Zhao H (eds) Heavy Metals - Their Environmental Impacts and Mitigation. IntechOpen

Ramirez-Mora T, Retana-Lobo C, Valle-Bourrouet G (2018) Biochemical characterization of extracellular polymeric substances from endodontic biofilms. PLoS ONE 13:e0204081. https://doi.org/10.1371/journal.pone.0204081

Rani RP, Anandharaj M, Sabhapathy P, Ravindran AD (2017) Physiochemical and biological characterization of novel exopolysaccharide produced by Bacillus tequilensis FR9 isolated from chicken. International Journal of Biological Macromolecules 96:1–10. https://doi.org/10.1016/j.ijbiomac.2016.11.122

Razzak SA, Faruque MO, Alsheikh Z, et al (2022) A comprehensive review on conventional and biological-driven heavy metals removal from industrial wastewater. Environmental Advances 7:100168. https://doi.org/10.1016/j.envadv.2022.100168

Reddy KV, Ranjit P, Priyanka E, et al (2024) Bioremediation of heavy metals-contaminated sites by microbial extracellular polymeric substances – A critical view. Environmental Chemistry and Ecotoxicology S2590182624000109. https://doi.org/10.1016/j.enceco.2024.05.002

Reek JNH, De Bruin B, Pullen S, et al (2022) Transition Metal Catalysis Controlled by Hydrogen Bonding in the Second Coordination Sphere. Chem Rev 122:12308–12369. https://doi.org/10.1021/acs.chemrev.1c00862

Reglero MM, Taggart MA, Monsalve-González L, Mateo R (2009) Heavy metal exposure in large game from a lead mining area: Effects on oxidative stress and fatty acid composition in liver. Environmental Pollution 157:1388–1395. https://doi.org/10.1016/j.envpol.2008.11.036

Rekha K, Usha B, Keeran NS (2021) Role of ABC transporters and other vacuolar transporters during heavy metal stress in plants. In: Metal and Nutrient Transporters in Abiotic Stress. Elsevier, pp 55–76

Rezayian M, Niknam V, Ebrahimzadeh H (2019) Oxidative damage and antioxidative system in algae. Toxicology Reports 6:1309–1313. https://doi.org/10.1016/j.toxrep.2019.10.001

Rizvi A, Saghir Khan Mohd (2019) Putative Role of Bacterial Biosorbent in Metal Sequestration Revealed by SEM–EDX and FTIR. Indian J Microbiol 59:246–249. https://doi.org/10.1007/s12088-019-00780-7

Romero-Puertas MC, Corpas FJ, Sandalio LM, et al (2006) Glutathione reductase from pea leaves: response to abiotic stress and characterization of the peroxisomal isozyme. New Phytol 170:43–52. https://doi.org/10.1111/j.1469-8137.2006.01643.x

Rubino F (2015) Toxicity of Glutathione-Binding Metals: A Review of Targets and Mechanisms. Toxics 3:20–62. https://doi.org/10.3390/toxics3010020

Ruttkay-Nedecky B, Nejdl L, Gumulec J, et al (2013) The Role of Metallothionein in Oxidative Stress. IJMS 14:6044–6066. https://doi.org/10.3390/ijms14036044

Ryu H, Fuwad A, Yoon S, et al (2019) Biomimetic Membranes with Transmembrane Proteins: State-of-the-Art in Transmembrane Protein Applications. IJMS 20:1437. https://doi.org/10.3390/ijms20061437

Rzymski P, Poniedzialek B, Niedzielski P, et al (2014) Cadmium and lead toxicity and bioaccumulation in *Microcystis aeruginosa*. Front Environ Sci Eng 8:427–432. https://doi.org/10.1007/s11783-013-0566-4

Saavedra R, Muñoz R, Taboada ME, et al (2018) Comparative uptake study of arsenic, boron, copper, manganese and zinc from water by different green microalgae. Bioresource Technology 263:49–57. https://doi.org/10.1016/j.biortech.2018.04.101

Salam KA (2019) https://www.biofueljournal.com/article_88261.html. Biofuel Res J 6:948–961. https://doi.org/10.18331/BRJ2019.6.2.2

Sánchez-Bayo A, Morales V, Rodríguez R, et al (2020) Cultivation of Microalgae and Cyanobacteria: Effect of Operating Conditions on Growth and Biomass Composition. Molecules 25:2834. https://doi.org/10.3390/molecules25122834

Santos S, Torcato I, Castanho MARB (2012) Biomedical applications of dipeptides and tripeptides. Biopolymers 98:288–293. https://doi.org/10.1002/bip.22067

Sargın İ, Arslan G (2015) Chitosan/sporopollenin microcapsules: Preparation, characterisation and application in heavy metal removal. International Journal of Biological Macromolecules 75:230–238. https://doi.org/10.1016/j.ijbiomac.2015.01.039

Schaedle M, Bassham JA (1977) Chloroplast Glutathione Reductase. Plant Physiol 59:1011–1012. https://doi.org/10.1104/pp.59.5.1011

Schiewer S, Patil SB (2008) Modeling the effect of pH on biosorption of heavy metals by citrus peels. Journal of Hazardous Materials 157:8–17. https://doi.org/10.1016/j.jhazmat.2007.12.076

Sears ME (2013) Chelation: Harnessing and Enhancing Heavy Metal Detoxification—A Review. The Scientific World Journal 2013:1–13. https://doi.org/10.1155/2013/219840

Sedighi O, Zargari M, Varshi G (2014) Effect of Selenium Supplementation on Glutathione Peroxidase Enzyme Activity in Patients With Chronic Kidney Disease: A Randomized Clinical Trial. Nephro Urol Mon 6:. https://doi.org/10.5812/numonthly.17945

SenthilKumar P, Ramalingam S, Sathyaselvabala V, et al (2011) Removal of copper(II) ions from aqueous solution by adsorption using cashew nut shell. Desalination 266:63–71. https://doi.org/10.1016/j.desal.2010.08.003

Shameer S (2016) Biosorption of lead, copper and cadmium using the extracellular polysaccharides (EPS) of Bacillus sp., from solar salterns. 3 Biotech 6:194. https://doi.org/10.1007/s13205-016-0498-3

Shamim S (2018) Biosorption of Heavy Metals. In: Derco J, Vrana B (eds) Biosorption. InTech

Shanab S, Essa A, Shalaby E (2012) Bioremoval capacity of three heavy metals by some microalgae species (Egyptian Isolates). Plant Signaling and Behavior 7:392–399. https://doi.org/10.4161/psb.19173

Shankar T, Palpperumal S, Kathiresan D, et al (2021) Biomedical and therapeutic potential of exopolysaccharides by Lactobacillus paracasei isolated from sauerkraut: Screening and characterization. Saudi Journal of Biological Sciences 28:2943–2950. https://doi.org/10.1016/j.sjbs.2021.02.030

Sharma P, Jha AB, Dubey RS, Pessarakli M (2012) Reactive Oxygen Species, Oxidative Damage, and Antioxidative Defense Mechanism in Plants under Stressful Conditions. Journal of Botany 2012:1–26. https://doi.org/10.1155/2012/217037

Sharma SS, Dietz K, Mimura T (2016) Vacuolar compartmentalization as indispensable component of heavy metal detoxification in plants. Plant Cell and Environment 39:1112–1126. https://doi.org/10.1111/pce.12706

Shartooh SM, Kasim SA, Obaid RH, et al (2014) Lettuce Leaves as Biosorbent Material to Remove Heavy Metal Ions from Industerial Wastewater. Baghdad SciJ 11:1164–1170. https://doi.org/10.21123/bsj.2014.11.3.1164-1170

Shcolnick S, Keren N (2006) Metal Homeostasis in Cyanobacteria and Chloroplasts. Balancing Benefits and Risks to the Photosynthetic Apparatus. Plant Physiology 141:805–810. https://doi.org/10.1104/pp.106.079251

Shen L, Chen R, Wang J, et al (2021) Biosorption behavior and mechanism of cadmium from aqueous solutions by *Synechocystis* sp. PCC6803. RSC Adv 11:18637–18650. https://doi.org/10.1039/D1RA02366G

Shen Y, Zhu W, Li H, et al (2018) Enhancing cadmium bioremediation by a complex of water-hyacinth derived pellets immobilized with Chlorella sp. Bioresource Technology 257:157–163. https://doi.org/10.1016/j.biortech.2018.02.060

Sheng Y, Abreu IA, Cabelli DE, et al (2014) Superoxide Dismutases and Superoxide Reductases. Chem Rev 114:3854–3918. https://doi.org/10.1021/cr4005296

Shuhong Y, Meiping Z, Hong Y, et al (2014) Biosorption of Cu2+, Pb2+ and Cr6+ by a novel exopolysaccharide from Arthrobacter ps-5. Carbohydrate Polymers 101:50–56. https://doi.org/10.1016/j.carbpol.2013.09.021

Siddiqui K, Bawazeer N, Scaria Joy S (2014) Variation in Macro and Trace Elements in Progression of Type 2 Diabetes. The Scientific World Journal 2014:1–9. https://doi.org/10.1155/2014/461591

Siegel BZ, Siegel SM (1973) The Chemical Composition of Algal Cell Walls. CRC Critical Reviews in Microbiology 3:1–26. https://doi.org/10.3109/10408417309108743

Simkin AJ, Kapoor L, Doss CGP, et al (2022) The role of photosynthesis related pigments in light harvesting, photoprotection and enhancement of photosynthetic yield in planta. Photosynth Res 152:23–42. https://doi.org/10.1007/s11120-021-00892-6

Singh JS, Kumar A, Rai AN, Singh DP (2016) Cyanobacteria: A Precious Bio-resource in Agriculture, Ecosystem, and Environmental Sustainability. Front Microbiol 7:. https://doi.org/10.3389/fmicb.2016.00529

Singh S, Sran KS, Pinnaka AK, Roy Choudhury A (2019) Purification, characterization and functional properties of exopolysaccharide from a novel halophilic Natronotalea sambharensis sp. nov. International Journal of Biological Macromolecules 136:547–558. https://doi.org/10.1016/j.ijbiomac.2019.06.080

Singh VK, Jha S, Rana P, et al (2023) Resilience and Mitigation Strategies of Cyanobacteria under Ultraviolet Radiation Stress. IJMS 24:12381. https://doi.org/10.3390/ijms241512381

Slobodian MR, Petahtegoose JD, Wallis AL, et al (2021) The Effects of Essential and Non-Essential Metal Toxicity in the Drosophila melanogaster Insect Model: A Review. Toxics 9:269. https://doi.org/10.3390/toxics9100269

Smječanin N, Nuhanović M, Sulejmanović J, et al (2023) Highly effective sustainable membrane based cyanobacteria for uranium uptake from aqueous environment. Chemosphere 313:137488. https://doi.org/10.1016/j.chemosphere.2022.137488

Sodhi KK, Mishra LC, Singh CK, Kumar M (2022) Perspective on the heavy metal pollution and recent remediation strategies. Current Research in Microbial Sciences 3:100166. https://doi.org/10.1016/j.crmicr.2022.100166

Solmaz K, Ozcan Y, Mercan Dogan N, et al (2018) Characterization and Production of Extracellular Polysaccharides (EPS) by Bacillus Pseudomycoides U10. Environments 5:63. https://doi.org/10.3390/environments5060063

Sooksawat N, Meetam M, Kruatrachue M, et al (2016) Equilibrium and kinetic studies on biosorption potential of charophyte biomass to remove heavy metals from synthetic metal solution and municipal wastewater. Bioremediation Journal 20:240–251. https://doi.org/10.1080/10889868.2016.1212810

Spain O, Funk C (2022) Detailed Characterization of the Cell Wall Structure and Composition of Nordic Green Microalgae. J Agric Food Chem 70:9711–9721. https://doi.org/10.1021/acs.jafc.2c02783

Spain O, Plöhn M, Funk C (2021) The cell wall of green microalgae and its role in heavy metal removal. Physiologia Plantarum 173:526–535. https://doi.org/10.1111/ppl.13405

Srivastava A, Ko S-R, Ahn C-Y, et al (2016) Microcystin Biosynthesis and *mcyA* Expression in Geographically Distinct *Microcystis* Strains under Different Nitrogen, Phosphorus, and Boron Regimes. BioMed Research International 2016:1–13. https://doi.org/10.1155/2016/5985987

Stewart RRC, Bewley JD (1980) Lipid Peroxidation Associated with Accelerated Aging of Soybean Axes. Plant Physiol 65:245–248. https://doi.org/10.1104/pp.65.2.245

Sudha Bai R, Abraham TE (2003) Studies on chromium(VI) adsorption–desorption using immobilized fungal biomass. Bioresource Technology 87:17–26. https://doi.org/10.1016/S0960-8524(02)00222-5

Sudhakar MS, Aggarwal A, Sah MK (2020) Engineering biomaterials for the bioremediation: advances in nanotechnological approaches for heavy metals removal from natural resources. In: Emerging Technologies in Environmental Bioremediation. Elsevier, pp 323–339

Sudmalis D, Mubita TM, Gagliano MC, et al (2020) Cation exchange membrane behaviour of extracellular polymeric substances (EPS) in salt adapted granular sludge. Water Research 178:115855. https://doi.org/10.1016/j.watres.2020.115855

Sulaymon AH, Mohammed AA, Al-Musawi TJ (2013) Competitive biosorption of lead, cadmium, copper, and arsenic ions using algae. Environ Sci Pollut Res 20:3011–3023. https://doi.org/10.1007/s11356-012-1208-2

Sun Q, Li Y, Shi L, et al (2022) Heavy metals induced mitochondrial dysfunction in animals: Molecular mechanism of toxicity. Toxicology 469:153136. https://doi.org/10.1016/j.tox.2022.153136

Suzaki PYR, Munaro MT, Triques CC, et al (2017) Biosorption of binary heavy metal systems: Phenomenological mathematical modeling. Chemical Engineering Journal 313:364–373. https://doi.org/10.1016/j.cej.2016.12.082

Swenson H, Stadie NP (2019) Langmuir's Theory of Adsorption: A Centennial Review. Langmuir 35:5409–5426. https://doi.org/10.1021/acs.langmuir.9b00154

Tangahu BV, Sheikh Abdullah SR, Basri H, et al (2011) A Review on Heavy Metals (As, Pb, and Hg) Uptake by Plants through Phytoremediation. International Journal of Chemical Engineering 2011:1–31. https://doi.org/10.1155/2011/939161

Tchounwou PB, Yedjou CG, Patlolla AK, Sutton DJ (2012) Heavy Metal Toxicity and the Environment. In: Luch A (ed) Molecular, Clinical and Environmental Toxicology. Springer Basel, Basel, pp 133–164

Thevarajah B, Nishshanka GKSH, Premaratne M, et al (2023) Cyanobacterial pigment production in wastewaters treated for heavy metal removal: Current status and perspectives. Journal of Environmental Chemical Engineering 11:108999. https://doi.org/10.1016/j.jece.2022.108999

Thévenod F, Fels J, Lee W-K, Zarbock R (2019) Channels, transporters and receptors for cadmium and cadmium complexes in eukaryotic cells: myths and facts. Biometals 32:469–489. https://doi.org/10.1007/s10534-019-00176-6

Tkachenko Y, Niedzielski P (2022) FTIR as a Method for Qualitative Assessment of Solid Samples in Geochemical Research: A Review. Molecules 27:8846. https://doi.org/10.3390/molecules27248846

Torres E (2020) Biosorption: A Review of the Latest Advances. Processes 8:1584. https://doi.org/10.3390/pr8121584

Tseng R-L, Wu F-C, Juang R-S (2010) Characteristics and applications of the Lagergren's first-order equation for adsorption kinetics. Journal of the Taiwan Institute of Chemical Engineers 41:661–669. https://doi.org/10.1016/j.jtice.2010.01.014

Tsuneda S, Aikawa H, Hayashi H, et al (2003) Extracellular polymeric substances responsible for bacterial adhesion onto solid surface. FEMS Microbiology Letters 223:287–292. https://doi.org/10.1016/S0378-1097(03)00399-9

Tzabar N, Ter Brake HJM (2016) Adsorption isotherms and Sips models of nitrogen, methane, ethane, and propane on commercial activated carbons and polyvinylidene chloride. Adsorption 22:901–914. https://doi.org/10.1007/s10450-016-9794-9

Uddin MM, Zakeel MCM, Zavahir JS, et al (2021) Heavy Metal Accumulation in Rice and Aquatic Plants Used as Human Food: A General Review. Toxics 9:360. https://doi.org/10.3390/toxics9120360

Ullah R, Jo MH, Riaz M, et al (2020) Glycine, the smallest amino acid, confers neuroprotection against d-galactose-induced neurodegeneration and memory impairment by regulating c-Jun N-terminal kinase in the mouse brain. J Neuroinflammation 17:303. https://doi.org/10.1186/s12974-020-01989-w

Vandenbossche M, Jimenez M, Casetta M, Traisnel M (2015) Remediation of Heavy Metals by Biomolecules: A Review. Critical Reviews in Environmental Science and Technology 45:1644–1704. https://doi.org/10.1080/10643389.2014.966425

Vašák M, Schnabl J (2016) Sodium and Potassium Ions in Proteins and Enzyme Catalysis. In: Sigel A, Sigel H, Sigel RKO (eds) The Alkali Metal Ions: Their Role for Life. Springer International Publishing, Cham, pp 259–290

Vatansever F, De Melo WCMA, Avci P, et al (2013) Antimicrobial strategies centered around reactive oxygen species – bactericidal antibiotics, photodynamic therapy, and beyond. FEMS Microbiol Rev 37:955–989. https://doi.org/10.1111/1574-6976.12026

Vigdorowitsch M, Pchelintsev A, Tsygankova L, Tanygina E (2021) Freundlich Isotherm: An Adsorption Model Complete Framework. Applied Sciences 11:8078. https://doi.org/10.3390/app11178078

Vijayaraghavan K, Yun Y-S (2008) Bacterial biosorbents and biosorption. Biotechnology Advances 26:266–291. https://doi.org/10.1016/j.biotechadv.2008.02.002

Vilar VJP, Botelho CMS, Boaventura RAR (2008) Metal biosorption by algae Gelidium derived materials from binary solutions in a continuous stirred adsorber. Chemical Engineering Journal 141:42–50. https://doi.org/10.1016/j.cej.2007.10.011

Villa JA, Bernal B (2018) Carbon sequestration in wetlands, from science to practice: An overview of the biogeochemical process, measurement methods, and policy framework. Ecological Engineering 114:115–128. https://doi.org/10.1016/j.ecoleng.2017.06.037

Volesky B, Holan ZR (1995) Biosorption of heavy metals. Biotechnol Prog 11:235–250. https://doi.org/10.1021/bp00033a001

Wang B, Wang X, Hu Y, et al (2015a) The combined effects of UV-C radiation and H 2 O 2 on *Microcystis aeruginosa* , a bloom-forming cyanobacterium. Chemosphere 141:34–43. https://doi.org/10.1016/j.chemosphere.2015.06.020

Wang F, Lu X, Li X (2016) Selective removals of heavy metals (Pb2+, Cu2+, and Cd2+) from wastewater by gelation with alginate for effective metal recovery. Journal of Hazardous Materials 308:75–83. https://doi.org/10.1016/j.jhazmat.2016.01.021

Wang J, Guo X (2020) Adsorption kinetic models: Physical meanings, applications, and solving methods. Journal of Hazardous Materials 390:122156. https://doi.org/10.1016/j.jhazmat.2020.122156

Wang J, Guo X (2022) Rethinking of the intraparticle diffusion adsorption kinetics model: Interpretation, solving methods and applications. Chemosphere 309:136732. https://doi.org/10.1016/j.chemosphere.2022.136732

Wang J, Zhao X, Tian Z, et al (2015b) Isolation and Characterization of Exopolysaccharide-Producing Lactobacillus plantarum SKT109 from Tibet Kefir. Pol J Food Nutr Sci 65:269–279. https://doi.org/10.1515/pjfns-2015-0023

Wang L-L, Wang L-F, Ren X-M, et al (2012) pH Dependence of Structure and Surface Properties of Microbial EPS. Environ Sci Technol 46:737–744. https://doi.org/10.1021/es203540w

Wang Q, Wei N, Jin X, et al (2021) Molecular characterization of the COPT/Ctr-type copper transporter family under heavy metal stress in alfalfa. International Journal of Biological Macromolecules 181:644–652. https://doi.org/10.1016/j.ijbiomac.2021.03.173

Wang S, Yang Z, Yang H, Lu B, Li S and Lu Y (2004). Copper-induced stress and antioxidative responses in roots of *Brassica juncea* L. Botanical Bulletin of Academia Sinica 45: 203-212.

Wang X, Cheng B, Zhang L, et al (2022a) Synthesis of MgNiCo LDH hollow structure derived from ZIF-67 as superb adsorbent for Congo red. Journal of Colloid and Interface Science 612:598–607. https://doi.org/10.1016/j.jcis.2021.12.176

Wang X, Wang C, Zhang Z, Shi G (2022b) Genome-wide Identification of Metal Tolerance Protein Genes in Peanut: Differential Expression in the Root of Two Contrasting Cultivars Under Metal Stresses. Front Plant Sci 13:791200. https://doi.org/10.3389/fpls.2022.791200

Wang Y, Branicky R, Noë A, Hekimi S (2018) Superoxide dismutases: Dual roles in controlling ROS damage and regulating ROS signaling. Journal of Cell Biology 217:1915–1928. https://doi.org/10.1083/jcb.201708007

Wang Y, Li C, Liu P, et al (2010) Physical characterization of exopolysaccharide produced by Lactobacillus plantarum KF5 isolated from Tibet Kefir. Carbohydrate Polymers 82:895–903. https://doi.org/10.1016/j.carbpol.2010.06.013

Waqar R, Kaleem M, Iqbal J, et al (2023) Kinetic and Equilibrium Studies on the Adsorption of Lead and Cadmium from Aqueous Solution Using Scenedesmus sp. Sustainability 15:6024. https://doi.org/10.3390/su15076024

Were D, Kansiime F, Fetahi T, et al (2019) Carbon Sequestration by Wetlands: A Critical Review of Enhancement Measures for Climate Change Mitigation. Earth Syst Environ 3:327–340. https://doi.org/10.1007/s41748-019-00094-0

Weydert CJ, Cullen JJ (2010) Measurement of superoxide dismutase, catalase and glutathione peroxidase in cultured cells and tissue. Nat Protoc 5:51–66. https://doi.org/10.1038/nprot.2009.197

Witkowska D, Słowik J, Chilicka K (2021) Heavy Metals and Human Health: Possible Exposure Pathways and the Competition for Protein Binding Sites. Molecules 26:6060. https://doi.org/10.3390/molecules26196060

Woitzik D, Weckesser J, Jurgens UJ (1988) Isolation and Characterization of Cell Wall Components of the Unicellular Cyanobacterium Synechococcus sp. PCC 6307. Microbiology 134:619–627. https://doi.org/10.1099/00221287-134-3-619

Wu F-C, Tseng R-L, Juang R-S (2009) Initial behavior of intraparticle diffusion model used in the description of adsorption kinetics. Chemical Engineering Journal 153:1–8. https://doi.org/10.1016/j.cej.2009.04.042

Wu Y, Li Z, Yang Y, et al (2021) Extracellular Polymeric Substances Facilitate the Adsorption and Migration of Cu2+ and Cd2+ in Saturated Porous Media. Biomolecules 11:1715. https://doi.org/10.3390/biom11111715

Wu Z, Zhang D, Xia T, Jia X (2022) Characteristics, sources and risk assessments of heavy metal pollution in soils of typical chlor-alkali residue storage sites in northeastern China. PLoS ONE 17:e0273434. https://doi.org/10.1371/journal.pone.0273434

Xiao R, Zheng Y (2016) Overview of microalgal extracellular polymeric substances (EPS) and their applications. Biotechnology Advances 34:1225–1244. https://doi.org/10.1016/j.biotechadv.2016.08.004

Xie A, Li H, Hao Y, Zhang Y (2021) Tuning the Toxicity of Reactive Oxygen Species into Advanced Tumor Therapy. Nanoscale Res Lett 16:142. https://doi.org/10.1186/s11671-021-03599-8

Xie X, He Z, Chen N, et al (2019) The Roles of Environmental Factors in Regulation of Oxidative Stress in Plant. BioMed Research International 2019:1–11. https://doi.org/10.1155/2019/9732325

Yaashikaa PR, Kumar PS, Saravanan A, Vo D-VN (2021) Advances in biosorbents for removal of environmental pollutants: A review on pretreatment, removal mechanism and future outlook. Journal of Hazardous Materials 420:126596. https://doi.org/10.1016/j.jhazmat.2021.126596

Yadav APS, Dwivedi V, Kumar S, et al (2020) Cyanobacterial Extracellular Polymeric Substances for Heavy Metal Removal: A Mini Review. J Compos Sci 5:1. https://doi.org/10.3390/jcs5010001

Yadav G, Sekar M, Kim S-H, et al (2021) Lipid content, biomass density, fatty acid as selection markers for evaluating the suitability of four fast growing cyanobacterial strains for biodiesel production. Bioresource Technology 325:124654. https://doi.org/10.1016/j.biortech.2020.124654

Yang T, Chen M-L, Wang J-H (2015) Genetic and chemical modification of cells for selective separation and analysis of heavy metals of biological or environmental significance. TrAC Trends in Analytical Chemistry 66:90–102. https://doi.org/10.1016/j.trac.2014.11.016

Yemm EW, Willis AJ (1954) The estimation of carbohydrates in plant extracts by anthrone. Biochemical Journal 57:508–514. https://doi.org/10.1042/bj0570508

Yin Y, Hu Y, Xiong F (2011) Sorption of Cu(II) and Cd(II) by extracellular polymeric substances (EPS) from Aspergillus fumigatus. International Biodeterioration and Biodegradation 65:1012–1018. https://doi.org/10.1016/j.ibiod.2011.08.001

Yu P, Cui H, Bai J, et al (2022) Adsorption and desorption of Cu, Zn, Pb, and Cd on surface sediments from a shallow lake, North China. Ecohydrology and Hydrobiology S1642359322000027. https://doi.org/10.1016/j.ecohyd.2022.01.002

Yu X-Z, Lin Y-J, Zhang Q (2019) Metallothioneins enhance chromium detoxification through scavenging ROS and stimulating metal chelation in Oryza sativa. Chemosphere 220:300–313. https://doi.org/10.1016/j.chemosphere.2018.12.119

Yuzugullu Karakus Y (2020) Typical Catalases: Function and Structure. In: Dulce Bagatini M (ed) Glutathione System and Oxidative Stress in Health and Disease. IntechOpen

Zakar T, Laczko-Dobos H, Toth TN, Gombos Z (2016) Carotenoids Assist in Cyanobacterial Photosystem II Assembly and Function. Front Plant Sci 7:. https://doi.org/10.3389/fpls.2016.00295

Zeng G, He Y, Liang D, et al (2022) Adsorption of Heavy Metal Ions Copper, Cadmium and Nickel by *Microcystis aeruginosa*. IJERPH 19:13867. https://doi.org/10.3390/ijerph192113867

Zhang B, Lewis JA, Kovacs F, et al (2023) Activity of Cytosolic Ascorbate Peroxidase (APX) from Panicum virgatum against Ascorbate and Phenylpropanoids. IJMS 24:1778. https://doi.org/10.3390/ijms24021778

Zhang C, Yang Q, Zhang X, et al (2021) Genome-Wide Identification of the HMA Gene Family and Expression Analysis under Cd Stress in Barley. Plants 10:1849. https://doi.org/10.3390/plants10091849

Zhang F-Q, Wang Y-S, Lou Z-P, Dong J-D (2007) Effect of heavy metal stress on antioxidative enzymes and lipid peroxidation in leaves and roots of two mangrove plant seedlings (Kandelia candel and Bruguiera gymnorrhiza). Chemosphere 67:44–50. https://doi.org/10.1016/j.chemosphere.2006.10.007

Zhang Z, Cai R, Zhang W, et al (2017) A Novel Exopolysaccharide with Metal Adsorption Capacity Produced by a Marine Bacterium Alteromonas sp. JL2810. Marine Drugs 15:175. https://doi.org/10.3390/md15060175

Zheng X, Chen L, Li X (2018) Arabidopsis and rice showed a distinct pattern in ZIPs genes expression profile in response to Cd stress. Bot Stud 59:22. https://doi.org/10.1186/s40529-018-0238-6

Zhou C, Tesfamariam EG, Tang Y, Li A (2023) Contributions of adsorption, bioreduction and desorption to uranium immobilization by extracellular polymeric substances. Frontiers of Environmental Science and Engineering 17:107. https://doi.org/10.1007/s11783-023-1707-z

Zhou H-X, Pang X (2018) Electrostatic Interactions in Protein Structure, Folding, Binding, and Condensation. Chem Rev 118:1691–1741. https://doi.org/10.1021/acs.chemrev.7b00305

Zhou Q, Sun W-W, Chen J-C, et al (2022) Phenylalanine impairs insulin signaling and inhibits glucose uptake through modification of IRβ. Nat Commun 13:4291. https://doi.org/10.1038/s41467-022-32000-0

Zhou Q, Yang N, Li Y, et al (2020) Total concentrations and sources of heavy metal pollution in global river and lake water bodies from 1972 to 2017. Global Ecology and Conservation 22:e00925. https://doi.org/10.1016/j.gecco.2020.e00925

Zhou W, Min M, Li Y, et al (2012) A hetero-photoautotrophic two-stage cultivation process to improve wastewater nutrient removal and enhance algal lipid accumulation. Bioresource Technology 110:448–455. https://doi.org/10.1016/j.biortech.2012.01.063

Zinicovscaia I, Duca G, Cepoi L, et al (2015) Biotechnology of Metal Removal from Industrial Wastewater: Zinc Case Study. CLEAN Soil Air Water 43:112–117. https://doi.org/10.1002/clen.201200570

(2014) Biosorption of Arsenic by Living and Dried Biomass of Fresh Water Microalgae - Potentials and Equilibrium Studies. J Bioremed Biodeg 05: https://doi.org/10.4172/2155-6199.1000249

BIO-DATA

Name	:	Sengjrang Ch Momin
Father's Name		Nickinson N Arengh
Mother's Name		Setnilla Ch Momin
Permanent Address	:	Kusimkolgre, Williamnagar, East Garo Hills, Meghalaya
Nationality	:	Indian
Date of Birth	:	28-03-1994
Sex	:	Male
Marital Status	:	Unmarried
Contact Number	:	9485168195
Email Address	:	xrangmomin@gmail.com

ACADEMIC QUALIFICATIONS (STARTING FROM THE HIGHEST DEGREE)

Sl. no.	Name of the degree/exam	Subject	Board/ University	Year of passing	% Marks/ Grade
1	Ph. D.	Botany	Mizoram University (MZU)	2025	
2	M. Sc.	Botany	Mizoram University (MZU)	2016	75.0
3	B. Sc.	Botany	North-Eastern Hill University (NEHU)	2014	61.63
4	HSSLC	Science	Meghalaya Board of School Education (MBOSE)	2011	52.0
5	SSLC	Science	Meghalaya Board of School Education (MBOSE)	2009	67.5

LIST OF PUBLICATION

Patent Publication

1. Mehta S. K, **Momin S Ch**, Pradhan R. B (2024). Methods for removing heavy metals from aqueous solutions using extracellular polymeric substance from *Microcystis aeruginosa*. Application No. 202431032536 A. Patent office journal No. 18/2024 Dated: 03/05/2024

Paper Publication

1. **Momin S Ch**, Pradhan RB, Nath J, et al (2024b) Metal sequestration by *Microcystis* extracellular polymers: a promising path to greener water treatment. Environmental Science and Pollution Research 31:11192–11213. **(Impact Factor-5.8)**

2. **Momin S Ch**, Nath J, Mahana A, et al (2024a) Chemical activation of *Microcystis aeruginosa* biomass: a promising approach for enhanced diclofenac sorption and water treatment. Journal of Chemical Technology and Biotechnology 99:149–163. **(Impact Factor-3.4)**

3. Mahana A, Guliy OI, **Momin S Ch**, et al (2020) Sunlight-driven photocatalytic degradation of methylene blue using ZnO nanowires prepared through ultrasonication-assisted biological process using aqueous extract of *Anabaena doliolum*. Optical Materials 108:110205. **(Impact Factor-3.9)**

4. Lalremdika R, Pradhan R. B, **Momin S. Ch**, et al (2024) Carbon dioxide sequestration and sustainable domestic sewage bioremediation by Microcystis aeruginosa and Chlorella vulgaris. Ecology, Environment and Conservation 30: S108-S119.

PRESENTATION AND WORKSHOP

1. Paper presentation in International Conference on Science and Technology for Innovative and Sustainable Development (STISD-2023) jointly organized by Department of Chemistry and Department of Industrial Chemistry, Mizoram University during 28-30th June, 2023.

2. Paper presentation in International Conference on Biotechnology for Environment and Health (ICBEH), organized by School of Bio Sciences and Technology, Vellore Institute of Technology along with Association of Biotechnology and Pharmacy, from November 25 – 27th, 2021.

3. Paper presentation in International Conference on Molecular Biology of Stress Responses in Phototrophs on 12-14th, November 2016 organized by Department of Biotechnology, Indira Gandhi National Tribal University, Amarkantak, Madhya Pradesh, India.

4. Participation at One Day Awareness Program cum Workshop on Invasive Alien Plants in Himalayas: Status, Ecological Imapact and Management (Mizoram and Tripura Chapter), organized by Botanical Survey of India in collaboration with Department of Botany, Mizoram University on 26th April, 2019 under National Mission for Himalyan Studies.

5. Participation in the National workshop on Hands on Training on DNA Barcoding and Phylogenetics held during 20-25th March 2017 organized by State Biotech-Hub Facility, Department of Biotechnology, Mizoram University sponsored by Department of Biotechnology (DBT) New Delhi. India.

PARTICULARS OF THE CANDIDATE

NAME	:	Sengjrang Ch Momin
DEGREE	:	Ph. D
DEPARTMENT	:	Botany
TITLE OF THESIS	:	Characterization of cyanobacterial cell surface for removal of heavy metals from aqueous solutions.
DATE OF ADMISSION	:	16th August, 2016
DATE OF APPROVAL OF RESEARCH PROPOSAL:		
1. DRC	:	24th April, 2017
2. BOS	:	1st May, 2017
3. SCHOOL BOARD	:	26th May, 2017
MZU REGISTRATION NO.	:	7050 of 2014
PH. D REGISTRATION NO. and DATE	:	MZU/Ph. D/1014 of 26.05.2017
EXTENSION (IF ANY)	:	No. 16-2/MZU(Acad)/21/179-182 30th August 2022

Head

Department of Botany

ABSTRACT

CHARACTERIZATION OF CYANOBACTERIAL CELL SURFACE FOR REMOVAL OF HEAVY METALS FROM AQUEOUS SOLUTIONS

AN ABSTRACT SUBMITTED IN PARTIAL FULFILLMENT OF THE REQUIREMENTS FOR THE DEGREE OF DOCTOR OF PHILOSOPHY

SENGJRANG CH MOMIN

MZU Reg. No.: 7050 of 2014

Ph. D Reg. No.: MZU/Ph.D./1014 of 26.05.2017

DEPARTMENT OF BOTANY

SCHOOL OF LIFE SCIENCES

MAY, 2024

CHARACTERIZATION OF CYANOBACTERIAL CELL SURFACE FOR REMOVAL OF HEAVY METALS FROM AQUEOUS SOLUTIONS

By

SENGJRANG CH MOMIN
DEPARTMENT OF BOTANY

SUPERVISOR
DR. SURYA KANT MEHTA

SUBMITTED

IN PARTIAL FULFILLMENT OF THE REQUIREMENT OF THE DEGREE OF DOCTOR OF PHILOSOPHY IN BOTANY OF MIZORAM UNIVERSITY, AIZAWL

ABSTRACT

Heavy metal contamination of aquatic ecosystems has emerged as a global environmental concern, posing a serious threat to the health of our planet and its inhabitants. Unlike many organic pollutants, heavy metals cannot be degraded by natural processes. They persist in the environment for extended periods, accumulating in sediments and entering the food chain through a process known as bioaccumulation. This progressive concentration of heavy metals as they move up the food chain poses a significant risk to various life forms, including humans.

These heavy metals, such as Cd^{2+}, Cu^{2+}, and Ni^{2+}, can exert a multitude of detrimental effects on living organisms. They can disrupt essential biological processes by interfering with enzyme function, causing oxidative stress, and damaging cellular structures. Even at low concentrations, chronic exposure to heavy metals can lead to a range of health problems in humans, including neurological disorders, kidney and liver damage, and an increased risk of cancer.

The widespread presence of heavy metals in water bodies necessitates the development of effective and sustainable remediation strategies. Traditional methods for heavy metal removal often rely on expensive and energy-intensive techniques like chemical precipitation or filtration. These methods can also generate toxic byproducts, creating additional environmental challenges.

In recent years, bioremediation has emerged as a promising alternative for heavy metal removal from contaminated water. This eco-friendly approach harnesses the natural ability of microorganisms and their by-products to bind and sequester heavy metals. Biosorption utilizes the unique properties of certain microorganisms, such as bacteria and algae, which possess functional groups on their cell walls or secrete biomolecules with high metal-binding affinity. These biomolecules, known as Extracellular Polymeric Substances (EPS), play a significant role in metal biosorption by providing additional binding sites for metal ions.

This thesis investigated the biosorption potential of *M. aeruginosa* and *A. doliolum* for removing Cd^{2+},Cu^{2+} and Ni^{2+} ions from aqueous solutions. The study explored the efficacy of biomass and Extracellular Polymeric Substances (EPS), with a focus on understanding the underlying mechanisms and reusability aspects.

Additionally, the research examined the impact of metal exposure on the organisms, and their tolerance mechanisms and oxidative stress response.

Objectives:

- To evaluate the biosorption capacity of *M. aeruginosa* and *A. doliolum* biomass and EPS for Cd^{2+}, Cu^{2+}, and Ni^{2+} ions.
- To characterize cell surface of the test organisms for the adsorption of metal ions.
- To investigate the influence of co-existing metal ions on individual metal biosorption using isotherm models.
- To assess the reusability and regeneration potential of the biosorbents through desorption studies.
- To study the toxicity and the tolerance mechanisms employed by the test organisms to cope with metal stress.

Methodology

The freshwater cyanobacteria *A. doliolum* and *M. aeruginosa* were used in this study. The cyanobacteria were collected from a paddy field in Aizawl, Mizoram, India. To ensure the purity of the culture, an agar-plating method was used. The purified cultures were then grown and maintained in CHU-10 medium at a pH of 7.2 ± 0.2. A controlled light-dark cycle of 10-14 hours was provided, along with a temperature range of 30-35°C to mimic natural conditions and promote optimal growth.

After cultivating cyanobacteria, EPS production was stimulated, and the EPS was isolated from the culture broth. The supernatant was separated by centrifugation, concentrated, and then precipitated with acetone. The collected EPS was subsequently purified through re-dissolution and re-precipitation steps, followed by dialysis to remove contaminants. Finally, freeze-drying yielded concentrated EPS for further analysis. The chemical composition of both cyanobacteria and EPS was determined. Total saccharide content, total sugars, protein content were measured using a dye-binding assay, and total amino acid content was assessed using the Ninhydrin method. High-resolution transmission electron microscopy (TEM) revealed the ultrastructure

of the samples, while scanning electron microscopy (SEM) examined surface characteristics. Energy-dispersive X-ray (EDAX) spectroscopy identified and quantified elements within the samples, and Fourier-transform infrared (FTIR) spectroscopy determined the functional groups present in EPS and cyanobacteria, providing insights into potential interactions with heavy metals.

The ability of cyanobacteria biomass and EPS to remove Cu^{2+} and Ni^{2+} from water was investigated. Various concentrations of metal solutions were mixed with biomass or EPS, shaken, and the remaining metal concentration in the solution was measured using AAS. The difference between initial and final metal concentration indicated the amount adsorbed. Experiments were performed to assess the impact of pH on metal removal and the rate of metal uptake over time. Mathematical models were then used to analyze the adsorption data for both biomass and EPS.

Thermodynamic parameters like enthalpy, entropy, and Gibbs free energy were determined to understand the energetic nature and spontaneity of the metal removal process at different temperatures. Mathematical models were used to analyze the kinetics of metal adsorption, considering pseudo-first-order, pseudo-second-order, and intra-particle diffusion mechanisms. Furthermore, the impact of co-existing metal ions on the adsorption of Cu^{2+} and Ni^{2+} was investigated. Additionally, three isotherm models, Langmuir, Freundlich, and Temkin, were employed to describe the relationship between the amount of metal adsorbed and its equilibrium concentration in the solution. The study also included a potentiometric titration to assess the functional groups on the cyanobacteria cell surface that might be involved in metal binding. Finally, desorption experiments were conducted to evaluate the reusability of the biomass and EPS for heavy metal removal. The percentage of metal desorbed using Milli-Q water was measured to assess the reversibility of the adsorption

As described above, the study explored the efficacy of both live cells (biomass) and Extracellular Polymeric Substances (EPS) for biosorption, with a focus on understanding the underlying mechanisms and reusability aspects. However, the research also examined the impact of metal exposure on the organisms, including their tolerance mechanisms and oxidative stress response.

The study investigated the effects of heavy metals on two freshwater cyanobacteria, *A. doliolum* and *M. aeruginosa*. Collected from a local paddy field, the

cyanobacteria were purified and cultured under controlled conditions (10-14 hour light/dark cycle, 30-35°C temperature, CHU-10 medium at pH 7.2). To assess heavy metal impact, cultures were exposed to varying concentrations of Cd^{2+}, Cu^{2+}, and Ni^{2+} (0-100 mg L^{-1}) for 96 hours. Cell growth was monitored by measuring optical density at 663 nm every 24 hours. A specific growth rate formula was used to analyze the results.

The protein content of both cyanobacteria was measured using Lowry's method with Bovine Serum Albumin for calibration. Total carbohydrates were estimated using the Anthrone method with glucose as the standard. To quantify photosynthetic pigments, cells were pelleted and re-suspended in ethanol for pigment extraction. The resulting supernatant was then used to measure Chlorophyll-a and Carotenoid content using a UV/VIS spectrophotometer at specific wavelengths as described by Mimuro & Fujita (1977) and Kirk & Allen (1965).

To assess oxidative stress, the extent of lipid damage (TBARS), hydrogen peroxide (H_2O_2) concentration, and superoxide radical (O_2^-) generation measured. For superoxide radicals, a mixture containing buffer, electron donor, and osmotic protectant was incubated with cyanobacteria under light to stimulate O_2^- production. The resulting blue formazan was measured at 530 nm to quantify O_2^-. Due to the fleeting nature of hydroxyl radicals (OH-), direct measurement is impossible. However, OH^- damage was assessed by measuring cellular damage to a substrate (2-deoxyribose) using a method involving homogenization, centrifugation, and spectrophotometric analysis of a colored byproduct.

In order to investigate the antioxidant defense mechanisms employed by cyanobacteria under stressful conditions, several antioxidant enzymes were extracted and their activities were assessed. Following the disruption of cell walls, enzymes including superoxide dismutase (SOD), catalase (CAT), ascorbate peroxidase (APX), and glutathione reductase (GR) were extracted. The ability of SOD to inhibit photoreduction of NBT caused by superoxide radicals was measured to determine its activity. CAT activity was determined by monitoring the disappearance of hydrogen peroxide. The consumption of ascorbate used to reduce hydrogen peroxide was followed to assess APX activity. Finally, GR activity was measured by monitoring the

conversion of another molecule (NADPH) involved in the antioxidant pathway. The activity of each enzyme was expressed in units per milligram of protein.

To assess the total antioxidant pool within cyanobacteria, the concentration of various thiol groups (T-SH) was measured using methods by Sedlak and Lindsay (1968). Ellman's reagent (DTNB) was employed in all assays. Total T-SH directly reacted with DTNB to form a yellow product (TNB) measured at 412 nm, with higher absorbance indicating greater total thiol content. Non-protein thiols (NP-SH) were specifically measured after protein precipitation to remove protein-bound thiols, following the same principle of TNB formation and absorbance measurement. Finally, reduced glutathione (GSH), an important cellular antioxidant, was isolated through protein precipitation and then reacted with DTNB to quantify GSH concentration based on the resulting TNB absorbance at 412 nm.

Results

I. Biosorption of Heavy Metals

The ability of live canobacteria biomass and their isolated exopolysaccharides (EPS) to remove Cu^{2+}, Ni^{2+} and Cd^{2+} from water was investigated. Live *M. aeruginosa* and *A. doliolum* cultures were grown under controlled conditions. Separately, EPS was isolated from these 30 days old cultures. The biomass and EPS were then exposed to various concentrations of Cu^{2+}, Ni^{2+}, and Cd^{2+} solutions. After incubation, the amount of metal remaining in the solution was measured to determine the biosorption capacity. The study aimed to compare the effectiveness of live cyanobacteria and EPS in removing these heavy metals from water.

The composition of cyanobacteria biomass and EPS was investigated to understand their potential for metal adsorption. The content of saccharides, proteins, and amino acids was quantified, revealing higher concentrations within the biomass compared to the EPS for both *M. aeruginosa* and *A. doliolum*. This suggests a primary location within the cells for these biomolecules, where they regulate metal ion concentrations to maintain metal homeostasis. However, their presence, albeit at lower levels, in the EPS indicates a possible secondary role in interacting with and immobilizing metal ions from the surrounding environment. This highlights the

potential of EPS as a bioadsorbent for heavy metals, even though their primary function within the EPS may differ. Structural differences between the EPS of the two species were revealed using Scanning Electron Microscopy (SEM). *Microcystis* EPS possessed a well-defined 3D structure with interconnected voids, while *A. doliolum* EPS exhibited a solid surface with a flowery structure. Both displayed porosity and smooth surfaces. Energy-Dispersive X-ray analysis (EDX) was employed to identify the elemental composition of these components. Carbon and oxygen were dominant elements in both biomass and EPS, with trace elements also being detected. Notably, the EPS of both species contained higher levels of sodium compared to the biomass, suggesting a potential role in metal interactions. Additionally, the presence of specific elements such as Cu^{2+} and chlorine in *Microcystis* EPS and nitrogen in *A. doliolum* EPS suggests their possible involvement in metal binding or other functionalities.

Fourier Transform Infrared (FTIR) spectroscopy revealed changes in *Microcystis* biomass and EPS upon interaction with metal ions. Peaks indicated binding with aromatic structures, C-O bonds, and carbonyl oxygen atoms. Similar results were observed for A. *doliolum*. Liquid Chromatography-Mass Spectrometry (LCMS) analysis revealed dipeptides as the major component in *Microcystis* EPS, suggesting a more rigid structure with limited flexibility. In contrast, *A. doliolum* EPS exhibited a wider variety of molecules, including longer peptides like tetrapeptides. This suggests a more complex and adaptable structure in *A. doliolum* EPS compared to *Microcystis* EPS. These variations in EPS composition likely influence their physical properties, interactions with the environment, and overall functions in each organism. For example, the presence of more polar amino acids in *Microcystis* EPS might contribute to its role in nutrient acquisition, while the wider variety of molecules in *A. doliolum* EPS could provide more adaptability to different environmental conditions.

Acid-base titration was used to assess the surface properties of cyanobacteria (*M. aeruginosa* and *A. doliolum*) and their ability to bind heavy metals. When exposed to acid, the cells take up hydrogen ions (H+) due to functional groups on their surface. This process (protonation) can affect the cell's surface charge. The experiment measured the amount of acid needed to neutralize the cells (equivalence point). Metal-treated cells (Cu^{2+}, Cd^{2+} and Ni^{2+}) generally required less acid to reach the equivalence

point compared to untreated cells. This suggests metal binding alters the surface chemistry, potentially reducing the availability of sites for H+ binding.

The study examined how pH impacts cyanobacteria and their isolated EPS in removing Cu^{2+}, Cd^{2+}, and Ni^{2+} from water. *M. aeruginosa* showed peak Cu^{2+} removal at pH 6.5, while Ni^{2+} removal remained stable across pH levels. Cd^{2+} removal increased with pH up to 7. A. doliolum exhibited stable Cu^{2+} removal and a gradual rise in Ni^{2+} removal with increasing pH. Cd^{2+} removal in A. doliolum surged at higher pH (7-8). Isolated EPS from both species displayed high initial removal for Cu^{2+} and Ni^{2+} at low pH (2.0). Cd^{2+} removal by both EPS types was low at low pH but increased significantly at higher pH (7), likely due to electrostatic interactions.

Kinetic studies suggest a two-phase heavy metal uptake process in cyanobacteria. The first rapid phase, likely passive binding to the cell wall, achieves over 90% of total uptake within a mere 30-45 minutes. This is followed by a slower phase, potentially involving active transport of metals into the cells. Interestingly, Ni^{2+} uptake is generally faster than Cu^{2+} or Cd^{2+} uptake, as evidenced by higher intraparticle diffusion rate constants (k_d) for Ni^{2+}. For example, *M. aeruginosa* showed a k_d of 0.0047 mg g-1 min^-1/2 for Cd^{2+} compared to a significantly higher 0.0164 mg g-1 min^-1/2 for Ni^{2+}. Diffusion also plays a more prominent role in EPS compared to whole cells. This is clear from the higher k_d values observed for EPS compared to whole cell biomass. For instance, *M. aeruginosa* EPS exhibited a k_d of 0.36 mg g-1 min^-1/2 for Ni^{2+}, whereas M. aeruginosa biomass had a much lower k_d of 0.0047 mg g-1 min^-1/2 for Cd^{2+}.

While both cyanobacteria and their isolated EPS adsorbed Ni^{2+}, Cu^{2+}, and Cd^{2+}, the mechanisms differed. Biomass adsorption, though exothermic (releasing heat), was unfavorable (nonspontaneous), suggesting a need for external energy for efficient metal removal. In contrast, EPS showed favorable (spontaneous) adsorption for all metals, with Cd^{2+} uptake being uniquely endothermic (absorbing heat). This highlights the promise of EPS for spontaneous heavy metal removal, while biomass may require optimization and further study is needed to understand the endothermic Cd^{2+} uptake by EPS.

Isolated EPS from cyanobacteria adsorbed more Ni^{2+}, Cu^{2+}, and Cd^{2+} than the cyanobacteria themselves, making EPS more promising for metal removal. The

Langmuir and Freundlich isotherm models effectively described the adsorption process, indicating a favorable and complex interaction between the metal ions and the EPS. The Langmuir model suggests monolayer adsorption on a homogenous surface, while the Freundlich model implies multilayer adsorption on a heterogeneous surface. This combination suggests a complex reality, where both even and uneven binding sites are likely present on the EPS, allowing for multiple layers of metal ions to be adsorbed. Interestingly, the presence of one metal reduced the adsorption of another, indicating competition for binding sites on the EPS. This highlights the potential of EPS for metal removal but also the need to consider co-existing contaminants.

The study examined how well the cyanobacteria and their EPS could be reused to remove metals. They desorbed the metals with water and found that EPS released a much higher percentage of the captured Cd^{2+}, Cu^{2+}, and Ni^{2+} compared to the leftover cyanobacteria cells. This suggests EPS is not only good at grabbing metals but also easier to clean and reuse. However, the ease of releasing the metals varied between the metals themselves, with Ni^{2+} being harder to desorb from both types of material.

II. Toxicity and tolerance of heavy metals in the test organisms

The study investigated how Cu, Ni, and Cd affect two cyanobacteria species, *M. aeruginosa* and *A. doliolum*. All three metals inhibited the growth of both cyanobacteria species in a dose-dependent manner. Cd^{2+} had the strongest inhibitory effect, followed by Cu^{2+} and then Ni^{2+}. The heavy metals caused a reduction in protein, carbohydrate, chlorophyll-a, and carotenoid content in both species. Again, Cd^{2+} had the strongest effect, followed by Cu^{2+} and Ni^{2+}. Exposure to the metals increased the production of malondialdehyde (MDA), hydrogen peroxide (H_2O_2), and superoxide radicals (O_2^-) in both cyanobacteria. These are all indicators of oxidative stress, which can damage cells. Cd^{2+} caused the most significant increase in these markers, again followed by Cu^{2+} and Ni^{2+}. Interestingly, *A. doliolum* seemed more prone to oxidative stress than *M. aeruginosa*. *M. aeruginosa* showed a significant increase in hydroxyl radical production with all three metals, with Cu^{2+} causing the most. *A. doliolum* displayed a different pattern, with a much smaller overall increase in hydroxyl radicals compared to *M. aeruginosa*. This suggests *A. doliolum* might be better at mitigating

hydroxyl radical production. Overall, the study shows that Cd^{2+} (Cd) has the most detrimental effect on cyanobacteria growth and physiology compared to Cu^{2+} (Cu) and Ni^{2+} (Ni). Interestingly, *A. doliolum* appeared to be more susceptible to oxidative stress than *M. aeruginosa*, but also showed a better ability to manage hydroxyl radicals.

When exposed to Cu^{2+}, Ni^{2+}, and Cd^{2+}, *M. aeruginosa* and *A. doliolum*, suffered increased oxidative stress. In response to this stress, both species upregulated the production of antioxidant enzymes, including superoxide dismutase (SOD), catalase, and ascorbate peroxidase (APX). *A. doliolum* generally had higher basal activity of all antioxidant enzymes compared to *M. aeruginosa*. *A. doliolum* showed a stronger increase in catalase and APX activity in response to heavy metals compared to *M. aeruginosa*. *M. aeruginosa* showed a larger increase in SOD activity compared to *A. doliolum*. The activity of this enzyme increased slightly in both species with heavy metal exposure, but the increase was lower compared to other antioxidant enzymes.